



<https://theses.gla.ac.uk/>

Theses Digitisation:

<https://www.gla.ac.uk/myglasgow/research/enlighten/theses/digitisation/>

This is a digitised version of the original print thesis.

Copyright and moral rights for this work are retained by the author

A copy can be downloaded for personal non-commercial research or study,
without prior permission or charge

This work cannot be reproduced or quoted extensively from without first
obtaining permission in writing from the author

The content must not be changed in any way or sold commercially in any
format or medium without the formal permission of the author

When referring to this work, full bibliographic details including the author,
title, awarding institution and date of the thesis must be given

Enlighten: Theses

<https://theses.gla.ac.uk/>
research-enlighten@glasgow.ac.uk

NONLINEAR ANALYSIS OF 2D AND SHELL REINFORCED
CONCRETE STRUCTURES INCLUDING CREEP AND SHRINKAGE

By

L I B O R J E N D E L E

A thesis submitted for the degree of
Doctor of Philosophy

Department of Civil Engineering
University of Glasgow

© L. Jendele
June 1992

ProQuest Number: 11011472

All rights reserved

INFORMATION TO ALL USERS

The quality of this reproduction is dependent upon the quality of the copy submitted.

In the unlikely event that the author did not send a complete manuscript and there are missing pages, these will be noted. Also, if material had to be removed, a note will indicate the deletion.



ProQuest 11011472

Published by ProQuest LLC (2018). Copyright of the Dissertation is held by the Author.

All rights reserved.

This work is protected against unauthorized copying under Title 17, United States Code
Microform Edition © ProQuest LLC.

ProQuest LLC.
789 East Eisenhower Parkway
P.O. Box 1346
Ann Arbor, MI 48106 – 1346

DECLARATION

I hereby declare that the following thesis has been composed by me, that it is a record of work carried out by myself, and that it has not been presented in any previous application for a higher degree.

ACKNOWLEDGEMENT

The work presented in this thesis was carried out in the Department of Civil Engineering and was supervised by Dr. D. V. Phillips. I wish to express my thanks to him and to other staff of the Civil Engineering Department, especially to Prof. D. R. Green, Dr. A. H. C. Chan and Prof. D. M. Wood, the Head of the Department, for their strong support, help and encouragement throughout my whole studies in Glasgow.

My thanks are also due to the staff of Electrical Department, particularly to Dr. D. Muir. His help with the university computer facilities is very appreciated.

My studies were funded by the Postgraduate Scholarship of the University of Glasgow and by ORS awards offered by the Senate of British Principals and Chancellors, London. Without these supports my work in Glasgow would not be possible and I am very grateful for them.

I acknowledge also full support and interest in my studies by my employers, SKODA Power Plant, Prague, Czechoslovakia, particularly to Dr. M. Trnka, the Chairman of Department of Technical Design.

Last, but not the least, my thanks are reserved for my wife, parents and parents-in-law. They showed a great understanding and encouragement to me during my stay in Glasgow.

ABSTRACT

The work deals with the static analysis of plane stress, plane strain, axisymmetric and shell reinforced concrete structures subject to short and long term loading conditions. Nonlinear short term material properties and structural nonlinear geometric behavior is considered. The effect of time factors is adopted in a linear form because of the lack of well established nonlinear models for creep and shrinkage of concrete.

The Total and Updated Lagrangian formulation of the problem is used to derive structural governing equations via the principle of virtual displacements. The adopted formulation is suitable for structures with large deflections, large rotations but small strains. Constitutive smeared-type equations for both 2D and 3D analysis of reinforced concrete are also considered.

For the 2D analysis isoparametric elements with variable number of nodes (four to nine) with Lagrangian approximation of geometry and displacements are employed using a simple linear material model accounting for cracking, crushing as well as for smooth tension stiffening of concrete. The reinforcement is modeled by piece-wise linear elastic isotropic constitutive equations.

For shell analysis, the degenerated Ahmad's shell element using Serendipity, Lagrange and Heterosis geometry and displacement interpolating hierarchical approach is adopted. Special attention is focused on the problem of shear locking and thus full, selective and reduced integration rules are dealt with. Constitutive equations are assumed which are elastic-plastic for both concrete and steel materials. Also tension stiffening and compression hardening and softening of concrete is included.

Nonlinear solution techniques are comprehensively reviewed and consequently some of them are significantly improved. A new algorithm for the solution of nonlinear equations, which is based on Newton-Raphson, Arc-length and Line search methods, has been developed.

Analysis considering shrinkage and creep has also been developed. The Step-by-step analysis using the Dirichlet series ap-

proximation to the creep function was adopted and its problem of numerical instability has been overcome.

The derived theory has been extensively tested for both short and long term loading conditions. Short term analyses focus especially on the accuracy of the material models being used and on shell behavior near the loss of stability. This type of analysis has been feasible only with the implementation of a very robust nonlinear equation solver, which is capable of dealing with structural snap through and snap back phenomena. The long term analyses concentrate on the accuracy of various simplified solution techniques, comparing these results with the Step-by-step method. The collective results show that full time analysis is necessary to assess serviceability structural conditions, whilst the time factor is negligible for the total structural strength with a failure mechanism being controlled mainly by time-independent reinforcement. The above conclusions are applicable for the structures investigated herein, (i.e. relatively thin and well reinforced), and should not be generalized for any arbitrary structure.

All developments in the work have been programmed into the nonlinear program NONSAP (University of Berkeley, USA) and CONCRETE (University of Swansea, U.K.). In addition other software has been created, such as material preprocessing program, library with graphics accessible from the FORTRAN environment etc.

TABLE OF CONTENTS

	Page
1. Introduction	1
1.1 Brief overview	1
1.2 Objective and scope, starting position	6
1.3 Thesis layout	11
2. General continuum governing equations	14
2.1 General problem formulation	17
2.2 Stress tensors	20
2.3 Strain tensors	22
2.4 The principle of virtual displacement applied to Total and Updated formulations	24
3. Constitutive equation	31
3.1 Experimental evidence about concrete behavior	32
3.2 Basic entities	38
3.3 Failure criteria	42
3.3.1 Overview of failure criteria for concrete	42
3.3.2 Mohr-Coulomb failure criterion combined with Rankine Cut-off criterion used in program NONSAP	48
3.3.3 Failure criterion used in program CONCRETE	49
3.3.4 Crushing coefficient	50
3.3.5 Failure criteria for steel	52
3.3.6 Interaction of concrete and reinforcing bars in cracks	52
3.4 Linear elastic constitutive models with failure cri- teria accounting for cracking and crushing	54
3.5 Nonlinear constitutive equation for concrete	72
3.5.1 Isotropic models	72
3.5.1.1 Model with variable E_s and μ_s	73
3.5.1.2 Model with variable bulk K_s and shear G_s modulus	75
3.5.2 Orthotropic models	79
3.5.2.1 Orthotropic model for monotonic loading	80
3.5.2.2 Orthotropic model for cyclic loading	82
3.5.3 Elastic-plastic models	85
3.5.4 Other types of constitutive equations	99

3.6	Constitutive equations for steel	100
3.7	Constitutive equations for reinforced concrete	101
3.8	Material and failure models used in programs NONSAP and CONCRETE	102
4.	Two dimensional axisymmetric, plane stress and plane strain elements	105
4.1	Geometry and displacement approximation	106
4.2	Element matrices assembly	113
5.	General shell element	125
5.1	Geometry and displacement fields for degenerated element	128
5.2	Strain and stresses definition	132
5.3	General governing equation for degenerated element	145
5.4	Serendipity, Lagrangian and Heterosis variant of degenerated shell element	149
5.5	Shear correction factor	156
5.6	Normal and shear forces, bending moment	158
5.7	The analysis of rank deficiency of the Ahmad's dege- nerate element for shell analysis	161
6.	Numerical Method For Solution Of Nonlinear Equations	183
6.1	Newton-Raphson method	184
6.2	Modified Newton-Raphson method	187
6.3	Quasi-Newton method	188
6.4	Arc-length method	193
6.4.1	Vector n_i lies in the plane normal to t_i (Normal update plane method)	198
6.4.2	Consistently linearized method	199
6.4.3	Explicit orthogonal method	201
6.4.4	The Crisfield method	204
6.5	Line search method	209
6.6	Parameter β	212
6.7	The new solution algorithm	214
6.8	Final remarks on nonlinear solution schemes	219
7.	Analysis of structures subject to short-term loading.	220
7.1	Simple two truss elements structure.	221
7.2	Ramm's shell.	227
7.3	Ramm's shell in reinforced concrete.	233

7.4 R/C slabs <i>A</i> and <i>B</i> .	235
7.5 R/C slab <i>C</i> .	257
7.6 Cylindrical R/C shell [67].	259
7.7 Summary.	277
8. Creep and Shrinkage Analysis	278
8.1 Models of creep and shrinkage prediction	280
8.1.1 American Concrete Institute (ACI) 1978 model	282
8.1.2 CEB - FIP 1978 model	289
8.1.3 Bazant and Panula's model II, 1978	296
8.2 Methods of creep and shrinkage analysis	301
8.2.1 Effective modulus method (EM method)	301
8.2.2 Rate of creep method (RC method)	302
8.2.3 Rate of flow method (RF method)	304
8.2.4 Improved Dischinger method (ID method)	305
8.2.5 Rheological models (RM method)	307
8.2.6 Step by step method	309
8.2.7 The Trost - Bazant method (TB method)	313
8.3 Step-by-step procedure using Dirichlet series for creep function	317
9. Analysis of structures subject to long-term loading.	329
9.1 Beam analysis subject to three years loading, 2D analysis.	330
9.1.1 Comparison between element meshes and integ- ration rules.	333
9.1.2. Comparison between creep and shrinkage mo- dels.	335
9.1.3. Effect of material non-linearity.	337
9.1.4. Effect of time integration densities.	338
9.1.5 Effect of retardation times.	339
9.2 Beam analysis subject to three years loading, shell analysis.	340
9.2.1 Comparison between creep and shrinkage mo- dels.	342
9.3 Analysis of concrete samples.	343
9.4 Comparison of the present Step by step method with solution techniques.	350
9.5 Approximation of creep function by Dirichlet's se-	

ries, rejection of excessive modes.	361
9.6 Summary.	364
10. User's and programmer's consideration of the developed software in a PC environment.	365
10.1 General considerations.	365
10.2 Hardware requirements.	366
10.3 User's considerations.	367
10.4 Programmer's considerations.	369
11. Conclusion and summary	381
References	387

FIGURES

	Page
Fig. 2.1 The movement of body of structure in Cartesian coordinate system.	18
Fig. 3.1 Typical uniaxial compressive stress-strain diagram [40].	33
Fig. 3.2 Uniaxial tensile stress-elongation curve [62].	34
Fig. 3.3 Uniaxial compressive stress-strain curves for concrete [64].	35
Fig. 3.4 Influence of specimen height on uniaxial stress-strain curve [65].	36
Fig. 3.5 Stress-strain curves under multiaxial compression (stress, strain positive in compression).	36
Fig. 3.6 Volumetric strain under biaxial compression [40].	37
Fig. 3.7 Cyclic uniaxial compressive stress-strain curve [63].	38
Fig. 3.8 Stress state at point P in principle stress coordinate system.	40
Fig. 3.9 Deviatoric and meridian cross sections of failure criteria discussed in Sec. 3.3.	43
Fig. 3.10 Notation for axisymmetric problem.	56
Fig. 3.11 Crack pattern in x-y plane.	58
Fig. 3.12 Evaluation of $\sigma_{y'}$ and $G_{x'y'}$ - method a/.	63
Fig. 3.13 Evaluation of $\sigma_{y'}$ and $G_{x'y'}$ - method b/.	65
Fig. 3.14 The functions $f_{\sigma}(\varepsilon_{y'})$ and $f_G(\varepsilon_{y'})$ in model d/.	68
Fig. 3.15 Diagram for $\sigma - \varepsilon$ according to SARGIN - (uniaxial case).	74
Fig. 3.16 The $\mu_s - \beta$ diagram.	75
Fig. 3.17 Loading condition.	83
Fig. 3.18 Hardening rules.	88
Fig. 3.19 Uniaxial case for $K'(\varepsilon^P)$.	91
Fig. 3.20 2D representation of failure criterion in CONCRETE.	98
Fig. 3.21 Yield and loading functions in the program CONCRETE.	99
Fig. 3.22 Hardening function H' in the program CONCRETE.	99

Fig. 4.1	Two dimensional element, natural and global coordinate systems.	106
Fig. 4.2	Example of some interpolation functions h_k .	110
Fig. 5.1	Three dimensional shell element, (a) and the corresponding degenerate shell element, (b,c).	127
Fig. 5.2	Degenerate shell nodal and curvilinear, (a) and local axes, (b) coordinate system.	130
Fig. 5.3	Node notation for element variants of quadratic element.	150
Fig. 5.4	Integration schemes and sampling points notation.	153
Fig. 5.5	Extension of bilinear approximation functions for arbitrary rectangular.	155
Fig. 5.6	The layer model.	156
Fig. 5.7	Shear retention factor.	157
Fig. 5.8	Stress resultant sign convention.	160
Fig. 5.9	Rank analysis of the Ahmad's element, the geometry of the two element structure.	162
Fig. 5.10	Rank analysis of the Ahmad's element, the eigenmodes of the Lagrangian approximation using the full integration rule.	164
Fig. 5.11	Rank analysis of the Ahmad's element, the eigenmodes of the Lagrangian approximation using the selective integration rule.	165
Fig. 5.12	Rank analysis of the Ahmad's element, the eigenmodes of the Lagrangian approximation with the reduced integration rule.	166
Fig. 5.13	Rank analysis of the Ahmad's element, the eigenmodes of the Heterosis approximation with the full integration rule.	167
Fig. 5.14	Rank analysis of the Ahmad's element, the eigenmodes of the Heterosis approximation with the selective integration rule.	168
Fig. 5.15	Rank analysis of the Ahmad's element, the eigenmodes of the Heterosis approximation with the reduced integration rule.	169
Fig. 5.16	Rank analysis of the Ahmad's element, the eigenmodes of the Serendipity approximation with the full	

integration rule.	170
Fig. 5.17 Rank analysis of the Ahmad's element, the eigenmodes of the Serendipity approximation with the selective rule.	171
Fig. 5.18 Rank analysis of the Ahmad's element, the eigenmodes of the Serendipity approximation with the reduced rule.	172
Fig. 5.19 Rank analysis of the Ahmad's element, the eigenmodes of the Lagrangian approximation, full integration - plastic material condition in the longitudinal direction.	177
Fig. 5.20 Rank analysis of the Ahmad's element, the eigenmodes of the Lagrangian approximation, full integration - fully cracked material in the longitudinal direction.	180
Fig. 6.1 Newton-Raphson method.	186
Fig. 6.2 Modified Newton-Raphson method.	188
Fig. 6.3 The Arc-length method notation and convergence performance.	195
Fig. 6.4 The vectors \underline{t}_1 , \underline{n}_1 and scalar β .	197
Fig. 6.5 Normal update plane for solution $\Delta\lambda_{i-1}$.	199
Fig. 6.6 Consistently linearized method for $\Delta\lambda_{i-1}$.	200
Fig. 6.7 Explicit orthogonal method for $\Delta\lambda_{i-1}$.	202
Fig. 6.8 The choice of the proper $\Delta\lambda_{i-1}$ root.	205
Fig. 6.9 Solution flow chart (part 1).	217
Fig. 6.9 Solution flow chart (part 2).	218
Fig. 7.1 Structure and loading condition to test nonlinear solver.	222
Fig. 7.2 Load vs. displacement relationship of the truss structure to test the nonlinear solver.	223
Fig. 7.2 Load vs. displacement relationship of the truss structure to test the nonlinear solver (cont.).	224
Fig. 7.3 Ramm's shell; geometry, loading and deflections at points c , i .	228
Fig. 7.4 Deflection at point c of Ramm's shell; different meshes, with and without geometrical nonlinearity.	231
Fig. 7.5 Deflection at point i of Ramm's shell; different	

meshes, with and without geometrical nonlinearity.	232
Fig. 7.6 Ramm's shell from reinforced concrete.	235
Fig. 7.7 Plate A: geometry, reinforcement, loading and boundary conditions.	237
Fig. 7.8 Plate A: finite element mesh and structural deformations.	240
Fig. 7.9 Plate A: load-deformation diagram.	241
Fig. 7.10 Plate A: comparison of the nonlinear solvers.	243
Fig. 7.11 Plate A: comparison of results for reduced and selective integration scheme.	245
Fig. 7.12 Plate A: mesh no. 1 and mesh no. 2.	247
Fig. 7.13 Plate A: mesh no. 1, loading 1 to 6.	248
Fig. 7.14 Plate A: results for mesh no. 1 and no. 2.	249
Fig. 7.15 Plate B: geometry, loading and boundary conditions.	251
Fig. 7.16 Plate B: reinforcement near top and bottom.	252
Fig. 7.17 Plate B: finite element mesh and deformations for the third load increment.	253
Fig. 7.18 Plate B: the deflection near the plate center (at point 'B').	255
Fig. 7.19 Plate B: the deflection at the mid of free plate edge (at point 'A').	256
Fig. 7.20 Plate C: load-displacement relationships.	258
Fig. 7.21 Geometry and reinforcement details of the cylindrical shell.	261
Fig. 7.22 Shell, model No. 1.	263
Fig. 7.23 Shell, model No. 2.	264
Fig. 7.24 Mid-span displacement of shell edge beams.	265
Fig. 7.25 Shell deformation for $\lambda=10.3$, model No. 1.	266
Fig. 7.26 Shell deformation for $\lambda=10.3$, model No. 2.	267
Fig. 7.27 Shell, model No. 1, failure zone progression.	268
Fig. 7.27 Shell, model No. 1, failure zone progression (cont.).	269
Fig. 7.28 Shell internal forces for $\lambda=4.3$, model No. 1.	271
Fig. 7.29 Shell internal forces for $\lambda=11.96$, model No. 1.	272
Fig. 7.30 Shell internal forces for $\lambda=19.52$, model No. 1.	273
Fig. 7.31 Shell internal forces for $\lambda=29.23$, model No. 1.	274

Fig. 7.32 Influence of geometrical nonlinearity and various modeling of concrete compression on the shell behavior, model No. 1.	276
Fig. 8.1 RC method.	303
Fig. 8.2 RF method.	305
Fig. 8.3 ID method.	307
Fig. 8.4 Burger' model.	309
Fig. 8.5 Superposition of virgin creep curves.	310
Fig. 8.6 Notation adopted in step-by-step procedure.	312
Fig. 8.7 Examples of $\chi(t, t')$ diagram (CEB - FIP).	316
Fig. 8.8 Notation for Step-by-step procedure using Dirichlet series approximation of creep function.	320
Fig. 8.9 Representation of Dirichlet series.	324
Fig. 9.1 Geometry and reinforcement of typical floor specimen.	331
Fig. 9.2 Geometry of the models used for 2D analysis.	334
Fig. 9.3 Creep and shrinkage analysis, the mid span deflection of the tested RC beam, 2D analysis.	334
Fig. 9.4 Influence of different creep models on mid-span deflection, 2D analysis.	336
Fig. 9.5 Crack development with time, 2D analysis.	336
Fig. 9.6 Effect of matrix B on the mid-span deflection, 2D analysis.	337
Fig. 9.7 Comparison between different integration steps.	339
Fig. 9.8 Comparison between different retardation times, 2D analysis.	340
Fig. 9.9 Geometry of the model used for shell analysis.	341
Fig. 9.10 The mid span deflection of the tested R/C beam, shell analysis.	342
Fig. 9.11 Shrinkage of concrete samples.	345
Fig. 9.12 Compressive strength of concrete samples.	346
Fig. 9.13 Strain in sample bars due to stress and shrinkage.	347
Fig. 9.14 Different time integration methods to analyze uniaxial concrete specimen.	348
Fig. 9.15 Maximum displacement of the structures, cases A-D.	354
Fig. 9.16 Maximum displacement of the structures, cases A-D, expressed in % of the results according to method	

a/.	355
Fig. 9.17 Maximum displacements development calculated by method a/.	356
Fig. 9.18 Short term and long term load-displacement curves, (case A).	360
Fig. 9.19 Analysis of Dirichlet's series modal spectrum	363
Fig. 10.1 Menu to define material characteristics for Bazant-Panula model 1.	369
Fig. 10.2 NONSAP layout.	370

TABLES

	Page
Table 4.1 Interpolation functions for 2D element.	111
Table 5.1 Analytical and discretized form of equilibrium equation.	146
Table 5.2 Ahmad's elements, locking and spurious energy modes summary, [41].	152
Table 5.3 Rank analysis of Ahmad's degenerated shell elements, maximum deformation of the 2-element cantilever in 10^{-4} m.	162
Table 5.4 Rank analysis of Ahmad's elements, number of spurious energy modes of one element.	173
Table 5.5 Rank analysis of Ahmad's elements, their layout for the analysis of communicability of spurious energy modes.	174
Table 5.6 Rank analysis of Ahmad's element, number of spurious energy modes of meshes of two or more elements.	174
Table 5.7 Rank analysis of the Ahmad's element, the eigenmodes of the Lagrangian approximation, selective integration - plastic condition in the longitudinal direction.	178
Table 5.8 Rank analysis of the Ahmad's element, the eigenmodes of the Lagrangian approximation, selective integration - fully cracked material in the longitudinal direction.	181
Table 7.1 Results of truss analysis testing the nonlinear solver.	225
Table 7.2 Plate A: joint loading for 9 element mesh.	238
Table 7.3 Plate A: joint loading for 36 element mesh.	246
Table 7.4 Plate B: nodal loading forces.	254
Table 7.5 Material properties for shell analysis.	262
Table 8.1 ACI 78 model, creep coefficient k'_4 .	284
Table 8.2 Definition of average and effective thicknesses.	285
Table 8.3 ACI 78 model, constants A and B .	286
Table 8.4 ACI 78 model, coefficient q'_4 .	288
Table 8.5 ACI 78 model, shrinkage age coefficient q'_5 .	288

Table 8.6 Expressions for CEB-FIP model for creep predictions.	292
Table 8.6 Expressions for CEB-FIP model for creep predictions (cont.).	293
Table 8.7 Comparison of total results of creep prediction using CEB - FIP approximation expressions and Neville et al. functions.	293
Table 8.8 Expressions for CEB-FIP model for shrinkage predictions.	295
Table 9.1 Integration time steps.	338
Table 9.2 Retardation time sets.	340

NOTATION

In this work the following system of notation is used:

- 1/ Matrix, vector and scalar variables are printed in bold, underlined and italic fonts respectively, e.g. \mathbf{K} , \underline{p} , i . Constant scalars are written in standard font, e.g. E . For some special scalar constants and/or variables greek alphabetic is used.
- 2/ For indexed entities the left superscript denotes the time corresponding to the value of the entity, the left subscript denotes the configuration with respect to which the value is measured and subscripts on the right identify the relationships to the coordinate axis. Thus for example ${}_{0}^{t+dt}\tau_{ij}$ denotes element i, j of stress tensor τ at time $t+dt$ with respect to the original (undeformed) configuration.
- 3/ For derivatives the abbreviated notation will be used, i.e. all right subscripts that appear after a comma declare derivatives. For example:

$${}_{0}^{t+dt}u_{1,j} = \frac{\partial}{\partial X_j} {}_{0}^{t+dt}u_1$$

It follows a list of the most frequently used symbols. More detailed description is available near the text or equation where the particular symbol referred.

$a, b, c, \dots, A, B, C, \dots, \alpha, \beta, \dots$ = material constants

tV = volume at time t

β = angle of cracks

C^E = elastic material rigidity matrix

C^{EP} = elastic plastic material rigidity matrix

${}_{0}C_{ijrs}$ = i, j, r, s element of the tangential material rigidity tensor

$\delta()$ = variation operator

$\delta_{ij} = i, j$ element of Kronecker's delta tensor.

$\frac{\partial e_{ij}^t}{\partial t} = i, j$ element of strain rate tensor at time t

$e_{0ij} = i, j$ element of the linear part of strain increment

$e_{mn}^t = m, n$ element of ordinary strain tensor at time t

$\varepsilon_{0ij}^t = i, j$ element of Almansi strain tensor at time t

$\varepsilon_{0ij}^t = i, j$ element of Green-Lagrange strain tensor at time t

$c_{0ij}^t = i, j$ element of Cauchy-Green strain tensor at time t

η = acceleration/dumping coefficient for Line search method

ε^P = plastic part of strain

ε_{cr} = strain when material cracked

E = Young's modulus

$E(t')$ = function for Young's modulus

f'_c = material compression strength

$f'_t = f_{tu}$ = material tension strength

${}^tF(\dots), {}^t f(\dots)$ = yield (loading) functions

${}^{t+\Delta t} \underline{F}_0^{(i-1)}$ = the vector of nodal point forces equivalent to the
internal stresses from previous iterations

$\Phi(t, t') = \frac{1}{E(t')} [1 + \phi(t, t')] =$ creep compliance function

G = shear modulus

${}^tH(\dots)$ = hardening function

h_k = k -th shape function in natural coordinate system

I_1, I_2, I_3 = 1st, 2nd and 3rd invariants of Cauchy stress tensor

I'_1, I'_2, I'_3 = 1st, 2nd and 3rd invariants of strain tensor

J_1, J_2, J_3 = 1st, 2nd and 3rd invariants of deviatoric Cauchy
stress tensor

J'_1, J'_2, J'_3 = 1st, 2nd and 3rd invariants of deviatoric strain
tensor

J = Jacobian of transformation to natural coordinate system

K = bulk modulus

${}^t_0 K_L$ = linear part of stiffness matrix

${}^t_0 K_{NL}$ = nonlinear part of stiffness matrix

λ = load multiplier for Arc length method

${}^0\eta_{ij}$ = i, j element of the nonlinear part of strain increment

${}^{t+dt}_0 R$ = the work of external forces at time t

$\sigma_1, \sigma_2, \sigma_3$ = principal stresses

r, s, t = coordinates in natural coordinate system

σ_{oct} = octahedral normal stress

σ_m = mean normal stress

σ_{ij} = i, j element of Cauchy stress tensor

s_{ij} = i, j element of deviatoric Cauchy stress tensor

${}^t_0 S_{ij}$ = i, j element of 2nd Piola-Kirchhoff tensor at time t

${}^t S$ = surface area at time t

τ_{oct} = octahedral shear

τ_m = mean shear

${}^t\tau_{ij}$ = i, j element of Cauchy stress tensor at time t

${}^t\dot{\tau}_{ij}$ = i, j element of Jaumann stress rate tensor at time t

t = time of our interest of structural behavior

t' = time, when the structure was loaded

${}^t u_1, {}^t u_2, {}^t u_3$ = point displacements at time t

$u_i = {}^{t+dt}X_i - {}^tX_i$ is i -th element of vector of displacement increments at time t

$\Delta \underline{u}^{(i)} = \underline{u}^{(i)} - \underline{u}^{(i-1)}$ is the displacement increment in the i -th iteration

${}^tX_1, {}^tX_2, {}^tX_3$ = point coordinates at time t

ξ, χ, Θ coordinates in the principal stress coordinate system

1. INTRODUCTION

1.1 Brief overview.

Concrete in the form of a structural material has been used since Roman times. In ancient times the most important problem was its very low strength in tension, but fortunately the discovery that concrete can be reinforced by steel bars has nowadays reduced this drawback.

At the time of the industrial revolution interest in reinforced concrete significantly increased and this involved interest in more accurate analysis of reinforced concrete structures. Many researchers and engineers have produced many methods to analyze various types of reinforced concrete structure but most were based on empirical formulae and engineer's professional judgment rather than on mathematical and mechanical theories of material and structural behavior. This was due to the inherent complexity of reinforced concrete material behavior as a composite of steel and concrete, as well as the different material characteristics of concrete in compression and tension regimes.

Another problem was the mathematical modeling of structures themselves. Again only empirical formulae based on experimental results or experience with already finished structures were available and only later some theories based on linear approach has been introduced.

Nowadays the situation in structural analysis and material modeling is much better. The development of the finite element method and the availability of very powerful computer techniques enable relatively accurate predictions of structural response to loading even near to collapse. This has encouraged designers to consider lighter and more efficient structures.

This trend has been accompanied by the efforts of scientists to solve emerging problems which were earlier unattractive. For example, stability problems ^{require} nonlinear treatment of structural geometry and material response etc. However despite the enormous

work already being done there are still many problems to be solved in the future.

Another problem in this area is the practical employment of theoretical research results. People working in design enterprises usually have no time to systematically study sophisticated methods being produced by universities, research institutes etc. and the only way to pass to them the newly developed theories is to produce simplified design instructions in building codes or preferably to produce powerful software background. This software must guide them in a "user friendly" way through a whole analysis and eventually check user provided data. Programs of this sort are usually called Expert Systems and they are constructed as a "rational" superstructure above computer-aided design systems (CAD).

Today many programs for structural analysis are available. The vast majority, however, are based on linear finite element theories. These are supplemented by programs for detailed concrete design (dimensions, reinforcement etc.) according to building codes. Hence nonlinear design procedures provided in building standards are used in conjunction within accurate results obtained by overall linear analysis of a structure. If we are restricted to use only about fifty percent of the material strength and if we do not design some especially light structures the above software is quite justified and the adopted simplifications cause only negligible errors. Unfortunately attempts to produce more economic structures as well as attempts to build structures which were in earlier times technically impossible, force engineers to provide more accurate solutions and designs, and obviously nonlinearity must be considered during the whole analysis.

Today there are some powerful nonlinear solution systems available in the world. Some of the most advanced are ADINA, DIANA, NASTRAN and LUSAS, whilst STRUDL and PAFEC support some limited nonlinearity. In addition there are many single purpose nonlinear programs that solve, for instance, plane beam structures,

shell buckling analysis etc. However there is still a high demand for new nonlinear software.

The primary purpose of this work is the modeling of reinforced concrete structures, particularly plane stress, plane strain, axisymmetric and shell structures. This will be now discussed in more detail. The problem can be divided into the following parts:

- Assembling of overall governing equations that characterize structure shape, loading etc.,
- Material behavior prediction,
- Solution of assembled set of nonlinear equations,
- Results interpretation.

The most usual method for considering the governing structural equations is the principle of virtual work. It is a versatile tool for defining structural behavior and can be used for any type of material model, loading condition, structural shape etc. Because the displacement variant of structural analysis is usually preferred, the particular principle of virtual displacement is employed. However, for particular problems some other structural definition can be utilized, for example, variational principles, Clapeyron principles etc.

Material behavior, and especially reinforced concrete behavior, represents a very difficult problem. The traditional Hooke's law, that leads to linear analysis, can now be replaced by much more sophisticated models. They comprise, for example, nonlinear hyperelastic and incremental hypoelastic models, elastic plastic models with hardening in compression zones and stiffening in tension zones (near cracks), endochronic, progressive fracture models and many others. Nevertheless most nonlinear programs use "traditional" elasto-plastic models for concrete in compression and linearized models for cracking in tension regimes. Many yield and loading functions have been developed as well as expressions for hardening and tension stiffening. Despite this there is still a lack of information for general three dimensional cases and also most results are applicable only for short-

term monotonically increasing loading. Additional problems are in obtaining the proper material constants for the above models. Realizing that some endochronic models comprise twenty and even more material characteristics it is apparent that here experimental work is very important.

In practice less complicated material models are usually used in conjunction with material values recommended in building codes, and supplemented by some laboratory tests. Reinforcing steel is quite satisfactorily modeled by elastic-plastic material (Von Mises) or by part-linear models.

The assembled nonlinear set of equations are solved iteratively and the loading is applied by increments. The well established procedure for equation solution is the Newton-Raphson method or its simplified version, the Modified Newton-Raphson method. In recent times new methods have been developed (Quasi Newton methods, Arc-length methods, Line search etc.).

A special group of solution procedures are perturbation methods. They have advantages, especially in stability problems, when whole classes of possible structural imperfections can be studied. However their practical use is difficult because they are very complex and there exists no proof that the computed results give the "lowest" energy and hence the most probable structural response. Thus they are used by people with an adequate theoretical background rather than as a practical design tool for ordinary engineers.

The way results are interpreted is not unique. Some CAD software are capable of providing facilities up to the final drawing stage of structural design including sophisticated and powerful graphics etc. On the other hand ordinary nonlinear programs usually finish by printing and plotting of displacements and internal stresses.

The study of reinforced concrete structures under long-term loading has received little attention. There is a lack of both experimental data and practical software development. This is due to the fact that long-term laboratory tests are expensive and

analytical solution, comprising the combination of geometrical nonlinear solution, material nonlinearity and time phenomena such as creep and shrinkage, represents very complex and challenging analysis. It is only in very recent times that such a solution could be attempted. The problem is particularly difficult for shell analysis. Since there is a high interest in very thin structures spanning over tens of meters it is evident that it is worthwhile to be concerned with this problem. Although shrinkage and creep may not significantly influence the stresses in many cases, the importance of creep on structural deformations and thus serviceability is indisputable. It can be ^{the} limiting factor for bearing capacity of this type structures.

1.2 Objective and scope, starting position.

This work deals with the nonlinear analysis of reinforced concrete structures. Particular attention is focused on two dimensional plane stress, plane strain and axisymmetric structures as well as to degenerated three dimensional shell structures.

Several aspects of nonlinear analysis are considered, including the creation and assembly of the general governing equations using the principle of virtual work applied to both Total and Updated Lagrangian formulations for geometric nonlinearity, the modeling of constitutive equations, and procedures for the solution of the nonlinear equations. Special attention is paid to the time dependent factors of concrete, i.e. to creep and shrinkage.

In addition to this theoretical development, the major part of this work was the extension of two software packages, NONSAP [44], [45] and CONCRETE [42], into which all developed theory has been programmed, tested and prepared for practical use.

A major objective was to develop all software for PC computers so that as many users as possible can make use of them. The software was developed for people who need to perform accurate analysis of reinforced structures without access to a supercomputer or Cray-like techniques and without first-hand theoretical and practical experience of this type of analysis. Therefore analysis and programs aim for user friendliness and require no special computing facilities.

The basic objectives can be summarized in detail as follows:

Theoretical part:

1/ To produce a state-of-art report on some current concepts used in nonlinear analysis of reinforced concrete. This comprises the following aspects:

-Problem formulation using Total and Updated Lagrangian

- approaches applied under the principle of virtual work,
- Review of the currently most widely used material models for concrete and steel materials,
 - Description and discussion of the procedures based on the Newton-Raphson method and their modification for the solution of nonlinear equations,
 - Overview of methods for creep and shrinkage analysis.

2/ To introduce compression hardening and softening into elasto-plastic material model for concrete.

3/ To develop more powerful algorithms for the solution of nonlinear equations.

4/ To use the step-by-step solution method for creep and shrinkage analysis. This includes the development of procedures for approximations of creep and shrinkage functions by Dirichlet series [38] and in particular treatments for dealing with ill conditioning and stability of this problem.

5/ To test the above theoretical models and provide analytical evidence on structural behavior with special emphasis to:

- short and long term constitutive equations,
- robustness and efficiency of the developed nonlinear equations solver,
- comparison of the accuracy of various simplified creep and shrinkage methods with the Step-by-step methods. Here both serviceability and ultimate structural conditions should be investigated. The effect of reinforcement ratio and structural loading level is also a matter of concern.

Comparison of the obtained results with results from independent sources.

Practical part:

The above theories are applied for two dimensional plane strain/stress structures, axisymmetric structures and thin and moderately thick 3D shell structures. Two nonlinear finite element programs have been used as a basis for the new developments: "NONSAP" produced by K. J. Bathe, [44], [45], for 2D RC structures, and "CONCRETE" developed by E. Hinton and D. R. J. Owen, [42], for 3D degenerated RC shells (called CONCR2 by authors). The work includes the following:

1/ In order to develop software for PC environment the first step was to modify and transfer mainframe versions of the programs NONSAP and CONCRETE to PCs and MSDOS operating system.

2/ Programming and implementing the newly derived nonlinear equations solver into NONSAP and CONCRETE. The algorithm can work either fully automatically or by manual adjustment of optional solution parameters (step length, type of Arc-length constraint, employment of Line search etc.). NONSAP uses the band variable sky-line housekeeping procedures whilst the CONCRETE uses the frontal solution techniques. Therefore two sets of procedures were created.

3/ The development of a small graphics library for plotting using ICL CG 6400 graphic terminals, HP plotters, .DXF interfaces in cooperation with AUTOCAD software as well as IBM PC compatible video monitors (HERCULES, CGA, EGA etc.). In order to save internal memory no standard graphic package is used, the whole graphics being supported only by a standard FORTRAN environment.

The developed library is used for graphic output of geometry and deformations from nonlinear analysis performed by the NONSAP (the program NONGRAPH) as well as by the CONCRETE (the program CONCRPLOT).

Both NONGRAPH and CONCRPLOT work in interactive mode and support some basic functions such as zooming, plotting of selected parts of structure (boxing, by group of elements) etc. In addition the .DXF interface enables the use of all facilities provided by AUTOCAD, for example 'hide' function, and modifying created pictures.

4/ Programming a material preprocessor for the following creep and shrinkage models (the program MATERIAL):

- CEB FIB 1978 model [31],
- ACI 78 model [32],
- Bazant-Panula model I [48],
- Bazant-Panula model II [32],

and the creation of the software for their approximation by Dirichlet series. In order to avoid numerical stability problems the program automatically deselects excessive shape modes from a total class of approximation functions.

The data from this are compatible with both NONSAP and CONCRETE programs (in binary form) and are plotted on the graphic monitor. Hence the user has a very convenient control over this step of the problem solution. Also the input data for material definition is required in a very user friendly form.

To enable a quick orientation in results pertaining to particular creep and shrinkage model in conjunction with the user supplied data (material constants and loading condition) a simple analysis of a concrete bar is available directly within the program MATERIAL. This very fast step can avoid a time expensive solution of an analyzed structure with improper concrete model. Also a direct graphic interpretation of results is available.

5/ The implementation of the Step-by-step method into CONCRETE and NONSAP programs to include creep and shrinkage analysis.

Despite the fact that all created software is developed for PC computers, the programs and subroutines are written in standard Fortran 77 and thus ^{are} simply transferable to any other machine. Small difficulties might emerge in the case of graphic functions. Hence these are cumulated in a separated library, are described in detail and thus it should be no problem to modify them for any other particular configuration.

1.3 Thesis layout.

The objective of this section is to give information about the thesis layout.

Chapter Two deals with the derivation of the general continuum governing equations for Total and Updated Lagrangian formulation. All expressions are based on the incremental form of the principle of virtual displacements.

Chapter Three brings together the many possibilities of material modeling of concrete. Special attention is focused on linearized models which account for cracking, crushing and mixed mode failure, to nonlinear initially isotropic models (hyperelastic, incremental hypoelastic etc), to orthotropic and to elasto-plastic models. The essential part of this chapter deals with formulation of failure criteria. A variety of failure models is presented from the simplest with only one parameter to very advanced formulations with many material constants. This chapter also includes detailed description of constitutive equations used in the developed software, including their enhancements.

The steel constitutive equations are not discussed directly but it can be used by part linear Hooke's rule or elasto-plastic model with Von Mises yield condition.

Chapter Four is concerned with the implementation of theories derived in Chapter Two (the governing equations) and Chapter Three (material models) for 2D problems. Plane stress/strain and axisymmetric analyses are discussed. This is in fact the theoretical description of the finite element used in the program NON-SAP.

Chapter Five deals with shell analysis. All resulting equations are presented in detailed form prepared for direct algorithmisation. Some problems such as locking etc. are overviewed. The discussed theories are used in the program CONCRETE.

Chapter Six is concerned with the solution of the governing nonlinear equations. Some current "standard" solution techniques are presented after which the Arc-length and Line search methods

are employed to compile new efficient solution schemes. This comprises a possible variable step length constraints as well as the optimization of some other parameters. The theoretical results of this chapter are used to improve the original band variable skyline solver in NONSAP and the frontal solver in the program CONCRETE. The primary aim is to construct all subroutines in the most independent way and hence to make them simple to use in any other nonlinear finite element package.

Chapter Seven brings together all practical results of short-term analyses using the developed software. At the very beginning a list of all performed analyses is given, each with a brief explanation about which particular problems are dealt with. In addition the header of every analysis contains detailed description of the studied phenomena.

The objective of Chapter Eight is creep and shrinkage analysis. At first some recognized material models are discussed, thereafter the most widely used methods for time dependent analysis are reviewed. Finally attention is focused on the step by step procedure using approximations by Dirichlet series [38]. This method is used in both CONCRETE and NONSAP programs.

Chapter Nine presents results of several long-term analyses. The method of presentation is similar to that in Chapter Seven. This chapter and Chapter Seven tests in practice all theoretical developments derived in the thesis.

Chapter Ten contains user's and programmer's considerations of the developed software. The first section describes general aspects of the environment. Several versions of the software have been developed. Their efficiency and hardware requirements are discussed in the second section of this chapter. The third chapter brings a brief picture of user-software communication. An example of input data for material preprocessing program MATERIAL is given. Finally, the fourth and last section deals with technical and programmer's considerations. A short description of all subroutines used in the software is given as well as for example programs' overlay structures etc. This section is valuable only

for those aiming to enhance the program environment.

The work is concluded and summarized in Chapter eleven.

2. GENERAL CONTINUUM GOVERNING EQUATIONS.

In this chapter the general governing continuum equations for nonlinear analysis will be presented. It should be noted that there are many variants of nonlinear analysis depending on how many nonlinear effects are accounted for.

For a linear analysis we must satisfy the following simplifications:

- 1/ The constitutive equations must be linear, in other words we use the generalized form of Hooke's law, leading to a materially linear solution.
- 2/ The geometric equations relating strains and displacements must be linear, that is quadratic terms are neglected.
- 3/ Both loading and boundary conditions must be conservative. This means that they are constant throughout the whole analysis irrespective of structure deformation, time etc.

Provided all three restrictions are satisfied the relationships between loading and deflection are linear. A linear solution is much simpler than a nonlinear one and therefore it is important to know when such a simplification is acceptable and their adoption does not cause too high an error.

Generally linear constitutive equations can be employed for a material which is far from its failure point, usually up to about 50% of maximum strength. Of course this depends on the type of material, e.g. rubber needs to be considered as a nonlinear material much earlier. But for usual civil engineering materials this is satisfactory.

Geometric equations can be linearized if the deflections of a structure are much smaller than its dimensions. This must be satisfied not only for the whole structure but also for its parts. The geometric equations for the loaded structure can then be written using the original (unloaded) geometry.

Also important is that a linear solution is permissible only in the case of small strains. This is closely related to material properties because if strains are high, the stresses are usually,

although not necessarily, high also.

Despite the fact that for the vast majority of structures linear simplifications are quite acceptable, there are structures when it is necessary to take in account some nonlinearity. The resulting governing equations are then much more complicated and normally do not have a closed form solution. Consequently some nonlinear iterative solution scheme must be used. In addition computation costs increase enormously and without computer support practical nonlinear analysis is impossible. Hence the first aim of every engineer is to apply linear relationships if at all possible.

Nonlinear analysis can be classified into various levels:

- a/ Nonlinear material behavior only needs to be accounted for. This is the most common case for ordinary reinforced concrete structures. Because of serviceability limitations, deformations are relatively small. However the very low tensile strength of concrete needs to be accounted for.
- b/ Deformations (either displacements only or both displacements and rotations) are large enough that the equilibrium equations must use the deformed shape of the structure. However the relative deformations (strains) are still small. The complete form of the geometric equations, including quadratic terms, have to be employed but constitutive equations are linear. This group of nonlinear analysis includes most stability problems.
- c/ The last group uses both material and geometric nonlinear equations. In addition it is usually not possible to suddenly apply the total value of load but it is necessary to integrate in time and/or loading increments. This is the most accurate and general approach but unfortunately is also the most complicated.

Before carrying out a complex nonlinear analysis it is

always good practice to perform an independent linear solution in order to obtain some "feel" for the response of a structure, and to be able to evaluate the influence of linear simplifications on the response of the structure. It sometimes happens that a nonlinear solution will miss the lowest energy solution. For example this is the case for the perturbation method where there is no proof that "lowest" deformation mode has really been found. In these situations it is usually worthwhile to understand the linear behavior of a structure.

There are two basic possibilities for formulating the general structural behavior based on its deformed shape:

Lagrange formulation.

In this case we are interested in the behavior of infinitesimal particles of volume dV . Their volume will vary dependent on the loading level applied and, consequently, on a scale of current deformations. This method is usually used to compute structural behavior in civil engineering.

Euler formulation.

The essential idea of Euler's formulation is to study the "flow" of the structural material through infinitesimal and fixed volumes of the structure. This is the favourite formulation for fluid analysis, analysis of gas flow, tribulation etc. where large material flows exist.

For structural analysis, however, Lagrangian formulation is better and therefore attention will be restricted to this. Two forms of the Lagrangian formulation are possible. The governing equations can either be written with respect to the undeformed original configuration at time $t = 0$ or with respect to the most recent deformed configuration at time t . The former case is called Total Lagrangian formulation (TL) whilst the latter is

called the Updated Lagrangian formulation (UL).

It is difficult to say which formulation is better because both have their advantages and drawbacks. Usually it depends on a particular structure being analyzed and which one to use is a matter of engineering judgment. Generally, provided the constitutive equations are adequate, the results for both methods are identical. The problem of which one to use will be discussed later when the necessary theoretical background has been developed.

2.1 General problem formulation.

In most cases a structure must be loaded by many loading increments and at each increment an iterative scheme needs to be employed to obtain a solution. This is the basic idea of so-called incremental iterative procedures.

The total loading is divided into many increments which are subsequently applied to the structure at different times. The main task of an analysis is to compute the response of the structure after applying a load increment. In order to do this we need to know the state of the structure at time t before applying the loading increment and we analyze the structural behavior at time $t + \Delta t$ after its application. This procedure is repeated as many times as necessary to reach the final (total) level of loading.

This is depicted in Figure 2.1. At time $t = 0$ the volume of structure is 0V , the surface area is 0S and any arbitrary point M has coordinates 0X_1 , 0X_2 and 0X_3 . Similarly at time t the same structure has a volume tV , surface area tS and coordinates of point M tX_1 , tX_2 and tX_3 . Similar definitions apply for time $t+dt$ also by replacing t by $(t + \Delta t)$.

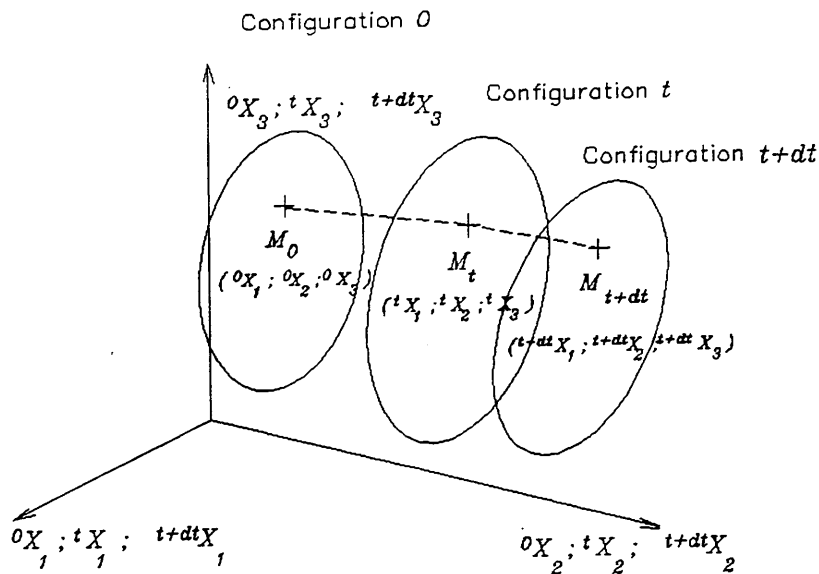


Fig. 2.1 The movement of body of structure in Cartesian coordinate system.

For the derivations of nonlinear equations it is important to use clear and simple notation. In this thesis the system of notation used in [1] will be adopted throughout, although sometimes it may not be the most convenient.

- Displacements u are defined in a similar manner to that adopted for coordinates, hence ${}^t u_i$ is the i -th element of the displacement vector at time t ,

- $u_i = {}^{t+dt} X_i - {}^t X_i$ is i -th element of vector of displacement increments at time t , (for the sake of simplicity index t is already omitted: we are always interested in the "current" time increment),

- Generally the left superscript denotes the time corresponding to the value of the entity, the left subscript denotes the configuration with respect to which the value is measured and subscripts on the right identify the relationships to the coordinate axis. Thus for example ${}^{t+dt} {}_0 \tau_{ij}$ denotes element i, j of

stress tensor τ at time $t+dt$ with respect to the original (undeformed) configuration.

- For derivatives the abbreviated notation will be used, i.e. all right subscripts that appear after a comma declare derivatives. For example:

$${}^{t+dt}u_{0\ 1,j} = \frac{\partial}{\partial X_j} {}^{t+dt}u_1$$

The general governing equations can be derived in the form of a set of partial differential equations (for example by using the displacement method) or an energy approach can be used. The final results are the same.

One of the most general methods of establishing the governing equations is to apply the principle of virtual work. There are three basic variants of this:

- 1/ The principle of virtual displacements,
- 2/ The principle of virtual forces,
- 3/ The Clapeyron divergent theorem.

Using the virtual work theorems it is possible to derive several different variational principles (Lagrange principle, Clapeyron principle, Hellinger-Reissner principle, Hu-Washizu principle etc.). These are popular especially in linear analysis. They can be used to establish equilibrium equations, to study possible deformation modes in finite element discretization etc. Unfortunately in nonlinear analysis they do not always work.

All the following derivations will be presented in their displacement form and consequently the principle of virtual displacements will be used throughout this thesis. Details of other formulations of the continuum equations can be found in [3].

The following section deals with the definition of the stress and strain tensors which are usually used in nonlinear analysis. All are symmetric.

2.2 Stress tensors.

Nowadays many different types of stress tensor are used in nonlinear mechanics. However only three of them are totally satisfactory and these will now be defined:

Cauchy stress tensor.

This tensor is well known from linear mechanics. It expresses the forces that act on infinitesimal small areas of the deformed body at time t . Sometimes these are also called "engineering" stress. The Cauchy stress tensor is the main entity for checking ultimate stress values in materials. In the following text it will be denoted by τ .

2nd Piola-Kirchhoff stress tensor.

The 2nd Piola-Kirchhoff tensor is a fictitious entity, having no physical representation as in the case of the Cauchy tensor. It expresses the forces which act on infinitesimal areas of body in the undeformed configuration. Hence it relates forces to the shape of the structure which no longer exists.

The mathematical definition is given by:

$${}^tS_{ij} = \frac{{}^0\rho}{{}^t\rho} * {}^0X_{i,m} * {}^t\tau_{mn} * {}^0X_{j,n} \quad /2.1/$$

where $\frac{{}^0\rho}{{}^t\rho}$ is the ratio of density of the material at time 0 and t ,

${}^t\tau_{mn}$ is the Cauchy stress tensor at time t ,

${}^0X_{i,m}$ is the derivative of coordinates

Using inverse transformation, we can express the Cauchy stress tensor in terms of the 2nd Piola-Kirchhoff stress tensor, i.e.:

$${}^t\tau_{mn} = \frac{{}^t\rho}{\rho} * {}^tX_{m,i} * {}^tS_{ij} * {}^tX_{n,j} \quad /2.2/$$

The elements ${}^tX_{m,i}$ are usually collected in the so-called Deformation gradient matrix:

$${}^tX = \left(\nabla \cdot {}^t\underline{X}^T \right)^T \quad /2.3/$$

$$\text{where } \nabla^T = \left[\frac{\partial}{\partial X_1}; \frac{\partial}{\partial X_2}; \frac{\partial}{\partial X_3} \right]^T$$

$${}^t\underline{X}^T = \left[{}^tX_1; {}^tX_2; {}^tX_3 \right]$$

The ratio $\frac{{}^t\rho}{\rho}$ can be computed using:

$$\rho = {}^t\rho * \det {}^tX \quad /2.4/$$

Expression /2.4/ is based on the assumption that the weight of an infinitesimal particle is constant during the loading process.

Some important properties can be deduced from definition /2.1/:

- at time 0, i.e. the undeformed configuration, there is no distinction between 2nd Piola-Kirchhoff and Cauchy stress tensors because ${}^0X = E$, the unity matrix, and the density ratio $\frac{{}^t\rho}{\rho} = 1.$,

- 2nd Piola-Kirchhoff tensor is an objective entity in the sense that it is independent of any movement of the body provided the loading conditions are frozen. This is a very important property. The Cauchy stress tensor does not satisfy this because it is sensitive to the rotation of the body.

Jaumann stress rate tensor.

Contrary to the previous tensors, the Jaumann stress rate tensor expresses not direct stress values but their rates. It is also a fictitious entity and is usually used in the most complicated nonlinear analysis when load (time) increments must be integrated (and not applied suddenly). It is also objective and is defined by:

$${}^t\dot{\tau}_{ij} = \frac{\partial {}^t\tau_{ij}}{\partial t} - {}^t\tau_{ip} * {}^t\Omega_{pj} - {}^t\tau_{jp} * {}^t\Omega_{pi} \quad /2.5/$$

$$\text{where } {}^t\Omega_{ij} = \frac{1}{2} \left(\frac{\partial^2 {}^t u_j}{\partial t \partial X_i} - \frac{\partial^2 {}^t u_i}{\partial t \partial X_j} \right) \quad /2.6/$$

The value of Jaumann stress tensor depends not only on current loading condition but also on the loading history (e.g. in the case of hypoelastic materials).

2.3 Strain tensors.

Similar to stress tensors, there are many strain tensors suitable for nonlinear analysis, but we will restrict our descriptions to the five which are energy conjugate with the above stress tensors:

Green-Lagrange strain

This is the energy conjugate of the 2nd Piola-Kirchhoff tensor and its properties are similar (i.e. objective etc.). It is defined by:

$${}^t\varepsilon_{ij} = \frac{1}{2} \left(\begin{matrix} {}^t u_{i,j} + {}^t u_{j,i} + {}^t u_{k,i} * {}^t u_{k,j} \end{matrix} \right) \quad /2.7a/$$

It can be proved [1], [3] that this tensor represents accurate values of strains. It can be demonstrated that if we calculate the length of an infinitesimal fibre prior and after deformation in the original coordinates, we get directly the terms of the Green-Lagrange tensor.

Cauchy-Green tensor

Cauchy-Green tensor is an arbitrary tensor defined by:

$${}^t_{C_{ij}} = {}^t_{X_{k,i}} * {}^t_{X_{k,j}} \tag{2.8/}$$

and is often used to calculate the Green-Lagrange tensor by:

$${}^t_{\epsilon_{ij}} = \frac{1}{2} \left({}^t_{C_{ij}} - \delta_{ij} \right) \tag{2.7b/}$$

where δ_{ij} denotes the Kronecker's delta tensor.

Strain rate tensor:

The Strain rate tensor is the energy conjugate of the Jaumann stress rate tensor and its properties are similar. Its definition is given by:

$$\frac{\partial {}^t e_{ij}}{\partial t} = \frac{1}{2} \left(\frac{\partial^2 {}^t u_i}{\partial t * \partial {}^t X_j} + \frac{\partial^2 {}^t u_j}{\partial t * \partial {}^t X_i} \right) \tag{2.9/}$$

Ordinary strain tensor:

This is the most commonly used strain tensor, comprising strains which are often called Engineering strains. Its main importance is that it is used in linear mechanics as a counterpart to the Cauchy stress tensor.

$${}^t e_{mn} = \frac{1}{2} \left(\frac{\partial u_m}{\partial {}^t X_n} + \frac{\partial u_n}{\partial {}^t X_m} \right) \quad /2.10/$$

This is a very important but unobjective entity. The following very helpful relation can be proved:

$$\delta({}_0^t \varepsilon_{ij}) = \frac{\partial {}^t X_m}{\partial {}^0 X_i} * \frac{\partial {}^t X_n}{\partial {}^0 X_j} \delta({}_t e_{mn}) \quad /2.11/$$

where δ is the operator for variation.

Using /2.11/ it is simply demonstrated that the 2nd Piola-Kirchhoff tensor is the energy conjugate of the Green-Lagrange strain tensor.

Almansi strain tensor.

This is the energy conjugate of the Cauchy stress tensor and its properties are similar (i.e. non-objective etc.). It is defined by:

$${}_0^t \varepsilon_{ij} = \frac{1}{2} \left({}_0^t u_{i,j} + {}_0^t u_{j,i} - {}_0^t u_{k,i} * {}_0^t u_{k,j} \right) \quad /2.12/$$

The Almansi strain and Cauchy stress tensors are sometimes preferred to the Green-Lagrange and 2nd Piola-Kirchhoff tensors when a material model defined in engineering stresses and strains is used and the analysis is defined in the UL formulation.

2.4 The principle of virtual displacements applied to Total and Updated Lagrangian formulations.

The objective of this section is to present how the principle of virtual displacement can be applied to the analysis of a structure. For completeness both the Lagrangian Total and

Updated formulations will be discussed. In all derivations it is assumed that the response of the structure up to time t is known. Now at time $t + \Delta t$ we apply a load increment and using the principle of virtual displacement we can define the response of the structure during that time. Hence we are interested in a so-called incremental solution.

From virtual work of the structure we can write:

for Total formulation:

$${}^0_V \int \left\{ {}^{t+dt} S_{ij} * \delta ({}^{t+dt} \epsilon_{ij}) \right\} dV = {}^{t+dt} R_0 \quad /2.13/$$

for Updated formulation:

$${}^t_V \int \left\{ {}^{t+dt} S_{ij} * \delta ({}^{t+dt} \epsilon_{ij}) \right\} dV = {}^{t+dt} R_t \quad /2.14/$$

where 0_V , t_V denotes the structure volume corresponding to time 0 and t and ${}^{t+dt} R$ is the total virtual work of the external forces. The symbol δ denotes the variation of the following entity.

Since energy must be invariant with respect to the reference coordinate system, /2.13/ and /2.14/ must lead to identical results. After substitution we get:

a/ Lagrange total formulation.

From /2.1/ and /2.7/,

$${}^{t+dt} S_{ij} = \frac{{}^0 \rho}{{}^{t+dt} \rho} * {}^{t+dt} X_{i,m} * {}^{t+dt} \tau_{mn} * {}^{t+dt} X_{j,n}$$

/2.15/

$$\delta \left(\begin{matrix} t+dt \\ 0 \end{matrix} \varepsilon_{ij} \right) = \delta \left(\frac{1}{2} \left(\begin{matrix} t+dt \\ 0 \end{matrix} u_{i,j} + \begin{matrix} t+dt \\ 0 \end{matrix} u_{j,i} + \right. \right. \\ \left. \left. + \begin{matrix} t+dt \\ 0 \end{matrix} u_{k,i} * \begin{matrix} t+dt \\ 0 \end{matrix} u_{k,j} \right) \right) \quad /2.16/$$

In incremental form:

$$\begin{matrix} t+dt \\ 0 \end{matrix} S_{ij} = \begin{matrix} t \\ 0 \end{matrix} S_{ij} + \begin{matrix} S \\ 0 \end{matrix} S_{ij} \quad /2.17/$$

$$\begin{matrix} t+dt \\ 0 \end{matrix} \varepsilon_{ij} = \begin{matrix} t \\ 0 \end{matrix} \varepsilon_{ij} + \begin{matrix} e \\ 0 \end{matrix} e_{ij} + \begin{matrix} \eta \\ 0 \end{matrix} \eta_{ij} \quad /2.18/$$

where

$$\begin{matrix} e \\ 0 \end{matrix} e_{ij} = \frac{1}{2} \left(\begin{matrix} u \\ 0 \end{matrix} u_{i,j} + \begin{matrix} u \\ 0 \end{matrix} u_{j,i} + \begin{matrix} u \\ 0 \end{matrix} u_{k,i} * \begin{matrix} u \\ 0 \end{matrix} u_{k,j} + \begin{matrix} u \\ 0 \end{matrix} u_{k,j} * \begin{matrix} u \\ 0 \end{matrix} u_{k,i} \right) \quad /2.19/ \\ = \text{the linear part of strain increment}$$

$$\begin{matrix} \eta \\ 0 \end{matrix} \eta_{ij} = \frac{1}{2} \begin{matrix} u \\ 0 \end{matrix} u_{k,i} * \begin{matrix} u \\ 0 \end{matrix} u_{k,j} \quad /2.20/ \\ = \text{the nonlinear part of strain increment}$$

$$\begin{matrix} t+dt \\ 0 \end{matrix} u_{i,j} = \begin{matrix} t \\ 0 \end{matrix} u_{i,j} + \begin{matrix} u \\ 0 \end{matrix} u_{i,j} \quad /2.21/$$

$$\delta \left(\begin{matrix} t+dt \\ 0 \end{matrix} \varepsilon_{ij} \right) = \delta \left(\begin{matrix} e \\ 0 \end{matrix} e_{ij} \right) + \delta \left(\begin{matrix} \eta \\ 0 \end{matrix} \eta_{ij} \right),$$

$$\delta \left(\begin{matrix} t \\ 0 \end{matrix} \varepsilon_{ij} \right) = 0$$

Substituting /2.16/ through /2.21/ in /2.13/ we get:

$$\begin{aligned} \int_0^V \left(\begin{matrix} t+dt \\ 0 \end{matrix} S_{ij} * \delta \left(\begin{matrix} t+dt \\ 0 \end{matrix} \varepsilon_{ij} \right) \right) dV &= \int_0^V \left(\begin{matrix} t \\ 0 \end{matrix} S_{ij} + \begin{matrix} S \\ 0 \end{matrix} S_{ij} \right) * \\ &* \delta \left(\begin{matrix} e \\ 0 \end{matrix} e_{ij} + \begin{matrix} \eta \\ 0 \end{matrix} \eta_{ij} \right) dV = \\ \int_0^V \begin{matrix} t \\ 0 \end{matrix} S_{ij} * \delta \left(\begin{matrix} e \\ 0 \end{matrix} e_{ij} \right) dV &+ \quad (\text{this is always zero}) \\ + \int_0^V \begin{matrix} t \\ 0 \end{matrix} S_{ij} * \delta \left(\begin{matrix} \eta \\ 0 \end{matrix} \eta_{ij} \right) dV &+ \end{aligned}$$

$$\begin{aligned}
& + \int_{0V} {}^t S_{ij} * \delta({}_0 \eta_{ij}) dV + \\
& + \int_{0V} {}_0 S_{ij} * \delta({}_0^t \varepsilon_{ij}) dV + \quad \text{(this is also zero)} \\
& + \int_{0V} {}_0 S_{ij} * \delta(e_{ij}) dV + \\
& + \int_{0V} {}_0 S_{ij} * \delta({}_0 \eta_{ij}) dV \quad /2.22/
\end{aligned}$$

Introducing the constitutive relation:

$${}_0 S_{ij} = {}_0 C_{ijrs} * (e_{rs} + {}_0 \eta_{rs}) \quad /2.23/$$

$$\begin{aligned}
& \int_{0V} \left\{ {}_0 C_{ijrs} (e_{rs} + {}_0 \eta_{rs}) * \delta({}_0 e_{ij} + {}_0 \eta_{ij}) + \right. \\
& \quad \left. + {}_0^t S_{ij} * \delta({}_0 \eta_{ij}) \right\} dV = {}^{t+dt} R - \\
& - \int_{0V} {}^t S_{ij} * \delta({}_0 e_{ij}) dV \quad /2.24/
\end{aligned}$$

Now assuming linearization of the strain increment in the first term of /2.24/ we obtain the final form of the governing equations:

$$\begin{aligned}
& {}_0 e_{rs} + {}_0 \eta_{rs} \longrightarrow {}_0 e_{rs} \\
& \int_{0V} {}_0 C_{ijrs} {}_0 e_{rs} * \delta({}_0 e_{ij}) dV + \int_{0V} {}^t S_{ij} * \delta({}_0 \eta_{ij}) dV \\
& = {}^{t+dt} R - \int_{0V} {}^t S_{ij} * \delta({}_0 e_{ij}) dV \quad /2.25/
\end{aligned}$$

b/ Lagrangian Updated formulation:

For the deformed configuration, the derivation of the equi-

valent expression to /2.25/ is similar. The only differences are that the index for the reference configuration is changed from 0 to t and some terms of /2.19/ can be omitted.

From /2.1/ and /2.7/:

$${}^{t+dt}S_{ij} = \frac{{}^t\rho}{{}^{t+dt}\rho} * {}^{t+dt}X_{i,m} * {}^{t+dt}\tau_{mn} * {}^{t+dt}X_{j,n} \quad /2.26/$$

$$\delta \left({}^{t+dt}\varepsilon_{ij} \right) = \delta \left(\frac{1}{2} ({}^t u_{i,j} + {}^t u_{j,i} + {}^t u_{k,i} * {}^t u_{k,j}) \right) \quad /2.27/$$

In incremental form:

$${}^{t+dt}S_{ij} = {}^t\tau_{ij} + {}^tS_{ij} \quad /2.28/$$

$${}^{t+dt}\varepsilon_{ij} = {}^t\varepsilon_{ij} + {}^te_{ij} + {}^t\eta_{ij} \quad /2.29/$$

where

$${}^t\varepsilon_{ij} = 0$$

$${}^te_{ij} = \frac{1}{2} ({}^t u_{i,j} + {}^t u_{j,i}) \quad /2.30/$$

= the linear part of strain increment

$${}^t\eta_{ij} = \frac{1}{2} {}^t u_{k,i} * {}^t u_{k,j} \quad /2.31/$$

= the nonlinear part of strain increment

$${}^tS_{ij} = {}^tC_{ijrs} * ({}^te_{rs} + {}^t\eta_{rs}) \quad /2.32/$$

Similarly to the Total formulation:

$$\begin{aligned}
& \int_{tV} \left\{ C_{ijrs} \left(e_{rs} + \eta_{rs} \right) * \delta \left(e_{ij} + \eta_{ij} \right) + \right. \\
& \quad \left. + \tau_{ij} * \delta \left(\eta_{ij} \right) \right\} dV = {}^{t+dt}_t R - \\
& \quad - \int_{tV} \tau_{ij} * \delta \left(e_{ij} \right) dV \quad /2.33/
\end{aligned}$$

After linearization, $e_{rs} + \eta_{rs} \longrightarrow e_{rs}$ and the final equation takes the form:

$$\begin{aligned}
& \int_{tV} C_{ijrs} e_{rs} * \delta \left(e_{ij} \right) dV + \int \tau_{ij} * \delta \left(\eta_{ij} \right) dV = \\
& = {}^{t+dt}_t R - \int_{tV} \tau_{ij} * \delta \left(e_{ij} \right) dV \quad /2.34/
\end{aligned}$$

The work done by the external forces:

So far only the incremental virtual work has been considered. This work is balanced by the work done by the external forces, expressions for which are now briefly summarized. Their derivation is similar to that obtained using linear mechanics; moreover the differences between the Total and Updated formulations are negligible. Therefore only the final expression for the Total variant is presented:

$$\begin{aligned}
{}^{t+dt}_0 R &= \int_{0V} {}^{t+dt}_0 f b_1 * \delta \left({}_0 u_1 \right) dV + \\
&+ \int_{0S} {}^{t+dt}_0 f s_1 * \delta \left({}_0 u_1 \right) dS + \\
&+ \int_{0V} {}^0 \rho * \frac{\partial^2 {}^{t+dt}_0 u_1}{\partial t^2} * \delta \left({}_0 u_1 \right) dV \quad /2.35/
\end{aligned}$$

where $f s_1$, $f b_1$ are surface and body forces, ${}^0 S$ denotes integration with respect to the surface with the prescribed boundary forces and the last term of /2.35/ accounts for inertia forces (applicable for dynamic problems only).

Thus all the relationships for incremental analysis have now been presented. It should be noted that the assumption of linearization in /2.24/ and /2.33/ leading to /2.25/ or /2.34/ means that the structure must be solved in an iterative manner. In practice after every iteration (either at the same time or after a time increment) we must compare the resulting external and internal forces and if the differences are unacceptably high, another iteration is necessary to dissipate the difference. The applied forces (i.e. the R.H.S of /2.34/ or /2.25/) become these unbalanced forces.

The solution equations were presented in the compact analytical form but for practical examples (structures) it is now necessary to discretize them (both in space and time). Apart from the loading condition however, this depends on the elements being used to model the structure.

Two special groups of elements will be discussed later. Chapter Four deals with plane stress, plane strain and axisymmetric elements whilst Chapter Five is concerned with shell elements. The discretization procedure for many other elements are available in the literature (e.g. [1]).

3. CONSTITUTIVE EQUATIONS.

This chapter is concerned with the constitutive equations for reinforced concrete structures. The first part deals with experimental evidence about concrete behavior. The second part first introduces some basic mechanical entities (e.g. what it is deviatoric or π plane, definition of stress and strain invariants etc.) and thereafter, attention is focused on numerical modeling of concrete behavior. It includes failure criteria and constitutive equations, (both linear and nonlinear). Finally the material models used in programs CONCRETE and NONSAP are discussed.

Nowadays many different expressions for modeling the behavior of concrete and reinforced concrete exist. Despite this, there is still a lack of generally applicable models. This situation is caused by the fact that all practical material models deal with concrete from a macroscopic point of view. The material models are created either by data fitting from which general relationships between stress and strain are obtained or some purely mathematical model is extended which often has nothing in common with the real material.

Unfortunately these alternatives can not be used in all situations. Usually they work satisfactory provided that the structure is analyzed in material conditions similar to those during the experiment. Over the years many models have been postulated which are applicable for special circumstances but under other conditions give poor performance.

Recently there has been increasing interest in the study of concrete at microscopic level but practical usable results have not yet been provided.

In the following, each model will be accompanied by a description of conditions for which it is applicable. Some of the models will be given in total form, some in incremental form but it should be noted that both CONCRETE and NONSAP work in incremental form only. The only exception to this strategy is in the program CONCRETE in the tension-tension zone for concrete in

order to simplify the formulation of tension stiffening relations.

3.1 Experimental evidence about concrete behavior.

Concrete has been used as a building material for many years and therefore an enormous number of different experimental tests have been done to study its behavior. To date uniaxial stress-strain behavior is well documented and many results have also been collected for two dimensional loading situations. One of the most widely used studies are the results published by Kupfer et. al. [40] which nearly covers the complete range of possible 2D loading conditions. In the case of three dimensional loading the situation is much worse and to the author's knowledge work similar to [40] is still lacking. Of course this lack of experimental data is caused by the large amount of different types of 3D loading possibilities as well as the demand on laboratory equipment.

An especially neglected area is experiments dealing with long-term loading. Usually available data are based on measurements done on some important real structure and hence are applicable only for special types of loading, structural shape and type of concrete. This problem will be discussed in more detail in Chapter 6 which considers time-dependent phenomena for concrete, i.e. shrinkage and creep.

Concrete is a composite material of coarse aggregate and mortar which comprises a mixture of small aggregate particles, cement paste and water. Its physical behavior is very complex and depends on the structure of the composite material. The most important properties are water-cement ratio, ratio of cement to aggregate, aggregate properties etc. Concrete is a brittle material with tensile strength about one tenth of its compressive strength. This complicates all models for constitutive equations. Its stress-strain behavior is affected mainly by micro- and macrocracks which are located mostly at the interface between coarse aggregate and mortar. Many microcracks occur in concrete before

loading. They are caused by shrinkage, thermal expansion of cement paste, segregation etc. After loading the progression of these cracks and the creation of new ones is mainly responsible for nonlinear stress-strain behavior.

A typical stress-strain curve in uniaxial compression test is shown in Figure 3.1. There are three basic stages in this diagram. In the first stage for stress up to about 30% of maximum compressive stress f'_c , the stress-strain relationship is nearly linear. The stress $0.3f'_c$ is called the limit of elasticity. Further on, up to about 75% of f'_c , concrete exhibits nonlinear behavior. However the crack propagation at this second stage is still stable. In the third stage, up to failure, unstable fracture propagation is the main characteristic. It is primarily caused by cracks through the mortar. These cracks join bond cracks at the surface of nearby aggregates and form crack zones. After this further deformations localize and finally major cracks parallel to the direction of applied load cause failure of specimen.

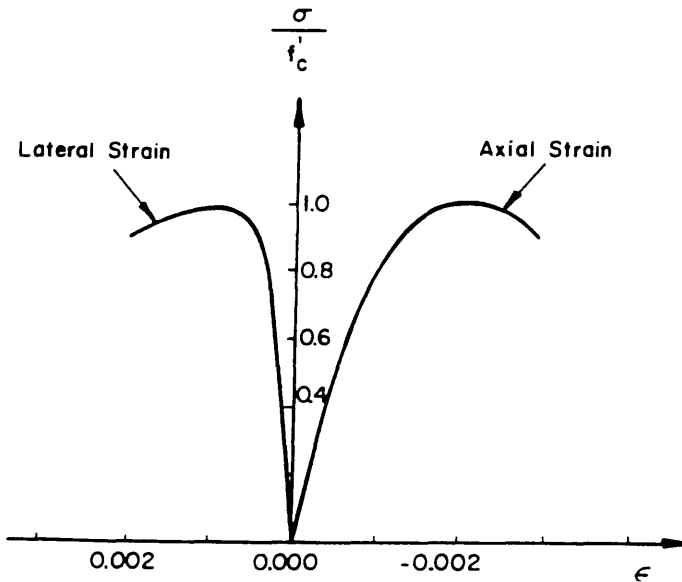


Fig. 3.1 Typical uniaxial compressive stress-strain diagram [40].

Uniaxial tension stress-strain tests show that limit of elasticity is in this case about 65-80% of the ultimate tensile strength f'_t . The regime of stable crack propagation is much shorter.

ter and the unstable crack propagation starts very soon. That is why concrete is quite brittle in nature. The typical stress-strain curve of concrete specimen subject to uniaxial tension is depicted in Figure 3.2.

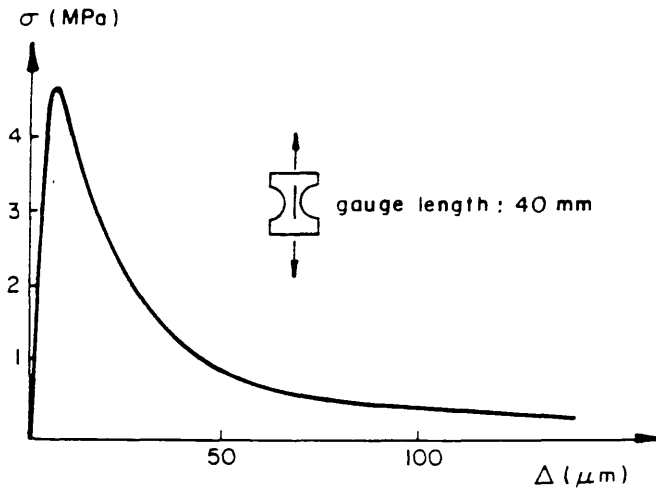


Fig. 3.2 Uniaxial tensile stress-elongation curve [62].

A very important property of concrete is strain softening. This is applicable for compression as well as for tension regimes. Figure 3.3 shows typical uniaxial compressive stress-strain curves obtained from strain controlled tests.

It is still debated whether the softening branch of the curves reflects material property or it represents rather the response of the structure formed by the specimen together with its complete loading system (van Mier, 1984). The latter hypothesis is supported in Figure 3.4 which presents post-peak uniaxial compression stress-strain curves for cylindrical specimens of different height (van Mier, 1984). The observed curves significantly differ. However if we plot the stresses against elongations (displacements) rather than strains, the three curves exhibit nearly identical pattern.

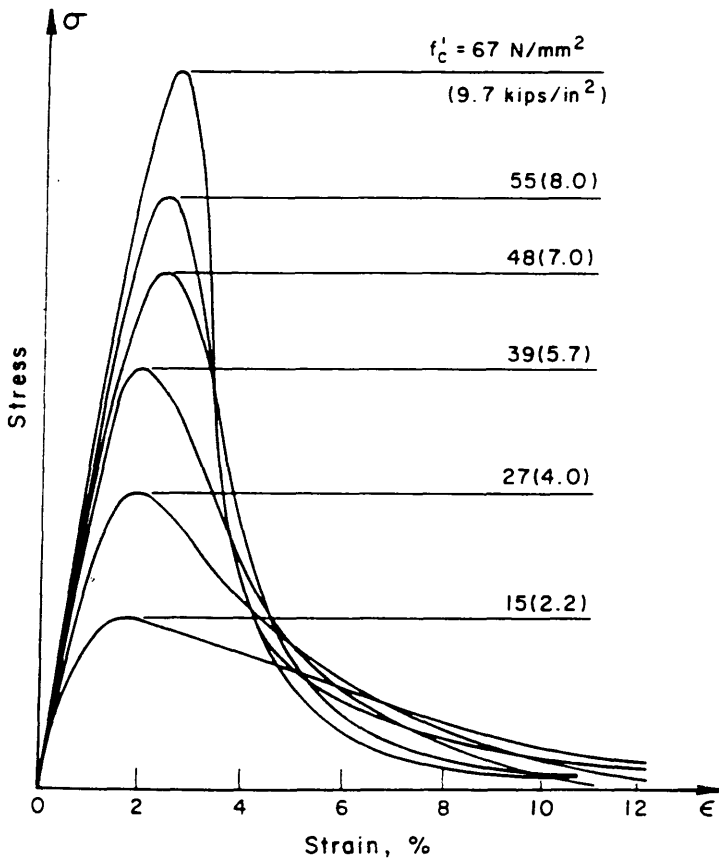


Fig. 3.3 Uniaxial compressive stress-strain curves for concrete [64].

Even after creation of major cracks concrete still contributes to the total strength of reinforced concrete elements. A reason of this, for example, is the bond between reinforcement and concrete macro-particles which yet has not cracked or crushed. This phenomenon is called tension stiffening. In practice it is very difficult to distinguish between strain softening and stiffening and therefore the constitutive equations usually simulate them both together.

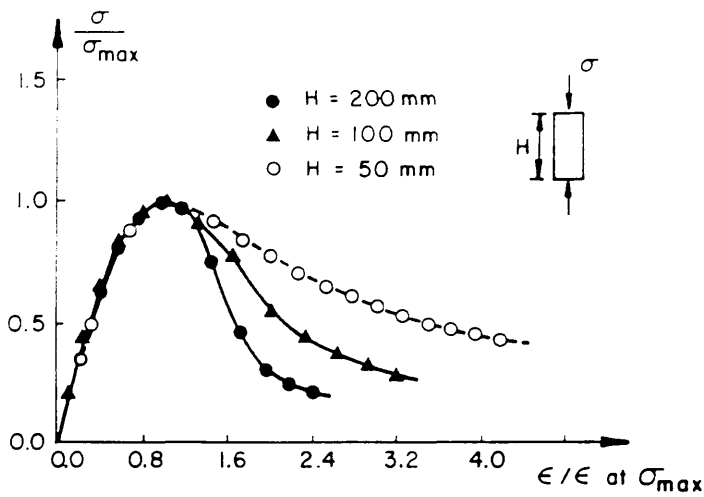


Fig. 3.4 Influence of specimen height on uniaxial stress-strain curve [65].

Typical stress-strain diagrams for multiaxial compressive loading of cylindrical specimens are shown in Figure 3.5 [61].

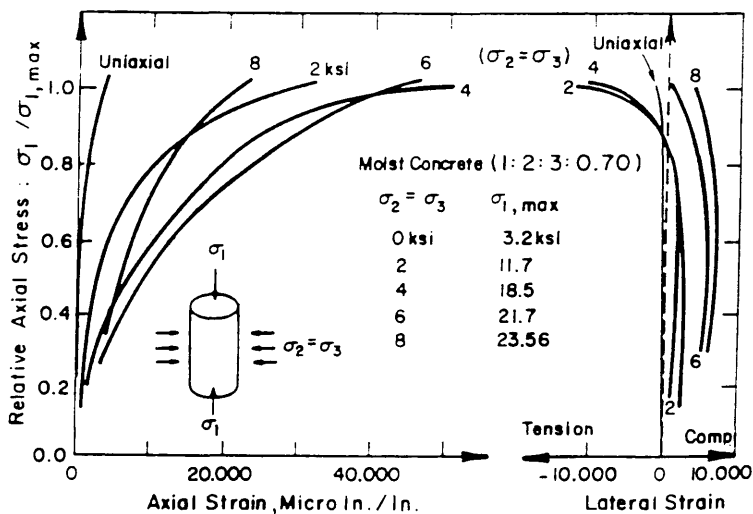


Fig. 3.5 Stress-strain curves under multiaxial compression (stress, strain positive in compression).

It is now well known that concrete behavior in one direction is significantly influenced by stress conditions in the other directions. The lateral confining and axial strains at failure increase with increasing confining stress, however beyond some threshold the further increasing of lateral stresses will decrease the values of axial strains at failure. This property is obvious from Figure 3.6 where volumetric strain is plotted against the stress in biaxial compression tests.

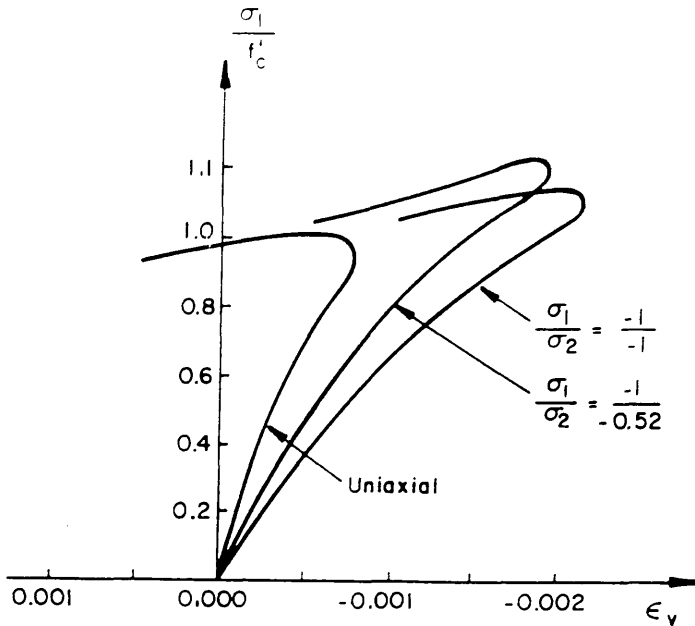


Fig. 3.6 Volumetric strain under biaxial compression [40].

It can be seen that under compressive loading with confining pressure concrete exhibits a certain degree of ductility before failure. In a two dimensional equal compression-compression stress-state the concrete strength increases approximately by 20% compared to the uniaxial strength f'_c . The Poisson's ratio is about 0.18 for nearly all types of concretes, The higher is compression strength the lower value of Poisson's ratio. Its value is stable until about 75 % of peak loading. Thereafter it increases to 0.5 near to the failure stage, (i.e. incompressible state).

A typical uniaxial working diagram of concrete subject to cyclic loading is depicted in Figure 3.7.

The increasing number of cycles gradually degrades the material stiffness. This property is well simulated by plastic-fracturing material models.

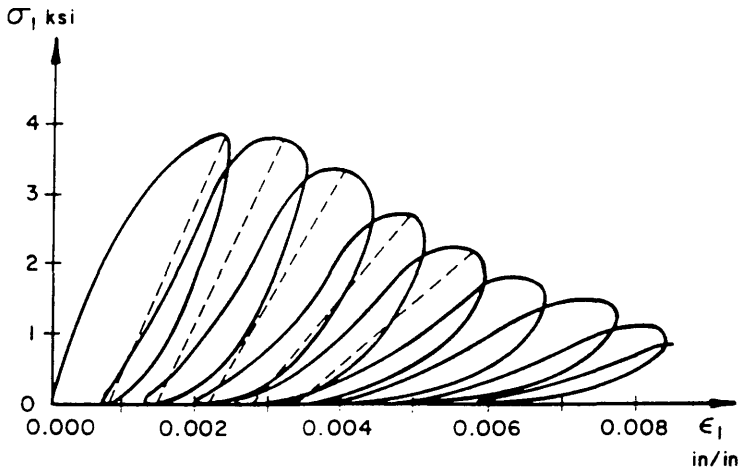


Fig. 3.7 Cyclic uniaxial compressive stress-strain curve [63].

More information about the experimental behavior of concrete is provided in ref. [2] which gives an overview of the experimental results. Other information is also presented in ref. [41], particularly for plate bending conditions.

3.2 Basic entities.

The stress state at a particular point can be expressed with respect to many coordinate systems. For the purposes of constitutive equations the most commonly used are Cauchy stresses (i.e. real stresses) in a coordinate system which is defined by the directions of the principal stresses at this point.

The essential feature of this coordinate system is that volumetric strain axis can be defined ($\sigma_1 = \sigma_2 = \sigma_3$), perpendicular to which are octahedral planes. See Fig. 3.8. The deviatoric plane is a special case of the octahedral plane lying in the first quadrant of principal stress space.

The π plane is a deviatoric plane which satisfies the equation $\sum \sigma_{11} = 0$, that is the plane in which the hydrostatic part of stress equals zero.

The following notation will be used:

$[\sigma_1; \sigma_2; \sigma_3]$ - coordinate system created by the principal stress vector at a particular point,

$[I_1; I_2; I_3]$ - 1st, 2nd and 3rd invariants of the Cauchy stress tensor,

$[J_1; J_2; J_3]$ - 1st, 2nd and 3rd invariants of the deviatoric Cauchy stress tensor,

where

$$I_1 = \sigma_{ii} = \sigma_1 + \sigma_2 + \sigma_3$$

$$I_2 = \frac{1}{2} * (I_1^2 - \sigma_{ij} * \sigma_{ij}) = \sigma_1 * \sigma_2 + \sigma_1 * \sigma_3 + \sigma_3 * \sigma_2$$

$$I_3 = \frac{1}{3} * \sigma_{ij} * \sigma_{ik} * \sigma_{jk} = \sigma_1 * \sigma_2 * \sigma_3 \quad /3.1/$$

$$\sigma_{oct} = \frac{1}{3} * \sigma_{ii} = \frac{1}{3} * I_1 = \sigma_m$$

$$s_{ij} = \sigma_{ij} - \sigma_m * \delta_{ij}$$

$$\tau_{oct} = \sqrt{\frac{2}{3} * J_2}$$

$$\tau_m = \sqrt{\frac{2}{5} * J_2}$$

and where:

σ_{ij} is an element of the Cauchy stress tensor,

s_{ij} is an element of the deviatoric Cauchy stress tensor,

σ_{oct} and τ_{oct} are the normal and shear components of stress in the deviatoric plane,

σ_m and τ_m are the normal and shear components of stress acting on an infinitesimal sphere of the body.

Deviatoric stress invariants are computed by replacing σ_{ij} by s_{ij} . We can also define strain invariants I'_1, I'_2 and I'_3 and deviatoric strain invariants J'_1, J'_2 and J'_3 by replacing the elements of the stress tensor by terms of the strain tensor.

The stress state at a material point can also be described by using ξ, χ and Θ coordinates. The ξ coordinate represents the volumetric part of the stress (the direction coincides with the normal to the π plane), χ is deviatoric part of the stress (acting in the π plane) and Θ defines the angle of shear in the π plane, measured from the projection of the σ_1 coordinate axis onto the π plane to the vector χ . Anti-clockwise rotation is defined as positive (see Fig. 3.8).

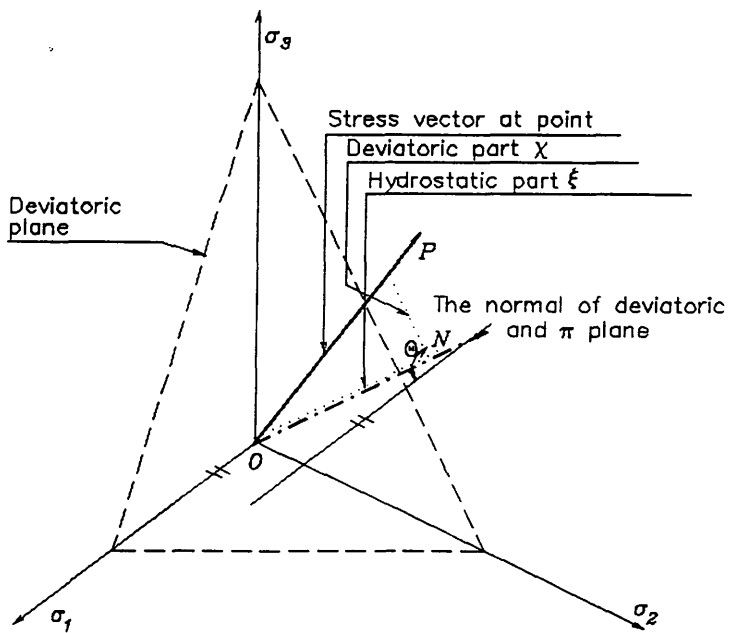


Fig. 3.8 Stress state at point P in principal stress coordinate system.

The principal stresses are ordered according to:

$$\sigma_1 > \sigma_2 > \sigma_3 \quad /3.2/$$

and the following relationships exist for ξ , χ and Θ :

$$\xi = \sqrt{(3)} * \sigma_m = \sqrt{(3)} * \sigma_{oct}$$

$$\chi = \tau\sqrt{(5)} * \tau_m = \sqrt{(3)} * \tau_{oct}$$

$$\cos(3*\Theta) = \frac{3\sqrt{(3)}}{2} * \frac{J_3}{J_2^{(3/2)}} \quad 0 < \Theta < \pi/3 \quad /3.3/$$

In addition the following relationships also exist:

$$\begin{bmatrix} \sigma_1 \\ \sigma_2 \\ \sigma_3 \end{bmatrix} = \begin{bmatrix} \sigma_{oct} \\ \sigma_{oct} \\ \sigma_{oct} \end{bmatrix} + \frac{2\sqrt{(J_2)}}{\sqrt{(3)}} * \begin{bmatrix} \cos(\Theta) \\ \cos(\Theta - \frac{2}{3}\pi) \\ \cos(\Theta + \pi * \frac{2}{3}) \end{bmatrix}$$

$$0 < \Theta < \frac{\pi}{3}; \quad \sigma_1 > \sigma_2 > \sigma_3 \quad /3.4/$$

The strain level at a point in a structure is described by a strain tensor ϵ_{ij} , or the volumetric strain e_v and deviatoric strain tensor e_{ij} , defined by

$$e_{ij} = \epsilon_{ij} - \frac{1}{3} * \epsilon_v * \delta_{ij} \quad /3.5/$$

where $\epsilon_v = \epsilon_{11} = I'_1$.

3.3 Failure criteria for concrete.

3.3.1 Overview of failure criteria.

Failure criteria are of central importance in modeling constitutive equations. Usually they distinguish a pre-failure material state from a material in the fatal state. Many failure criteria have been postulated, most being derived from experimental results.

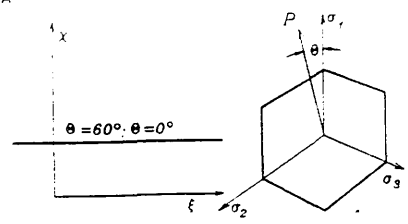
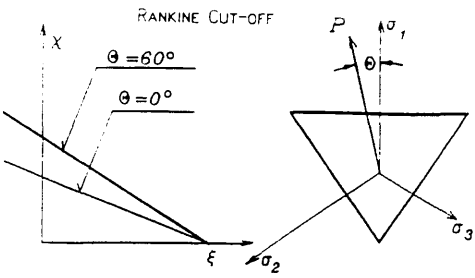
The following general characteristics have been identified for concrete near failure

- in pure hydrostatic compression, failure cannot happen,
- the curve describing material failure is directly related to the level of hydrostatic stress ξ (I_1). The higher the compression the higher the allowable χ ,
- the shape of failure envelopes in deviatoric planes is nearly circular under high hydrostatic compression and more triangular under low hydrostatic compression or hydrostatic tension,
- the tension-compression strength ratio (the ratio of the tension-compression meridian) is always less than one, i.e. $\frac{\chi_t}{\chi_c} < 1$, (the compression and tension meridians correspond to $\Theta = 60^\circ$, and $\Theta = 0^\circ$ respectively),
- for the π plane, ($\Sigma \sigma_{ii} = 0$), the above ratio $\frac{\chi_t}{\chi_c}$ is approximately 0.5 whilst for nearly hydrostatic compression it is close to 0.8,
- the envelope on the deviatoric plane and the meridian failure envelope are smooth and convex.

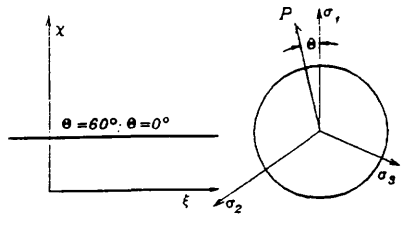
Some of the most commonly used failure models will be briefly discussed. They will be presented according to the number of variables defining the criterion. More information can be found in refs. [2] and [60]. Their meridians and cross sections near failure are shown in Fig. 3.9. Finally failure models used in the present work will be presented in more detail.

ONE PARAMETER CRITERIA

TRESCA

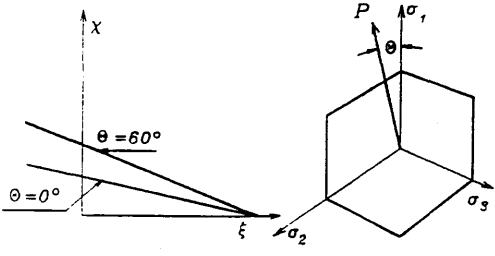


VON MISES

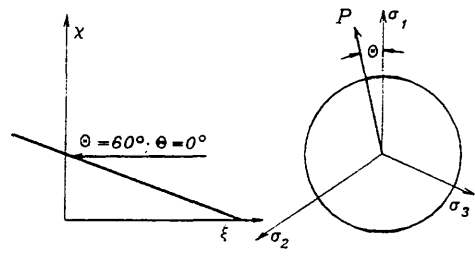


TWO PARAMETERS CRITERIA

MOHR - COULOMB

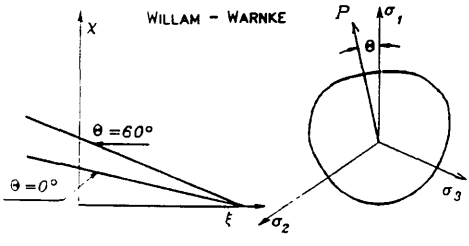


DRUCKER - PRAGER

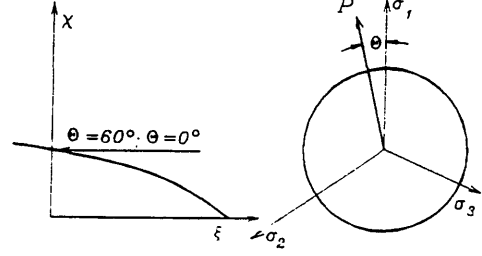


THREE PARAMETERS CRITERIA

WILLAM - WARNKE

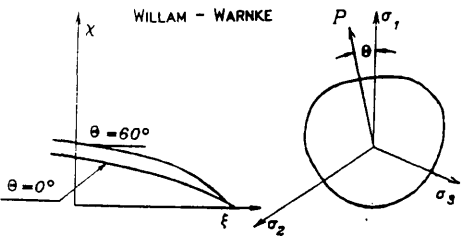


BRESLER - PISTER



FIVE PARAMETERS CRITERION

WILLAM - WARNKE



FOUR PARAMETERS CRITERION

HSIEH

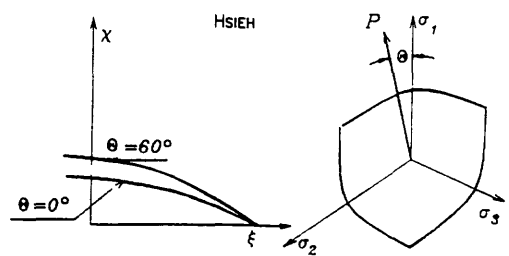


Fig. 3.9 Deviatoric and meridian cross sections of failure criteria discussed in Sec. 3.3.

One parameter models.

This group of failure criteria represents the most simple models and provide only a coarse approximation to real behavior. The failure stage of the material is characterized by one material parameter which is readily identified.

The Cut-off criterion [2] is the most widely used stress-based criterion and was first published by Rankine in 1876. Failure occurs if any principal stress exceeds the fixed value defined for maximum normal stress. This value is quite independent of the stress condition in the material prior to failure. It is often used as an additional criterion to other failure criteria, and is most often employed for tension zones in concrete where it has provided satisfactory accuracy.

It was found that failure in concrete, especially in compressive zones, is more sensitive to the value of mean shear than principal stresses. This is the main idea of the shear-based Tresca failure criterion. In this, failure occurs if the mean shear in concrete is higher than the maximum allowable shear.

This criterion fits experimental data much better than the Rankine Cut-off criterion, but unfortunately it is not smooth. This can cause problems during numerical iterative solutions. An alternative is the Von Mises failure criterion where the maximum mean shear is replaced by the maximum octahedral shear, leading to a smooth failure surface.

The Tresca and Von Mises failure criteria are most suitable for concrete under stress conditions close to hydrostatic pressure. In particular the Von Mises criterion in combination with the Rankine Cut-off (for tension) provides reasonable results.

Two parameter models.

Experimentally obtained stress-strain curves show that the peak stress value in concrete is directly dependent on the value

of hydrostatic stress. Hence it is advantageous to use a variable failure threshold which depends on the hydrostatic stress. This is the basic idea of two parameter models such as Mohr-Coulomb and Drucker-Prager models.

Two parameters failure criteria use variable cross-sections of the failure surface. However there is affinity between them which is contrary to experimental evidence. Despite this inaccuracy both criteria are often used (Mohr-Coulomb for concrete and Drucker-Prager for rocks).

MOHR-COULOMB failure criterion:

According to Mohr-Coulomb, failure occurs if the shear stress exceeds a value which is a linear function of normal stresses σ . The Tresca criterion is a special case of this. The failure surface in deviatoric plane is hexahedral in shape.

Used in combination with the Rankine Cut-off criterion the three parameter Cowan criterion [2] is obtained, (originally published in 1953). This criterion has been satisfactorily used in practice, and is also used in program NONSAP. It will be discussed in more detail later.

DRUCKER - PRAGER failure criterion:

This criterion is an extension of the Von Mises criterion. The failure surface in the deviatoric plane has ^{the} shape of ^a cone. Setting the constant corresponding to hydrostatic compression equal to zero leads to the Von Mises criterion.

Three parameter models.

There are two basic inaccuracies associated with two parameters models. The first is the affinity of cross sections with respect to volumetric compression and the other is the linear relationship between volumetric stress and volume of failure envelopes in deviatoric planes. This should be parabolic at least.

This group of failure models is capable of avoiding one of

these drawbacks, whilst the other remains. Hence they can be divided into two basic groups:

Group a:

A parabolic relationship defines the meridian whilst there is affinity between cross sections which remain always circular. The BRESLER-PISTER criterion (1958) [2] is an example of failure criteria of this group. For low value of ξ it provides results close to those using the Rankine Cut-off criterion.

Group b:

The relationship between volumetric stress and the meridian value remains linear but deviatoric-cross sections are no longer circular, their shape being a function of the angle of similarity. The WILLAM - WARNKE criterion [2], [60] is probably the most widely used criterion of this type. Its failure surface is smooth and convex. It creates a base for the five parameter WILLAM-WARNKE criterion [2] (discussed later). Accurate results have been obtained with this criterion.

Nowadays there are many other criteria of this type available, for example ARGYRIS (1974), [2]. More information is provided in refs. [2] and [60].

Four parameter failure criteria.

Using one more material parameter, it is possible to establish more accurate models for failure prediction. However increasing the number of material constants also increases the numerical labour and, more seriously, it becomes more difficult to obtain the relevant material constants used by the model. Hence sometimes the benefit from using better failure criterion is a priori neutralized by using inaccurate input data for the material constants.

An example is the OTTOSEN failure criterion (1974), [2]. This criterion is suitable for any stress combination in concrete.

te, its meridian sections are parabolic and cross-sections change their shape from nearly circular to triangular depending on the value of volumetric stress. With a parameter setting of constant the criterion degrades to the Von Mises criterion.

Another example is the HSIEH failure criterion [2] which satisfies all convexity requirements. However the deviatoric cross sections are not smooth.

Five parameters failure criteria.

An example of five parameters failure criteria is the five parameters WILLAM-WARNKE failure criterion [2]. This is direct extension of the three parameter Willam - Warnke criterion which has been already mentioned. All experimentally established properties of the failure surface are satisfied (smoothness, convexity etc.).

The only drawback is that the convexity requirements leads to failure when only hydrostatic compression is present, which contradicts experimental evidence.

Failure criteria based on fracture mechanics.

The other possible approach to the problem of concrete failure can be based on fracture mechanics. Nowadays a massive literature on this topic is available, for example works of Bazant and Tsubaski [8]. The main concept is that occurrence of failure depends not only on the stress state at one distinct point but also on its surrounding area. Energy criteria then determine whether a crack will propagate into the surrounding area. The result is that these models also observe areas close to their position and predicted results are usually more accurate. Unfortunately their use is also more complicated.

We will not discuss these models here in more detail since it involves the concept of damage theory, which is outside the

scope of this work. Further details can be found in [60] and the work of Dougill (1975,1976) and others.

3.3.2 Mohr-Coulomb failure criterion combined with Rankine Cut-off used in program NONSAP.

The failure criterion defined by a combination of the Mohr-Coulomb and Rankine Cut-off criteria represents one of the most popular failure surfaces for two dimensional problems. The given accuracy is usually satisfactory and the criterion is at the same time simple to use. For compression-compression and compression-tension zones the Mohr-Coulomb criterion is used. For the tension-tension zone, Mohr-Coulomb usually overestimates the material strength and thus the Rankine Cut-off criterion is used instead to define the ultimate tension in concrete.

The ultimate quantity defining failure is mean shear stress and this will now be discussed in more detail for 2D condition. Mathematically the failure is expressed by:

$$\sigma_1 \frac{1 + \sin\phi}{2C \cos\phi} - \sigma_2 \frac{1 - \sin\phi}{2C \cos\phi} = 1 \quad /3.06/$$

where $\sigma_1 > \sigma_2$ are principal stresses and ϕ , C are two material constants, the angle of internal friction and the material cohesion. The derivation of /3.06/ is straightforward using Mohr circles.

The material constants ϕ and C can be identified from uniaxial strength in compression f'_c and tension f'_t , (or alternatively in shear f'_s). Substituting $\sigma_2 = -f'_c$ and $\sigma_1 = 0$ into /3.06/ leads to one equation. Similarly $\sigma_1 = f'_t$, (or $\sigma_1 = f'_s$) and $\sigma_2 = 0$ leads to a second equation. The solution of the required material constants from those equations is then straightforward.

A third material constant is necessary to define the peak value for tension for Rankine Cut-off criterion, usually the tensile strength f'_t in the form:

$$\max(\sigma_1; \sigma_2) = f'_t \quad /3.07/$$

3.3.3 Failure criterion used in program CONCRETE.

The program CONCRETE uses an elastic-plastic material model for the constitutive equation, in which both compression hardening and tension stiffening are included. It implies that the material state is primarily defined by a plasticity Yield function or a subsequent loading surface. These will be presented later in the section concerned with constitutive equation modeling. Similar to the model used in NONSAP, the main failure criterion here is also combined with the Rankine Cut-off for the tension-tension zone.

The function defining the loading surface after the beginning of plasticity in a material must also be limited. Theoretically it is possible to design expressions for loading functions so that they are applicable until the material is completely destroyed, however in practice this is very difficult to achieve and is not very useful. Due to serviceability and additional reasons, it is satisfactory to define loading functions for a limited stress or strain range, so that if damage in the material exceeds some ultimate level, the total loss of both rigidity and stress in the material can be assumed.

There are many possibilities for defining this additional ultimate failure surface. In program CONCRETE an expression very similar to the loading surface is used for the sake of simplicity. The only difference is that stress entities are replaced by strain entities. Its mathematical form is given by:

$$\beta(-3J'_2) + \alpha I'_1 = \epsilon_u^2 \quad /3.08/$$

where ϵ_u is ultimate value of total strain extrapolated from uniaxial test results,

J'_2 is the second deviatoric strain invariant,

I'_1 is the first strain invariant and

α , β are material constants and are the same as defined for the yield function. They are calculated to fit the Kupfer et. al [40] failure surface. These will be discussed when presenting the Yield function in Section 3.5.3.

The expression /3.08/ does not represent the most sophisticated solution, nevertheless it works well for most practical examples. Note that some other authors (e.g. Hinton [42]) use as a J'_2 a negative value defined by /3.1/.

3.3.4 Crushing coefficient.

A natural question is how to define material behavior after material failure has occurred in a particular part of the structure.

The simplest solution is to omit rigidity and stresses in the failure zone, but this is a very coarse approximation. Usually it is necessary to adopt more accurate treatment within failed areas, according to their mode of failure. This is the main idea for introducing a crushing coefficient.

Generally there are two basic modes of concrete failure. The first is the consequence of excessive values of tensile stress, (either due to tension or shear), leading to the creation of cracks. The second is the crushing of concrete in which case the concrete degrades to a material with properties similar to a loose material (e.g. sand).

In the latter case complete loss of material rigidity and internal stress is justified but in the former we have to account

for material stiffness in direction parallel to cracks. This is done by assuming an orthotropic material with nearly zero rigidity perpendicular to the crack but with the original rigidity value parallel to the crack. However if the material is partly destroyed by cracking and partly by crushing, an accurate solution is very difficult. One possibility is to use a linear combination of rigidities corresponding to both failure modes. The coefficients defining this combination are established according to how much each particular mode of failure participated in the failure condition.

The pure crack failure mode can be roughly characterized by:

$$\sigma_1 \geq 0; \sigma_1 > \sigma_2 > \sigma_3 \quad /3.09/$$

or alternatively using stress invariants:

$$\sqrt{J_2} \cos\theta + \frac{1}{2\sqrt{3}} I_1 \geq 0; \quad 0^\circ \leq \theta \leq 60^\circ$$

The simplest way to mathematically characterize crushing failure mode in a material is to assume that all strains corresponding to principal stresses must be negative. Thus:

$$\varepsilon_1 \leq 0 \quad /3.10/$$

Assuming elasticity the substitution of stresses to /3.10/ leads to

$$\sigma_1 - \mu(\sigma_2 + \sigma_3) \leq 0$$

or /3.11/ if stress invariants are used

$$\sqrt{J_2} \cos\theta + \frac{(1 - 2\mu)}{2\sqrt{3} (1 + \mu)} I_1 \leq 0 \quad 0^\circ \leq \theta \leq 60^\circ \quad /3.11/$$

A comparison of /3.09/ and /3.11/ leads directly to the so called crushing coefficient:

$$\alpha = - \frac{I_1}{2\sqrt{3} \sqrt{J_2} \cos\theta} \quad /3.12/$$

If $\alpha \leq 1$ we assume that material failure is due to a pure cracking mode. On the other hand if $\alpha \geq \frac{1 + \mu}{1 - 2\mu}$, pure crushing occurs. For intermediate values of α , a coefficient ν defines the ratios of failure modes such that for cracking $\nu = 1$ and for crushing $\nu = 0$ and intermediate values are linearly interpolated.

After failure it is assumed that the orthotropic material has nearly zero rigidity perpendicular to the crack and ν times the rigidity of the original material for directions parallel to the crack.

This approach is only a first approximation for dealing with multi-mode failure criteria, but based on experience with program NONSAP its use is generally satisfactory.

3.3.5 Failure criteria for steel.

Steel behaves as a isotropic elastic-plastic material and thus a failure criterion can be defined by the ultimate loading surface similar to its Yield function. The situation is further simplified considering that reinforcing bars are only one dimensional elements. This approach is employed in this work.

3.3.6. Interaction of concrete and reinforcing bars in cracks.

Experimental evidence shows that after cracks have been formed concrete continues to contribute to structural rigidity in

a direction perpendicular to the cracks. This is because cracks occur at finite intervals and the surround material between them can still contribute to the structural stiffness, especially if reinforcement is present. Two possible solutions have been suggested for dealing with this phenomena. The first one accounts for a post-cracking concrete contribution by artificially increasing the reinforcing bar rigidity near ϵ_{cr} , the concrete ultimate strain in the uniaxial tension test.

The second approach, (used here), assumes some post cracking residual material rigidity in the concrete. This is usually defined by a tension stiffening rule which will be discussed in Section 3.4.

More information about behavior close to cracks, which is not relevant to this thesis, is summarized in ref. [41]. It should be noted that the bond-slip between the concrete and reinforcing bars is important in some situations, especially in detailed studies. For the sake of simplicity this phenomena are not accounted for in this work.

3.4 Linear elastic constitutive models for concrete accounting for cracking and crushing.

The simplest constitutive equations for any material, including concrete, is their linear modeling by Hooke's law. If in addition, crack occurrence is accounted for, the resulting material model serves as a fair approximation to real material behavior. This model is quite applicable to a large range of structures which fail due to yielding of reinforcement rather than compression collapse of concrete. Hence it is especially applicable for shell or moderately deep bending structures etc. In the case of high volumetric compression levels the results tend to overestimate concrete stiffness because no ductility, (or plasticity), is assumed.

In order to specify crack creation as well as crushing of concrete, the models need to be supplemented by simple failure criteria. In the case of crushing failure we usually assume a complete loss of material rigidity and stresses whilst in the case of cracking, an orthotropic material is adopted. The orthotropic axis are assumed to coincide either with the principal stress axes or with directions of principal strains. The stiffness in the direction parallel to a crack is assumed unchanged. The stiffness in the perpendicular direction is set to zero and appropriate normal stress is released unless tension stiffening is adopted. If in subsequent loading history the crack closes again, the original isotropic material is reinstated.

Some models take into account normal and shear residual stiffness across the crack, (due to aggregate interlocking, reinforcing dowel etc.), and they will be discussed later.

In cases of mixed crack/crushing failure modes the crushing coefficient approach presented in Section 3.3.4 is often employed.

In the following, simple linear constitutive models will be presented for the case of two dimensional and axisymmetric loading conditions. Its extension to shell analysis is straightforward.

ward and will not be given explicitly. Also in this case we assume that cracks can occur perpendicular to the element plane only and hence the similarity with 2D models.

Constitutive equations of this type are based on Hooke's law specifying linear relationships between strains and stresses. These equations are well known and only final expressions are presented.

For general three dimensional loading:

$$\Delta\sigma_{ij} = \frac{E}{(1 + \mu)} \Delta\varepsilon_{ij} + \frac{\mu E}{(1 + \mu)(1 - 2\mu)} \Delta\varepsilon_{kk} \delta_{ij} \quad /3.13/$$

where E is Young's modulus, μ is Poisson's ratio and $\Delta\sigma$ and $\Delta\varepsilon$ are stress and strain increments. δ_{ij} is the Kronecker's δ tensor ($\delta_{ij} = 1$ for $i = j$, $\delta_{ij} = 0$ for $i \neq j$)

In the case of 2D problems /3.13/ can be abbreviated to:

Axisymmetric problem (z-axis is axis of symmetry):

($\gamma_{z\Theta} = \gamma_{\Theta r} = \tau_{z\Theta} = \tau_{\Theta r} = 0$). See Fig. 3.10 showing the adopted notation.

$$\begin{bmatrix} \Delta\sigma_r \\ \Delta\sigma_z \\ \Delta\tau_{rz} \\ \Delta\sigma_\Theta \end{bmatrix} = \frac{E}{(1 + \mu)(1 - 2\mu)} \begin{bmatrix} (1 - \mu) & \mu & 0 & \mu \\ & (1 - \mu) & 0 & \mu \\ \text{sym.} & & (1 - 2\mu)/2 & 0 \\ & & & (1 - \mu) \end{bmatrix} \begin{bmatrix} \Delta\varepsilon_r \\ \Delta\varepsilon_z \\ \Delta\gamma_{rz} \\ \Delta\varepsilon_\Theta \end{bmatrix} \quad /3.14/$$

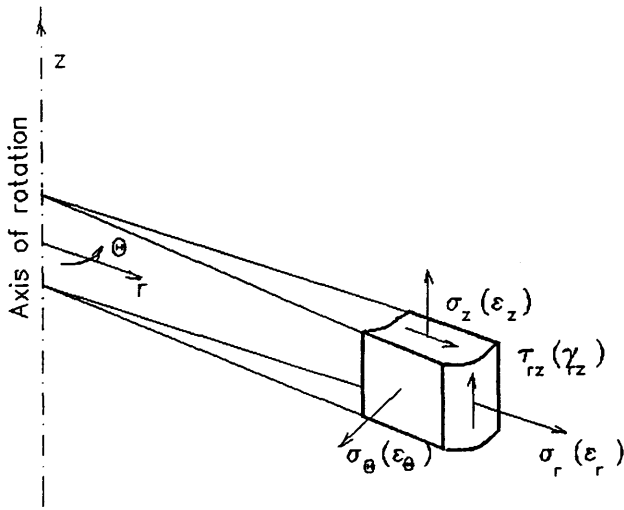


Fig. 3.10 Notation for axisymmetric problem.

Plane strain in plane (x-y):

$$(\epsilon_z = \gamma_{zy} = \gamma_{zx} = \tau_{zy} = \tau_{zx} = 0)$$

$$\begin{bmatrix} \Delta\sigma_x \\ \Delta\sigma_y \\ \Delta\tau_{xy} \end{bmatrix} = \frac{E}{(1 + \mu)(1 - 2\mu)} \begin{bmatrix} (1 - \mu) & \mu & 0 \\ & (1 - \mu) & 0 \\ \text{sym.} & & (1 - 2\mu)/2 \end{bmatrix} \begin{bmatrix} \Delta\epsilon_x \\ \Delta\epsilon_y \\ \Delta\gamma_{xy} \end{bmatrix}$$

/3.15/

$\Delta\sigma_z$ can be calculated using /3.13/:

$$\Delta\sigma_z = \frac{E \mu}{(1 + \mu)(1 - 2\mu)} (\Delta\epsilon_x + \Delta\epsilon_y) = \mu(\Delta\sigma_x + \Delta\sigma_y) \quad /3.16/$$

Plane stress in plane (x-y):

$$(\sigma_z = \gamma_{zy} = \gamma_{zx} = \tau_{zy} = \tau_{zx} = 0)$$

$$\begin{bmatrix} \Delta\sigma_x \\ \Delta\sigma_y \\ \Delta\tau_{xy} \end{bmatrix} = \frac{E}{(1 - \mu^2)} \begin{bmatrix} 1 & \mu & 0 \\ & 1 & 0 \\ \text{sym.} & & (1 - 2\mu)/2 \end{bmatrix} \begin{bmatrix} \Delta\gamma_x \\ \Delta\gamma_y \\ \Delta\tau_{xy} \end{bmatrix} \quad /3.17/$$

$$\Delta\sigma_z = 0,$$

$$\Delta\epsilon_z = \frac{\mu}{\mu - 1} (\Delta\epsilon_x + \Delta\epsilon_y) \quad /3.18/$$

Although equations /3.14/ through /3.18/ were presented for stress and strain increments, because of their linearity the same form can be used for relationships between total values.

Proceeding to the constitutive equation for cracked concrete, because of our restriction to 2D problems, a crack can be created in the x-y plane only (see Figure 3.11). The coordinate system x'-y' parallel with the crack is based on the assumption that x' axis is normal to direction of principal stress responsible for the crack creation. The angle between axes x and x' is denoted β and is positive for an anti-clockwise rotation.

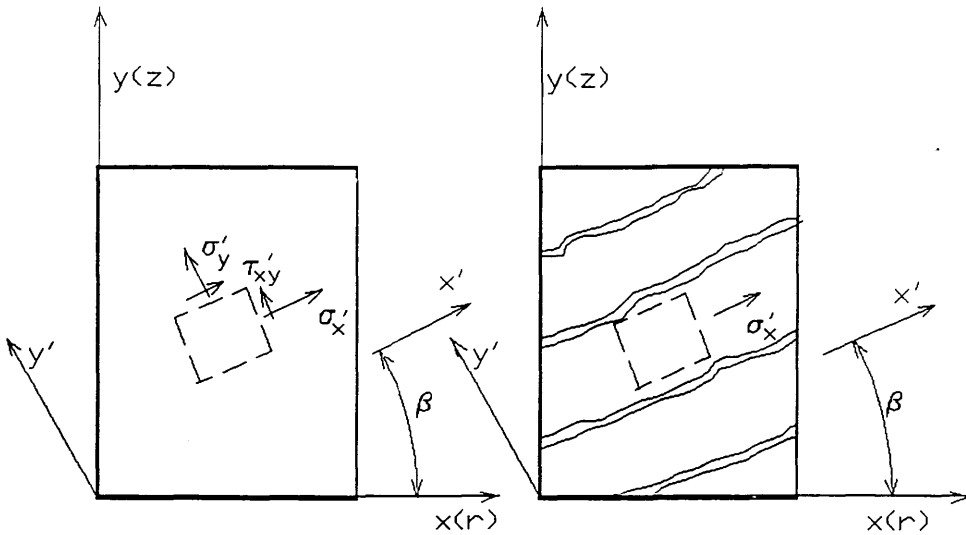


Fig. 3.11 Crack pattern in x-y plane.

After crack occurrence the equations /3.14/ to /3.18/ are replaced by /3.19/:

$$\begin{bmatrix} \Delta\sigma_{x'} \\ \Delta\sigma_{y'} \\ \Delta\tau_{x'y'} \\ \Delta\sigma_z \end{bmatrix} = \begin{bmatrix} E_{x'} & 0 & 0 & \mu E_{x'} \\ & E_{y'} & 0 & 0 \\ & & G_{x'y'} & 0 \\ \text{sym.} & & & E_z \end{bmatrix} \begin{bmatrix} \Delta\epsilon_{x'} \\ \Delta\epsilon_{y'} \\ \Delta\gamma_{x'y'} \\ \Delta\epsilon_z \end{bmatrix}$$

/3.19/

where $E_{x'} = E_z = E'$ is the original Young's modulus and $E_{y'}$ and $G_{x'y'}$ are residual values of Young's modulus perpendicular to the crack and the shear modulus along the crack.

For the cases of plane strain and axisymmetry after the crack formation, we deal with a plane stress problem in plane $x'-z$ and hence $E' = \frac{E}{1 - \mu^2}$, whilst in the case of a plane stress problem after cracking the solution degrades to a one dimension situation with $E' = E$. Here E is Young's modulus for a virgin concrete in one dimension, μ is Poisson's ratio. Notice that Poisson's ratio in the $x'-y'$ plane is assumed zero ($\mu_{x'y'} = 0$).

This is justified (see for example refs. [9], [10], [14]).

Equations /3.19/ are provided in x'-y' coordinate system and therefore it is necessary to transform them to the original x-y system. This takes the form:

$$\underline{\Delta\sigma} = D \underline{\Delta\varepsilon} ,$$

where:

$$D = \begin{bmatrix} C^4; S^2C^2; S C^3; \mu C^2 \\ S^4; S^3C; \mu S^2 \\ \text{sym.} & S^2C^2; \mu SC \\ & & 1 \end{bmatrix} E' +$$

$$\begin{bmatrix} S^4; S^2C^2; -S C^3; 0 \\ C^4; -S^3C; 0 \\ \text{sym.} & S^2C^2; 0 \\ & & 0 \end{bmatrix} E_{y'} + \quad /3.20/$$

$$\begin{bmatrix} 2S^2C^2; -2S^2C^2; -SC(C^2 - S^2) ; 0 \\ 2S^2C^2; SC(C^2 - S^2) ; 0 \\ \text{sym.} & (C^2 - S^2)^2/2 ; 0 \\ & & 0 \end{bmatrix} G_{x'y'}$$

where $C = \cos\beta$, $S = \sin\beta$ and β is the crack angle.

β is computed using the direction of principal stresses just prior to failure:

$$n_x = 1$$

$$n_y = \frac{\sigma_x - \sigma_1}{\tau_{xy}} \quad /3.21/$$

$$\beta = \arctg\left(\frac{n_y}{n_x}\right)$$

Note that $\sigma_1 > \sigma_2$, and is the in-plane principal stress prior to cracking.

Similar to equation /3.21/ we can derive transformation relations for the stress vector $[\sigma_{x'}, \sigma_{y'}, \tau_{x'y'}, \sigma_z]$ to the x-y coordinate system.

$$\sigma_{x'} = \sigma_x \cos^2 \beta + \sigma_y \sin^2 \beta - \sin 2\beta \tau_{x'y'}$$

$$\sigma_{y'} = \sigma_x \sin^2 \beta + \sigma_y \cos^2 \beta + \sin 2\beta \tau_{x'y'}$$

$$\tau_{x'y'} = (\sigma_{x'} - \sigma_{y'}) \sin \beta \cos \beta + \tau_{x'y'} \cos 2\beta$$

Note, that in order to be able to use the transformation rule for tensors, in $\Delta \underline{\varepsilon}$ we have to consider not γ_{xy} but $\varepsilon_{xy} = \frac{1}{2} \gamma_{xy}$ [3] and after transformation to reset γ_{xy} back again.

Equations /3.20/ and /3.21/ were presented for an x-y-z coordinate system with a crack in the x-y plane. For axisymmetric situation it is necessary to replace indexes x, y, z by r, s, θ respectively. In the case of plane stress (plane strain) problems σ_z (ε_z) equals zero and expressions similar to /3.18/ and /3.16/ must be derived.

An important feature of this model is that after cracks have occurred, the residual rigidities $E_{y'}$ and $G_{x'y'}$ are retained.

This is in agreement with experimental evidence. Nevertheless, some authors (for the sake of simplicity) neglect them both leading to the following expressions (recommended in [2]):

a/ Plane stress (plane x-y):

$$\underline{\sigma} = [\sigma_x; \sigma_y; \tau_{xy}]^T \dots \text{stress vector}$$

$\underline{\varepsilon} = [\varepsilon_x; \varepsilon_y; \varepsilon_{xy}]^T$... strain vector

$\underline{\Delta\sigma} = [\Delta\sigma_x; \Delta\sigma_y; \Delta\tau_{xy}]^T$... increment of stress due to
increment of strain $\underline{\Delta\varepsilon}$

$\underline{\Delta\varepsilon} = [\Delta\varepsilon_x; \Delta\varepsilon_y; \Delta\varepsilon_{xy}]^T$... strain increment

β ... angle of crack.

$\underline{b}(\beta)^T = [\cos^2(\beta), \sin^2(\beta), \sin(\beta)\cos(\beta)]$

$\underline{b}'(\beta)^T = [\cos^2(\beta), \sin^2(\beta), 2\sin(\beta)\cos(\beta)]$

E ... Young's modulus

I ... identity matrix

μ ... Poisson's ratio

$$\underline{\Delta\sigma} = (E \{ \underline{b}(\beta) * \underline{b}(\beta)^T \} * \underline{\Delta\varepsilon} - (I - \{ \underline{b}(\beta) * \underline{b}'(\beta)^T \} * \underline{\sigma}) \quad /3.22/$$

b/ Plane strain:

$$\underline{\Delta\sigma} = (\frac{E}{1 - \mu^2} \{ \underline{b}(\beta) * \underline{b}(\beta)^T \} * \underline{\Delta\varepsilon} - (I - \{ \underline{b}(\beta) * \underline{b}'(\beta)^T \} * \underline{\sigma}) \quad /3.23/$$

c/ Axisymmetric problem:

$$\begin{bmatrix} \Delta\sigma_r \\ \Delta\sigma_z \\ \Delta\tau_{rz} \\ \Delta\sigma_\Theta \end{bmatrix} = \frac{E}{1-\mu^2} * \begin{bmatrix} \underline{b}(\beta)*\underline{b}(\beta)^T & ; & \mu\underline{b}(\beta) \\ \mu\underline{b}(\beta)^T & ; & 1 \end{bmatrix} * \begin{bmatrix} \Delta\varepsilon_r \\ \Delta\varepsilon_z \\ \Delta\varepsilon_{rz} \\ \Delta\varepsilon_\Theta \end{bmatrix} \\ - \begin{bmatrix} (I-\underline{b}(\beta)*\underline{b}'(\beta)^T); & 0 \\ 0 & ; & 0 \end{bmatrix} * \begin{bmatrix} \sigma_r \\ \sigma_z \\ \tau_{rz} \\ \sigma_\Theta \end{bmatrix}$$

/3.24/

Note that equations /3.22/ through /3.24/ comprise stress changes $\Delta\sigma$ due to strain changes $\Delta\varepsilon$ (first term) and also stress changes due to crack occurrence (released stresses, in the second term of R.H.S). Hence they are applicable only for the step when the concrete has just cracked. For the following steps (or iterations) the second terms of /3.22/ to /3.24/ are omitted.

Returning to the general case which includes residual material rigidities after cracking, it is necessary to specify correctly the shear modulus $G_{x,y}$, and Young modulus E_y , in equation /3.20/. In the following, four often used methods are presented.

Model a/.

The simplest way of establishing $G_{x,y}$, and E_y , is shown in Figure /3.12/:

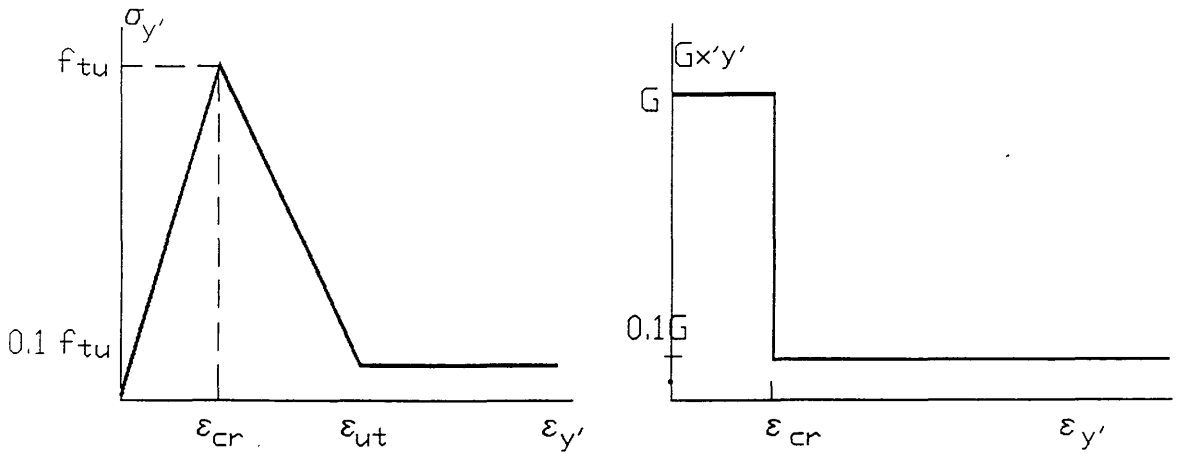


Fig. 3.12 Evaluation of $\sigma_{y'}$ and $G_{x'y'}$ - method a/.

The model assumes a piece wise linear relationship diagram for the normal stress perpendicular to the crack. The model assumes that the strain normal to the crack, $\epsilon_{y'}$, can be taken as a measure of the crack width. The wider the crack the smaller the normal stress. Beyond ϵ_{ut} (the ultimate tensile uniaxial strain) the corresponding stress is constant and equal to ^afraction ^{of} the original tensile strength. Young's modulus $E_{y'}$ is computed by taking the derivative of $\sigma_{y'}$ with respect to ϵ .

The shear modulus after cracking is also reduced to about 10% its original value and kept constant for further loading.

Mathematically the model is expressed by:

Normal stress:

$$\sigma_{y'} = \frac{f_{tu}}{2} \left(1 + \frac{\epsilon_{ut} - \epsilon_{y'}}{\epsilon_{ut} - \epsilon_{cr}} \right) \quad \text{for } \epsilon_{ut} > \epsilon_{y'} \geq \epsilon_{cr}$$

$$E_{y'} = \frac{\partial \sigma_{y'}}{\partial \epsilon_{y'}} = \frac{f_{tu}}{2} \left(\frac{1}{\epsilon_{cr} - \epsilon_{ut}} \right) \quad /3.25/$$

and

$$\sigma_{y'} = \frac{f_{tu}}{10}; E_{y'} = 0 \quad \text{for } \epsilon_{y'} > \epsilon_{ut}$$

where f_{tu} is ultimate tension normal to the crack just before its creation,

ϵ_{cr} is strain ϵ_y corresponding to f_{tu} , (usually $f_{tu} = f'_t$),

ϵ_{ut} is ultimate one dimensional strain .

Shear modulus:

$$G_{x',y'} = 0.05G \text{ to } 0.15G \quad /3.26/$$

This model represents a very simple approach which causes some difficulties with the numerical treatment of the problem (to be discussed later). More details are available in ref. [9].

Model b/.

In order to provide a more accurate model the following expressions have also been recommended [10], and are shown in Fig. 3.13. These comprise also linear relationships.

Normal stress:

$$\sigma_{y'} = \frac{\alpha_2 f_{tu} \left(\alpha_1 - \frac{\epsilon_{y'}}{\epsilon_{cr}} \right)}{\alpha - 1} \quad \text{for } \alpha_1 \epsilon_{cr} > \epsilon_{y'} \geq \epsilon_{cr} \quad /3.27/$$

$$E_{y'} = \frac{\alpha_2 f_{tu}}{\alpha_1 - 1} \left(-\frac{1}{\epsilon_{cr}} \right)$$

$$\text{and } \sigma_{y'} = 0; E_{y'} = 0 \quad \text{for } \epsilon_{y'} > \alpha_1 \epsilon_{cr}$$

Shear modulus:

$$G_{x',y'} = G \frac{(\beta_1 - \beta_2)}{(\beta_3 - 1)} \left(\beta_3 - \frac{\epsilon_{y'}}{\epsilon_{cr}} \right) + \beta_2 G \quad /3.28/$$

$$\text{for } \beta_3 \epsilon_{cr} > \epsilon_{y'} \geq \epsilon_{cr}$$

$$G_{x'y'} = \beta_2 G \quad \text{for } \varepsilon_{y'} > \beta_3 \varepsilon_{cr}$$

The additional material constants α_1 , α_2 , β_1 , β_2 and β_3 are set experimentally or numerically.

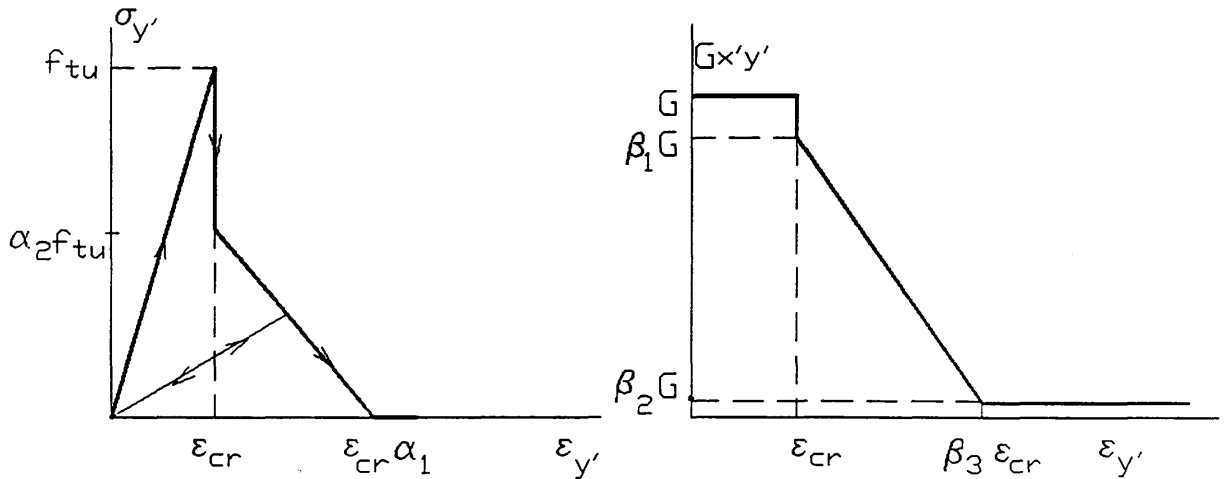


Fig. 3.13 Evaluation of $\sigma_{y'}$ and $G_{x'y'}$ - method b/.

Based on results presented in [10] the following values are suggested:

$$\alpha_1 = 10; \quad \alpha_2 = 0.6; \quad \beta_1 = 1; \quad \beta_2 = 0.1; \quad \beta_3 = 10$$

The other possibility is to relate constants α_1 and α_2 to fracture energy G_f of concrete (i.e. energy which is necessary to create a crack of unit surface):

$$G_f = \int_{\varepsilon_{cr}}^{\alpha_1 \varepsilon_{cr}} (\sigma_{y'}, l_c d\varepsilon) \quad /3.29/$$

where l_c is a characteristic crack length.

Substituting /3.27/ to /3.29/ we get:

$$G_f = 0.5 \alpha_1 \alpha_2 l_c f_{tu} \varepsilon_{cr}$$

$$\text{i.e. } \alpha_1 \alpha_2 = \frac{2 G_f}{l_c f_{tu} \varepsilon_{cr}} \quad /3.30/$$

and length l_c can be assumed for 2D situations as:

$$l_c = \sqrt{A} \quad /3.31/$$

where A is the area corresponding to the sampling point. The fracture energy for normal concretes varies between 50 N/m to 200N/m.

Model c/.

This model represents a different approach. The basic idea is to divide the total value of strain in the direction normal to the crack $\varepsilon_{y'}$, into two parts. The first part $\Delta\varepsilon_{co}$ corresponds to the strain in the uncracked concrete and the second part $\Delta\varepsilon_{cr}$ to the strain in the crack [14], i.e. $\varepsilon_{y'} = \Delta\varepsilon_{co} + \Delta\varepsilon_{cr}$.

The above equations can be derived from the assumption that after cracking stress equilibrium must be satisfied:

$$\Delta\sigma_{y'} = \Delta\sigma_{cr} = \Delta\sigma_{co}$$

where:

$$\Delta\sigma_{cr} = \Delta\varepsilon_{cr} E_t \quad \text{stress in crack (the second part of strain),}$$

$$\Delta\sigma_{co} = \Delta\varepsilon_{co} E \quad \text{stress in virgin concrete (the first part of strain),}$$

and the compatibility condition:

$$\Delta \varepsilon_{y'} = \Delta \varepsilon_{cr} + \Delta \varepsilon_{co}.$$

Using the above equations we can write:

$$\Delta \sigma_{y'} = \frac{E E_t}{E - E_t} \Delta \varepsilon_{y'} \quad /3.32/$$

$$\Delta \tau_{x'y'} = \frac{\beta}{1 - \beta} \left(\frac{E}{2(1 + \mu)} \right) \Delta \gamma_{x'y'}$$

and for unloading phase:

$$\Delta \sigma_{y'} = \frac{E E_{sec}}{E - E_{sec}} \Delta \varepsilon_{y'} \quad /3.33/$$

$$\Delta \tau_{x'y'} = \frac{\beta}{1 - \beta} \left(\frac{E}{2(1 + \mu)} \right) \Delta \gamma_{x'y'}$$

where:

$\Delta \sigma_{y'}$, $\Delta \varepsilon_{y'}$, $\Delta \gamma_{x'y'}$, $\Delta \tau_{x'y'}$ are as previously defined,

E_t is Young's modulus which relates the change of stress in the direction normal to the crack $\Delta \sigma_{y'}$, to the change of strain in direction normal to the crack $\varepsilon_{y',cr}$, (the first part),

E_{sec} is the secant modulus based on $\sigma_{y'}$ and $\varepsilon_{y'}$, (for unloading only),

β is a material parameter defining shear reduction after crack formation.

The shear and Young's modulus are calculated as usual by taking appropriate derivatives.

Model d/.

The above models provide results of satisfactory accuracy, but unfortunately their discontinuities sometimes causes serious trouble for nonlinear equation solvers. Thus smoother methods of modeling the residual rigidities have been recommended [39]:

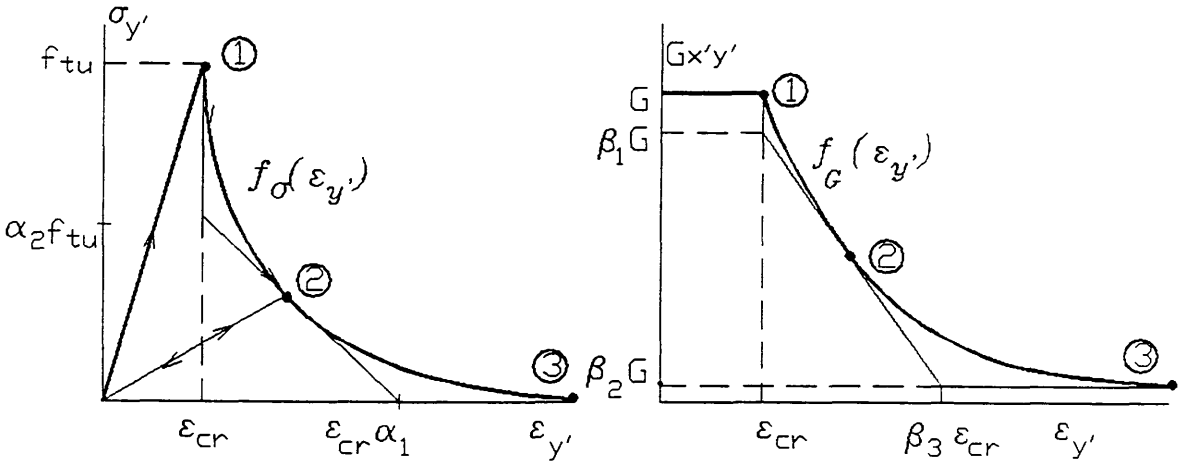


Fig. 3.14 The functions $f_{\sigma}(\epsilon_{y'})$ and $f_G(\epsilon_{y'})$ in model d/.

This model is similar in shape to model b/ but the piece wise linear relationships are replaced by a hyperbolic function for both $\sigma_{y'}$ and $G_{x'y'}$, as follows:

$$y = f(\epsilon_{y'}) = a + \frac{k}{\epsilon_{y'} - b} \quad /3.34/$$

where y and $f(\epsilon_{y'})$ are either $\sigma_{y'}$ or $G_{x'y'}$, and constants a , b , k are computed from the requirements that $f(\epsilon_{y'})$ must fit points 1, 2 and is tangential to a constant residual value (see Figure 3.14), i.e. point 3 is at ∞ .

This leads to:

$$G_{x'y'} = G \left(\beta_2 + (1 - \beta_2) \frac{\epsilon_{cr} - b}{\epsilon_{y'} - b} \right) \quad /3.35/$$

where β_1 , β_2 and β_3 are three material constants to be set experimentally or numerically and

$$b = \frac{AC - B}{A - 1}$$

where

$$A = \frac{\beta_1 - \beta_2}{2(1 - \beta_2)} ; \quad B = \varepsilon_{cr} ; \quad C = \frac{\varepsilon_{cr}}{2} (1 + \beta_3)$$

Similarly for $\sigma_{y'}$:

$$\sigma_{y'} = f_{tu} \left(\frac{\varepsilon_{cr} - b}{\varepsilon_{y'} - b} \right) \quad /3.36/$$

where α_1 , α_2 are additional material constants and

$$b = \frac{AC - B}{A - 1}$$

where

$$A = \frac{\alpha_1}{2} ; \quad B = \varepsilon_{cr} ; \quad C = \frac{\varepsilon_{cr}}{2} (1 + \alpha_2).$$

Young's modulus is calculated by taking the derivative:

$$E_{y'} = \frac{\partial \sigma_{y'}}{\partial \varepsilon_{y'}} = -f_{tu} \frac{\varepsilon_{cr} - b}{(\varepsilon_{y'} - b)^2} \quad /3.37/$$

Some final remarks on the above material models:.

The last model, method d/, was implemented into NONSAP and some previously reported numerical troubles, such as oscillation around the structural response corresponding to cracked and uncracked material conditions, disappeared. For shell analysis, (program CONCRETE), method b/ is used thru this work.

The value f_{tu} in model /d is not constant, (providing that the Mohr-Coulomb criterion failed) and depends particularly on the level of volumetric stress. Hence for every sampling point with a crack, in order to preserve the continuity of the normal stress across the crack, the peak tension f_{tu} must be remembered. If more crack directions are allowed then for every new direction an additional value must be stored. Obviously this strategy demands a lot of computer storage. For this reason some authors (models a/, b/) prefer to sacrifice the continuity and use a reduced uniaxial tension strength f'_t instead. In addition, a similar situation arises with the shear moduli in cracks.

If residual rigidities are neglected after cracking then the stress state degrades to one a dimensional problem, and hence the next failure leads to total failure.

If, however, residual rigidities are taken into account, it allows creation of an additional set of cracks after some further loading. There are two possibilities for treating these. The first is based on the simple assumption that the second set of cracks must be normal to the previous cracks and no additional set is possible. This is used in program CONCRETE. The second approach is to calculate the direction of the second set of cracks using the current stress state. It is assumed again that the crack direction is the direction of the principal stress σ_1 .

In addition to the above approaches we should mention so-called fixed and rotating crack models. The basic concept of the former is that a crack, once created, doesn't change its direction. The latter calculates a new crack direction every time the material rigidity matrix is evaluated. In practice this causes the crack to "rotate". This idea is justified by some experimental evidence which suggests a single crack is never created but rather small areas of micro cracks occurs. The particular direction of material weakening is then a function of current loading (or stress) state in appropriate zone.

The fixed crack models are adopted thru this work.

A final source of doubt is whether to base crack directions on principal stresses or on principal strains. In the author's opinion this question has not yet been resolved. Nevertheless principal stresses are used more for their easier treatment rather than for more accurate results.

3.5 Nonlinear constitutive equation for concrete.

The objective of this section is to present some of the most widely used nonlinear constitutive equations for concrete. They are usually combined with the linear models discussed in the previous section and can be used with any of the failure criteria discussed previously.

Generally nonlinear constitutive equations are usually used only for the compression regime whilst the tension regime is covered adequately by linear relationships. There are many types of nonlinear equations, for example hyperelastic, hypoelastic, elastic-plastic, endochronic etc. and there are special groups based on fracture mechanics. As in the previous section nonlinear models can also be treated as smeared or discrete. An important additional division of nonlinear models is whether they are assumed to predict concrete response for monotonic or cycling loading conditions or even for dynamic loading. Some models are of the secant type (hyperelastic models) where the current stress-strain relationships is independent of previous history; hypoelastic models, on the other hand, are examples of constitutive equations which account for all previous loading paths.

In the following, examples of initially isotropic, orthotropic and elastic-plastic models are presented because they are the most frequently used material models in current nonlinear finite elements methods.

3.5.1 Isotropic models.

This group of models is characterized by the assumption of initial isotropy in the concrete. During the loading process an anisotropic material is created. There are two basic types in this group. The first extrapolates uniaxial nonlinear stress-strain behavior to 2D and 3D solutions using a form of constitutive equations similar to /3.13/ with variable Young's modulus

and Poisson's ratio. The second type is based on nonlinear relations defining the bulk and shear moduli.

3.5.1.1 Model with variable E_s and μ_s .

This is one of the simplest nonlinear models for concrete. The basic entities are variable Young's modulus E_s and Poisson's ratio μ_s . In order to extend uniaxial relationships for E_s and μ_s to 2D or 3D situation a nonlinearity index β is introduced which defines the ratio of the maximum current stress to the critical compression stress at failure.

The compression at failure is computed using any failure criterion in which the ratios of main and lateral stresses are the same as for the current loading condition. In other words the critical compression stresses are assumed to be a multiple of the current stresses.

For the uniaxial relationship between E_s and strain ϵ Sargin (1971) [2] derived the following relationship:

$$\frac{-\sigma}{f'_c} = \frac{-A \left(\frac{\epsilon}{\epsilon_c} \right) + (D-1) \left(\frac{\epsilon}{\epsilon_c} \right)^2}{1 - (A-2) \left(\frac{\epsilon}{\epsilon_c} \right) + D \left(\frac{\epsilon}{\epsilon_c} \right)^2} \quad /3.38/$$

where A is ratio the $\frac{E_0}{E_c}$,

E_0 is initial (virgin) Young's modulus,

$E_c = \frac{f'_c}{\epsilon_c}$ is the secant modulus at failure,

D is a parameter defining the shape of descending part of the stress-strain diagram,

ϵ_c is the maximum compressive strain at failure,

ϵ is the current compression strain.

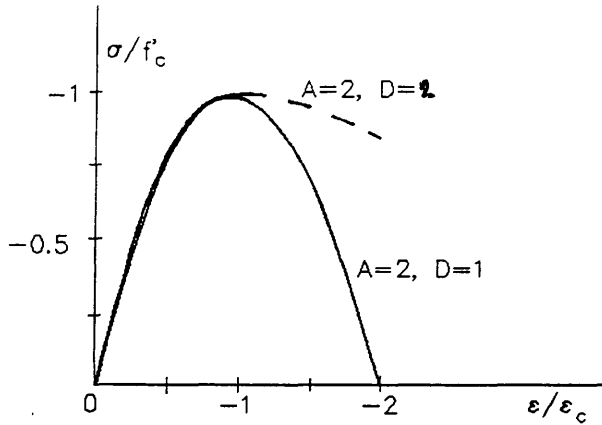


Fig. 3.15 Diagram for $\sigma - \epsilon$ according to Sagrin - (uniaxial case).

The function for Poisson's ratio μ_s is recommended in the form:

$$\mu_s = \mu_f - (\mu_f - \mu_0) \sqrt{1 - \left(\frac{\beta - \beta_a}{1 - \beta_a} \right)^2} \quad \text{for } 1 \geq \beta \geq \beta_a$$

$$\mu_s = \mu_0 \quad \text{for } \beta \leq \beta_a$$

/3.39/

where β is the nonlinearity index,

β_a is set approximately to 0.7,

μ_s and μ_0 are the secant and initial Poisson's ratios,

μ_f is Poisson's ratio at failure (0.5).

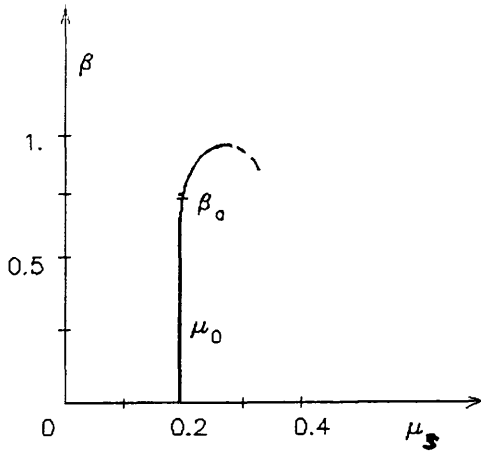


Fig. 3.16 The $\mu_s - \beta$ diagram.

In practice a factor λ , the multiple of current loading compared to failure, is first calculated; $\beta = \lambda^{-1}$. The second step is to obtain the maximum compression strain ϵ_c corresponding to failure. Thereafter the ratio ϵ/ϵ_c is calculated from which the stress σ and Poisson's ratio μ are computed using equations /3.38/ and /3.39/. Hence using the values of σ and ϵ the current secant modulus is calculated which is then substituted into equation /3.13/ with Poisson's ratio in order to calculate all stresses.

The main advantages of this model is its simplicity and the smooth modeling of the descending part of the stress-strain diagram. The uniaxial stress - strain relationship provided by Sargin can be replaced by any other suitable equation.

3.5.1.2 Model with variable bulk K_s and shear G_s modulus.

The main idea of this model is very similar to the previous model, the only difference being that the variable material constants E_s and μ_s are replaced by variable bulk modulus K_s and shear modulus G_s .

Approximate functions for both K_s and G_s are established by fitting numerous experimental results for 2D stress states to

functions $K_s = K_s(I_1)$ and $G_s = G_s(J_2)$ or $K_s = K_s(\sigma_{oct})$ and $G_s = G_s(\tau_{oct})$.

The independent variables I_1 and J_2 are used in order to ensure the independence of the loading history. Alternatively strain entities can be used instead. These models can be subdivided into those which use secant relationships or those which use tangential relationship.

a/ Secant relationships.

1/ 2D state: $K_s = K_s(\gamma_{oct})$, $G_s = G_s(\gamma_{oct})$ /3.40/

$$\begin{bmatrix} \sigma_x \\ \sigma_y \\ \tau_{xy} \end{bmatrix} = \frac{4G_s(3K_s + G_s)}{3K_s + 4G_s} \begin{bmatrix} 1 & ; 3K_s - 2G_s & ; 0 \\ & \frac{2(3K_s + G_s)}{2(3K_s + G_s)} & \\ \left\{ \frac{3K_s - 2G_s}{2(3K_s + 4G_s)} \right\} & ; 1 & ; 0 \\ 0 & ; 0 & ; \frac{3K_s + 4G_s}{4(3K_s + G_s)} \end{bmatrix} \begin{bmatrix} \epsilon_x \\ \epsilon_y \\ \epsilon_{xy} \end{bmatrix}$$

/3.41/

The experimentally derived functions K_s , G_s are supplemented by the failure criterion:

$$\sigma_1 = f'_t \geq \sigma_2 \text{ for the tension-tension zone,}$$

$$\sigma_1 = (1 + 0.8 \sigma_2 / f'_c) f'_t \text{ for the tension-compression zone,}$$

$$\left(\frac{\sigma_1}{f'_c} + \frac{\sigma_2}{f'_c} \right)^2 + \frac{\sigma_2}{f'_c} + 3.65 \frac{\sigma_1}{f'_c} = 0$$

$$(\sigma_1 \geq \sigma_2) \text{ for the compression-compression zone.}$$

/3.42/

where f'_t , f'_c are the uniaxial tensile and compressive strengths respectively,

ε_{oct} , γ_{oct} are the octahedral volumetric and shear strains respectively.

$$2/ \text{ 3D problem: } K_s = K_s(\varepsilon_{\text{oct}}), \quad G_s = G_s(\gamma_{\text{oct}})$$

For the 3D case we must use $K_s = K_s(\varepsilon_{\text{oct}})$ and $G_s = G_s(\gamma_{\text{oct}})$ because the previous assumption $K_s = K_s(\gamma_{\text{oct}})$ involves a linear relationship between volumetric changes and hydrostatic stress [2].

The detailed derivation of equations similar to /3.41/ is trivial. Suitable expressions for functions K_s and G_s [2] are:

$$K_s(\varepsilon_{\text{oct}}) = K_0 [a b^{\varepsilon_{\text{oct}}/c} + d]$$

$$G_s(\gamma_{\text{oct}}) = G_0 [m q^{-\gamma_{\text{oct}}/r} - n \gamma_{\text{oct}} + t]$$

/3.43/

where a,b,c,d,m,q,r,n,t are material constants and K_0 and G_0 are the initial bulk and shear moduli. They must be identified experimentally.

The 3D situation /3.43/ must also be accompanied by appropriate failure criteria.

b/ Tangential relationships.

Tangential relationships are based on the same functions for bulk and shear moduli as the secant relationships but now it is necessary to take appropriate derivatives. For the 3D case these take the form:

$$\Delta \tau_{\text{oct}} = \left(G_s + \gamma_{\text{oct}} * \frac{\partial G_s}{\partial \gamma_{\text{oct}}} \right) \Delta \gamma_{\text{oct}} = G_T \Delta \gamma_{\text{oct}}$$

$$\Delta\sigma_{\text{oct}} = 3 \left(K_s + \varepsilon_{\text{oct}} * \frac{\partial K_s}{\partial \varepsilon_{\text{oct}}} \right) \Delta\varepsilon_{\text{oct}} = K_T \Delta\varepsilon_{\text{oct}}$$

/3.44/

where $\Delta\tau_{\text{oct}}$, $\Delta\sigma_{\text{oct}}$, $\Delta\gamma_{\text{oct}}$ and $\Delta\varepsilon_{\text{oct}}$ are increments of corresponding entities.

For the 2D case, (i.e. $K_s = K_s(\gamma_{\text{oct}})$, $G_s = G_s(\gamma_{\text{oct}})$), the equation for $\Delta\sigma_{\text{oct}}$ is replaced by:

$$\Delta\sigma_{\text{oct}} = \left(\delta_{kl} K_s + 4 \frac{\varepsilon_{\text{oct}}}{\gamma_{\text{oct}}} * \frac{\partial K_s}{\partial \gamma_{\text{oct}}} e_{kl} \right) \Delta\varepsilon_{kl}$$

/3.45/

where δ_{kl} is k,l element of the Kronecker's delta tensor and e_{kl} is element k,l of the deviatoric strain tensor.

After some manipulation similar equations to /3.41/ in incremental form can be obtained.

It should be noted that these models are only suitable for monotonic loading conditions and that the volumetric and shear behavior are treated independently of each other. This is contrary to experimental evidence and the following model attempts to remedy this.

Experimental evidence shows that pure deviatoric stress causes not only deviatoric but also volumetric strains. Hence the basic idea of this model is to calculate some "pseudo" volumetric stress σ'_{oct} due to ε_{oct} despite the fact that it is actually caused by τ_{oct} , i.e.

$$\sigma'_{\text{oct}} = 3 K_s \varepsilon_{\text{oct}} \quad /3.46/$$

The value for σ'_{oct} is given by equation /3.47/, which is based purely on experimental results:

$$\frac{\sigma'_{\text{oct}}}{f'_c} = \frac{1.3}{\left[1 + 0.444 \left(\frac{\sigma_{\text{oct}}}{f'_c}\right)^{-2.45}\right]} \frac{\tau_{\text{oct}}}{f'_c} \quad /3.47/$$

Thus the strain - stress relationships take the form:

$$\gamma_{\text{oct}} = \frac{\tau_{\text{oct}}}{G_s}$$

$$\epsilon_{\text{oct}} = \frac{[\sigma_{\text{oct}} + \sigma'_{\text{oct}}]}{3K_s} \quad /3.48/$$

Having established these constitutive equations for octahedral strains their modification into a form similar to equation /3.41/ is straightforward.

3.5.2 Orthotropic models.

Orthotropic models represent another large group of constitutive equations used to model concrete behavior. The basic idea is to consider concrete as a orthotropic material in which its properties in a particular direction are calculated with regard to the stress level in this direction.

Instead of using ϵ_{ij} in direction i we introduce a single strain ϵ_{iu} which simulates the effect of ϵ_{ij} , ($j = 1, 2, 3$), into the 1D state.

$$\epsilon_{iu} = \frac{\epsilon_i}{1 - \mu \frac{\sigma_j + \sigma_k}{\sigma_i}} \quad /3.49/$$

where σ_i is principal stress in direction i .

σ_j, σ_k are principal stresses in lateral directions
 j, k .

Because ε_{iu} ($i = 1, 2, 3$) fully represents the strains in the material established under the assumption of one dimensional conditions, we can now simply use any uniaxial stress - strain relationship applied independently for each direction $i = 1, i = 2$ etc. and obtain the corresponding stresses.

Alternatively it is also possible to use a direct formulation of orthotropic equations. However the presented approach is usually used because of its simplicity and clarity.

3.5.2.1 Orthotropic model for monotonic loading.

The above concept will be now demonstrated on a simple 3D hypoelastic model for concrete (i.e. the model is dependent on loading history).

The essential uniaxial relationship between the strain ε_{iu} and stress σ_i is assumed in the form [2]:

$$\frac{\sigma_i}{\sigma_{ic}} = \frac{n}{n - 1 + \left(\frac{\varepsilon_{iu}}{\varepsilon_{ic}} \right)^n} \frac{\varepsilon_{iu}}{\varepsilon_{ic}} \quad /3.50/$$

where σ_i is the principal stress i , $i = 1, 2, 3$,

σ_{ic} is ultimate value of the principal stress i ,

ε_{ic} is ultimate strain corresponding to σ_{ic} ,

ε_{iu} is the uniaxial strain simulating the effect of

ε_{1j} , $j=1, 2, 3$; defined by /3.49/,

n influences the shape of the curve defined by

/3.50/ and is given by:

$$n = \frac{E_0 \varepsilon_{1c}}{E_0 \varepsilon_{1c} - \sigma_{1c}} \quad /3.51/$$

where E_0 is the initial Young's modulus.

Taking the derivative of /3.50/ we obtain the tangential Young's modulus E_1 in the form:

$$E_1 = \frac{\partial \sigma_1}{\partial \varepsilon_{1u}} = \frac{\left[1 - \left(\frac{\varepsilon_{1u}}{\varepsilon_{1c}} \right)^n \right] n(n-1) \frac{\sigma_{1c}}{\varepsilon_{1c}}}{\left[n - 1 + \left(\frac{\varepsilon_{1u}}{\varepsilon_{1c}} \right)^{n-2} \right]}$$

/3.52/

Hence the final form of constitutive equations is:

$$\begin{bmatrix} \Delta \sigma_1 \\ \Delta \sigma_2 \\ \dots \\ \Delta \tau_{13} \end{bmatrix} = \begin{bmatrix} E_1 & & & 0 \\ & E_2 & & \\ & & \text{sym} & \\ & & & G_{13} \end{bmatrix} \begin{bmatrix} \Delta \varepsilon_1 \\ \Delta \varepsilon_2 \\ \dots \\ \Delta \varepsilon_{13} \end{bmatrix} =$$

$$= \begin{bmatrix} E_1(1-\mu_{32}^2); \sqrt{E_1 E_2}(\mu_{12}\mu_{23} + \mu_{13}); \sqrt{E_1 E_3}(\mu_{12}\mu_{32} + \mu_{13}); 0; 0; 0 \\ E_2(1-\mu_{13}^2) ; \sqrt{E_2 E_3}(\mu_{12}\mu_{13} + \mu_{23}); 0; 0; 0 \\ E_3(1-\mu_{12}^2) ; 0; 0; 0 \\ G_{12}; 0; 0 \\ G_{23}; 0 \\ G_{13} \end{bmatrix} *$$

$$* \Phi \begin{bmatrix} \Delta \epsilon_1 \\ \Delta \epsilon_2 \\ \Delta \epsilon_3 \\ \Delta \epsilon_{12} \\ \Delta \epsilon_{23} \\ \Delta \epsilon_{13} \end{bmatrix}$$

/3.53/

where:

$$\mu_{12}^2 = \mu_{12} \mu_{21}; \quad \mu_{13}^2 = \mu_{13} \mu_{31}; \quad \mu_{23}^2 = \mu_{23} \mu_{32}$$

$$\Phi = (1 - \mu_{12}^2 - \mu_{13}^2 - \mu_{23}^2 - 2\mu_{12}\mu_{13}\mu_{23})$$

$$G_{ij} = \frac{1}{4\Phi} \left[E_i + E_j - 2\mu_{ij} \sqrt{E_i E_j} - \left(\mu_{jk} \sqrt{E_i} + \mu_{ki} \sqrt{E_j} \right)^2 \right]$$

The volumetric and shear properties are quite independent. These relationships have been presented for the 3D situation but its modification for 2D or axisymmetric conditions is straightforward.

3.5.2.2 Orthotropic model for cyclic loading.

This model [11] is similar to the model presented in the previous section but now the uniaxial stress - strain relationships also include unloading and subsequent reloading stages. (See Fig. 3.17). Using notation defined in Fig. 3.17 then:

1. Loading phase:

For loading (i.e. the path A in Fig. 3.17) the previous model for monotonic loading is used.

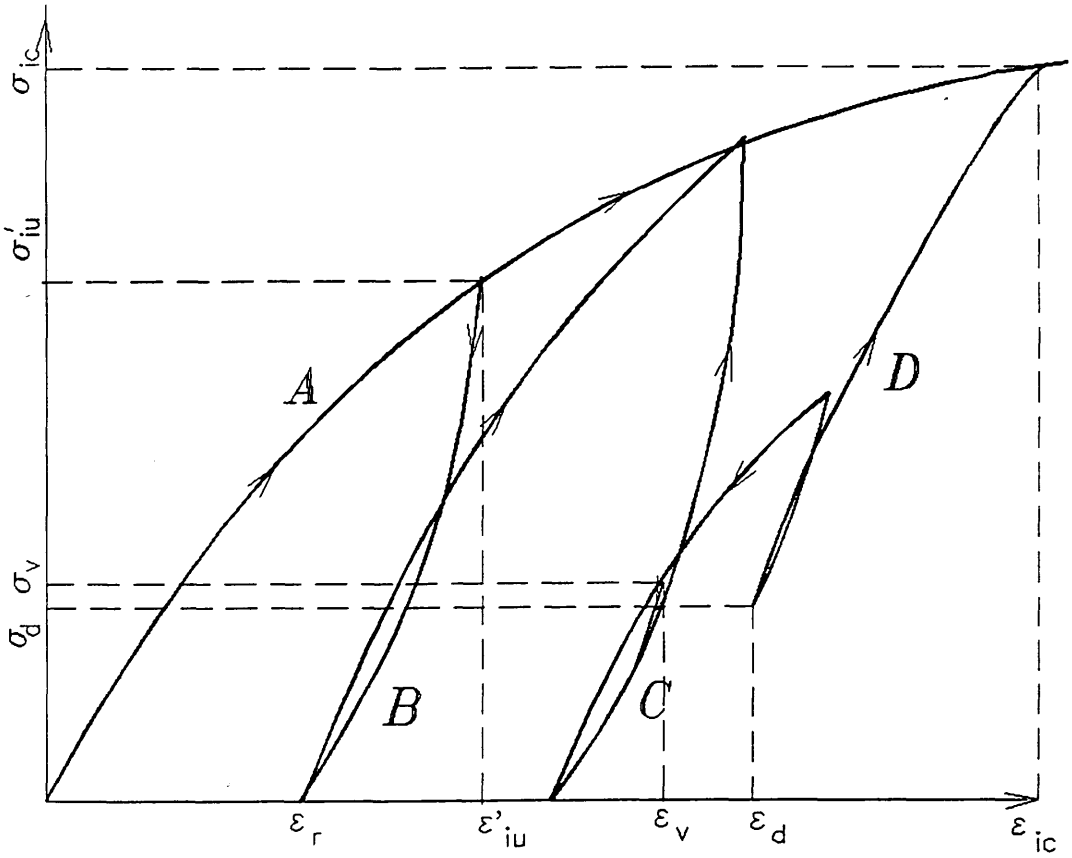


Fig. 3.17 Loading condition.

2. Unloading from the envelope curve:

The unloading curve is defined by a parabola having infinite slope at $(\sigma'_{iu}; \epsilon'_{iu})$, i.e. the point where unloading occurs (see path *B* in Fig. 3.17):

$$\frac{\epsilon_r}{\epsilon_{ic}} = 0.162 \left(\frac{\epsilon'_{iu}}{\epsilon_{ic}} \right) + 0.334 \left(\frac{\epsilon'_{iu}}{\epsilon_{ic}} \right)^2 \quad /3.54a/$$

This curve intersects the strain axis, i.e. for $\sigma_1 = 0.$, at strain ϵ_r :

$$\varepsilon_r = 0.162\varepsilon'_{1u} + \frac{0.334\varepsilon'^2_{1u}}{\varepsilon_{1c}} \quad /3.54b/$$

and final expressions for the uniaxial unloading are then:

Stress-strain curve:

$$(\varepsilon_{1u} - \varepsilon'_{1u}) = \frac{(\varepsilon'_{1u} - \varepsilon_r)}{\sigma'^2_{1u}} (\sigma_i - \sigma'_{1u})^2 \quad /3.54c/$$

Tangential Young's modulus:

$$E_i = \frac{1}{2 \sqrt{\left[\frac{\varepsilon'_{1u} - \varepsilon_r}{\sigma'^2_{1u}} (\varepsilon'_{1u} - \varepsilon_{1u}) \right]}} \quad /3.54d/$$

3. Unloading at intermediate stress:

Unloading phase from intermediate stress, i.e. from the point $(\sigma_v; \varepsilon_v)$, (path C in Fig. 3.17), is similar to the path B. Equations /3.54/ are used again, but the point $(\sigma'_{1u}; \varepsilon'_{1u})$ is replaced by the point $(\sigma_v; \varepsilon_v)$.

4. Reloading at intermediate case:

In this case, (path D in Fig. 3.17), similar expressions to those for the loading phase A are used. However the initial Young's modulus E_0 is replaced by E_{r0i} defined by

$$E_{r0i} = \frac{\sigma'_{1u} - \sigma_d}{\varepsilon'_{1u} - \varepsilon_d} \quad /3.55a/$$

where the point $(\sigma_d; \varepsilon_d)$ is the point from which reloading occurs. The final expressions for the stress-strain curve and Young's modulus are then in the following form:

Stress-strain curve:

$$\frac{\sigma_i - \sigma_d}{\sigma_{ic} - \sigma_d} = \frac{n}{n - 1 + \left(\frac{\epsilon_{iu} - \epsilon_r}{\epsilon_{ic} - \epsilon_r} \right)^n} \left(\frac{\epsilon_{iu} - \epsilon_r}{\epsilon_{ic} - \epsilon_r} \right) \quad /3.55b/$$

$$n = \frac{E_{r0i} (\epsilon_{ic} - \epsilon_d)}{E_{r0i} (\epsilon_{ic} - \epsilon_d) - (\sigma_{ic} - \sigma_d)} \quad /3.55c/$$

Young's modulus:

$$E_i = \frac{\left[1 - \left(\frac{\epsilon_{iu} - \epsilon_r}{\epsilon_{ic} - \epsilon_r} \right)^n \right] n(n - 1) \left(\frac{\sigma_{ic} - \sigma_d}{\epsilon_{ic} - \epsilon_r} \right)}{\left[n - 1 + \left(\frac{\epsilon_{iu} - \epsilon_r}{\epsilon_{ic} - \epsilon_r} \right)^n \right]^2} \quad /3.55d/$$

3.5.3. Elastic-plastic models.

One of the most widely used material model are elastic-plastic constitutive equations. Similar to the previous models, these equations are usually used only for compression and mixed compression-tension loading conditions whilst for pure tension zones linear-elastic models with cracking procedures are satisfactory.

The elastic-plastic material model is based on the existence of the following functions:

- a yield function which defines under what stress conditions plastic yielding in the material starts,
- a flow rule which defines the relationship between the stresses and plastic deformations,
- a loading function which modifies the definition of the Yield

function with respect to the amount of plastic deformation. This is achieved by using a so-called hardening function.

In classical theory of plasticity the total strains are divided into two parts. The first, ${}^t\varepsilon_{ij}^E$, corresponds to elastic behavior of material (i.e. strain due to Hooke's law) and the second part, ${}^t\varepsilon_{ij}^P$, corresponds to plastic flow, i.e. ${}^t\varepsilon_{ij} = {}^t\varepsilon_{ij}^E + {}^t\varepsilon_{ij}^P$. Assuming isothermic conditions and isothermic hardening rules we can write:

$${}^t f({}^t\sigma_{ij}) - {}^t K(k) = 0 \quad \text{or}$$

$${}^t F({}^t\sigma_{ij}, {}^t K) = 0 \quad /3.56/$$

where ${}^t K(k)$ is a hardening function of an arbitrary parameter k , (usually plastic strains ${}^t\varepsilon_{ij}^P$),
 ${}^t f({}^t\sigma_{ij})$ is a Yield function (or loading surface for higher loading levels),
 ${}^t F({}^t\sigma_{ij}, {}^t K)$ is another form of the Yield function.

It should be noted that both ${}^t f({}^t\sigma_{ij})$ and ${}^t K(k)$ represent stresses and are in units of stresses.

The simplest definition of flow rule is the so-called normality rule which assumes plastic strains to be normal to the loading surface ${}^t F({}^t\sigma_{ij}, {}^t K)$, hence its name.

Mathematically this can be expressed by:

$$\delta\varepsilon_{ij}^P = {}^t\lambda \frac{\partial {}^t F}{\partial {}^t\sigma_{ij}} \quad /3.57/$$

where ${}^t\lambda$ is a scalar factor dependent on the loading history. There are some objections to the use of this flow rule for concrete because experimental evidence suggests that there is no affinity between the yield and failure surfaces. In addition con-

crete properties in compression differ from those in tension. Consequently other nonassociative and nonproportional rules have been developed (e.g. [4] and [60]). However, for the sake of simplicity, the normality rule is still used most often for concrete, without sacrificing too much accuracy.

The main problem with nonassociative rules is that they produce nonsymmetric material rigidity matrices. Nonproportional rules, in addition, assume a nonlinear form of the plastic strain definition in /3.57/.

As already mentioned the ${}^tK(k)$ function expresses hardening in the material beyond the initial yielding surface. Basically there are three possibilities (Fig. 3.18):

- 1/ Function ${}^tK(k)$ is constant, independent of the plastic state in the material and leads to a perfectly plastic material model.
- 2/ Kinematic strain hardening, in which case the volume of the yield surface is constant but the Yield function itself moves with respect to plastic strains.
- 3/ Isotropic strain hardening, when the Yield function does not move but its volume changes dependent on the plastic strains. Based on the experimental evidence it was found that for concrete this is the best choice and thus in the following this type of hardening will be used.

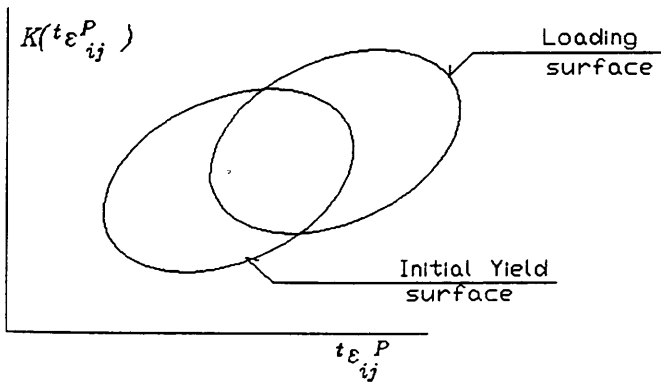
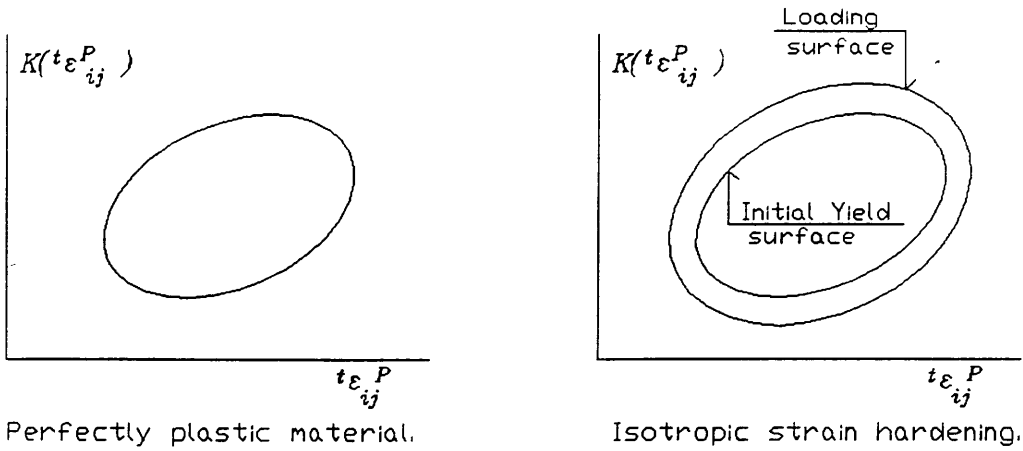


Fig. 3.18 Hardening rules.

The parameter k in the hardening function ${}^tK(k)$ represents work hardening due to plasticity and is defined by:

$$k = {}^tW_p = \int_{t_v} {}^t\sigma_{ij} (d{}^t\varepsilon_{ij}^P) dV \quad /3.58/$$

Hence if we assume ${}^t f({}^t\sigma_{ij})$ and ${}^t\varepsilon_{ij}^P$ are independent, we can write:

$${}^tK(k) = {}^tK({}^t\varepsilon_{ij}^P) \quad /3.59/$$

which states only that the hardening function is a function of plastic strains.

Because ${}^tF = 0$ and also $d{}^tF = 0$ we can write:

$$\frac{\partial {}^tF}{\partial {}^t\sigma_{ij}} \delta\sigma_{ij} + \frac{\partial {}^tF}{\partial {}^t\varepsilon_{ij}^P} \delta\varepsilon_{ij}^P = 0 \quad /3.60/$$

and using the notation

$${}^tq_{ij} = \frac{\partial {}^tF}{\partial {}^t\sigma_{ij}} \quad /3.61/$$

$${}^tp_{ij} = -\frac{\partial {}^tF}{\partial {}^t\varepsilon_{ij}^P}$$

$${}^t\underline{q}^T = [{}^tq_{11}, {}^tq_{22}, {}^tq_{33}, 2*{}^tq_{12}, 2*{}^tq_{23}, 2*{}^tq_{13}]$$

$${}^t\underline{p}^T = [{}^tp_{11}, {}^tp_{22}, {}^tp_{33}, 2*{}^tp_{12}, 2*{}^tp_{23}, 2*{}^tp_{13}] \quad /3.62/$$

we can write for the factor ${}^t\lambda$ using equation /3.57/:

$${}^t\lambda = \frac{{}^t\underline{q}^T C^E \delta\underline{\varepsilon}}{{}^t\underline{p}^T {}^t\underline{q} + {}^t\underline{q}^T C^E {}^t\underline{q}} \quad /3.63/$$

and for the stress increment $\delta\underline{\sigma}$ we can write:

$$\delta\underline{\sigma} = C^E (\delta\underline{\varepsilon} - \delta\underline{\varepsilon}^P) = C^{EP} \delta\underline{\varepsilon} \quad /3.64/$$

where C^E is elastic rigidity material matrix,

C^{EP} is elastic-plastic material matrix,

$\delta\varepsilon$ and $\delta\varepsilon^P$ are the total and plastic strain increments

respectively.

The elastic plastic matrix C^{EP} is defined by:

$$C^{EP} = C^E - \frac{C^E \underline{t}_q (C^E \underline{t}_q)^T}{\underline{p}^T \underline{t}_q + \underline{t}_q^T C^E \underline{t}_q} \quad /3.65/$$

The equations /3.64/ and /3.65/ are defined for the loading conditions, i.e.:

$$d^t f = \frac{\partial \quad {}^t f({}^t \sigma_{ij})}{\partial \quad {}^t \sigma_{ij}} d^t \sigma_{ij} > 0 \quad /3.66/$$

or the equivalent condition:

$${}^t F({}^t \sigma_{ij}, {}^{t-\Delta t} K) > 0 \quad /3.67/$$

In other cases, i.e unloading and reloading up to the maximum loading level reached before, we assume an elastic material only and hence $C^{EP} = C^E$.

The scalar product $\underline{p}^T \underline{t}_q$ is a derivative of so-called hardening function $K({}^t \epsilon_{ij}^P)$. Its basic features are best illustrated by reference to the uniaxial loading case (Fig. 3.19). It is assumed that in the elastic range, Hook's law with Young's modulus E is applicable and beyond it, E_t can be used.

$${}^t F({}^t \sigma_{ij}, {}^t K) = {}^t \sigma - K({}^t \epsilon^P) = 0$$

$$\underline{t}_q = \frac{\partial {}^t F}{\partial \sigma} = 1 ; \quad \underline{t}_p = - \frac{\partial {}^t F}{\partial \epsilon^P} = K'({}^t \epsilon^P)$$

$$K'({}^t \varepsilon_{ij}^P) = \frac{\partial \sigma}{\partial \varepsilon^P} = \frac{\partial \sigma}{\partial \varepsilon - \partial \varepsilon^E} = \frac{1}{\frac{\partial \varepsilon}{\partial \sigma} - \frac{\partial \varepsilon^E}{\partial \sigma}} = \frac{1}{\frac{1}{E_t} - \frac{1}{E}} = \frac{E_t}{1 - E_t/E}$$

/3.68/

Substituting /3.68/ into /3.65/ leads to $C^{EP} = E_t$ in the plasticity range.

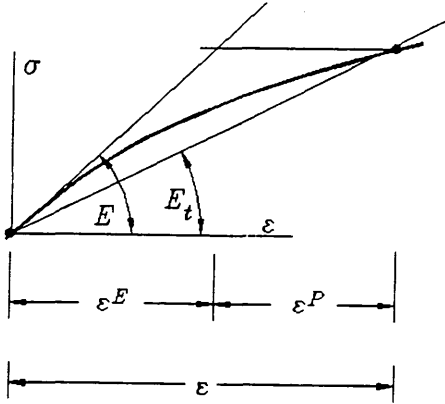


Fig. 3.19 Uniaxial case for $K'(\varepsilon^P)$.

Establishing the hardening function for a real material under multiaxial loading is a very difficult problem and hence the results from the uniaxial case are normally used. This is done by introducing an effective or generalized stress $\tilde{\sigma}^t$ and plastic strain $\tilde{\varepsilon}^P$ that represents the loading condition in the material.

$$\tilde{\sigma}^t = \sqrt{\frac{3}{2} t_{s_{ij}} t_{s_{ij}}}$$

/3.69/

$$\tilde{\varepsilon}^P = \sqrt{\frac{2}{3} t_{e_{ij}}^P t_{e_{ij}}^P}$$

where $t_{s_{ij}}$, $t_{e_{ij}}^P$ are the deviatoric stress and deviatoric plastic strain respectively.

It can be shown that for the uniaxial case ($t_{\sigma_1} \neq 0$, $t_{\sigma_2} = t_{\sigma_3} = 0$; $t_{\varepsilon_1}^P \neq 0$, $t_{\varepsilon_2}^P = t_{\varepsilon_3}^P = -\frac{1}{2} t_{\varepsilon_1}^P$ due to plastic flow) these corresponds to $\tilde{\sigma}^t$ and $\tilde{\varepsilon}^P$, the total stress and plastic strain, as follows:

$$\begin{aligned} t_{\sigma}^{\sim} &= \sqrt{\frac{3}{2} t_{s_{ij}} t_{s_{ij}}} = \sqrt{\frac{3}{2} \left\{ [t_{\sigma_1} - (t_{\sigma_1} + t_{\sigma_2} + t_{\sigma_3})/3]^2 + 2[-t_{\sigma_1}]^2 \right\}} = \\ &= t_{\sigma_1} = t_{\sigma} \end{aligned} \quad /3.70/$$

and

$$\begin{aligned} t_{\varepsilon}^{\sim P} &= \sqrt{\frac{2}{3} t_{e_{ij}^P} t_{e_{ij}^P}} = \sqrt{\frac{2}{3} \left\{ [t_{\varepsilon_1^P} - \underbrace{(t_{\varepsilon_1^P} + t_{\varepsilon_2^P} + t_{\varepsilon_3^P})/3}_{=0}]^2 + 2[-\frac{1}{2} t_{\varepsilon_1^P}]^2 \right\}} = \\ &= t_{\varepsilon_1^P} = t_{\varepsilon}^P \end{aligned} \quad /3.71/$$

Thus in practice, the hardening parameter is measured for the uniaxial test and its extrapolation to the multiaxial case is achieved by employing effective stress and effective plastic strain in place of uniaxial stress and plastic strain.

A different possible approach to extrapolate the hardening parameter from the uniaxial conditions is as follows:

From the previous definition of plastic strain (eq. /3.57/), $t_{\underline{q}}$ (eq. /3.62/) and k (eq. /3.58/) we can write:

$$t_{\varepsilon_{ij}^P} = t_{\varepsilon_{ij}^P} - \Delta t_{\varepsilon_{ij}^P} + \Delta t_{\varepsilon_{ij}^P} = t_{\varepsilon_{ij}^P} + t_{\lambda} \frac{\partial t_{\underline{F}}}{\partial t_{\sigma_{ij}}} = t_{\varepsilon_{ij}^P} + t_{\lambda} t_{\underline{q}} \quad /3.72/$$

$$k = t_{\underline{W}_P} = \int_{t_V} t_{\sigma_{ij}} (d t_{\varepsilon_{ij}^P}) dV \cong t_{\sigma} - \Delta t_{\sigma} \Delta t_{\varepsilon}^P = t_{\sigma} - \Delta t_{\sigma} t_{\lambda} t_{\underline{q}}$$

Similarly for the uniaxial case:

$$t_{\varepsilon^P} = t_{\varepsilon^P} - \Delta t_{\varepsilon^P} + \Delta t_{\varepsilon^P} = t_{\varepsilon^P} + t_{\lambda} 1$$

/3.73/

$$k = \frac{t_W}{t_V} = \int_{t_V}^{t_\sigma} (d^t \varepsilon^P) dV \cong t^{-\Delta t} \sigma \Delta^t \varepsilon^P = t^{-\Delta t} \sigma t_\lambda = f(t^{-\Delta t} \sigma) t_\lambda \quad /3.73'/$$

Hence comparing /3.73/ and /3.72/ we can write:

$$t^{-\Delta t} \sigma t_\lambda t_{\underline{q}} \cong f(t^{-\Delta t} \sigma) t_\lambda \quad \text{and}$$

$$t_\lambda \cong \frac{t^{-\Delta t} \sigma t_\lambda t_{\underline{q}}}{f(t^{-\Delta t} \sigma)} \quad /3.74/$$

Expression /3.74/ for t_λ is thereafter used directly in /3.73/ which leads to $t \varepsilon^P$ for the uniaxial case and hence we can use the hardening function $K'(t \varepsilon^P)$ for the uniaxial condition.

The program CONCRETE uses this latter approach.

It should be noted that the whole problem is nonlinear because in order to compute the stresses, we need to know the plastic strains and vice versa. Therefore all the equations above are solved step-by-step (i.e. a forward integration of the hardening function) and after several steps it is necessary to reduce the stresses back to the loading surface [1], [43]. The following number of integration steps are recommended in [43]:

$$n = 1 + \frac{8}{f'_c} \left(f(t_{\sigma_{1j}}) - f' \right) \quad /3.75/$$

where

f'_c is concrete compressive strength (positive),
 $f(t_{\sigma_{1j}})$ is the yield value for stress level computed under the assumption of elastic behavior in the current increment,
 f' is either the yield value from the previous step or for the current step when the concrete just starts to be plastic.

An example of one the simplest yield functions for concrete is the VON MISES criterion combined with the normality rules, i.e.:

$${}^tF = \frac{1}{2} {}^t s_{ij} {}^t s_{ij} - {}^tK \quad /3.76/$$

where ${}^t s_{ij}$ are the deviatoric stresses.

More complex yield functions with non-associative plastic strain flow rule are presented, for example, in [4], (for 2D case), and in [60], (for 3D case).

In this work, for plane stress, plane strain and axisymmetric analysis an elastic-plastic model is used. It comprises VON-MISES Yield condition and hardening defined similarly to /3.68/. In other words two values need to be defined for Young's modulus, one corresponding to the elastic regime (E) and one corresponding to the plastic regime (E_t).

For shell analysis a more accurate yield surface is defined by the function:

$${}^tF(I_1, J_2, {}^t\sigma_0) = \sqrt{\beta(-3J_2) + \alpha I_1} - {}^t\sigma_0 = 0 \quad /3.77/$$

where I_1 , J_2 are first and second deviatoric stress invariants,

α , β are material constants,

${}^t\sigma_0$ is the equivalent effective stress taken from the compressive stress of a uniaxial test,

and the sign of J_2 corresponds to the definition /3.1/.

Equation /3.77/ can be also expressed in terms of principal stresses by:

$$\beta \left[({}^t\sigma_1^2 + {}^t\sigma_2^2 + {}^t\sigma_3^2) - ({}^t\sigma_1 {}^t\sigma_2 + {}^t\sigma_1 {}^t\sigma_3 + {}^t\sigma_2 {}^t\sigma_3) \right] + \alpha ({}^t\sigma_1 + {}^t\sigma_2 + {}^t\sigma_3) = {}^t\sigma_0^2 \quad /3.78/$$

or in a global form as:

$$\beta \left[({}^t\sigma_{11}^2 + {}^t\sigma_{22}^2 + {}^t\sigma_{33}^2) - ({}^t\sigma_{11} {}^t\sigma_{22} + {}^t\sigma_{11} {}^t\sigma_{33} + {}^t\sigma_{22} {}^t\sigma_{33}) + 3 \left({}^t\tau_{12}^2 + {}^t\tau_{13}^2 + {}^t\tau_{23}^2 \right) \right] + \alpha ({}^t\sigma_{11} + {}^t\sigma_{22} + {}^t\sigma_{33}) = {}^t\sigma_0^2 \quad /3.79/$$

This Yield function is used for the the shell element in which ${}^t\sigma_{33}$ stress is zero, and hence its final form is:

$$\beta \left[({}^t\sigma_{11}^2 + {}^t\sigma_{22}^2) - {}^t\sigma_{11} {}^t\sigma_{22} + 3 \left({}^t\tau_{12}^2 + {}^t\tau_{13}^2 + {}^t\tau_{23}^2 \right) \right] + \alpha ({}^t\sigma_{11} + {}^t\sigma_{22}) = {}^t\sigma_0^2 \quad /3.80/$$

The material constants α , β were set according to the results of Kupfer et. al. [40] as follows:

$$\alpha = 0.355 {}^t\sigma_0 \quad /3.81/$$

$$\beta = 1.355$$

These correspond to biaxial data in which the equal biaxial compressive strength is 16% greater than the uniaxial compression strength. If we assume $\alpha = 0$ and $\beta = 1$, equation /3.80/ degrades to the VON MISES yield surface.

Substituting α and β into /3.80/ leads to the final expression:

$${}^t\sigma_0 = \gamma ({}^t\sigma_{11} + {}^t\sigma_{22}) + \left\{ \gamma^2 ({}^t\sigma_{11}^2 + {}^t\sigma_{22}^2 + 2 {}^t\sigma_{11} {}^t\sigma_{22}) + \beta \left[{}^t\sigma_{11}^2 + {}^t\sigma_{22}^2 - \right. \right.$$

$$- {}^t\sigma_{11} {}^t\sigma_{22} + 3 \left({}^t\tau_{12}^2 + {}^t\tau_{13}^2 + {}^t\tau_{23}^2 \right) \Big] \Big\}^{1/2} \quad /3.82/$$

where parameter $\gamma = \frac{\alpha}{2\sigma_0} = 0.1775$.

The resulting failure criterion and loading functions are depicted in Fig. 3.20 and Fig. 3.21 respectively.

To account for compression hardening and later strain softening effects the material model employs the conventional "Madrid Parabola" [42] for the ascending part of Fig. 3.22 and another parabolic function, derived here, for the descending part.

In the ascending part the material is assumed to be in elastic regime up to uniaxial stress $0.3f'_c$. Beyond that we can write:

$${}^t\sigma_0 = E_0 \varepsilon - \frac{1}{2} \frac{E_0}{\varepsilon_0} \varepsilon^2 \quad /3.83/$$

where E_0 is the initial elasticity modulus,

ε is total uniaxial strain, $\varepsilon \leq \varepsilon_0$,

ε_0 is total uniaxial strain at peak stress f'_c (i.e. at failure).

Substituting for elastic strain $\varepsilon^E = \frac{\sigma}{E_0}$ /3.83/, then

$${}^t\sigma_0 = - E_0 \varepsilon^P + \sqrt{2E_0^2 \varepsilon_0 \varepsilon^P} \quad /3.84/$$

for $0.3f'_c \leq {}^t\sigma_0 \leq f'_c$.

where ε^P is the plastic component of the uniaxial strain and ε_0 can be taken as $\frac{2f'_c}{E_0}$, or in other words we assume that near failure the plastic and elastic parts of strain are equal. The

function $K'(\epsilon^P)$ is derived by taking the derivative of /3.84/ with respect to plastic strain:

$$K'(\epsilon^P) = \frac{\partial \sigma_o}{\partial \epsilon^P} = E_o \left(-1 + \sqrt{\frac{\epsilon_o}{2\epsilon^P}} \right) \quad /3.85/$$

For the descending part, $\epsilon \in (\epsilon_o; \epsilon_{\max})$, another parabolic function is derived from the following requirements:

- compatibility of ascending and descending branches at strain ϵ_o ,
(functional values and their derivatives),
- for $\epsilon = \epsilon_{\max}$ must $\sigma_o = 0$.

The derivation of this parabolic function is similar to the one for the ascending branch and thus only the final equations are presented:

$$t_{\sigma_o} = \frac{-b + \sqrt{b^2 - 4ac}}{2a} \quad /3.85'/$$

where:

$$a = E_o^{-2}$$

$$b = \frac{\epsilon_{\max}^2}{f'_c} + \frac{2\epsilon^P - 4\epsilon_{\max}}{E_o}$$

$$c = \frac{4f'_c (\epsilon_{\max} - \epsilon^P)}{E_o} + (\epsilon^P)^2 - \epsilon_{\max}^2$$

and ϵ_{\max} is maximum compressive uniaxial strain in concrete. Beyond this value the material is assumed to crush resulting in zero rigidity and zero stresses. The function $K'(\epsilon^P)$ is equal to zero throughout the whole descending part.

Note that extrapolation from the uniaxial state in /3.85/ to the 3D state is performed using equations /3.74/ through /3.75/ and not by the effective stress and strain approach as expressed by equation /3.69/.

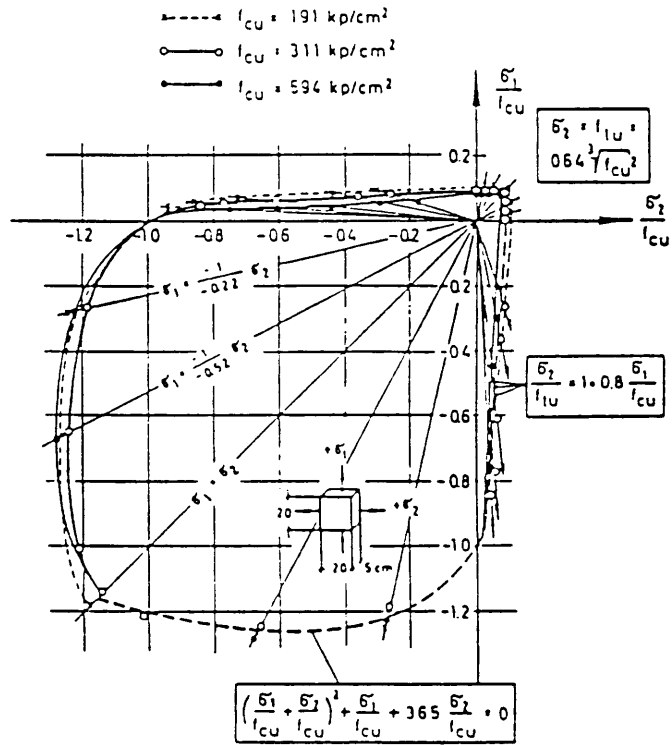


Fig. 3.20 2D representation of failure criterion in CONCRETE.

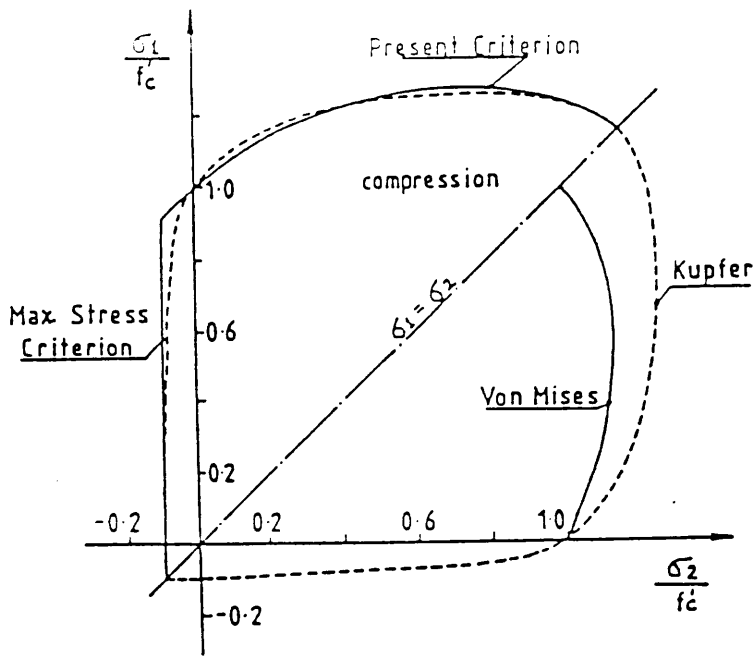


Fig. 3.21 Yield and loading functions in the program CONCRETE.

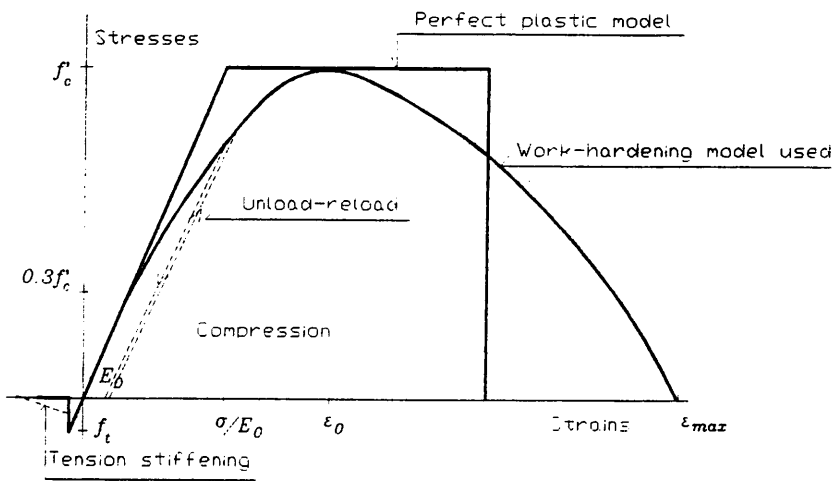


Fig. 3.22 Hardening function H' in the program CONCRETE.

3.5.4 Other types of constitutive equations.

In addition to the above constitutive equations there are many other ways of creating material models for concrete. Usually

these are more sophisticated and potentially more accurate, but careful consideration should be given as to whether a more accurate model is worthwhile or not. Sometimes inaccuracies in an analysis due to other phenomenon are more important than inaccuracies due to the material model, for example the finite element discretization, loading and boundary conditions, input material constants etc.

Generally, improvements of concrete models include the following features:

- 1/ Account is taken not only of the stress-strain condition at a particular point but also of conditions in its neighborhood.
- 2/ Unloading and reloading paths in concrete are more accurately defined.
- 3/ Account is taken of the additional factors such as creep, shrinkage, temperature and humidity effects etc.
- 4/ The behavior of concrete under dynamic conditions is included in order to carry out the dynamic analysis of reinforced concrete structures.

Among the more important work concerning more sophisticated concrete modeling are, for example, the progressive fracture model developed by DOUGILL [5], the endochronic models of SOERENSEN [6] and models presented by BAŽANT [7] based on fracture mechanics.

3.6 Constitutive models for steel.

In the previous section we were concerned with constitutive equations and failure criteria for concrete. Modeling of steel behavior is much simpler because steel is an isotropic material and its properties in the tension and compression regimes are similar. An important property of the stress-strain diagram is a relatively high ductility.

These properties make modeling of reinforcing steel

straightforward. The most widely used models for constitutive equations are piece wise linear elastic isotropic models and elastic plastic models in which the VON MISES Yield function is employed. Hardening, if accounted for, is assumed to be linear as depicted in Fig. 3.19.

Steel softening is neglected. The failure criterion is usually defined by the RANKINE Cut Off criterion or by a failure function in the shape of the VON MISES Yield function.

The fact that most reinforcing elements can be assumed as one dimensional also simplifies their modeling.

3.7 Constitutive equations for reinforced concrete.

Basically there are two methods for dealing with reinforced concrete. The first is to use so-called smeared modeling and the second is to employ discrete models.

The essential idea of the first group of models is to smear the heterogeneity caused by material failure, (e.g. cracks), within some area, which is the area usually associated with an integration point of the finite element mesh. Reinforced concrete constitutive equations are defined by superimposing concrete and steel contributions in the R/C composite. This implies the adoption of identical strains at any point in the reinforced concrete material and thus bond-slip etc. is not accounted for. Hence since material models for concrete and steel has already been specified, the constitutive equations for reinforced concrete are also defined. This approach is relatively simple and can be used to compute large and complex shaped structures. If we are interested in overall structural analysis this simplification is quite justified.

In the second group concrete and reinforcing steel are treated separately and in a different way prior and post failure. These models are called discrete models. Using the finite element

method it is necessary to employ different types of finite element for the steel bars, the surrounding concrete and also perhaps the interface elements which connect the concrete and steel. These models are accurate and can account for nearly all phenomena of a reinforced concrete composite. Unfortunately they are very computationally expensive. Thus this type of models is best restricted to local analysis or analysis of structural details. An additional disadvantage is that different types of finite element are needed for modeling cracks, crushed zones and so on. This implies that we must a priori specify where the failure zones will occur and if purely estimated the results of a long analysis can be nonsense. Hence due to the type of the present analysis, the computational demands and the above difficulties of discrete models, in this work the first group, i.e. smeared models, is preferred.

3.8 Material and failure models used in programs NONSAP and CONCRETE.

In summary a brief overview will be now given of the models used in this work including an explanation why these models were employed.

Both NONSAP and CONCRETE use smeared type constitutive equations in which the response of reinforced concrete is evaluated by superimposing concrete and steel responses. No bond slip between concrete and reinforcement is accounted for.

NONSAP.

Concrete:

The piece wise linear constitutive equations defined in Sec. 3.4 were used to model concrete behavior. This model is supplemented by the Mohr-Coulomb and Rankine Cut-Off failure

criteria (Sec. 3.2.2) and the tension stiffening model /d/ (eq. /3.35/-/3.37/).

After crushing no material rigidity and stresses are assumed. The post-cracking regime is governed by a tension stiffening law and only one set of cracks in a fixed direction, parallel to the maximum principal stress when the crack occurred, is defined. For cases when part crushing and part cracking failure occur the crushing coefficient is used (Sec. 3.3.4).

In addition the elastic plastic model with hardening was already available in the NONSAP library of material models, including the VON MISES Yield function.

Steel:

Reinforcement is modeled by one dimensional steel element for which piece wise linear constitutive equations are used. Shear effects are neglected and hence no dowel is accounted for.

These material models have been incorporated into NONSAP because of their simplicity. It is considered that NONSAP is created primarily for dynamic analyses and thus no sophisticated and time consuming models are feasible.

CONCRETE.

Concrete:

Concrete is modeled by elastic plastic constitutive equations, (Sec. 3.5.3). The Yield function and subsequent loading surfaces are defined by eq. /3.82/. Failure conditions are determined by expressions presented in Sec. 3.3.3. After crushing no material stresses and rigidity are assumed. For tension regimes, the Rankine Cut-Off criterion is used and the cracking regime is governed by the the stiffening model /b (eq. /3.27/-/3.31/). The fixed crack approach is used with the second set of cracks being perpendicular to the first one. The hardening and softening para-

bolos (eqs. /3.85/ ,/3.85'/) in compression were also implemented.

Steel:

Reinforcement is modeled by layers consisting of smeared uniaxial steel bars. For constitutive equations the elastic plastic model with linear hardening is used.

Most of these constitutive equations were already in the original version of the program. In this work compression hardening and softening were implemented to improve the high compression regime behavior. Collective experience proves this model to be a good compromise between computational cost and resulting accuracy.

4. TWO DIMENSIONAL AXISYMETRIC, PLANE STRESS AND PLANE STRAIN ELEMENTS.

This Chapter presents the complete formulation for two the dimensional isoparametric bilinear and biquadratic elements used in this work. Interest will focus on the overall formulation of element matrices pertaining to the element geometry. The isoparametric formulation of one, two and three dimensional elements belongs to "classic" element formulations. This is not because of its superior properties but due to the fact that it is a versatile and general approach and, also important, easy to understand. Some other types of element provide more accurate results, especially when restricted to static analysis. For example the family of hybrid elements usually give much better results for the stress fields. Nevertheless, isoparametric elements are used frequently because they contain no hidden difficulties, and are robust and reliable in use. This is very important in nonlinear analysis because there are usually problems enough, for example with material modeling, and it is undesirable to mix this sort of problem with, for instance, the fact that geometric equations are satisfied only in integral form (Hellinger-Reissner principle) etc.

The first part of this Chapter deals with the basic geometry of the elements, particularly the geometric and displacement approximations. The second part uses these to develop the complete formulation. Here we will follow the concepts of Chapter two, including notation.

It should be noted there is little difference in the formulation of plane stress and plane strain elements, the only difference being the material rigidity matrix. This was presented in Chapter three and will not be repeated here. For the axisymmetric element, the situation is more complex. Generally the coordinates x and y in plane stress/strain analysis correspond to coordinates r (radial) and s (parallel to axis of rotation) respectively and terms due to ϵ_{33} (circumferential direction) will be given separately.

For the sake of generality, both total and updated Lagrangian formulation will be discussed. The choice of which of them is more suitable for a particular analysis depends on the form of constitutive equations used.

4.1 Geometry and displacement approximation.

In isoparametric formulation the approximation of element geometry and displacements is identical. This is not the general case, however, because some elements use one approximation for geometry and a different approximation for displacement fields (e.g. semi-loof elements).

Let us consider the quadrilateral nine point element depicted in Fig. 4.1.

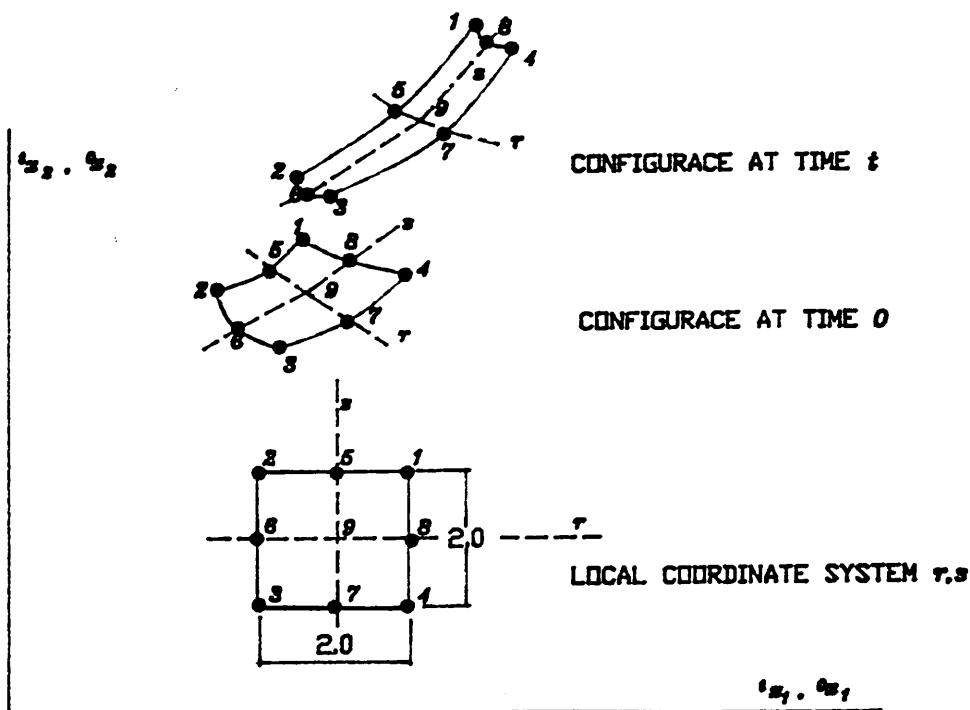


Fig 4.1. Two dimensional element, natural and global coordinate systems.

The approximation functions are constructed in such a way that only the four corner nodes and their corresponding modal shapes are mandatory. All other nodes can be, but need not be, incorporated.

If only four nodes are used, the element is bilinear, whilst a complete nine point definition corresponds to the biquadratic formulation including a "bubble" function in the centre of the element. This versatility of formulation is very advantageous because it allows mesh refining or use of more coarse divisions in some areas.

The main idea of coordinate approximation within the element is given by:

$$t_{x_1} = \sum_{k=1}^N h_k t_{x_1}^k$$

$$t_{x_2} = \sum_{k=1}^N h_k t_{x_2}^k$$

/4.1/

where h_k is a shape function corresponding to node k ,

$t_{x_1}^k, t_{x_2}^k$ are coordinates x_1 and x_2 of joint k at time t ,

t_{x_1}, t_{x_2} are coordinate of an arbitrary point within the element,

N is the number of element nodes.

The main idea of isoparametric formulation is to map the coordinate system x_1, x_2 to a natural coordinate system r, s , (see Figure 4.1), where an element of any original shape, including curved boundaries, is transformed to a regular quadrilateral with straight boundaries of size of 2×2 units. For example $t_{x_1}^1, t_{x_2}^1$ are transformed to $r_1 = 1, s_1 = 1$, $t_{x_1}^2, t_{x_2}^2$ to $r_2 = -1, s_2 = 1$ etc. This approach allows the element formulation to be independent of the original element shape.

The construction of the interpolation functions h_k is as follows:

- 1/ every function h_k must be equal to one for r, s corresponding to node k ,
- 2/ every function h_k must be equal to zero for r, s corresponding to any other element node.

As already mentioned, the four corner nodes and their modes are always incorporated. The expressions for the bilinear case are given by:

$$h_1 = \frac{1}{4} (1 + r)(1 + s)$$

$$h_2 = \frac{1}{4} (1 - r)(1 + s)$$

/4.2/

$$h_3 = \frac{1}{4} (1 - r)(1 - s)$$

$$h_4 = \frac{1}{4} (1 + r)(1 - s)$$

Now let us add, for example, the shape mode corresponding to node five which is located in the center between nodes one and two, (see Fig. 4.1):

In order to satisfy the condition that h_5 is equal to zero at points one through four, and at the same time equal to one at joint five, it is necessary to use a quadratic function in the r -direction whilst a linear function is sufficient in the s -direction. Hence the expression for h_5 is given by:

$$h_5 = \frac{1}{2} (1 - r^2)(1 + s) \quad /4.3/$$

It is easy to check that both the above constraints are satisfied by h_3, h_4 and h_5 , but the second constraint is violated by the previous definitions (4.2) for h_1 and h_2 for the new node five. The remedy is to subtract their values given by h_5 at node 5 from their values, (i.e. a half of h_5). Hence, including node five, the definition for h_1 and h_2 is as follows:

$$h_1 = \frac{1}{4} (1 + r)(1 + s) - \frac{1}{2} h_5 \quad /4.4/$$

$$h_2 = \frac{1}{4} (1 - r)(1 + s) - \frac{1}{2} h_5$$

Generally if we introduce any new node to the element approximation, the new shape function must satisfy the two constraints and thus for all previously defined nodes everything is satisfactory. Thereafter every previously defined function must be checked with respect to the new node. If its value is zero then no correction is required. If it is not zero, the value is zeroed by adding the appropriate fraction of the mode shape which corresponds to the newly introduced node.

This process is simply checked. The sum of all the incorporated shape functions at any point of the element must always be one, mathematically expressed by:

$$\sum_{k=1}^N h_k(r,s) = 1 \quad /4.5/$$

where r, s are coordinates of arbitrary element point.

Using this concept all nine interpolation functions are presented in Table 4.1. Note again that h_1 through h_4 are mandatory while h_5 through h_9 are optional. If any of the latter is used, the appropriate correction of previous functions must be made. Fig. 4.2 illustrate some of the mode shapes for h_1 . This concept of the natural coordinate system h_1 is sometimes called hierarchical natural coordinate system.

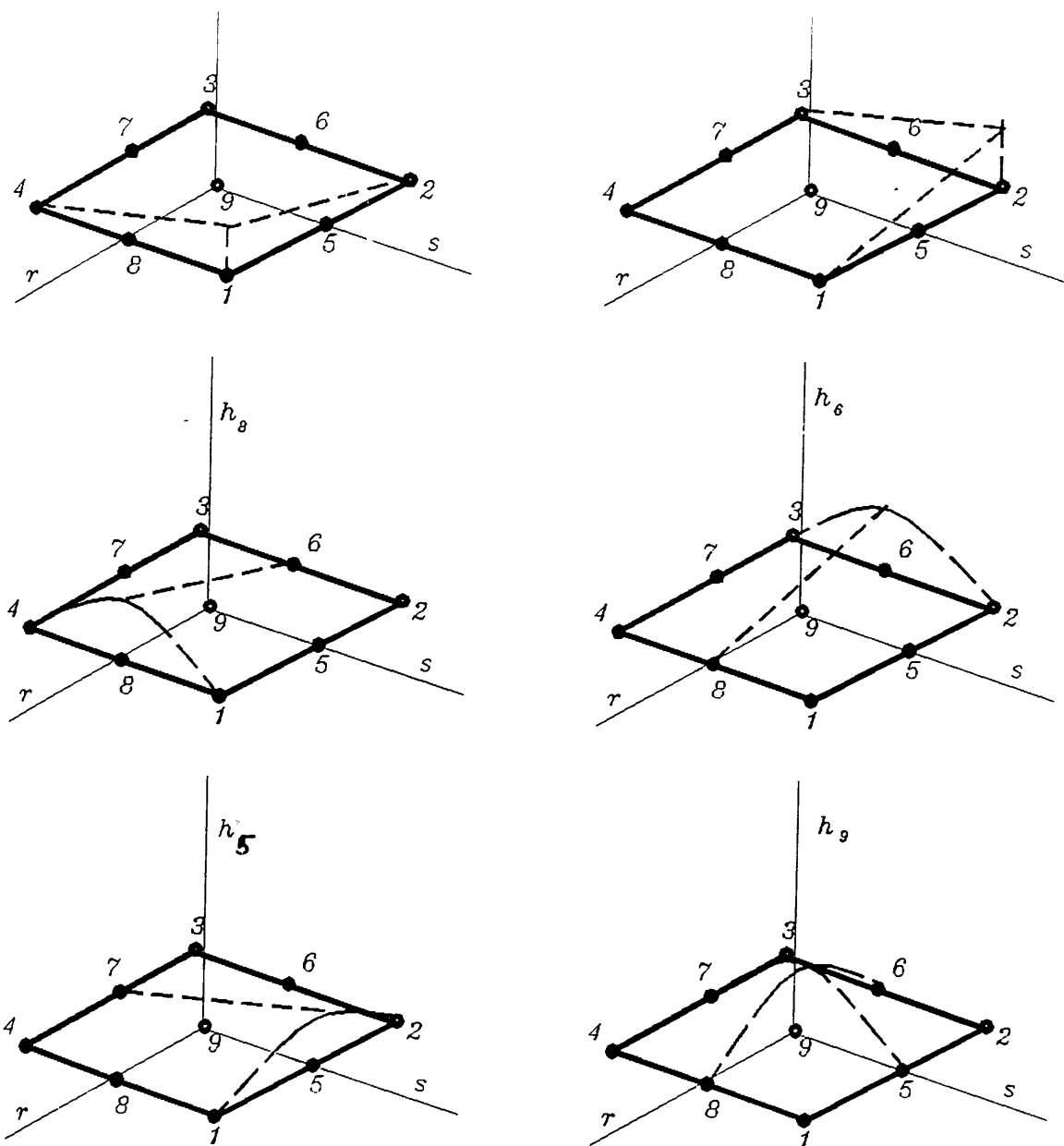


Fig. 4.2 Examples of some interpolation functions h_i .

No	Function	Additional correction in node j if defined:				
		$j=5$	$j=6$	$j=7$	$j=8$	$j=9$
h_1	$\frac{1}{4}(1+r)(1+s)$	$-\frac{1}{2}h_5$			$-\frac{1}{2}h_8$	$\frac{1}{4}h_9$
h_2	$\frac{1}{4}(1-r)(1+s)$	$-\frac{1}{2}h_5$	$-\frac{1}{2}h_6$			$\frac{1}{4}h_9$
h_3	$\frac{1}{4}(1-r)(1-s)$		$-\frac{1}{2}h_6$	$-\frac{1}{2}h_7$		$\frac{1}{4}h_9$
h_4	$\frac{1}{4}(1+r)(1-s)$			$-\frac{1}{2}h_7$	$-\frac{1}{2}h_8$	$\frac{1}{4}h_9$
h_5	$\frac{1}{2}(1-r^2)(1+s)$					$-\frac{1}{2}h_9$
h_6	$\frac{1}{2}(1-r)(1-s^2)$					$-\frac{1}{2}h_9$
h_7	$\frac{1}{2}(1-r^2)(1-s)$					$-\frac{1}{2}h_9$
h_8	$\frac{1}{2}(1+r)(1-s^2)$					$-\frac{1}{2}h_9$
h_9	$(1-r^2)(1-s^2)$					

Tab. 4.1 Interpolation functions for 2D element.

For displacements and displacement increments, exactly identical approximation functions are used. So analogous to /4.1/ we can define:

$${}^t u_1 = \sum_{k=1}^N h_k {}^t u_1^k \quad /4.6/$$

$${}^t u_2 = \sum_{k=1}^N h_k {}^t u_2^k$$

$$u_1 = \sum_{k=1}^N h_k u_1^k \quad /4.7/$$

$$u_2 = \sum_{k=1}^N h_k u_2^k$$

where ${}^t u_j^k, u_j^k$ ($j = 1, 2$) are the displacements and displacement increments, respectively for coordinate j at joint k and time t . Hence the simplicity of this formulation.

Both displacement and geometry of the element are defined by functions of the local coordinates r and s . The relationship between r, s and ${}^t x_1, {}^t x_2$ is given by /4.1/. To calculate element matrices we also need to derive expressions for the derivatives of displacement with respect to original coordinate system ${}^t x_1, {}^t x_2$.

It is easy to calculate the derivatives with respect to natural coordinate system r, s . Let us assume we have some function $f({}^t x_1, {}^t x_2)$ defined in r, s coordinate system so that we know its derivatives with respect to these local coordinates, i.e. $\frac{\partial f(r,s)}{\partial r}$ and $\frac{\partial f(r,s)}{\partial s}$.

Now $\frac{\partial f({}^t x_1, {}^t x_2)}{\partial {}^t x_1}$ and $\frac{\partial f({}^t x_1, {}^t x_2)}{\partial {}^t x_2}$ can be expressed by:

$$\frac{\partial f({}^t x_1, {}^t x_2)}{\partial {}^t x_1} = \frac{\partial f(r,s)}{\partial r} \frac{\partial r}{\partial {}^t x_1} + \frac{\partial f(r,s)}{\partial s} \frac{\partial s}{\partial {}^t x_1}$$

/4.8/

$$\frac{\partial f({}^t x_1, {}^t x_2)}{\partial {}^t x_2} = \frac{\partial f(r,s)}{\partial r} \frac{\partial r}{\partial {}^t x_2} + \frac{\partial f(r,s)}{\partial s} \frac{\partial s}{\partial {}^t x_2}$$

These can be used to express derivatives with respect to the original coordinates ${}^t x_1, {}^t x_2$ as follows:

$$\frac{\partial f(r,s)}{\partial r} = \frac{\partial {}^t x_1}{\partial r} \frac{\partial f({}^t x_1, {}^t x_2)}{\partial {}^t x_1} + \frac{\partial {}^t x_2}{\partial r} \frac{\partial f({}^t x_1, {}^t x_2)}{\partial {}^t x_2}$$

/4.9/

$$\frac{\partial f(r,s)}{\partial s} = \frac{\partial^t x_1}{\partial s} \frac{\partial f(t x_1, t x_2)}{\partial^t x_1} + \frac{\partial^t x_2}{\partial s} \frac{\partial f(t x_1, t x_2)}{\partial^t x_2}$$

Hence:

$$\frac{\partial f(t x_1, t x_2)}{\partial^t x_1} = J^{-1} \left(\frac{\partial^t x_2}{\partial s} \frac{\partial f(r,s)}{\partial r} - \frac{\partial^t x_2}{\partial r} \frac{\partial f(r,s)}{\partial s} \right)$$

/4.10/

$$\frac{\partial f(t x_1, t x_2)}{\partial^t x_2} = J^{-1} \left(-\frac{\partial^t x_1}{\partial s} \frac{\partial f(r,s)}{\partial r} + \frac{\partial^t x_1}{\partial r} \frac{\partial f(r,s)}{\partial s} \right)$$

$$\text{where } J = \det \begin{bmatrix} \frac{\partial^t x_1}{\partial r} & \frac{\partial^t x_2}{\partial r} \\ \frac{\partial^t x_1}{\partial s} & \frac{\partial^t x_2}{\partial s} \end{bmatrix} = \frac{\partial^t x_1}{\partial r} \frac{\partial^t x_2}{\partial s} - \frac{\partial^t x_2}{\partial r} \frac{\partial^t x_1}{\partial s}$$

J is sometimes called the Jacobian of transformation and is important because its value is equal to the area of element. Thus if we know the derivatives with respect to the local coordinate system, those with respect to the global system are simply calculated.

Note, that in the case of axisymmetric elements, the third direction (circumferential) is treated directly.

4.2 Element matrices assembly.

The general incremental continuum mechanics equations were presented in Chapter two and form the basis of general nonlinear displacement finite element analysis. Now using the expressions from the last section and invoking the principle of virtual dis-

placements the governing finite element equations will be formulated.

Problem formulation is similar to linear analysis, the only differences being that the final equations are assembled for load increments only and are based on the 2nd Piola-Kirchhoff (stress) and Green-Lagrange (deformation) tensors for Total Lagrangian formulation and on Cauchy (stress) and Almansi (deformation) tensors for the Updated Lagrangian formulation.

These tensors have already been defined in Chapter two. The objective here is to discretize the previously presented expressions.

All expressions will first be defined using Total Lagrangian formulation, after which they will be modified for Updated Lagrange formulation. We assume only static condition, but extensions to dynamics are obvious.

Total Lagrangian formulation.

The main governing equations take the form:

$$\left(\begin{matrix} t \\ 0 \end{matrix} \mathbf{K}_L + \begin{matrix} t \\ 0 \end{matrix} \mathbf{K}_{NL} \right) \Delta \underline{u}^{(i)} = \begin{matrix} t+\Delta t \\ 0 \end{matrix} \underline{R} - \begin{matrix} t+\Delta t \\ 0 \end{matrix} \underline{F}^{(i-1)} \quad /4.11/$$

where $\begin{matrix} t \\ 0 \end{matrix} \mathbf{K}_L$ is the linear part of stiffness matrix,

$\begin{matrix} t \\ 0 \end{matrix} \mathbf{K}_{NL}$ is the nonlinear part of stiffness matrix,

$\Delta \underline{u}^{(i)} = \underline{u}^{(i)} - \underline{u}^{(i-1)}$ is the displacement increment in the i -th iteration,

$\begin{matrix} t+\Delta t \\ 0 \end{matrix} \underline{R}$ is the loading vector applied at time $t + \Delta t$ (total),

$\begin{matrix} t+\Delta t \\ 0 \end{matrix} \underline{F}^{(i-1)}$ is the vector of nodal point forces equivalent to the internal stresses from previous iterations.

The following correspondence exists between analytical and discretized expressions:

$$\int_{\circ_V} {}^0 C_{ijrs} {}^0 e_{rs} \delta_0 e_{ij} {}^0 dV \approx {}^0 K_L \Delta \underline{u}^{(1)}$$

$${}^0 K_L = \int_{\circ_V} {}^0 B_L^T {}^0 C {}^0 B_L {}^0 dV$$

/4.12/

$$\int_{\circ_V} {}^0 S_{ij} \delta_0 \eta_{ij} {}^0 dV \approx {}^0 K_{NL} \Delta \underline{u}^{(1)}$$

$${}^0 K_{NL} = \int_{\circ_V} {}^0 B_{NL}^T {}^0 S {}^0 B_{LN} {}^0 dV$$

and finally

$$\int_{\circ_V} {}^0 S_{ij} \delta_0 e_{ij} {}^0 dV \approx {}^0 F = \int_{\circ_V} {}^0 B_L^T {}^0 \underline{S} {}^0 dV$$

where the notation is identical to Chapter two.

Expressions for ${}^0 B_L^T$, ${}^0 B_{NL}^T$, ${}^0 \underline{S}$ etc., pertaining to an element, will now be derived.

Starting with incremental strains, then:

$$\begin{aligned} {}^0 \varepsilon_{11} = & {}^0 u_{1,1} + {}^0 u_{1,1} {}^0 u_{1,1} + {}^0 u_{2,1} {}^0 u_{2,1} + \\ & + \frac{1}{2} \left[({}^0 u_{1,1})^2 + ({}^0 u_{2,1})^2 \right] \end{aligned} \quad /4.13 /$$

$$\begin{aligned} {}^0 \varepsilon_{22} = & {}^0 u_{2,2} + {}^0 u_{1,2} {}^0 u_{1,2} + {}^0 u_{2,2} {}^0 u_{2,2} + \\ & + \frac{1}{2} \left[({}^0 u_{1,2})^2 + ({}^0 u_{2,2})^2 \right] \end{aligned}$$

$$\begin{aligned} {}^0 \varepsilon_{12} = & \frac{1}{2} \left[{}^0 u_{1,2} + {}^0 u_{2,1} \right] + \frac{1}{2} \left[{}^0 u_{1,1} {}^0 u_{1,2} + {}^0 u_{2,1} {}^0 u_{2,2} + \right. \\ & + {}^0 u_{1,2} {}^0 u_{1,1} + {}^0 u_{2,2} {}^0 u_{2,1} \left. \right] + \frac{1}{2} \left[({}^0 u_{1,1} {}^0 u_{1,2}) + \right. \\ & \left. + ({}^0 u_{2,1} {}^0 u_{2,2}) \right] \end{aligned}$$

$${}^0\varepsilon_{33} = \frac{u_1}{{}^0x_1} + \frac{{}^t u_1 u_1}{({}^0x_1)^2} + \frac{1}{2} \left(\frac{u_1}{{}^0x_1} \right)^2 \quad (\text{for axisymmetric analysis only})$$

where:

${}^t u_{i,j}$, ${}^0 u_{i,j}$ are the derivatives with respect to j coordinate, $({}^0x_j)$, of the i -th element of the displacement vector and its increment respectively at time t , all measured in the original, undeformed coordinate system, and

${}^0\varepsilon_{ij}$ is the increment of element (i,j) of the Green-Lagrange strain tensor, again in the original coordinate system.

The linear strain-displacement transformation matrix takes the form:

$${}^0\mathbf{e} = {}^t\mathbf{B}_{0L} \Delta\mathbf{u}$$

where

$${}^0\mathbf{e} = \left[{}^0e_{11}; {}^0e_{22}; {}^0e_{12}; {}^0e_{33} \right]^T \quad \text{is the linear part of the strain increment,}$$

and

$$\Delta\mathbf{u} = \Delta\mathbf{u}^{(1)} = \left[u_1^1; u_2^1; u_1^2; u_2^2; u_1^3; u_2^3; \dots u_1^N; u_2^N \right] \text{ are displacement increments.}$$

N is the number of element nodes (4 through 9).

The matrix ${}^t\mathbf{B}_{0L}$ is divided into two parts:

$${}^t\mathbf{B}_{0L} = {}^t\mathbf{B}_{0L1} + {}^t\mathbf{B}_{0L2}$$

/4.14/

The first matrix is given by:

$${}^t\mathbf{B}_{0L1} =$$

$$= \begin{bmatrix} {}_0^h h_{1,1}; 0 & ; & {}_0^h h_{2,1}; 0 & ; & {}_0^h h_{3,1}; 0 & ; & \dots & ; & {}_0^h h_{N,1}; 0 \\ 0 & ; & {}_0^h h_{1,2}; 0 & ; & {}_0^h h_{2,2}; 0 & ; & {}_0^h h_{3,2}; & \dots & ; & 0 & ; & {}_0^h h_{N,2} \\ {}_0^h h_{1,2}; {}_0^h h_{1,1}; {}_0^h h_{2,2}; {}_0^h h_{2,1}; {}_0^h h_{3,2}; {}_0^h h_{3,1}; & \dots & ; & {}_0^h h_{N,2}; {}_0^h h_{N,1} \\ \frac{h_1}{{}_0^- x_1} & ; & 0 & ; & \frac{h_2}{{}_0^- x_1} & ; & 0 & ; & \frac{h_3}{{}_0^- x_1} & ; & 0 & ; & \dots & ; & \frac{h_N}{{}_0^- x_1} & ; & 0 \end{bmatrix}$$

where ${}_0^h h_{k,j} = \frac{\partial h_k}{\partial {}_0^- x_j}$,

$$u_j^k = {}^{t+\Delta t} u_j^k - {}^t u_j^k,$$

and ${}_0^- x_1 = \sum_{k=1}^N h_k {}_0^k x_1^k$.

The second part of ${}^t B_{0L}$ is given by:

$${}^t B_{0L2} =$$

/4.15/

$$\begin{bmatrix} l_{11} {}_0^h h_{1,1} & & ; & l_{21} {}_0^h h_{1,1} & & ; & \dots \\ l_{12} {}_0^h h_{1,2} & & ; & l_{22} {}_0^h h_{1,2} & & ; & \dots \\ \left(l_{11} {}_0^h h_{1,2} + l_{12} {}_0^h h_{1,1} \right); & \left(l_{21} {}_0^h h_{1,2} + l_{22} {}_0^h h_{1,1} \right); & & \dots \\ l_{33} \frac{h_1}{{}_0^- x_1} & & ; & 0 & & ; & \dots \end{bmatrix}$$

$$\left. \begin{array}{l}
 \dots ; l_{11} \begin{matrix} h \\ 0 \end{matrix}_{N,1} \qquad \qquad \qquad ; l_{21} \begin{matrix} h \\ 0 \end{matrix}_{N,1} \\
 \dots ; l_{12} \begin{matrix} h \\ 0 \end{matrix}_{N,2} \qquad \qquad \qquad ; l_{22} \begin{matrix} h \\ 0 \end{matrix}_{N,2} \\
 \dots ; \left(l_{11} \begin{matrix} h \\ 0 \end{matrix}_{N,2} + l_{12} \begin{matrix} h \\ 0 \end{matrix}_{N,1} \right) ; \left(l_{21} \begin{matrix} h \\ 0 \end{matrix}_{N,2} + l_{22} \begin{matrix} h \\ 0 \end{matrix}_{N,1} \right) \\
 \dots ; l_{33} \frac{h_N}{0_{X_1}} \qquad \qquad \qquad ; 0
 \end{array} \right]$$

where

$$l_{11} = \sum_{k=1}^N \begin{matrix} h \\ 0 \end{matrix}_{k,1} \begin{matrix} t \\ u \end{matrix}_1^k$$

$$l_{22} = \sum_{k=1}^N \begin{matrix} h \\ 0 \end{matrix}_{k,2} \begin{matrix} t \\ u \end{matrix}_2^k$$

$$l_{21} = \sum_{k=1}^N \begin{matrix} h \\ 0 \end{matrix}_{k,1} \begin{matrix} t \\ u \end{matrix}_2^k$$

$$l_{12} = \sum_{k=1}^N \begin{matrix} h \\ 0 \end{matrix}_{k,2} \begin{matrix} t \\ u \end{matrix}_1^k$$

$$l_{33} = \frac{\sum_{k=1}^N \begin{matrix} h \\ 0 \end{matrix}_{k,1} \begin{matrix} t \\ u \end{matrix}_1^k}{0_{X_1}}$$

The nonlinear strain-displacement transformation matrix takes the form:

$${}^t_{0NL}{}^B = \quad /4.16/$$

$$= \begin{bmatrix} {}_0h_{1,1}; 0 & ; {}_0h_{2,1}; 0 & ; {}_0h_{3,1}; 0 & ; \dots & ; {}_0h_{N,1}; 0 \\ {}_0h_{1,2}; 0 & ; {}_0h_{2,2}; 0 & ; {}_0h_{3,2}; 0 & ; \dots & ; {}_0h_{N,2}; 0 \\ 0 & ; {}_0h_{1,1}; 0 & ; {}_0h_{2,1}; 0 & ; {}_0h_{3,1}; 0 & ; \dots & ; 0 & ; {}_0h_{N,1} \\ 0 & ; {}_0h_{1,2}; 0 & ; {}_0h_{2,2}; 0 & ; {}_0h_{3,2}; 0 & ; \dots & ; 0 & ; {}_0h_{N,2} \\ \frac{{}_0h_1}{{}_0x_1} & ; 0 & ; \frac{{}_0h_2}{{}_0x_1} & ; 0 & ; \frac{{}_0h_3}{{}_0x_1} & ; 0 & ; \dots & ; \frac{{}_0h_N}{{}_0x_1} & ; 0 \end{bmatrix}$$

The 2nd Piola Kirchoff stress matrix and tensors take the form:

$${}^t_0\mathbf{S} = \begin{bmatrix} {}^t_0S_{11}; & {}^t_0S_{12}; & 0 & ; & 0 & ; & 0 \\ {}^t_0S_{21}; & {}^t_0S_{22}; & 0 & ; & 0 & ; & 0 \\ 0 & ; & 0 & ; & {}^t_0S_{11}; & {}^t_0S_{12} & 0 \\ 0 & ; & 0 & ; & {}^t_0S_{21}; & {}^t_0S_{22}; & 0 \\ 0 & ; & 0 & ; & 0 & ; & 0 & ; & {}^t_0S_{33} \end{bmatrix} ; \quad {}^t_0\underline{\mathbf{S}} = \begin{bmatrix} {}^t_0S_{11} \\ {}^t_0S_{22} \\ {}^t_0S_{12} \\ {}^t_0S_{33} \end{bmatrix}$$

/4.17/

All derivatives are with respect to the original coordinate system. Since the expressions are in the r, s natural coordinate system, it is necessary to differentiate using equations /4.10/.

Loading terms take form:

$$\int_{0V} {}^{t+\Delta t}{}^B_{0f_i} \delta u_i \, {}^0dV + \int_{0A} {}^{t+\Delta t}{}^A_{0f_i} \delta u_i \, {}^0dA \approx {}^{t+\Delta t}\underline{\mathbf{R}}$$

where

/4.18/

$${}^{t+\Delta t}\underline{\mathbf{R}} = \int_{0V} \mathbf{H}^T {}^{t+\Delta t}{}^B_{0f} \, {}^0dV + \int_{0A} \left(\mathbf{H}^s \right)^T {}^{t+\Delta t}{}^A_{0f} \, {}^0dA$$

H^S , H are surface and volume interpolation matrices, and ${}^{t+\Delta t}f_o^B$, ${}^{t+\Delta t}f_o^A$ are vectors of body and surface forces defined per unit volume and surface respectively.

The structure of H^S and H is trivial and therefore are not given explicitly. Their rows consist of interpolation functions h_j .

As discussed in Chapter two the Total formulation leads to more sophisticated expressions for the calculation of the Green-Lagrange strain tensor, but also uses the 2nd Piola Kirchhoff tensor which has no physical meaning. Thus if we are interested in real stresses, we must transform them to the Cauchy stress tensor. On the other hand, the linear part of the stiffness matrix is computed only once and stays constant through all subsequent computation.

This completes the definition of the Total Lagrangian formulation. The Updated Lagrangian formulation is presented next.

Updated Lagrangian formulation.

In the Updated formulation the coordinate system is defined by the original coordinates increased by the total displacements from the previous solution (iterations).

It is easier to calculate the Green-Lagrange strain tensor, because ${}^t u_{1,j}$ are zero. Also the 2nd Piola Kirchhoff tensor is identical to the Cauchy tensor (with respect to the t configuration the structure is not deformed) and no transformation is necessary. This is very important when we have to use constitutive equations defined in engineering stresses and strains. The penalty is that all computations must be repeated in every iteration.

The main governing equations take the form:

$$({}^t K_L + {}^t K_{NL}) \Delta \underline{u}^{(i)} = {}^{t+\Delta t} \underline{R} - {}^{t+\Delta t} \underline{F}^{(i-1)} \quad /4.19/$$

where ${}^t K_L$ is the linear part of the stiffness matrix,

${}^t\mathbf{K}_L$ is the nonlinear part of the stiffness matrix,

$\Delta \underline{u}^{(i)} = \underline{u}^{(i)} - \underline{u}^{(i-1)}$ is the displacement increment in the i -th iteration,

${}^{t+\Delta t}\underline{R}$ is loading the vector applied at time $t + \Delta t$ (total),

${}^{t+\Delta t}\underline{F}^{(i-1)}$ is the vector of nodal point forces equivalent to the internal stresses from previous iterations.

The following correspondence exists between analytical and discretized expressions:

$$\int_{t_V} {}^t C_{ijrs} {}^t e_{rs} \delta {}^t e_{ij} {}^t dV \approx {}^t \mathbf{K}_L \Delta \underline{u}^{(i)}$$

$${}^t \mathbf{K}_L = \int_{t_V} {}^t \mathbf{B}_L^T {}^t \mathbf{C} {}^t \mathbf{B}_L {}^t dV$$

and

/4.20/

$$\int_{t_V} {}^t \tau_{ij} \delta {}^t \eta_{ij} {}^t dV \approx {}^t \mathbf{K}_{NL} \Delta \underline{u}^{(i)}$$

$${}^t \mathbf{K}_{NL} = \int_{t_V} {}^t \mathbf{B}_{NL}^T {}^t \boldsymbol{\tau} {}^t \mathbf{B}_{LN} {}^t dV$$

$$\int_{t_V} {}^t \tau_{ij} \delta {}^t e_{ij} {}^t dV \approx {}^t \underline{F} = \int_{t_V} {}^t \mathbf{B}_L^T {}^t \boldsymbol{\tau} {}^t dV$$

where the notation is identical to Chapter two.

Expressions for ${}^t \mathbf{B}_L^T$, ${}^t \mathbf{B}_{NL}^T$, $\boldsymbol{\tau}$ etc., pertaining to an element will now be derived:

Starting with incremental strains then

$${}^t \varepsilon_{11} = {}^t u_{1,1} + \frac{1}{2} \left[({}^t u_{1,1})^2 + ({}^t u_{2,1})^2 \right] \quad /4.21/$$

$${}^t \varepsilon_{22} = {}^t u_{2,2} + \frac{1}{2} \left[({}^t u_{1,2})^2 + ({}^t u_{2,2})^2 \right]$$

$${}^t \varepsilon_{12} = \frac{1}{2} \left[{}^t u_{1,2} + {}^t u_{2,1} \right] + \frac{1}{2} \left[({}^t u_{1,1} {}^t u_{1,2}) + ({}^t u_{2,1} {}^t u_{2,2}) \right]$$

$${}^t \varepsilon_{33} = \frac{u_1}{t_{x_1}} + \frac{1}{2} \left(\frac{u_1}{t_{x_1}} \right)^2 \quad \text{(for axisymmetric analysis only)}$$

where:

${}^t u_{i,j}$, ${}^t u_{1,j}$ are derivatives with respect to j coordinate, $({}^t x_j)$, of the i -th element of the displacement vector and its increment respectively at time t , all measured in deformed coordinate system, (pertaining to the previous iteration),

${}^t \varepsilon_{ij}$ is increment of (i,j) element of Green-Lagrange strain tensor, again in the deformed coordinate system.

The linear strain-displacement transformation matrix takes the form:

$${}^t e = {}^t B_L \Delta \underline{u}$$

where

$${}^t e = \left[{}^t e_{11}; {}^t e_{22}; 2 {}^t e_{12}; {}^t e_{33} \right]^T \quad \text{is the linear part of the strain increment,}$$

and

$$\Delta \underline{u} = \Delta \underline{u}^{(i)} = \left[u_1^1; u_2^1; u_1^2; u_2^2; u_1^3; u_2^3; \dots u_1^N; u_2^N \right] \text{ are displacement increments,}$$

N is the number of element nodes (4 through 9).

The matrix ${}^t B_L$ is given by:

$$\begin{aligned}
 & \begin{matrix} {}^t\mathbf{B} \\ {}^t\mathbf{L} \end{matrix} = \\
 & = \begin{bmatrix}
 {}^t h_{1,1}; 0 & ; & {}^t h_{2,1}; 0 & ; & {}^t h_{3,1}; 0 & ; & \dots & ; & {}^t h_{N,1}; 0 \\
 0 & ; & {}^t h_{1,2}; 0 & ; & {}^t h_{2,2}; 0 & ; & {}^t h_{3,2}; & \dots & ; & 0 & ; & {}^t h_{N,2} \\
 {}^t h_{1,2}; & {}^t h_{1,1}; & {}^t h_{2,2}; & {}^t h_{2,1}; & {}^t h_{3,2}; & {}^t h_{3,1}; & \dots & ; & {}^t h_{N,2}; & {}^t h_{N,1} \\
 \frac{h_1}{{}^t\bar{x}_1} & ; & 0 & ; & \frac{h_2}{{}^t\bar{x}_1} & ; & 0 & ; & \dots & ; & \frac{h_N}{{}^t\bar{x}_1} & ; & 0
 \end{bmatrix}
 \end{aligned}$$

$$\text{where } {}^t h_{k,j} = \frac{\partial h_k}{\partial {}^t x_j}, \quad /4.22/$$

$$u_j^k = {}^{t+\Delta t} u_j^k - {}^t u_j^k,$$

$$\text{and } {}^t\bar{x}_1 = \sum_{k=1}^N h_k {}^t x_1^k.$$

The nonlinear strain-displacement transformation matrix takes the form:

$$\begin{aligned}
 & \begin{matrix} {}^t\mathbf{B} \\ {}^t\mathbf{NL} \end{matrix} = \quad /4.23/ \\
 & = \begin{bmatrix}
 {}^t h_{1,1}; 0 & ; & {}^t h_{2,1}; 0 & ; & {}^t h_{3,1}; 0 & ; & \dots & ; & {}^t h_{N,1}; 0 \\
 {}^t h_{1,2}; 0 & ; & {}^t h_{2,2}; 0 & ; & {}^t h_{3,2}; 0 & ; & \dots & ; & {}^t h_{N,2}; 0 \\
 0 & ; & {}^t h_{1,1}; 0 & ; & {}^t h_{2,1}; 0 & ; & {}^t h_{3,1}; & \dots & ; & 0 & ; & {}^t h_{N,1} \\
 0 & ; & {}^t h_{1,2}; 0 & ; & {}^t h_{2,2}; 0 & ; & {}^t h_{3,2}; & \dots & ; & 0 & ; & {}^t h_{N,2} \\
 \frac{h_1}{{}^t\bar{x}_1} & ; & 0 & ; & \frac{h_2}{{}^t\bar{x}_1} & ; & 0 & ; & \dots & ; & \frac{h_N}{{}^t\bar{x}_1} & ; & 0
 \end{bmatrix}
 \end{aligned}$$

and the 2nd Piola Kirchhoff stress matrix and tensors take the forms:

$${}^tT = \begin{bmatrix} {}^t\tau_{11}; & {}^t\tau_{12}; & 0; & 0; & 0 \\ {}^t\tau_{21}; & {}^t\tau_{22}; & 0; & 0; & 0 \\ 0; & 0; & {}^t\tau_{11}; & {}^t\tau_{12} & 0 \\ 0; & 0; & {}^t\tau_{21}; & {}^t\tau_{22}; & 0 \\ 0; & 0; & 0; & 0; & {}^t\tau_{33} \end{bmatrix}; \quad {}^t\underline{\tau} = \begin{bmatrix} {}^t\tau_{11} \\ {}^t\tau_{22} \\ {}^t\tau_{12} \\ {}^t\tau_{33} \end{bmatrix} \quad /4.24/$$

The loading takes the form:

$$\int_{{}^tV} {}^{t+\Delta t}{}_{\underline{f}}^B \delta u_1 {}^t dV + \int_{{}^tA} {}^{t+\Delta t}{}_{\underline{f}}^A \delta u_1 {}^t dA \approx {}^{t+\Delta t}{}_{\underline{R}}$$

where

/4.25/

$${}^{t+\Delta t}{}_{\underline{R}} = \int_{{}^tV} H^T {}^{t+\Delta t}{}_{\underline{f}}^B {}^t dV + \int_{{}^tA} (H^s)^T {}^{t+\Delta t}{}_{\underline{f}}^A {}^t dA$$

and H^s , H are surface and volume interpolation matrices and ${}^{t+\Delta t}{}_{\underline{f}}^B$, ${}^{t+\Delta t}{}_{\underline{f}}^A$ are vectors of body and surface forces defined per unit volume and surface respectively.

This completes the definition for the Updated Lagrangian formulation.

Finally it should be noted that the above discretized forms of expressions for both Total and Lagrangian formulations are integrated by the Gaussian integration rules at 2 x 2, 3 x 3 or 4 x 4 sampling points. Obviously, considering nonlinearity of the element, the more integration points, the better the results, for example the more gradual cracking of the element. Based on the collective experience, the 4 x 4 integration rule is a good compromise between accuracy and computational cost.

Both Total and Updated element formulations are used in this work. Reinforcement is modeled by isoparametric bar elements.

5. GENERAL SHELL ELEMENT.

The objective of this chapter is to present the shell element used in this work. Similar to the previous chapter all derivations will be based on the general formulation derived in Chapter two and the constitutive equations and failure criteria in Chapter three.

First a brief general overview of shell modeling is given. Thereafter attention will focus on Ahmad's degenerated shell element. Three modifications of this element are included: Lagrangian, Serendipity and Heterosis variants of geometry and displacement field approximation. Also in order to avoid or minimize element membrane and shear locking full, selective and reduced integrations are considered. The resulting element behavior is discussed at the end of the chapter.

Following Total Lagrangian formulation of the problem, the principle of virtual displacements will be used to assemble the incremental form of the governing equations. Transformation to Updated Lagrangian formulation is simple and hence will be not presented explicitly.

Shell structural analysis represents one of the most complicated of structural problems. Consequently many simplifying assumptions must be adopted. There are generally four main possibilities for shell element formulation.

The simplest way is to divide a shell structure into many triangular flat elements. It was and may still be the most popular approach to shell analysis. Elements are relatively simple because they do not deal with difficulties accompanying curvilinear geometry of the elements. Usually a shell element is constructed by simple overlaying of plate and plane stress elements. This concept however leads to discontinuities between element domains if the structure is not planar.

The second group of shell elements are those based directly on some particular shell theory for curvilinear elements. Now-

adays many formulations exists for both thin and deep shells. Unfortunately completely general shell theory would be too complex and consequently the problem arises as to which phenomena of shell behavior are important and which negligible.

The third group represents theories where shell structures are considered as complete 3D structures. Usually a 3D isoparametric element is used. This approach allows for structure curvatures and at the same time its formulation is relatively simple. The time cost of analysis is however higher, even if an efficient 15 point integration scheme is used. The other drawback of this approach is that bending stiffness is overestimated in the case of thin shells.

The last group of shell element formulations is based on the 3D element concept again but employing appropriate assumptions, the problem is transformed into 2D space. The element third dimension through the element thickness is integrated in analytical form or by trapezoidal numerical integration, (i.e. layer concept). The latter case is necessary for materially nonlinear analyses.

One of the most popular elements in the fourth group is the degenerate continuum element (see Fig 5.1), originally proposed by Ahmad et al. [54]. In this formulation the complexity of general shell theory is avoided by direct discretization of the 3D continuum equations. Following general shell element theory each node of an element has five degrees of freedom, i.e. three displacement and two rotations in planes normal to the mid-surface of element.

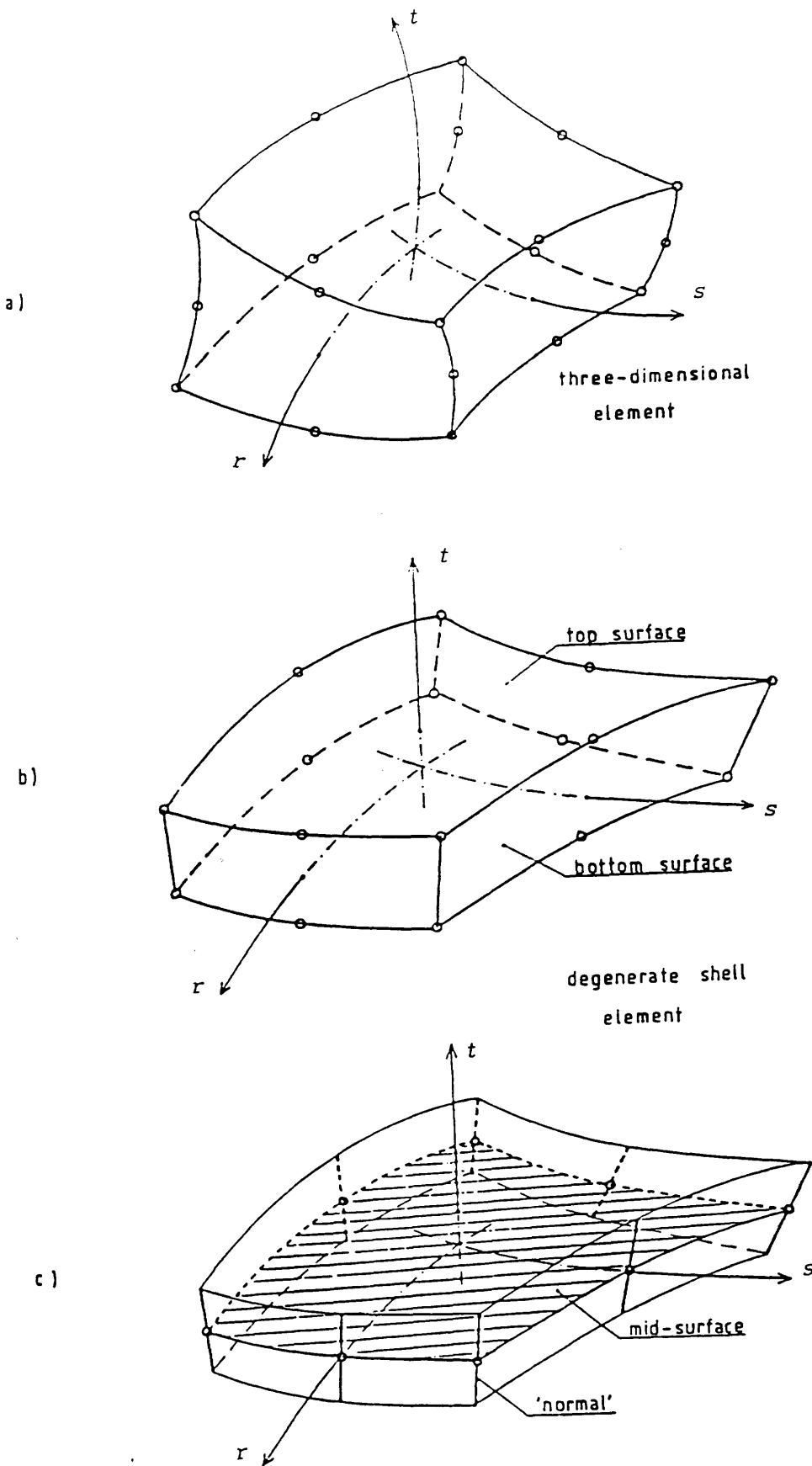


Fig 5.1 Three dimensional shell element, (a) and the corresponding degenerated shell element, (b, c).

Ahmad's original linear formulation of the element has been gradually but significantly improved by using reduced or selective integration schemes, Lagrange approximation of displacement etc. and by the introduction of nonlinear behavior. Because of its good properties this element has been adopted in this work and is now discussed in more detail.

5.1 Geometry and displacement fields for degenerated element.

Throughout all derivations of this element, isoparametric formulation is adopted.

Geometry.

The coordinates of top and bottom element surface is used to define the element geometry:

$$\begin{bmatrix} t_{X_1} \\ t_{X_2} \\ t_{X_3} \end{bmatrix} = t_{\underline{X}} = \sum_{k=1}^N h_k \frac{1+t}{2} \begin{bmatrix} t_{X_1}^{top} \\ t_{X_2}^{top} \\ t_{X_3}^{top} \end{bmatrix}_k + \sum_{k=1}^N h_k \frac{1-t}{2} \begin{bmatrix} t_{X_1}^{bot} \\ t_{X_2}^{bot} \\ t_{X_3}^{bot} \end{bmatrix}_k$$

/5.1/

where N is number of nodes per element,

$h_k(r,s)$ is the k -th interpolation function,

r, s, t are isoparametric coordinates (see Fig. 5.2),

$$\begin{bmatrix} t_{X_1}^{top} \\ t_{X_2}^{top} \\ t_{X_3}^{top} \end{bmatrix}_k \quad \text{and} \quad \begin{bmatrix} t_{X_1}^{bot} \\ t_{X_2}^{bot} \\ t_{X_3}^{bot} \end{bmatrix}_k$$

are vectors of the top and bottom

coordinates of point k (Fig.5.2).

At each nodal point a special coordinate system is defined by:

$$\underline{v1}_k = \begin{bmatrix} v1_1 \\ v1_2 \\ v1_3 \end{bmatrix}_k ; \quad \underline{v2}_k = \begin{bmatrix} v2_1 \\ v2_2 \\ v2_3 \end{bmatrix}_k ; \quad \underline{v3}_k = \begin{bmatrix} v3_1 \\ v3_2 \\ v3_3 \end{bmatrix}_k \quad /5.2/$$

Vector $\underline{v3}_k$ at point k is defined as a line joining the bottom and top coordinates at this point (prior to deformation).

The second vector defining local nodal point coordinate system, $\underline{v1}_k$, is normal to $\underline{v3}_k$ and is parallel to the plane of the global 0x_1 and 0x_3 axes. Hence:

$$[v1_1]_k = [v3_3]_k ; \quad [v1_2]_k = 0.0 \quad \text{and} \quad [v1_3]_k = - [v3_1]_k \quad /5.3/$$

or in the case that $\underline{v3}$ is parallel to 0x_2 (i.e. $[v3_1]_k = [v3_3]_k = 0$)

$$[v1_1]_k = - [v3_2]_k ; \quad [v1_2]_k = [v1_3]_k = 0.$$

The last vector is defined as a vector product of the two previous vectors:

$$\underline{v2}_k = \underline{v3}_k \times \underline{v1}_k$$

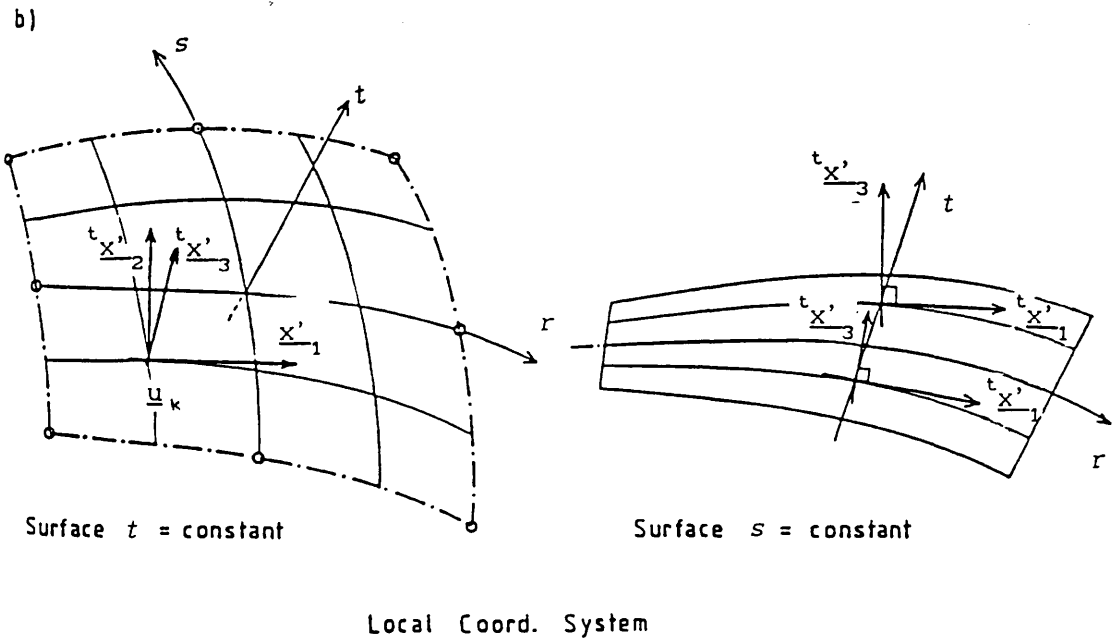
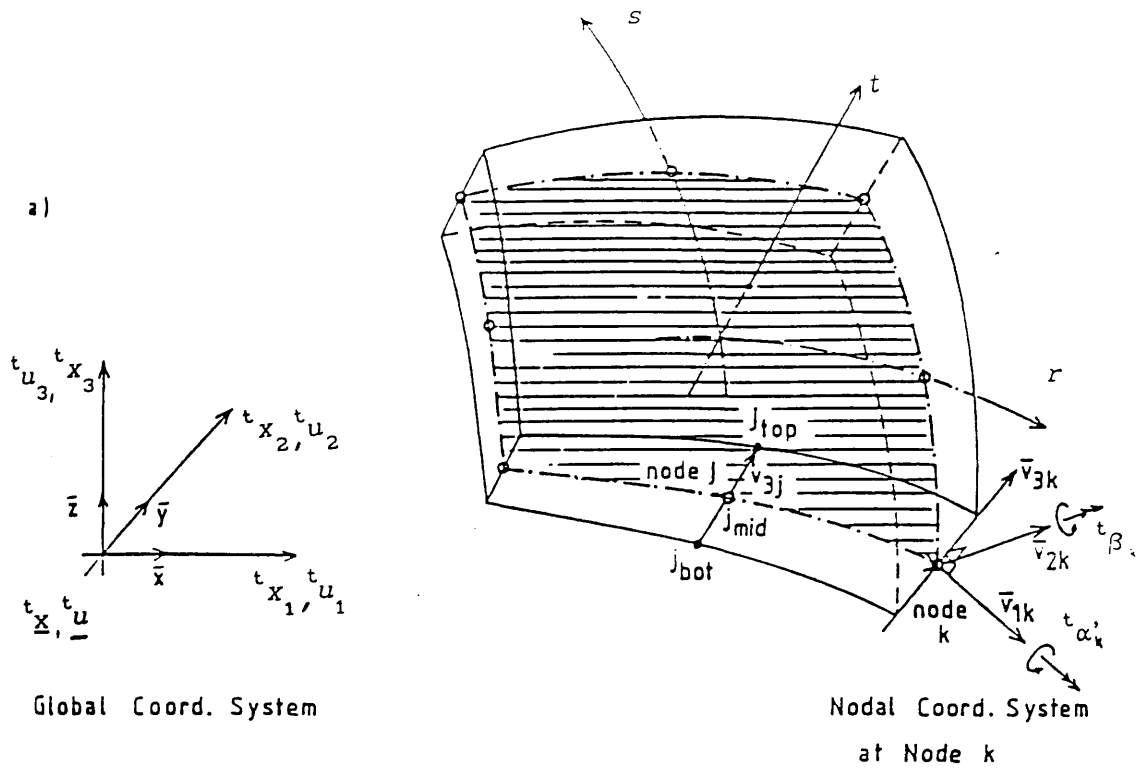


Fig 5.2 Degenerate shell nodal and curvilinear, (a) and local axes, (b) systems.

Using the above vectors equation /5.1/ can be rewritten in the following form:

$$\begin{bmatrix} t_{X_1} \\ t_{X_2} \\ t_{X_3} \end{bmatrix} = \underline{t}_X = \sum_{k=1}^N h_k \begin{bmatrix} t_{X_1}^{mid} \\ t_{X_2}^{mid} \\ t_{X_3}^{mid} \end{bmatrix}_k + \sum_{k=1}^N h_k \frac{t}{2} \begin{bmatrix} t_{v3_1} \\ t_{v3_2} \\ t_{v3_3} \end{bmatrix}_k [thick]_k \quad /5.4/$$

where $[thick]_k$ is element thickness at node k (i.e. distance between top and bottom points) and

$$\begin{bmatrix} t_{X_1}^{mid} \\ t_{X_2}^{mid} \\ t_{X_3}^{mid} \end{bmatrix}_k = \frac{1}{2} \left(\begin{bmatrix} t_{X_1}^{top} \\ t_{X_2}^{top} \\ t_{X_3}^{top} \end{bmatrix}_k + \begin{bmatrix} t_{X_1}^{bot} \\ t_{X_2}^{bot} \\ t_{X_3}^{bot} \end{bmatrix}_k \right) \quad /5.5/$$

are the coordinates of the mid surface, used whenever "global" access to the structure is necessary. Note that the definition of approximation functions $h_k(r,s)$ differs slightly from the 2D element depending on which variant for approximation is used, (Lagrange, Serendipity or Heterosis elements). Their definition is given later together with a discussion of element integration.

Displacement field approximation.

The displacement approximation is similar to the above approximation of geometry. Each node has three displacements in the direction of global coordinates axes 0x_1 , 0x_2 , 0x_3 and two rotations about vectors $\underline{v1}$ and $\underline{v2}$.

Thus the displacement vector takes the form:

$$\begin{bmatrix} {}^t u_1 \\ {}^t u_2 \\ {}^t u_3 \end{bmatrix} = {}^t u = \sum_{k=1}^N h_k \begin{bmatrix} {}^t u_1 \\ {}^t u_2 \\ {}^t u_3 \end{bmatrix}_k + \sum_{k=1}^N \left\{ h_k \frac{t}{2} [thick]_k \right.$$

/5.6/

$$\left. \begin{bmatrix} -{}^t v_{2_1}; & {}^t v_{1_1} \\ -{}^t v_{2_2}; & {}^t v_{1_2} \\ -{}^t v_{2_3}; & {}^t v_{1_3} \end{bmatrix}_k \begin{bmatrix} {}^t \alpha' \\ {}^t \beta' \end{bmatrix}_k \right\}$$

and the displacement vector at point k has the form:

$${}^t \underline{u}_k = [{}^t u_1; {}^t u_2; {}^t u_3; {}^t \alpha'; {}^t \beta']_k^T .$$

Its first three components are global displacements but the rotations are defined in the local point coordinate system (hence "" mark). The terms ${}^t \alpha'$, ${}^t \beta'$ mean rotation about ${}^t \underline{v}_{1_k}$ and ${}^t \underline{v}_{2_k}$ respectively. The three displacements are measured in the mid-surface plane.

5.2 Strain and stresses definition.

The 2nd Piola Kirchhoff stress and Green Lagrange strain tensors will be used again. In the case of linear and nonlinear compressive zones (i.e. where an elastic-plastic material model is applicable) constitutive equations are defined using stress and strain invariants independent of the geometric transformation of the elements. Thus, it does not matter whether the element constitutive equations are specified for deformed or undeformed element configurations. In tension zones (strain softening expressions), for the sake of simplicity, the difference between Cauchy and 2nd Piola Kirchhoff tensor is neglected and the latter tensor is directly used where "real" Cauchy stresses ought to be substituted. This simplification is feasible because in practice they do not significantly differ and tensile strength of con-

crete is low.

The constitutive equation for steel is based on an elastic-plastic material model.

The essential importance in the stress and strain definitions is that they have their own local coordinate system (this is different from the "node local coordinate system" explained in the previous section). This system corresponds to the mid-surface of the element and is used at sampling (integration) points.

Its coordinate vectors ${}^0\underline{x}'_1$, ${}^0\underline{x}'_2$ and ${}^0\underline{x}'_3$ are defined by:

$${}^0\underline{x}'_3 = \begin{bmatrix} \frac{\partial {}^0x_1}{\partial r} \\ \frac{\partial {}^0x_2}{\partial r} \\ \frac{\partial {}^0x_3}{\partial r} \end{bmatrix} \times \begin{bmatrix} \frac{\partial {}^0x_1}{\partial s} \\ \frac{\partial {}^0x_2}{\partial s} \\ \frac{\partial {}^0x_3}{\partial s} \end{bmatrix} \quad /5.7/$$

$${}^0\underline{x}'_1 = \begin{bmatrix} \frac{\partial {}^0x_1}{\partial r} \\ \frac{\partial {}^0x_2}{\partial r} \\ \frac{\partial {}^0x_3}{\partial r} \end{bmatrix} ; \quad {}^0\underline{x}'_2 = {}^0\underline{x}'_3 * {}^0\underline{x}'_1$$

where "*" denotes a vector product. The local coordinate system varies along the shell element but at a distinct point it remains fixed through all loading increments, due to the Total Lagrangian formulation used.

In order to establish relationship between local and global coordinate systems, a transformation matrix **T** is defined. Its columns are unit vectors parallel to vectors ${}^0\underline{x}'_1$, ${}^0\underline{x}'_2$ and ${}^0\underline{x}'_3$ respectively. Hence:

$$T = \left[\begin{array}{c} \frac{{}^0x'_1}{{}^0x'_1} ; \frac{{}^0x'_2}{{}^0x'_2} ; \frac{{}^0x'_3}{{}^0x'_3} \end{array} \right] \quad /5.8/$$

Green - Lagrange tensor.

The general definition for the Green-Lagrange strain tensor has the form (see /2.7a/):

$${}^t\varepsilon_{ij} = \frac{1}{2} \left(\begin{array}{cc} {}^t u_{i,j} + {}^t u_{j,i} + {}^t u_{k,i} & {}^t u_{k,j} \end{array} \right) \quad /5.9/$$

which after substitution leads to:

$$\left[\begin{array}{c} {}^t\varepsilon_{11} \\ {}^t\varepsilon_{22} \\ 2{}^t\varepsilon_{12} \\ 2{}^t\varepsilon_{13} \\ 2{}^t\varepsilon_{23} \end{array} \right] = \left[\begin{array}{c} \frac{\partial^t u_1}{\partial^t x_1} + \frac{1}{2} \left[\left(\frac{\partial^t u_1}{\partial^t x_1} \right)^2 + \left(\frac{\partial^t u_2}{\partial^t x_1} \right)^2 + \left(\frac{\partial^t u_3}{\partial^t x_1} \right)^2 \right] \\ \frac{\partial^t u_2}{\partial^t x_2} + \frac{1}{2} \left[\left(\frac{\partial^t u_1}{\partial^t x_2} \right)^2 + \left(\frac{\partial^t u_2}{\partial^t x_2} \right)^2 + \left(\frac{\partial^t u_3}{\partial^t x_2} \right)^2 \right] \\ \frac{\partial^t u_1}{\partial^t x_2} + \frac{\partial^t u_2}{\partial^t x_1} + \left[\frac{\partial^t u_1}{\partial^t x_1} \frac{\partial^t u_1}{\partial^t x_2} + \frac{\partial^t u_2}{\partial^t x_1} \frac{\partial^t u_2}{\partial^t x_2} + \frac{\partial^t u_3}{\partial^t x_1} \frac{\partial^t u_3}{\partial^t x_2} \right] \\ \frac{\partial^t u_1}{\partial^t x_3} + \frac{\partial^t u_3}{\partial^t x_1} + \left[\frac{\partial^t u_1}{\partial^t x_1} \frac{\partial^t u_1}{\partial^t x_3} + \frac{\partial^t u_2}{\partial^t x_1} \frac{\partial^t u_2}{\partial^t x_3} + \frac{\partial^t u_3}{\partial^t x_1} \frac{\partial^t u_3}{\partial^t x_3} \right] \\ \frac{\partial^t u_2}{\partial^t x_3} + \frac{\partial^t u_3}{\partial^t x_2} + \left[\frac{\partial^t u_1}{\partial^t x_3} \frac{\partial^t u_1}{\partial^t x_2} + \frac{\partial^t u_2}{\partial^t x_3} \frac{\partial^t u_2}{\partial^t x_2} + \frac{\partial^t u_3}{\partial^t x_3} \frac{\partial^t u_3}{\partial^t x_2} \right] \end{array} \right]$$

/5.10/

The expressions /5.10/ are very complicated and the present

work simplifies them significantly by adopting the Von-Karman assumptions as follows:

- a/ All strains are relatively small so their product can be neglected,
- b/ The deflection normal to mid surface of shell is of order of thickness,
- c/ Both curvatures are small,
- d/ The in-plane displacements are much smaller than transverse displacement and thus their derivatives in 2nd order terms can be neglected.

Applying the above assumptions the Green-Lagrange tensor can be written in the form:

$$\begin{bmatrix} {}^t\varepsilon_{11} \\ {}^t\varepsilon_{22} \\ 2 {}^t\varepsilon_{12} \\ {}^t\varepsilon_{13} \\ 2 {}^t\varepsilon_{23} \end{bmatrix} = \begin{bmatrix} \frac{\partial^t u_1}{\partial^t x_1} \\ \frac{\partial^t u_2}{\partial^t x_2} \\ \frac{\partial^t u_1}{\partial^t x_2} + \frac{\partial^t u_2}{\partial^t x_1} \\ \frac{\partial^t u_1}{\partial^t x_3} + \frac{\partial^t u_3}{\partial^t x_1} \\ \frac{\partial^t u_2}{\partial^t x_3} + \frac{\partial^t u_3}{\partial^t x_2} \end{bmatrix} + \begin{bmatrix} \frac{1}{2} \left(\frac{\partial^t u_3}{\partial^t x_1} \right)^2 \\ \frac{1}{2} \left(\frac{\partial^t u_3}{\partial^t x_2} \right)^2 \\ \frac{\partial^t u_3}{\partial^t x_1} \frac{\partial^t u_3}{\partial^t x_2} \\ 0 \\ 0 \end{bmatrix} = {}^t\varepsilon_{0-L} + {}^t\varepsilon_{0-NL} \quad /5.11/$$

The vectors ${}^t\varepsilon_{0-L}$ and ${}^t\varepsilon_{0-NL}$ represents the linear and nonlinear parts of the Green-Lagrange tensor.

The derivatives with respect to the global coordinates must be solved using derivatives with respect to local r, s, t coordinates (see /4.10/). Hence we can write:

$$\text{Jacobian } J = \begin{bmatrix} \frac{\partial^t x_1}{\partial r}; & \frac{\partial^t x_2}{\partial r}; & \frac{\partial^t x_3}{\partial r} \\ \frac{\partial^t x_1}{\partial s}; & \frac{\partial^t x_2}{\partial s}; & \frac{\partial^t x_3}{\partial s} \\ \frac{\partial^t x_1}{\partial t}; & \frac{\partial^t x_2}{\partial t}; & \frac{\partial^t x_3}{\partial t} \end{bmatrix} \quad /5.12/$$

The derivatives of the global coordinates with respect to isoparametric coordinates is given by:

$$\frac{\partial^t x_1}{\partial r} = {}^t X_{1,r} = \sum_{k=1}^N {}^0 h_{k,r} \left[{}^t X_{1 \text{ mid}} \right]_k + \sum_{k=1}^N {}^0 h_{k,r} \frac{t}{2} \begin{bmatrix} {}^t v3_1 \\ {}^t v3_2 \\ {}^t v3_3 \end{bmatrix}_k [\text{thick}]_k$$

$$\frac{\partial^t x_1}{\partial s} = {}^t X_{1,s} = \sum_{k=1}^N {}^0 h_{k,s} \left[{}^t X_{1 \text{ mid}} \right]_k + \sum_{k=1}^N {}^0 h_{k,s} \frac{t}{2} \begin{bmatrix} {}^t v3_1 \\ {}^t v3_2 \\ {}^t v3_3 \end{bmatrix}_k [\text{thick}]_k$$

$$\frac{\partial^t x_1}{\partial t} = {}^t X_{1,t} = \sum_{k=1}^N h_k \left[{}^t X_{1 \text{ mid}} \right]_k + \sum_{k=1}^N h_k \frac{1}{2} \begin{bmatrix} {}^t v3_1 \\ {}^t v3_2 \\ {}^t v3_3 \end{bmatrix}_k [\text{thick}]_k$$

/5.13/

Similar expression are applicable also for derivatives of ${}^t x_2$ and ${}^t x_3$ by replacing index 1 in ${}^t x_1$ by 2 and 3 respectively.

Using /5.12/ and /5.13/ we can write the displacement gradient matrix:

$$\begin{bmatrix} \partial_0^t u_{1,1}; & \partial_0^t u_{2,1}; & \partial_0^t u_{3,1} \\ \partial_0^t u_{1,2}; & \partial_0^t u_{2,2}; & \partial_0^t u_{3,2} \\ \partial_0^t u_{1,3}; & \partial_0^t u_{2,3}; & \partial_0^t u_{3,3} \end{bmatrix} = J^{-1} \begin{bmatrix} \partial_0^t u_{1,r}; & \partial_0^t u_{2,r}; & \partial_0^t u_{3,r} \\ \partial_0^t u_{1,s}; & \partial_0^t u_{2,s}; & \partial_0^t u_{3,s} \\ \partial_0^t u_{1,t}; & \partial_0^t u_{2,t}; & \partial_0^t u_{3,t} \end{bmatrix}$$

/5.14/

and by analogy to /5.13/ the derivatives of displacement can be calculated:

$$\frac{\partial^t u_1}{\partial r} = {}_0^t u_{1,r} = \sum_{k=1}^N {}_0 h_{k,r} \begin{bmatrix} {}^t u_1 \\ {}^t u_2 \\ {}^t u_3 \end{bmatrix}_k + \sum_{k=1}^N \left\{ {}_0 h_{k,r} \frac{t}{2} [thick]_k^* \right.$$

$$\left. \begin{bmatrix} {}^t v_{2_1}; & {}^t v_{1_1} \\ {}^t v_{2_2}; & {}^t v_{1_2} \\ {}^t v_{2_3}; & {}^t v_{1_3} \end{bmatrix}_k \begin{bmatrix} {}^t \alpha' \\ {}^t \beta' \end{bmatrix}_k \right\}$$

$$\frac{\partial^t u_1}{\partial s} = {}_0^t u_{1,s} = \sum_{k=1}^N {}_0 h_{k,s} \begin{bmatrix} {}^t u_1 \\ {}^t u_2 \\ {}^t u_3 \end{bmatrix}_k + \sum_{k=1}^N \left\{ {}_0 h_{k,s} \frac{t}{2} [thick]_k^* \right.$$

$$\left. \begin{bmatrix} {}^t v_{2_1}; & {}^t v_{1_1} \\ {}^t v_{2_2}; & {}^t v_{1_2} \\ {}^t v_{2_3}; & {}^t v_{1_3} \end{bmatrix}_k \begin{bmatrix} {}^t \alpha' \\ {}^t \beta' \end{bmatrix}_k \right\}$$

$$\frac{\partial^t u_1}{\partial t} = {}_0^t u_{1,t} = \sum_{k=1}^N h_k \begin{bmatrix} {}^t u_1 \\ {}^t u_2 \\ {}^t u_3 \end{bmatrix}_k + \sum_{k=1}^N \left\{ h_k \frac{1}{2} [thick]_k^* \right.$$

$$\left. \begin{matrix} \left[\begin{matrix} {}^t v_{2,1}; & {}^t v_{1,1} \\ {}^t v_{2,2}; & {}^t v_{1,2} \\ {}^t v_{2,3}; & {}^t v_{1,3} \end{matrix} \right]_k \left[\begin{matrix} {}^t \alpha' \\ {}^t \beta' \end{matrix} \right]_k \end{matrix} \right\}$$

/5.15/

The derivatives of ${}^t u_2$ and ${}^t u_3$ are computed in the same way.

Using /5.12/ through /5.15/, after substitution into /5.11/, the Green Lagrange strain tensor in the global coordinate system can be computed.

The governing equations are easier to formulate in the local coordinate system ${}^t \underline{x}'_1$, ${}^t \underline{x}'_2$ and ${}^t \underline{x}'_3$, hence all elements of /5.14/ are transformed into this system:

$$\begin{bmatrix} \partial_0^t u'_{1,1}; & \partial_0^t u'_{2,1}; & \partial_0^t u'_{3,1} \\ \partial_0^t u'_{1,2}; & \partial_0^t u'_{2,2}; & \partial_0^t u'_{3,2} \\ \partial_0^t u'_{1,3}; & \partial_0^t u'_{2,3}; & \partial_0^t u'_{3,3} \end{bmatrix} = \mathbf{T}^T \begin{bmatrix} \partial_0^t u_{1,1}; & \partial_0^t u_{2,1}; & \partial_0^t u_{3,1} \\ \partial_0^t u_{1,2}; & \partial_0^t u_{2,2}; & \partial_0^t u_{3,2} \\ \partial_0^t u_{1,3}; & \partial_0^t u_{2,3}; & \partial_0^t u_{3,3} \end{bmatrix} \mathbf{T}$$

/5.16/

where the additional symbol "'" refers to the ${}^t \underline{x}'_1$, ${}^t \underline{x}'_2$ and ${}^t \underline{x}'_3$ coordinate system, i.e. both displacements and the reference coordinate system (for derivatives) are transformed.

The elements of /5.16/ are finally assembled according to /5.11/ to create the strain tensor in the local coordinate system.

Using matrix notation, we can write:

$${}^t \underline{\varepsilon}_0 = {}^t \underline{\varepsilon}_{0-L} + {}^t \underline{\varepsilon}_{0-NL} \quad /5.17 /$$

where the linear part is computed by:

$${}^t_{0-L} \varepsilon = \sum_{k=1}^N \begin{bmatrix} {}^t_{0 \ L1} \mathbf{B} \end{bmatrix}_k {}^t_{\underline{u}}_k \quad /5.18/$$

$${}^t_{\underline{u}}_k = [{}^t_{u_1}; {}^t_{u_2}; {}^t_{u_3}; {}^t_{\alpha'}; {}^t_{\beta'}]_k^T$$

The detailed expression for matrix ${}^t_{0 \ L1} \mathbf{B}$ is far too complex to present it in matrix form and hence tensor notation is used, (the Einstein summation rule applies, i.e. through repeated indexes imply summation).

Starting again from the displacement field:

$${}^t_{u_i} = \sum_{k=1}^N [R_{ij}]_k [{}^t_{u_j}]_k$$

where submatrix $\mathbf{R}_k =$ /5.19/

$$\begin{bmatrix} h_k; 0; 0; h_k \frac{t}{2} [thick]_k [-{}^t_{v2_1}]_k; h_k \frac{t}{2} [thick]_k [{}^t_{v1_1}]_k \\ 0; h_k; 0; h_k \frac{t}{2} [thick]_k [-{}^t_{v2_2}]_k; h_k \frac{t}{2} [thick]_k^1 [{}^t_{v1_2}]_k \\ 0; 0; h_k; h_k \frac{t}{2} [thick]_k [-{}^t_{v2_3}]_k; h_k \frac{t}{2} [thick]_k [{}^t_{v1_3}]_k \end{bmatrix}$$

Now computing the derivatives with respect to global coordinates l :

$$\frac{\partial {}^t_{u_i}}{\partial {}^t_{x_1}} = {}^t_{0 \ u_{i,1}} = \sum_{k=1}^N \frac{\partial}{\partial {}^t_{x_1}} [R_{ij}]_k [{}^t_{u_j}]_k \quad /5.20/$$

expressing all derivatives using /5.12/ to /5.15/:

$${}^t_{0 \ u_{i,1}} = J_{1m}^{-1} \frac{\partial {}^t_{u_i}}{\partial {}^t_{\xi_m}} = \sum_{k=1}^N J_{1m}^{-1} \frac{\partial}{\partial {}^t_{\xi_m}} [R_{ij}]_k [{}^t_{u_j}]_k \quad /5.21/$$

and finally transforming to ${}^t_{x'_1}$, ${}^t_{x'_2}$; ${}^t_{x'_3}$ coordinate sys-

tem, we obtain the final expression for constructing the matrix in /5.14/:

$${}^t_{0\ i,1} u' = t_{s1} {}^t_{0\ r,s} u \quad t_{ri} = t_{s1} J_{sm}^{-1} \frac{\partial {}^t_{ur}}{\partial {}^t_{\xi_m}} t_{ri} =$$

/5.22/

$$t_{s1} \sum_{k=1}^N J_{sm}^{-1} \frac{\partial}{\partial {}^t_{\xi_m}} [R_{rj}]_k [{}^t_{uj}]_k t_{ri} =$$

$$\sum_{k=1}^N \left\{ t_{s1} J_{sm}^{-1} \frac{\partial}{\partial {}^t_{\xi_m}} [R_{rj}]_k t_{ri} \right\} [{}^t_{uj}]_k$$

where:

ξ_1 , ξ_2 and ξ_3 corresponds to r , s and t coordinates respectively, t_{ij} is element of T and J_{ij}^{-1} is element of matrix J^{-1} .

For the linear part of Green Lagrange tensor ${}^t_{0-L} \varepsilon$ we can write:

$$\begin{bmatrix} {}^t_{0\ \varepsilon_{11}} \\ {}^t_{0\ \varepsilon_{22}} \\ 2 {}^t_{0\ \varepsilon_{12}} \\ {}^t_{0\ \varepsilon_{13}} \\ 2 {}^t_{0\ \varepsilon_{23}} \end{bmatrix} = \sum_{k=1}^N \begin{bmatrix} t_{s1} J_{sm}^{-1} \frac{\partial}{\partial {}^t_{\xi_m}} [R]_k t_{r1} \\ t_{s2} J_{sm}^{-1} \frac{\partial}{\partial {}^t_{\xi_m}} [R]_k t_{r2} \\ t_{s2} J_{sm}^{-1} \frac{\partial}{\partial {}^t_{\xi_m}} [R]_k t_{r1} + t_{s1} J_{sm}^{-1} \frac{\partial}{\partial {}^t_{\xi_m}} [R]_k t_{r2} \\ t_{s3} J_{sm}^{-1} \frac{\partial}{\partial {}^t_{\xi_m}} [R]_k t_{r1} + t_{s1} J_{sm}^{-1} \frac{\partial}{\partial {}^t_{\xi_m}} [R]_k t_{r3} \\ t_{s2} J_{sm}^{-1} \frac{\partial}{\partial {}^t_{\xi_m}} [R]_k t_{r3} + t_{s3} J_{sm}^{-1} \frac{\partial}{\partial {}^t_{\xi_m}} [R]_k t_{r2} \end{bmatrix} *$$

$$* [{}^t u_1; {}^t u_2; {}^t u_3; {}^t \alpha'; {}^t \beta']_k^T = \sum_{k=1}^N \begin{bmatrix} {}^t B_{L1} \\ 0 \end{bmatrix}_k {}^t \underline{u}_k$$

/5.23/

Now proceeding to the evaluation of the nonlinear part of the Green - Lagrange tensor ${}^t \underline{\varepsilon}_{0-NL}$ which is defined by the second term of /5.11/, we must first express derivatives of ${}^t u_3$ with respect to coordinates ${}^t x_1$ and ${}^t x_2$ in a form similar to /5.21/.

$${}^t u_{3,1} = \sum_{k=1}^N \begin{bmatrix} {}^t g_x \\ 0 \end{bmatrix}_k^T \begin{bmatrix} {}^t u_j \end{bmatrix}_k \quad /5.24/$$

where vector g_x at point k adopts the form:

$$\begin{bmatrix} {}^t g_x \\ 0 \end{bmatrix}_k = {}^t s_{s1} J_{sm}^{-1} \frac{\partial}{\partial {}^t \xi_m} \begin{bmatrix} R_{rj} \end{bmatrix}_k {}^t r_{r3}$$

and similarly

$${}^t u_{3,2} = \sum_{k=1}^N \begin{bmatrix} {}^t g_y \\ 0 \end{bmatrix}_k^T \begin{bmatrix} {}^t u_j \end{bmatrix}_k \quad /5.25/$$

$$\begin{bmatrix} {}^t g_y \\ 0 \end{bmatrix}_k = {}^t s_{s2} J_{sm}^{-1} \frac{\partial}{\partial {}^t \xi_m} \begin{bmatrix} R_{rj} \end{bmatrix}_k {}^t r_{r3}$$

Hence we can write:

$${}^t_{0}\varepsilon_{NL} = \sum_{k=1}^N \begin{bmatrix} \frac{1}{2} \begin{bmatrix} t \\ \underline{u} \end{bmatrix}_k^T \begin{bmatrix} t \\ 0 \\ \underline{gX} \end{bmatrix}_k \begin{bmatrix} t \\ 0 \\ \underline{gX} \end{bmatrix}_k^T \begin{bmatrix} t \\ \underline{u} \end{bmatrix}_k \\ \frac{1}{2} \begin{bmatrix} t \\ \underline{u} \end{bmatrix}_k^T \begin{bmatrix} t \\ 0 \\ \underline{gY} \end{bmatrix}_k \begin{bmatrix} t \\ 0 \\ \underline{gY} \end{bmatrix}_k^T \begin{bmatrix} t \\ \underline{u} \end{bmatrix}_k \\ \begin{bmatrix} t \\ \underline{u} \end{bmatrix}_k^T \begin{bmatrix} t \\ 0 \\ \underline{gX} \end{bmatrix}_k \begin{bmatrix} t \\ 0 \\ \underline{gY} \end{bmatrix}_k^T \begin{bmatrix} t \\ \underline{u} \end{bmatrix}_k \\ 0 \\ 0 \end{bmatrix}$$

/5.26/

After derivation of the equations for the Green - Lagrange strains, we now proceed to similar expressions for their increments and variation of their increments:

$${}^t_{0}\varepsilon_{ij} = {}^{t+\Delta t}_{0}\varepsilon_{ij} - {}^t_{0}\varepsilon_{ij} \quad /5.27/$$

where ${}^{t+\Delta t}_{0}\varepsilon_{ij}$ is Green - Lagrange tensor at time $t + \Delta t$,

${}^{\Delta t}_{0}\varepsilon_{ij}$ is Green - Lagrange tensor at time t and

${}^{\varepsilon}_{0ij}$ is its increment.

Dividing ${}^t_{0}\varepsilon_{ij}$ into linear ${}^e_{0ij}$ and nonlinear ${}^{\eta}_{0ij}$ parts:

$${}^t_{0}\varepsilon_{ij} = {}^e_{0ij} + {}^{\eta}_{0ij} \quad /5.28/$$

we can write:

$${}_{0}\underline{e} = \sum_{k=1}^N \begin{bmatrix} {}^t\mathbf{B}_{L1} \\ {}_0 \end{bmatrix}_k \underline{u}_k + \begin{bmatrix} \begin{bmatrix} {}^t\underline{u} \\ {}_0 \end{bmatrix}_k^T \begin{bmatrix} {}^t\mathbf{gX} \\ {}_0 \end{bmatrix}_k \begin{bmatrix} {}^t\mathbf{gX} \\ {}_0 \end{bmatrix}_k^T \begin{bmatrix} \underline{u} \\ {}_0 \end{bmatrix}_k \\ \begin{bmatrix} {}^t\underline{u} \\ {}_0 \end{bmatrix}_k^T \begin{bmatrix} {}^t\mathbf{gY} \\ {}_0 \end{bmatrix}_k \begin{bmatrix} {}^t\mathbf{gY} \\ {}_0 \end{bmatrix}_k^T \begin{bmatrix} \underline{u} \\ {}_0 \end{bmatrix}_k \\ \begin{bmatrix} {}^t\underline{u} \\ {}_0 \end{bmatrix}_k^T \left\{ \begin{bmatrix} {}^t\mathbf{gY} \\ {}_0 \end{bmatrix}_k \begin{bmatrix} {}^t\mathbf{gX} \\ {}_0 \end{bmatrix}_k^T + \begin{bmatrix} {}^t\mathbf{gX} \\ {}_0 \end{bmatrix}_k \begin{bmatrix} {}^t\mathbf{gY} \\ {}_0 \end{bmatrix}_k^T \right\} \begin{bmatrix} \underline{u} \\ {}_0 \end{bmatrix}_k \\ 0 \\ 0 \end{bmatrix}$$

$${}_{0}\underline{\eta} = \sum_{k=1}^N \begin{bmatrix} \frac{1}{2} \begin{bmatrix} \underline{u} \\ {}_0 \end{bmatrix}_k^T \begin{bmatrix} {}^t\mathbf{gX} \\ {}_0 \end{bmatrix}_k \begin{bmatrix} {}^t\mathbf{gX} \\ {}_0 \end{bmatrix}_k^T \begin{bmatrix} \underline{u} \\ {}_0 \end{bmatrix}_k \\ \frac{1}{2} \begin{bmatrix} \underline{u} \\ {}_0 \end{bmatrix}_k^T \begin{bmatrix} {}^t\mathbf{gY} \\ {}_0 \end{bmatrix}_k \begin{bmatrix} {}^t\mathbf{gY} \\ {}_0 \end{bmatrix}_k^T \begin{bmatrix} \underline{u} \\ {}_0 \end{bmatrix}_k \\ \begin{bmatrix} \underline{u} \\ {}_0 \end{bmatrix}_k^T \begin{bmatrix} {}^t\mathbf{gX} \\ {}_0 \end{bmatrix}_k \begin{bmatrix} {}^t\mathbf{gY} \\ {}_0 \end{bmatrix}_k^T \begin{bmatrix} \underline{u} \\ {}_0 \end{bmatrix}_k \\ 0 \\ 0 \end{bmatrix}$$

/5.30/

where $\begin{bmatrix} \underline{u} \\ {}_0 \end{bmatrix}_k = \begin{bmatrix} {}^{t+\Delta t}\underline{u} \\ {}_0 \end{bmatrix}_k - \begin{bmatrix} {}^t\underline{u} \\ {}_0 \end{bmatrix}_k$ is the vector of displacement increments from time t to time $t + \Delta t$ at point k .

Variations of ${}_{0}\underline{e}$ and ${}_{0}\underline{\eta}$ are:

$$\delta \left\{ {}_{0}\underline{e} \right\} = \sum_{k=1}^N \begin{bmatrix} {}^t\mathbf{B}_{L1} \\ {}_0 \end{bmatrix}_k \delta \left\{ \begin{bmatrix} \underline{u} \\ {}_0 \end{bmatrix}_k \right\} + \quad /5.31/$$

$$\begin{aligned}
& \left[\begin{array}{l}
\mathcal{L} \left[\begin{array}{c} \underline{u} \\ \underline{u} \end{array} \right]_k^T \left[\begin{array}{c} \underline{gX} \\ \underline{0} \end{array} \right]_k \left[\begin{array}{c} \underline{gX} \\ \underline{0} \end{array} \right]_k^T \delta \left\{ \left[\begin{array}{c} \underline{u} \\ \underline{u} \end{array} \right]_k \right\} \\
\mathcal{L} \left[\begin{array}{c} \underline{u} \\ \underline{u} \end{array} \right]_k^T \left[\begin{array}{c} \underline{gY} \\ \underline{0} \end{array} \right]_k \left[\begin{array}{c} \underline{gY} \\ \underline{0} \end{array} \right]_k^T \delta \left\{ \left[\begin{array}{c} \underline{u} \\ \underline{u} \end{array} \right]_k \right\} \\
+ \mathcal{L} \left[\begin{array}{c} \underline{u} \\ \underline{u} \end{array} \right]_k^T \left\{ \left[\begin{array}{c} \underline{gY} \\ \underline{0} \end{array} \right]_k \left[\begin{array}{c} \underline{gX} \\ \underline{0} \end{array} \right]_k^T + \left[\begin{array}{c} \underline{gX} \\ \underline{0} \end{array} \right]_k \left[\begin{array}{c} \underline{gY} \\ \underline{0} \end{array} \right]_k^T \right\} \delta \left\{ \left[\begin{array}{c} \underline{u} \\ \underline{u} \end{array} \right]_k \right\} \\
0 \\
0
\end{array} \right] =
\end{aligned}$$

$$\sum_{k=1}^N \left\{ \left[\begin{array}{c} \underline{B}_{L1} \\ \underline{0} \end{array} \right]_k + \left[\begin{array}{c} \underline{B}_{L2} \\ \underline{0} \end{array} \right]_k \right\} \delta \left\{ \left[\begin{array}{c} \underline{u} \\ \underline{u} \end{array} \right]_k \right\}$$

$$\delta \left\{ \begin{array}{c} \underline{\eta} \\ \underline{0} \end{array} \right\} = \sum_{k=1}^N \left[\begin{array}{l}
\left[\begin{array}{c} \underline{u} \\ \underline{u} \end{array} \right]_k^T \left[\begin{array}{c} \underline{gX} \\ \underline{0} \end{array} \right]_k \left[\begin{array}{c} \underline{gX} \\ \underline{0} \end{array} \right]_k^T \delta \left\{ \left[\begin{array}{c} \underline{u} \\ \underline{u} \end{array} \right]_k \right\} \\
\left[\begin{array}{c} \underline{u} \\ \underline{u} \end{array} \right]_k^T \left[\begin{array}{c} \underline{gY} \\ \underline{0} \end{array} \right]_k \left[\begin{array}{c} \underline{gY} \\ \underline{0} \end{array} \right]_k^T \delta \left\{ \left[\begin{array}{c} \underline{u} \\ \underline{u} \end{array} \right]_k \right\} \\
\mathcal{L} \left[\begin{array}{c} \underline{u} \\ \underline{u} \end{array} \right]_k^T \left\{ \left[\begin{array}{c} \underline{gY} \\ \underline{0} \end{array} \right]_k \left[\begin{array}{c} \underline{gX} \\ \underline{0} \end{array} \right]_k^T + \left[\begin{array}{c} \underline{gX} \\ \underline{0} \end{array} \right]_k \left[\begin{array}{c} \underline{gY} \\ \underline{0} \end{array} \right]_k^T \right\} \delta \left\{ \left[\begin{array}{c} \underline{u} \\ \underline{u} \end{array} \right]_k \right\} \\
0 \\
0
\end{array} \right]$$

/5.32/

2nd Piola Kirchhoff tensor.

The stress state is measured by the 2nd Piola-Kirchhoff tensor, which is the energy conjugate of the Green - Lagrange tensor. Recall that all stresses except the normal stress perpendicular to the shell mid surface are accounted for, this being the reason why the local coordinate system was introduced. Obviously this system varies from point to point and strictly should be re-computed after every iteration, (a new transformation matrix $\begin{smallmatrix} t \\ 0 \end{smallmatrix} T$

is defined). However this is neglected here and the matrix 0T is kept fixed throughout the whole analysis. The resulting inaccuracy is acceptable if the Von Karman assumptions are obeyed.

For the solution of the internal forces the 2nd Piola Kirchhoff tensor is rearranged to vector form by:

$$\begin{bmatrix} t_S \\ 0 \end{bmatrix}_k = \begin{bmatrix} t_{S_{11}}; & t_{S_{22}}; & t_{S_{12}}; & t_{S_{13}}; & t_{S_{23}} \end{bmatrix}_k^T \quad /5.33/$$

and for computation of the nonlinear part of the stiffness matrix, the matrix form:

$$\begin{bmatrix} t_S \\ 0 \end{bmatrix}_k = \begin{bmatrix} t_{S_{11}}; & t_{S_{12}} \\ t_{S_{21}}; & t_{S_{22}} \end{bmatrix} \quad /5.34/$$

is used. Note that it is possible to abbreviate the full 3 by 3 element tensor to a 2 by 2 element only because of the Von Karman simplifying assumptions.

5.3 General governing equation for degenerated element.

After establishing all necessary relationships for strain and stress tensors we can now proceed to the final governing equations. They are presented in both continuum and equivalent discretized forms.

Using the expressions from Chapter Two the displacement increment during one iteration is expressed as follows:

$$\int_{{}_0V} {}^0C_{1jrs} e_{rs} \delta_0 e_{1j} {}^0dV + \int_{{}_0V} t_{S_{1j}} \delta_0 \eta_{1j} {}^0dV =$$

$${}^{t+\Delta t}R - \int_{{}_0V} t_{S_{1j}} \delta_0 e_{1j} {}^0dV \quad /5.35/$$

After discretization, equation /5.35/ takes the form:

$$\left(\begin{matrix} t \\ 0 \end{matrix} \mathbf{K}_L + \begin{matrix} t \\ 0 \end{matrix} \mathbf{K}_{NL} \right) \Delta \underline{u}^{(i)} = \begin{matrix} t \\ 0 \end{matrix} \Delta \underline{R} - \begin{matrix} t \\ 0 \end{matrix} \Delta t \underline{F}^{(i-1)} \quad /5.36/$$

where $\begin{matrix} t \\ 0 \end{matrix} \mathbf{K}_L$ is the linear part of the stiffness matrix,

$\begin{matrix} t \\ 0 \end{matrix} \mathbf{K}_{NL}$ is the nonlinear part of the stiffness matrix,

$\Delta \underline{u}^{(i)} = \underline{u} = \underline{u}^{(i)} - \underline{u}^{(i-1)}$ is the displacement increment in i -th iteration at time $t + \Delta t$,

$\begin{matrix} t \\ 0 \end{matrix} \Delta t \underline{R}$ is the vector of current (i.e. at time $t + \Delta t$) total loading,

$\begin{matrix} t \\ 0 \end{matrix} \underline{F}^{(i-1)}$ is the vector of internal forces.

Table 5.1 shows the correspondence between /5.35/ and /5.36/:

Analytical form	Discretized form
$\int_{\begin{matrix} 0 \\ v \end{matrix}} \begin{matrix} 0 \\ 0 \end{matrix} C_{ijrs} \begin{matrix} 0 \\ 0 \end{matrix} e_{rs} \delta \begin{matrix} 0 \\ 0 \end{matrix} e_{ij} \begin{matrix} 0 \\ 0 \end{matrix} dV$	$\begin{matrix} t \\ 0 \end{matrix} \mathbf{K}_L \Delta \underline{u}^{(i)}$
$\int_{\begin{matrix} 0 \\ v \end{matrix}} \begin{matrix} t \\ 0 \end{matrix} S_{ij} \delta \begin{matrix} 0 \\ 0 \end{matrix} \eta_{ij} \begin{matrix} 0 \\ 0 \end{matrix} dV$	$\begin{matrix} t \\ 0 \end{matrix} \mathbf{K}_{NL} \Delta \underline{u}^{(i)}$
$\begin{matrix} t \\ 0 \end{matrix} \Delta t \underline{R}$	$\begin{matrix} t \\ 0 \end{matrix} \Delta t \underline{R}$
$\int_{\begin{matrix} 0 \\ v \end{matrix}} \begin{matrix} t \\ 0 \end{matrix} S_{ij} \delta \begin{matrix} 0 \\ 0 \end{matrix} e_{ij} \begin{matrix} 0 \\ 0 \end{matrix} dV$	$\begin{matrix} t \\ 0 \end{matrix} \Delta t \underline{F}^{(i-1)}$

Table 5.1 Analytical and discretized form of equilibrium equation.

To derive $\begin{matrix} t \\ 0 \end{matrix} \mathbf{K}_L$ we can write:

$${}^t\mathbf{K}_{0L} \approx \sum_{k=1}^N \int_{o_v} \left[\begin{matrix} {}^t\mathbf{B}_{L1} + {}^t\mathbf{B}_{L2} \\ 0 \end{matrix} \right]_k^T \mathbf{C} \left[\begin{matrix} {}^t\mathbf{B}_{L1} + {}^t\mathbf{B}_{L2} \\ 0 \end{matrix} \right]_k {}^o dV \quad /5.37/$$

whereas for ${}^t\mathbf{K}_{0NL}$, using /5.32/:

$$\int_{o_v} {}^t\mathbf{S}_{ij} \delta_0 \eta_{ij} {}^o dV = \int_{o_v} {}^t\mathbf{S}^T \delta \left(\begin{matrix} \underline{\eta} \\ 0 \end{matrix} \right) = \quad /5.38/$$

$$= \int_{o_v} \sum_{k=1}^N \left[\begin{matrix} \delta \underline{u}^T \begin{matrix} {}^t\mathbf{g}_X & {}^t\mathbf{S}_{11} & {}^t\mathbf{g}_X^T \\ 0 & 0 & 0 \end{matrix} \underline{u} + \delta \underline{u}^T \begin{matrix} {}^t\mathbf{g}_Y & {}^t\mathbf{S}_{22} & {}^t\mathbf{g}_Y^T \\ 0 & 0 & 0 \end{matrix} \underline{u} + \right. \\ \left. \delta \underline{u}^T \left\{ \begin{matrix} {}^t\mathbf{g}_Y & {}^t\mathbf{S}_{12} & {}^t\mathbf{g}_X^T \\ 0 & 0 & 0 \end{matrix} + \begin{matrix} {}^t\mathbf{g}_X & {}^t\mathbf{S}_{12} & {}^t\mathbf{g}_Y^T \\ 0 & 0 & 0 \end{matrix} \right\} \underline{u} \right]_k {}^o dV =$$

$$= \sum_{k=1}^N \left[\delta \underline{u}^T \int_{o_v} \begin{matrix} {}^t\mathbf{G} & {}^t\mathbf{S} & {}^t\mathbf{G}^T \\ 0 & 0 & 0 \end{matrix} {}^o dV \underline{u} \right]_k$$

Hence:

$${}^t\mathbf{K}_{0NL} \approx \sum_{k=1}^N \left[\int_{o_v} \begin{matrix} {}^t\mathbf{G} & {}^t\mathbf{S} & {}^t\mathbf{G}^T \\ 0 & 0 & 0 \end{matrix} {}^o dV \right]_k \quad /5.39/$$

where the structure of the 2nd Piola-Kirchhoff tensor in matrix form (i.e. ${}^t\mathbf{S}$) and vector form (i.e. ${}^t\mathbf{S}$) is given by /5.34/ and /5.33/ respectively and matrix ${}^t\mathbf{G}$ consists of vectors ${}^t\mathbf{g}_X$ and ${}^t\mathbf{g}_Y$:

$${}^t\mathbf{G} = \left[\begin{matrix} {}^t\mathbf{g}_X \\ {}^t\mathbf{g}_Y \end{matrix} \right] \quad /5.40/$$

Note that in /5.37/ and /5.39/ the symbol " \approx " is used instead of "=" to imply that the above expressions consider contributions from one element node only. Thus summation through the remaining element nodes is necessary, which is relatively trivial.

For internal forces we can write:

$$\int_{o_V} {}^t S_{ij} \delta {}^o e_{ij} {}^o dV = \sum_{k=1}^N \int_{o_V} \delta \left[\underline{u} \right]_k \left\{ \begin{bmatrix} {}^t B_{L1} \\ 0 \end{bmatrix}_k + \begin{bmatrix} {}^t B_{L2} \\ 0 \end{bmatrix}_k \right\}^T \begin{bmatrix} {}^t S \\ 0 \end{bmatrix}_k {}^o dV$$

$${}^t \underline{F}^{(i-1)N} \cong \sum_{k=1}^N \int_{o_V} \left\{ \begin{bmatrix} {}^t B_{L1} \\ 0 \end{bmatrix}_k + \begin{bmatrix} {}^t B_{L2} \\ 0 \end{bmatrix}_k \right\}^T \begin{bmatrix} {}^t S \\ 0 \end{bmatrix}_k {}^o dV$$

/5.50/

where again appropriate assembly is necessary.

The last term of /5.35/ is the vector of external loading. This is not presented here because it is similar to the 2D case, (equations /4.25/).

Having established all general relationships we can now proceed to particular element variants.

5.4 Serendipity, Lagrangian and Heterosis variants of the degenerate shell element.

The shell element analysis uses eight noded interpolation for geometry and eight or nine noded interpolation for displacements (see Fig 5.3). The optional mode function h_9 comprises the difference only between the functional values using eight and nine noded approximations.

$$h_1(r,s) = \frac{1}{4} (1 - r)(1 - s)(-r - s - 1)$$

$$h_2(r,s) = \frac{1}{2} (1 - s)(1 - r^2)$$

$$h_3(r,s) = \frac{1}{4} (1 + r)(1 - s)(r - s - 1)$$

$$h_4(r,s) = \frac{1}{2} (1 + r)(1 - s^2)$$

$$h_5(r,s) = \frac{1}{4} (1 + r)(1 + s)(r + s - 1)$$

$$h_6(r,s) = \frac{1}{2} (1 + s)(1 - r^2)$$

$$h_7(r,s) = \frac{1}{4} (1 + r)(1 - s)(r - s - 1)$$

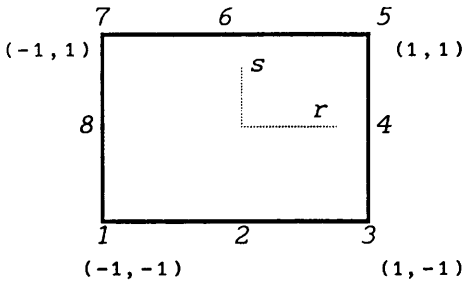
$$h_8(r,s) = \frac{1}{2} (1 - r)(1 - s^2) \quad /5.51/$$

$$h_9(r,s) = (1 - r^2)(1 - s^2)$$

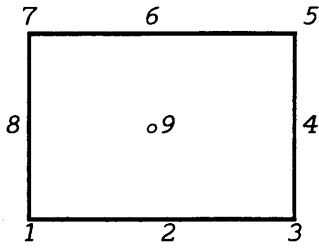
The actual values at the center point can be calculated by:

$$a_9 = \sum_{i=1}^8 h_i(r=0,s=0) a_i + \Delta a_9$$

where h_i are values of the interpolation function at point (0,0), a_i are corresponding node values, Δa_9 is the departure at the center (i.e. the computed value corresponding to the degree of freedom at the center) and a_9 is the total value at the center.

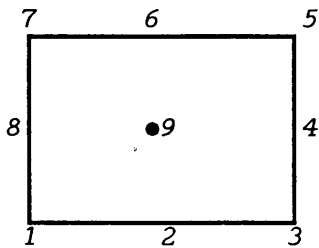


Eight noded Serendipity element



Heterosis element

(at no. 9 vertical or all displacements constrained)



Nine noded Lagrangian element

Fig.5.3 Node notation for element variants of quadratic element.

Depending on how many nodes and integration points are used the Serendipity, Lagrange and Heterosis degenerate element variants are distinguished as follows:

Serendipity element.

This element was used in Ahmad's original work. It comprises eight nodal points (the center point corresponding to the bubble function is omitted). Gauss integration scheme is used for in-plane element integration. Using full integration the element exhibits shear locking for thin and even moderately thick elements. If reduced integration is employed the problem of locking is significantly improved without creating spurious energy modes at the structural level, however the thin element suffers from two non

communicable spurious energy modes at element level.

Nine point Lagrangian element.

The nine point Lagrangian element is nowadays considered to be the most reliable variant of the degenerate element. Applying a full integration scheme there are no problems with membrane and shear locking provided it is used for very thin plate and shell structures. The behavior of moderately thick structures can be improved by using a reduced integration scheme. However in this case the element exhibits rank deficiency.

Heterosis element.

The Heterosis element is very similar to the Lagrangian element, the only difference being that the central node element displacements are constrained (sometimes only the displacement perpendicular to the element mid-surface at this point is constrained). The element behaves particularly well if selective integration is adopted.

The problem of membrane and shear locking for linear analysis are summarized in the Table 5.2, (data based on ref. [41]).

In the case of nonlinearity, especially material nonlinearity, the situation is much more complicated and depends primarily on the material state at sampling points. Moreover some discrepancies were found between the data in Table 5.2 and data provided by other sources [42], [55], [58]. For this reason a new rigorous study of this problem was carried out, the results of which are presented in Sect. 5.7. Unlike the previous studies element nonlinear effects are also considered.

Integ. rule	Shear locking	Number of mechanisms		
		Bending	Membrane	Total
Serendipity 8 node element				
R	$h/l < 0.02$	1*	1*	2*
S	no	0	0	0
Lagrangian 9 node element				
F	$h/l < 0.001$	0	0	0
R	no	3+1*	2+1*	5+2*
S	no	1*	2+1*	2+2*
Heterosis element				
R	no	2+1*	1*	2+2*
S	no	1*	0	1*

* Noncommunicable

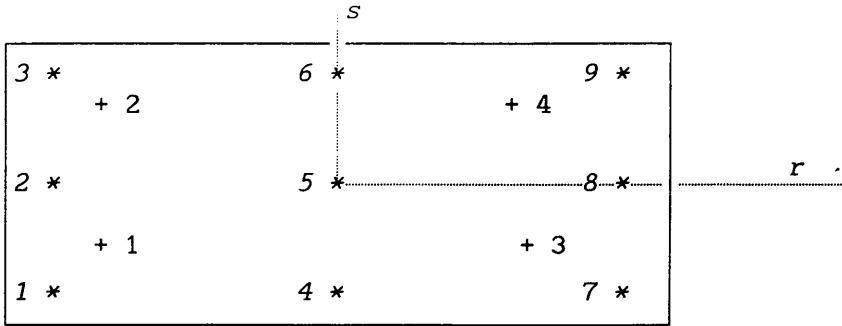
F = full integration, S = selective integration

R = reduced integration

Tab. 5.2 Ahmad's elements, locking and spurious energy modes summary, [41].

In previous paragraphs full, reduced and selective integration scheme has been mentioned. These procedures are demonstrated in Fig. 5.4.

The full and reduced integration schemes are original Gauss integrations at three by three and two by two integration points respectively and selective integration is full integration for membrane and bending actions whereas shear is integrated by reduced integration only.



Reduced integration scheme:	2 x 2 Gauss rule
	$r_i, s_i = \pm 0,57735$
	$i = 1, 2, 3, 4$
Full integration scheme:	3 x 3 Gauss rule
	$r_i, s_i = \pm 0,7746, 0.0$
	$i = 1, 2, \dots, 9$
Selective integration scheme:	
Bending, membrane ---	3 x 3 Gauss rule
	$r_i, s_i = \pm 0,7746, 0.0$
	$i = 1, 2, \dots, 9$
Shear ---	2 x 2 Gauss rule
(extrapolated to	$r_i, s_i = \pm 0,57735$
3 x 3 sampling points)	$i = 1, 2, 3, 4$

Fig. 5.4 Integration schemes and sampling point notation.

The steps during selective integration of shear can be explained by integration of an arbitrary function $f(r,s)$:

1/ First the value of f at sampling points corresponding to the two by two integration rule are calculated:

$$\begin{aligned}
 f_1 &= f(-0.5773, -0.5773) \\
 f_2 &= f(-0.5773, 0.5773) && /5.52/ \\
 f_3 &= f(0.5773, -0.5773) \\
 f_4 &= f(0.5773, 0.5773)
 \end{aligned}$$

2/ Using bilinear approximation the values of f at points cor-

responding to the three by three integration rule are calculated. There are two possibilities for this:

The first is based on the original area of the approximate area and the main idea is that the value of function f is calculated at the "corners" of the isoparametric element (i.e. $r = \pm 1.0$, $s = \pm 1.0$):

$$f_1 = \left[\sum_{k=1}^4 f_i^{\text{cor}} h_i \right]_{\substack{r=-0.5773 \\ s=-0.5774}}$$

$$f_2 = \left[\sum_{k=1}^4 f_i^{\text{cor}} h_i \right]_{\substack{r=-0.5773 \\ s=0.5774}}$$

/5.53/

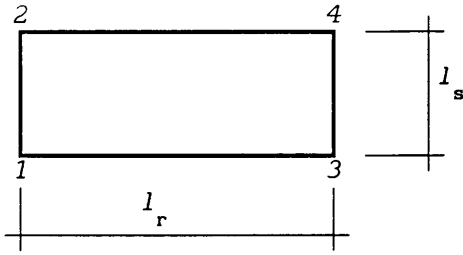
$$f_3 = \left[\sum_{k=1}^4 f_i^{\text{cor}} h_i \right]_{\substack{r=0.5773 \\ s=-0.5774}}$$

$$f_4 = \left[\sum_{k=1}^4 f_i^{\text{cor}} h_i \right]_{\substack{r=0.5773 \\ s=0.5774}}$$

where f_i^{cor} are corner values of function f and h_i are interpolation functions corresponding to the two by two interpolation and corner i .

The set of equations /5.53/ can be solved for f_i^{cor} . Having these values we can bilinearly approximate function f and compute the functional value at any point, including at the sampling points corresponding to the three by three integration rule.

The second and more elegant solution is a direct approximation. The interpolation function h_i are presented for an square area of the size two by two units but they can be extended to a rectangle of any size as shown in Fig. 5.5:



$$h'_1 = \frac{1}{4} \left(1 - \frac{2r}{l_r} \right) \left(1 - \frac{2s}{l_s} \right)$$

$$h'_2 = \frac{1}{4} \left(1 - \frac{2r}{l_r} \right) \left(1 + \frac{2s}{l_s} \right)$$

$$h'_3 = \frac{1}{4} \left(1 + \frac{2r}{l_r} \right) \left(1 - \frac{2s}{l_s} \right)$$

$$h'_4 = \frac{1}{4} \left(1 + \frac{2r}{l_r} \right) \left(1 + \frac{2s}{l_s} \right)$$

Fig. 5.5 Extension of bilinear approximation functions for arbitrary rectangular.

Since the functional values for the two by two sampling points in the corner of the square with $l_r = l_y = 2 \times 0.5775$ are available the approximation functions h'_i can be used directly to calculate the values of the function f at sampling points corresponding to the three by three integration rule.

Although the whole procedure was described for an arbitrary function f it is identical for shear functions. Instead of f we work with the approximate elements (rows) of the matrix \mathbf{B} which relate "shear" strains and nodal displacements.

For integration in the direction perpendicular to $r - s$ plane, i.e. is in the t -coordinate, it is also possible to use Gauss integration. However due to material nonlinearity it is more advantageous to use a trapezoidal scheme. This concept is called the Layer model.

The main idea is to divide the element through the thickness into layers. In every layer the values of strains and stresses are assumed constant and equal to their value at the center point of the layer. It has been found that to achieve good accuracy it is necessary to use about six to ten layers. The layer model has the additional advantages of enabling layers of reinforcing to be created and finer integration in areas with higher stress gradient.

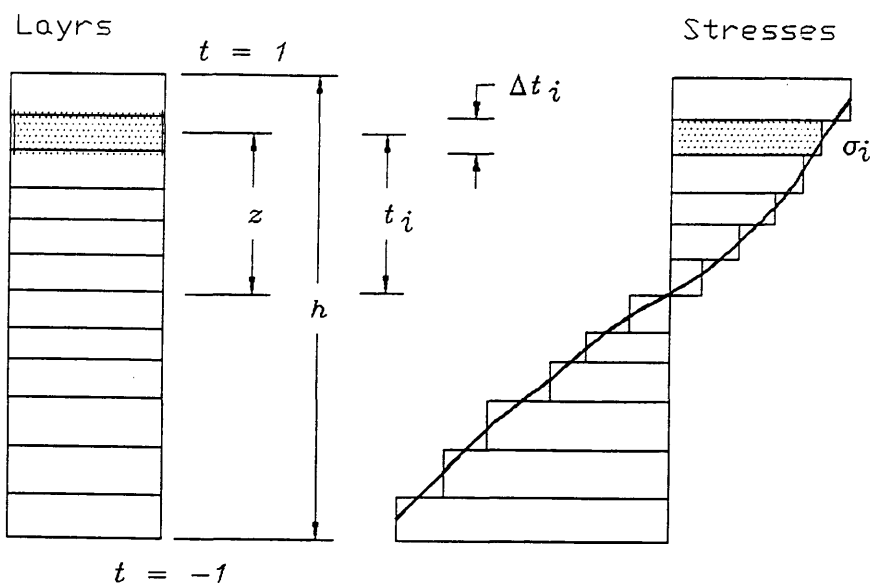


Fig. 5.6 The layer model.

5.5 Shear correction factor k .

The method of approximating displacements and the requirement of shear compatibility (i.e. between adjacent layers) cause both $\tau_{1,3}$, and $\tau_{2,3}$, to be constant throughout the element depth. This is contradictory to reality, where the well known parabolic distribution occurs.

In order to eliminate this inaccuracy, (at least in integral form), a correction factor k is introduced. For the sake of simplicity, the beam element with a rectangular cross section is considered (see Figure 5.7).

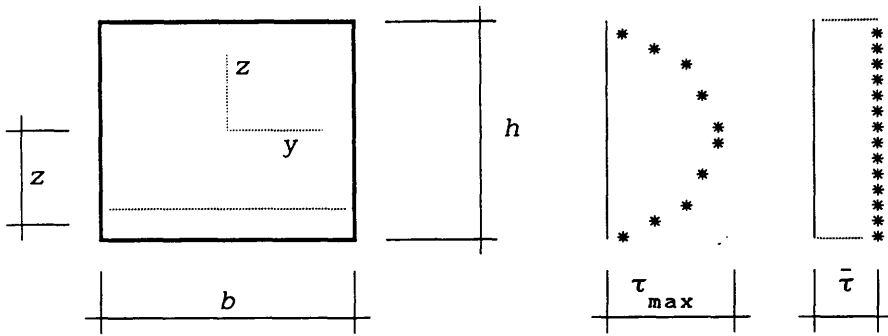


Fig. 5.7 Shear correction factor.

The equilibrium equation for x direction takes the form:

$$\frac{\partial \sigma_x}{\partial x} + \frac{\partial \tau_{xy}}{\partial y} + \frac{\partial \tau_{xz}}{\partial z} = 0 \quad (\text{if no volume forces are present})$$

/5.54/

and if we restrict ourselves to the case where $\frac{\partial \tau_{xy}}{\partial y} = 0$, then we can write:

$$\tau_{xz} = -\int_{-h/2}^z \frac{\partial \sigma_x}{\partial x} d\zeta = -\int_{-h/2}^z \frac{\partial M_x}{\partial x} \frac{1}{I} \zeta d\zeta = \frac{Q_{xz}}{I} g(z)$$

where G is shear modulus, and M_x and Q_{xz} are the moment and shear force in the plane $x - z$ respectively.

For a rectangular cross section, $g(z)$ and I are:

$$g(z) = \frac{h^2}{8} \left[1 - 4 \left(\frac{z}{h} \right)^2 \right]$$

$$I = \frac{1}{12} bh^3$$

and finally:

$$\tau_{\max} = \tau_{xz}(0) = \frac{3}{2} \frac{Q_{xz}}{bh}$$

which is a well known result.

The energy corresponding to this shear can be expressed:

$$\begin{aligned}
 W_{\text{shear}} &= \int_0^b \int_{-h/2}^{h/2} \gamma_{xz} \tau_{xz} dA = \frac{1}{G} \int_0^b \int_{-h/2}^{h/2} \gamma_{xz} \tau_{xz} dA = \\
 &= \frac{1}{G} b \int_{-h/2}^{h/2} \left(\frac{Q_{xz}}{I} g(z) \right)^2 d\zeta = \frac{Q_{xz}^2 b}{I^2 G} \int_{-h/2}^{h/2} g(z)^2 d\zeta = \\
 &= \frac{Q_{xz}^2 b}{I^2 G} \frac{1}{120} h^5 = \frac{5}{6} \frac{Q_{xz}^2}{G bh} \quad /5.55/
 \end{aligned}$$

In the case of constant shear we can write:

$$\bar{\tau} = \frac{Q_{xz}}{bh}$$

$$W_{\text{shear, const}} = \frac{Q_{xz}^2}{G bh} \quad /5.56/$$

Comparing /5.55/ and /5.56/ it is apparent that the value of $\bar{\tau}$ should be reduced by factor 5/6, i.e the value of k .

$$\bar{\tau} = \tau_{xz} = k G \gamma_{xz} = \frac{5}{6} G \gamma_{xz} \quad /5.57/$$

Although the correction factor was derived for a simple case, it is nevertheless adequate for plate elements (shells and plates) also and for both directions (τ_{xz} , τ_{yz}).

5.6 Normal and shear forces, bending moment.

Finally, referring to Fig. 5.8, the stress resultants are defined by the following expressions, where the notation for coordinate axes are simplified by:

$$x \approx {}^t x_1,; \quad y \approx {}^t x_2,; \quad z \approx {}^t x_3,$$

Normal forces:

/5.58/

$$N_x = \int_{-h/2}^{h/2} \sigma_x dz = \frac{h}{2} \int_{-1}^1 \sigma_x dt = \frac{h}{2} \sum_{i=1}^n \sigma_x^i \Delta t_i$$

$$N_y = \int_{-h/2}^{h/2} \sigma_y dz = \frac{h}{2} \int_{-1}^1 \sigma_y dt = \frac{h}{2} \sum_{i=1}^n \sigma_y^i \Delta t_i$$

Moments:

$$M_x = \int_{-h/2}^{h/2} \sigma_y z dz = \frac{h^2}{4} \int_{-1}^1 \sigma_y t dt = \frac{h^2}{4} \sum_{i=1}^n \sigma_y^i t_i \Delta t_i$$

$$M_y = -\int_{-h/2}^{h/2} \sigma_x z dz = -\frac{h^2}{4} \int_{-1}^1 \sigma_x t dt = -\frac{h^2}{4} \sum_{i=1}^n \sigma_x^i t_i \Delta t_i$$

$$M_{xy} = \int_{-h/2}^{h/2} \tau_{xy} z dz = \frac{h^2}{4} \int_{-1}^1 \tau_{xy} t dt = \frac{h^2}{4} \sum_{i=1}^n \tau_{xy}^i t_i \Delta t_i$$

Shear forces:

$$N_{xy} = \int_{-h/2}^{h/2} \tau_{xy} dz = \frac{h}{2} \int_{-1}^1 \tau_{xy} dt = \frac{h}{2} \sum_{i=1}^n \tau_{xy}^i \Delta t_i$$

$$Q_{xz} = \int_{-h/2}^{h/2} \tau_{xz} dz = \frac{h}{2} \int_{-1}^1 \tau_{xz} dt = \frac{h}{2} \sum_{i=1}^n \tau_{xz}^i \Delta t_i$$

$$Q_{yz} = \int_{-h/2}^{h/2} \tau_{yz} dz = \frac{h}{2} \int_{-1}^1 \tau_{yz} dt = \frac{h}{2} \sum_{i=1}^n \tau_{yz}^i \Delta t_i$$

All forces and moments are calculated for width equal to unit length.

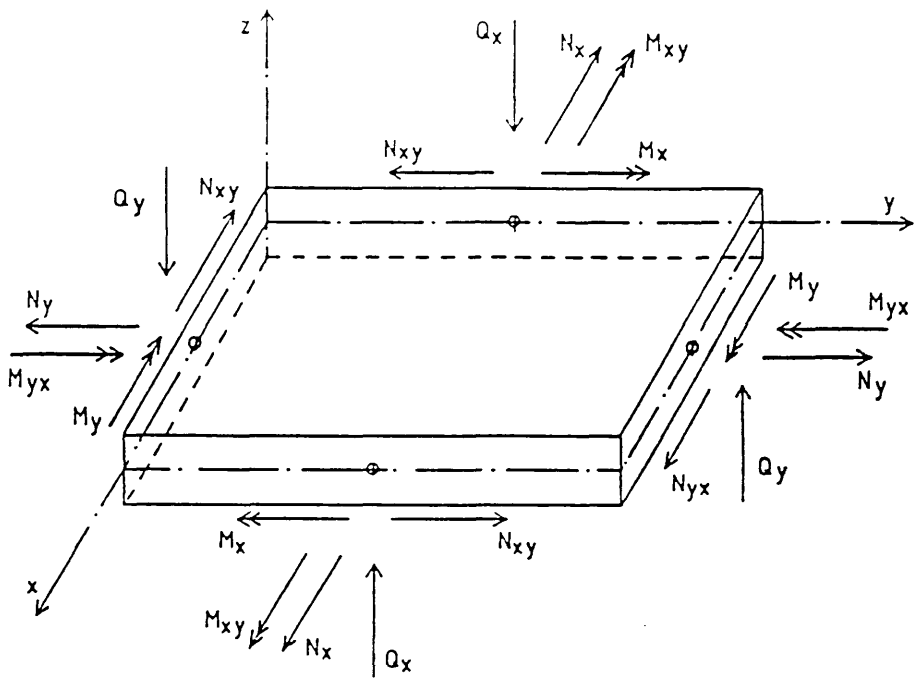


Fig 5.8 Stress resultant sign convention.

5.7 The analysis of rank deficiency of the Ahmad's degenerated element for shell analysis.

This section deals with the rank deficiency of the degenerated shell element of Ahmad [54]. A summary of these results have also been published elsewhere [58]. The correct rank of element matrices is vital for avoiding a singularity of the analysis.

There is an extensive amount of literature on this topic but unfortunately these usually deal with linear elastic plate elements only and specify conditions when the element stiffness matrix can be singular [55]. Other sources [42], [41] provide exact conditions for the matrix to be singular. However some differences have occurred between the results found here and these other sources.

To clarify this problem most of the common formulations of Ahmad's shell element have been analyzed. Geometric nonlinearity as well as the material condition, i.e. elastic, plastic and cracked state, are considered. The results are summarized in tables which provide, in conjunction with Figures of all element eigenmodes, a quick and convenient way to understand the behavior of a particular element formulation. The eigenmodes analysis of the stiffness matrix was performed by both the Householder tri-diagonalisation and QL methods [57], which are also able to analyze singular matrices. The GENSTAT [53], double precision eigenmodes solver was used. The analysis of sample structures, including element stiffness matrix evaluations, was performed by the program CONCRETE. Double precision arithmetic was used throughout, (i.e. 64 bits per variable).

Elastic condition.

In this section we assume geometrical nonlinearity only whilst the material is still in the elastic range, so that no failure occurred. Element properties are studied using the simple two element cantilever depicted in Fig. 5.9. Young's modulus E_0 was 29GPa and Poisson's ratio ν was taken as 0.18. The structu-

re was loaded by two forces of 0.1 kN at both end-nodes near the free end, (the mid-point was not loaded).

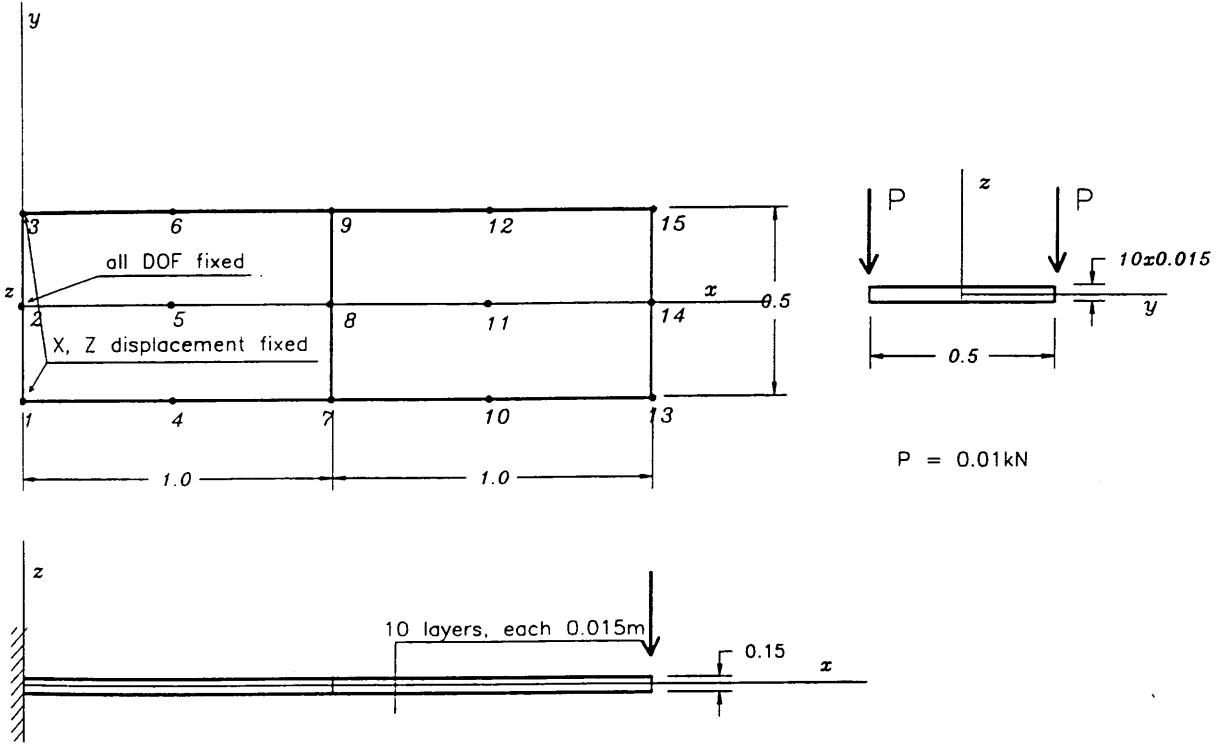


Fig. 5.9 Rank analysis of the Ahmad's element, the geometry of the two element structure.

Tab. 5.3 presents the maximum displacement pertaining to each particular element formulation.

Displacement approximation	Integration rule		
	Full	Selective	Reduced
Lagrangian	1.3164	1.5107	failed
Heterosis	1.3144	1.500	failed
Serendipity	1.2761	1.4096	1.4290

Tab. 5.3 Rank analysis of Ahmad's degenerated shell elements, maximum deformation of the 2-element cantilever in 10^{-4} m.

The above results were compared with the exact deformation, $1.30779 \cdot 10^{-4}$ m, calculated for a beam using Kirchhoff's theory. The closest result is provided, as anticipated, by the nine node Lagrangian displacement approximation and full integration scheme.

It should be noted that for extremely thin shells, it is sometimes recommended, e.g. [42], [56] that the Lagrangian or Heterosis approximation of displacement in combination with the selective in-plane integration be used. This significantly minimizes shear and membrane locking. However for ordinary thin and medium thick shells, which are the most usual case, there are no problems with locking and hence a mathematically more exact approximation and integration should be preferred.

Furthermore the analysis demonstrates the rank deficiency of the element stiffness matrix in the case of reduced integration for the nine node displacement approximation, i.e. the Lagrangian and Heterosis approaches.

In the following, the rank of the stiffness matrix of one element was examined. The first element of the cantilever was used. The results are depicted in Fig. 5.10 to 5.18. Note that $W(i)$ is the energy associated with the i -th eigenmode. Eigenvalues less than 0.5 can be treated as zeros, the non-zero value being caused by small round-off errors.

LAGRANGIAN APPROXIMATION - FULL INTEGRATION

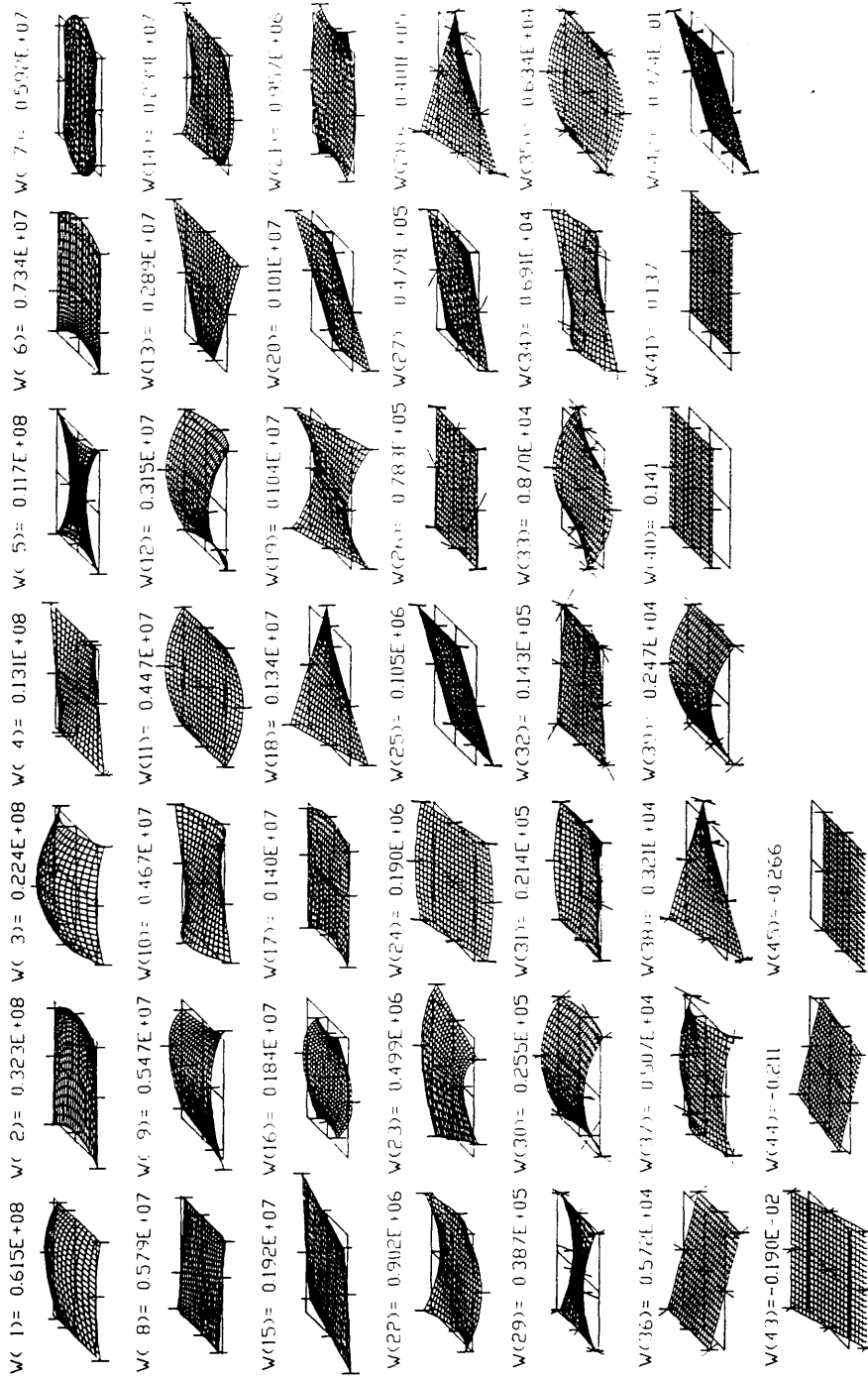


Fig. 5.10 Rank analysis of the Ahmad's element, the eigenmodes of the Lagrangian approximation using the full integration rule.

LAGRANGIAN APPROXIMATION - SELECTIVE INTEGRATION

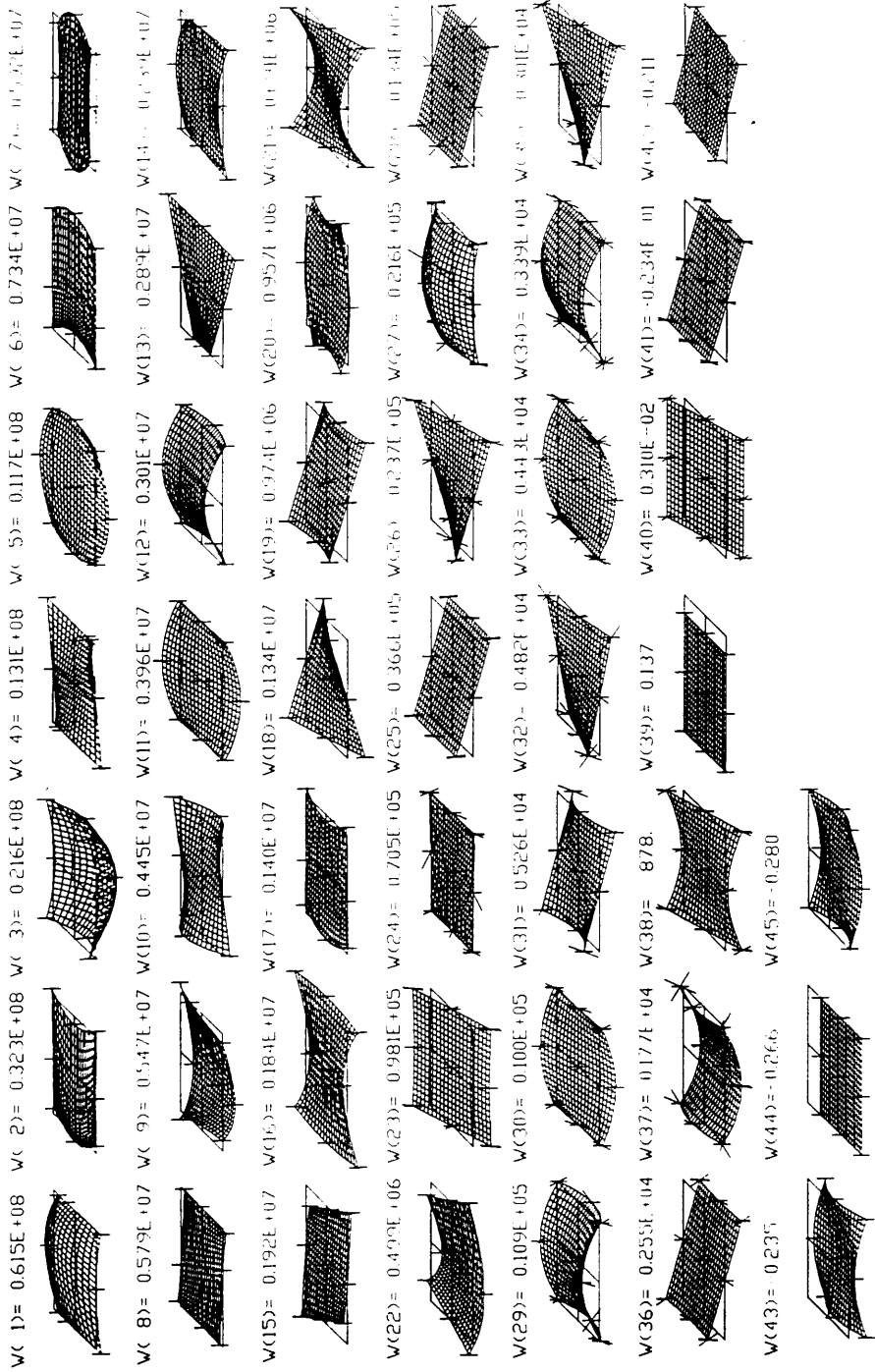


Fig. 5.11 Rank analysis of the Ahmad's element, the eigenmodes of the Lagrangian approximation using the selective integration rule.

LAGRANGIAN APPROXIMATION - REDUCED INTEGRATION

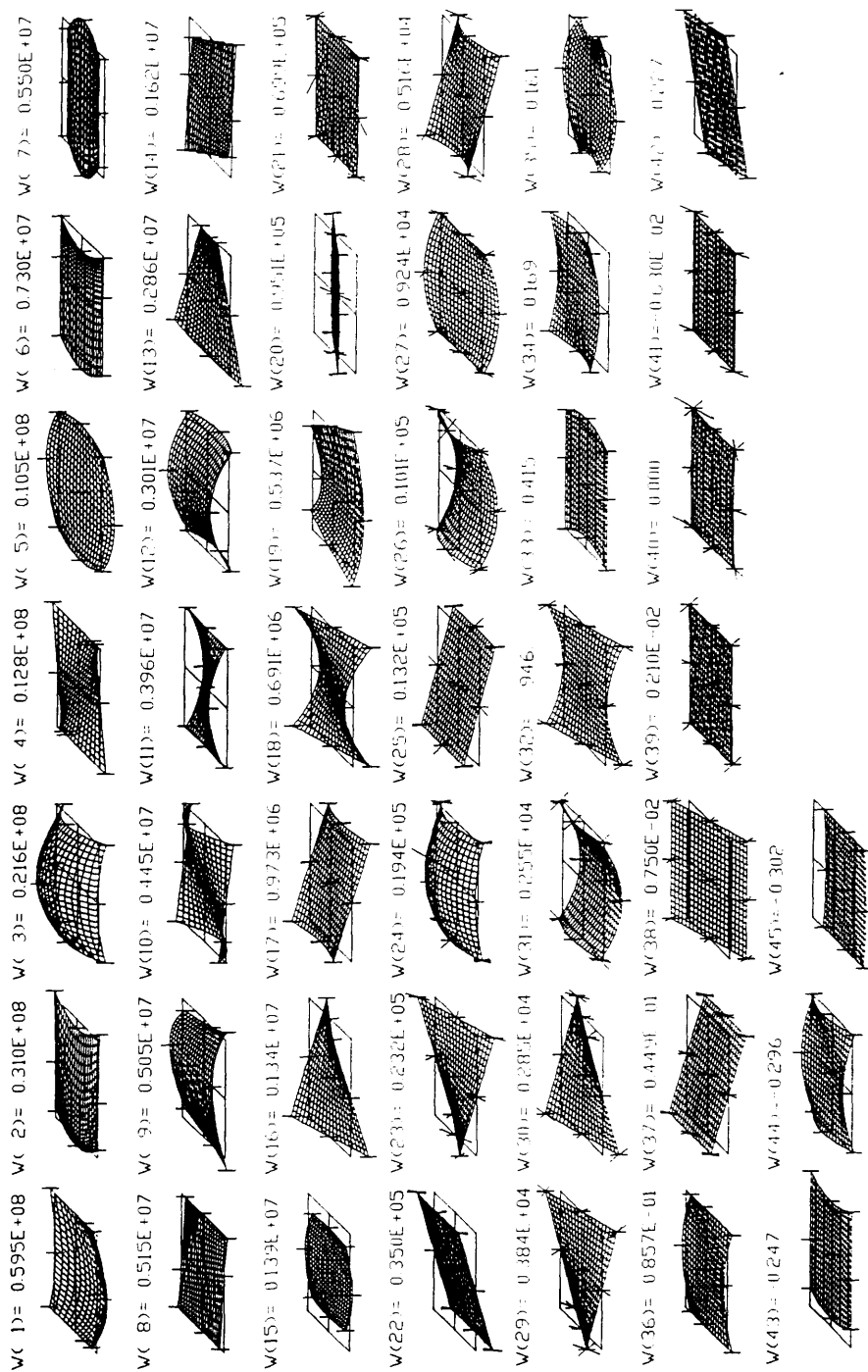


Fig. 5.12 Rank analysis of the Ahmad's element, the eigenmodes of the Lagrangian approximation with the reduced integration rule.

HETEROSIS ELEMENT - FULL INTEGRATION

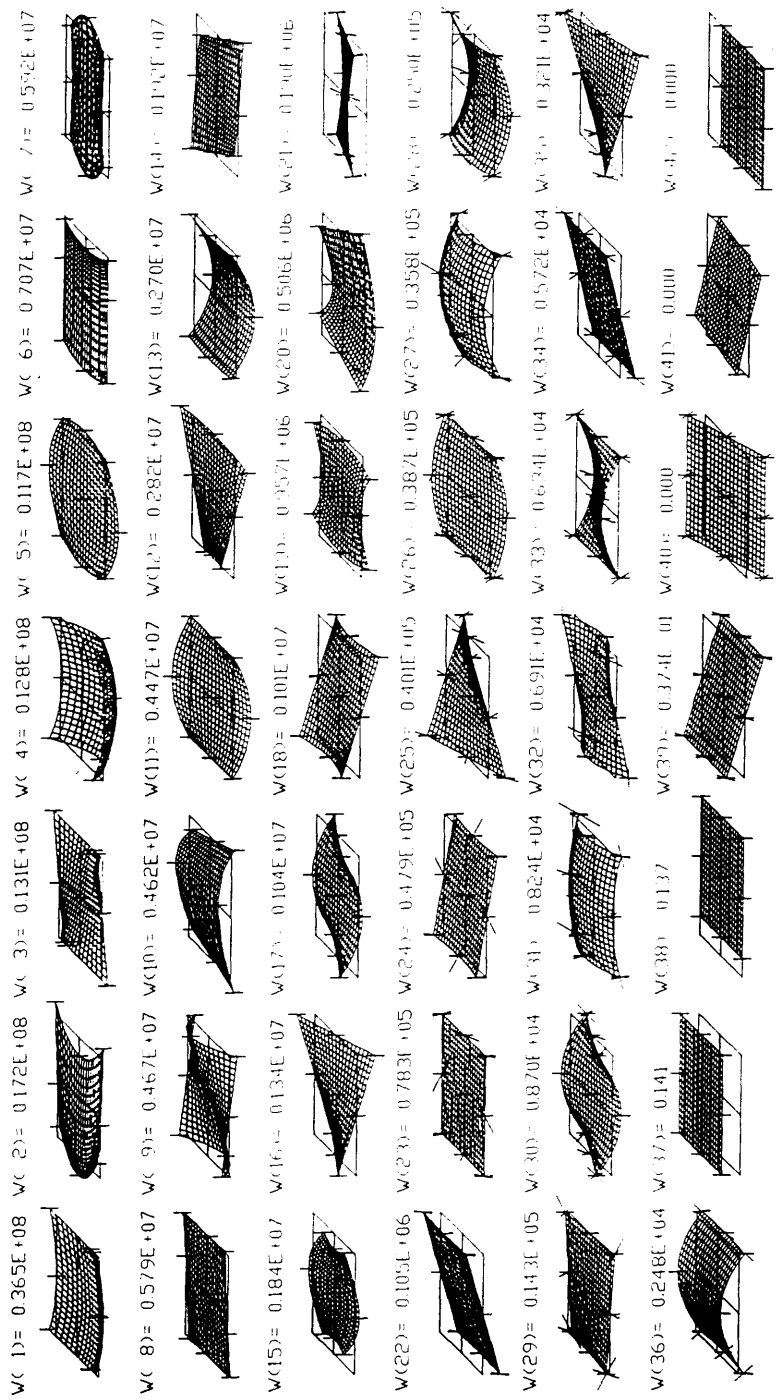


Fig. 5.13 Rank analysis of the Ahmad's element, the eigenmodes of the Heterosis approximation with the full integration rule.

HETEROSIS ELEMENT - SELECTIVE INTEGRATION

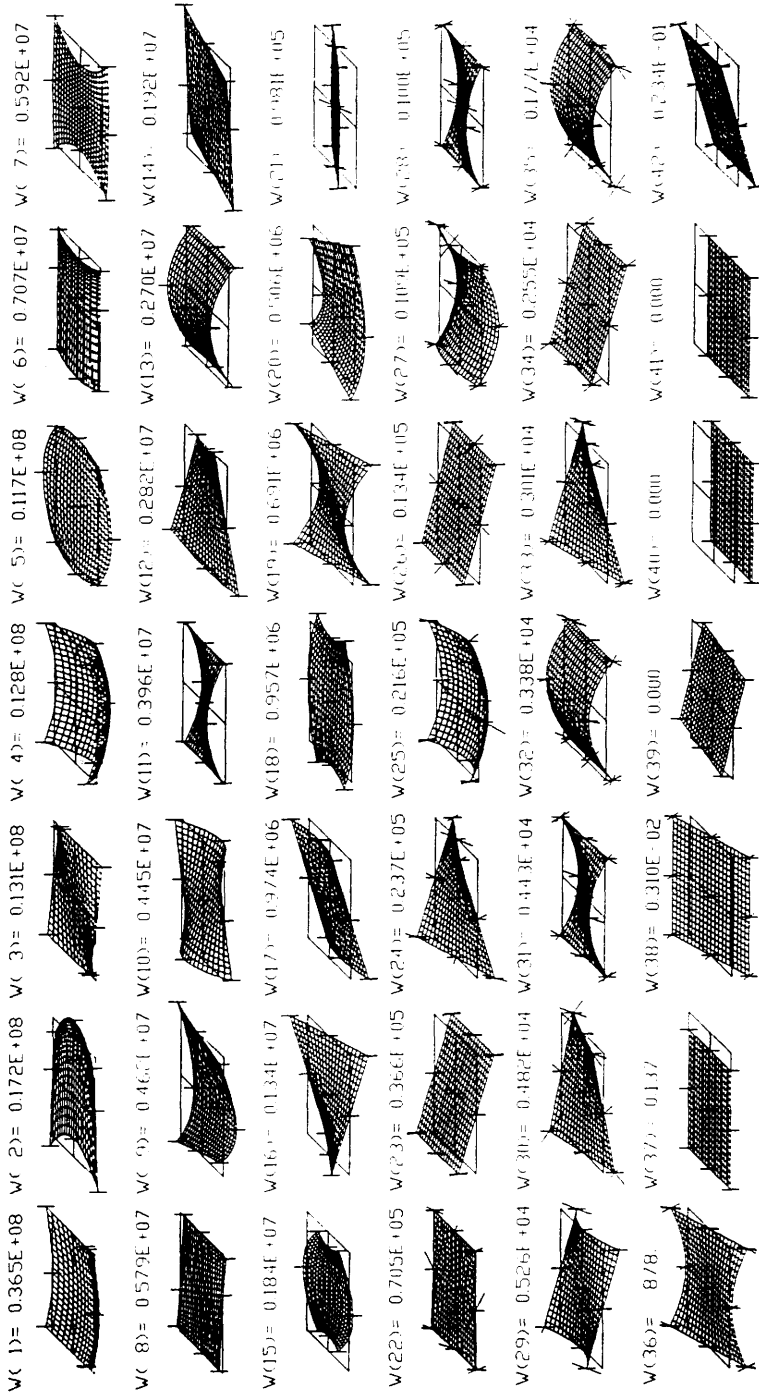


Fig. 5.14 Rank analysis of the Ahmad's element, the eigenmodes of the Heterosis approximation with the selective integration rule.

HETEROSIS ELEMENT - REDUCED INTEGRATION

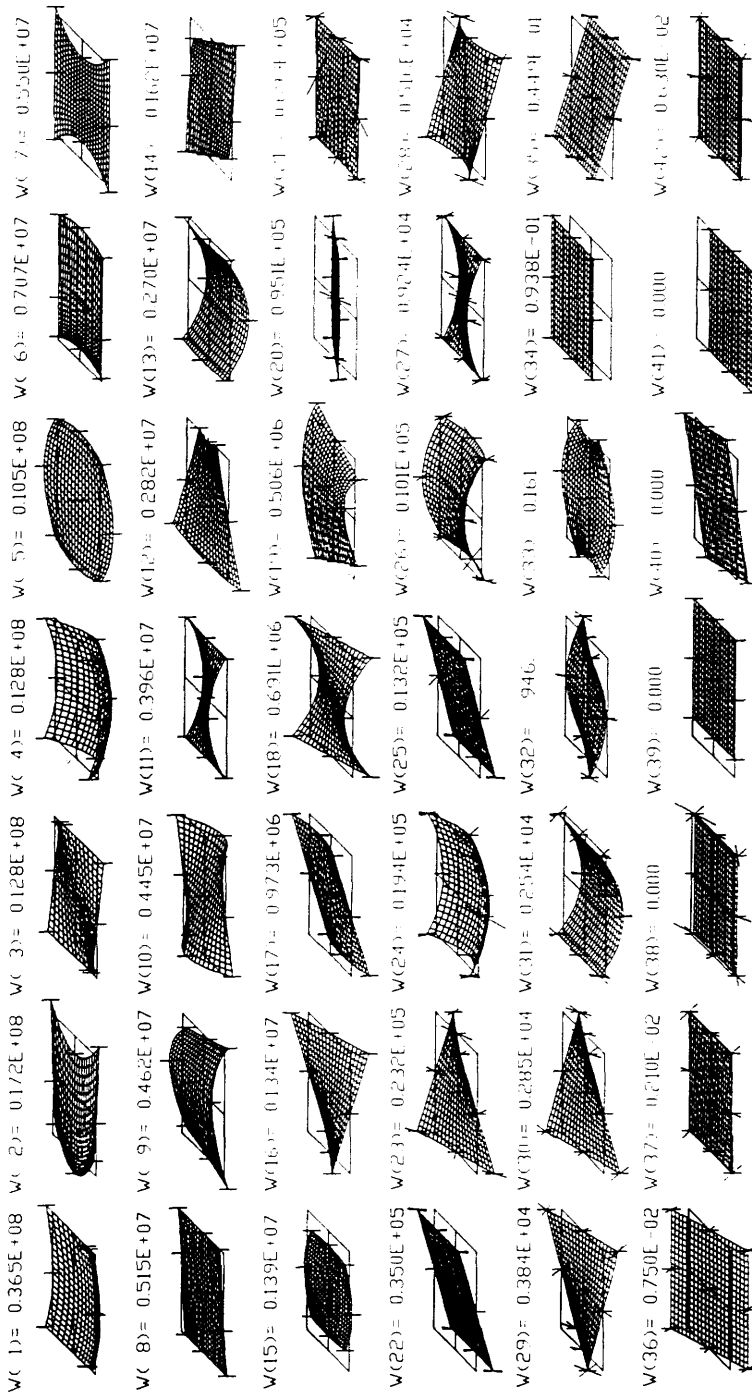


Fig. 5.15 Rank analysis of the Ahmad's element, the eigenmodes of the Heterosis approximation with the reduced integration rule.

SERENDIPITY APPROXIMATION - FULL INTEGRATION

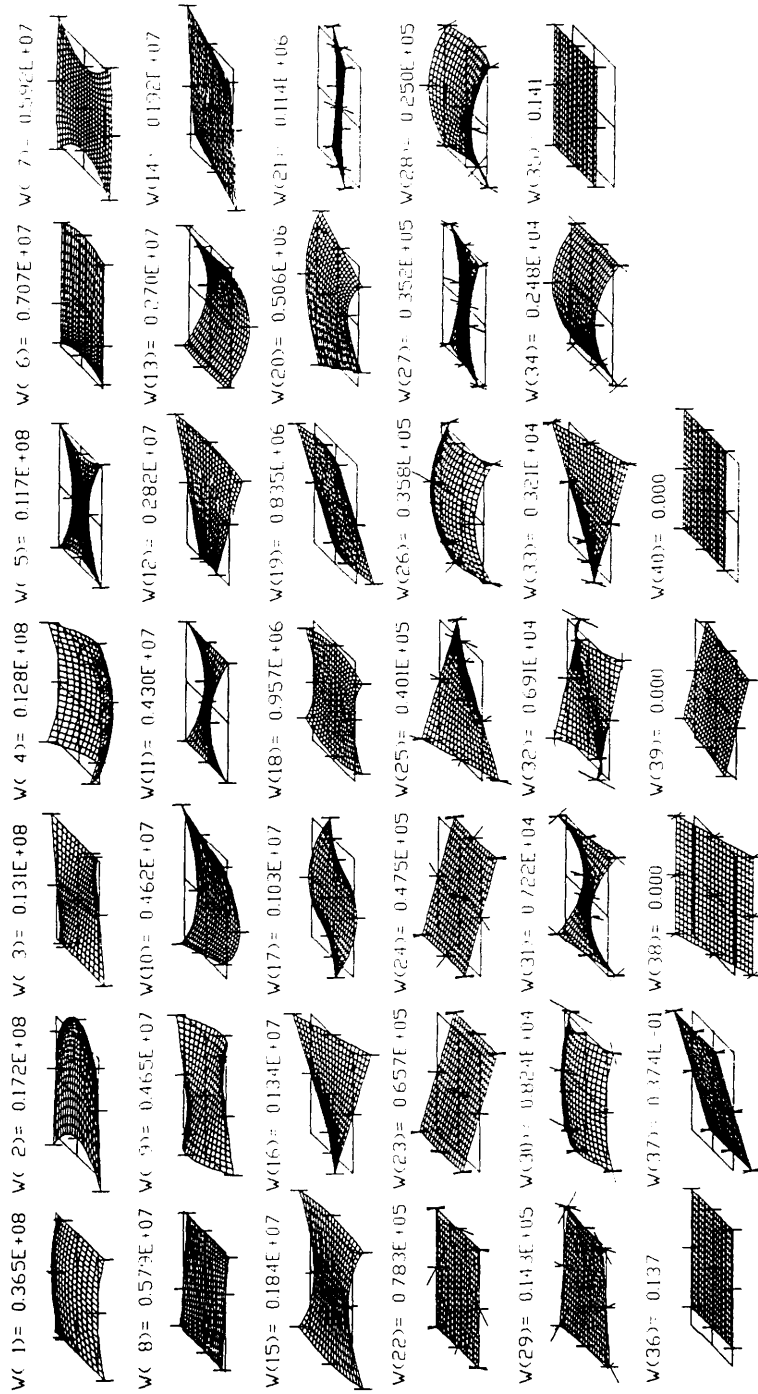


Fig. 5.16 Rank analysis of the Ahmad's element, the eigenmodes of the Serendipity approximation with the full integration rule.

SERENDIPITY APPROXIMATION - SELECTIVE INTEGRATION

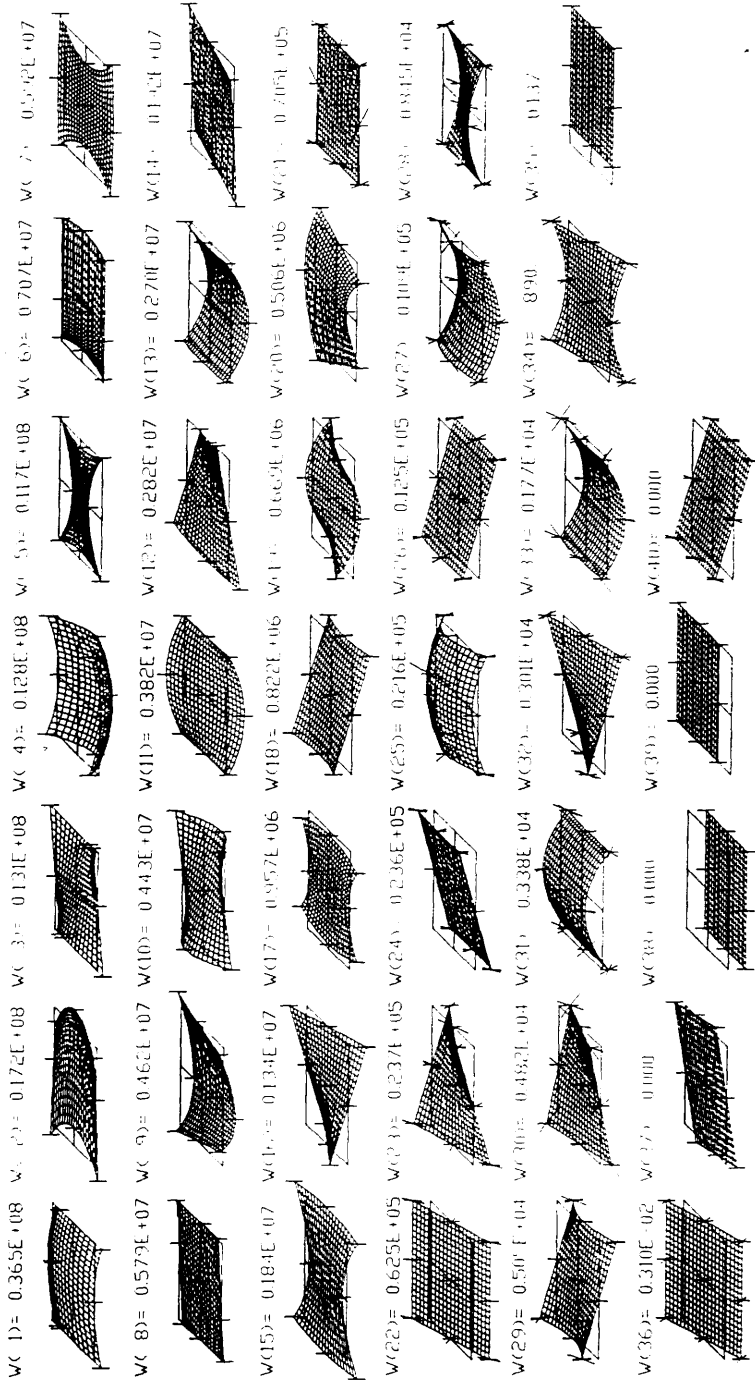


Fig. 5.17 Rank analysis of the Ahmad's element, the eigenmodes of the Serendipity approximation with the selective rule.

SERENDIPITY APPROXIMATION - REDUCED INTEGRATION

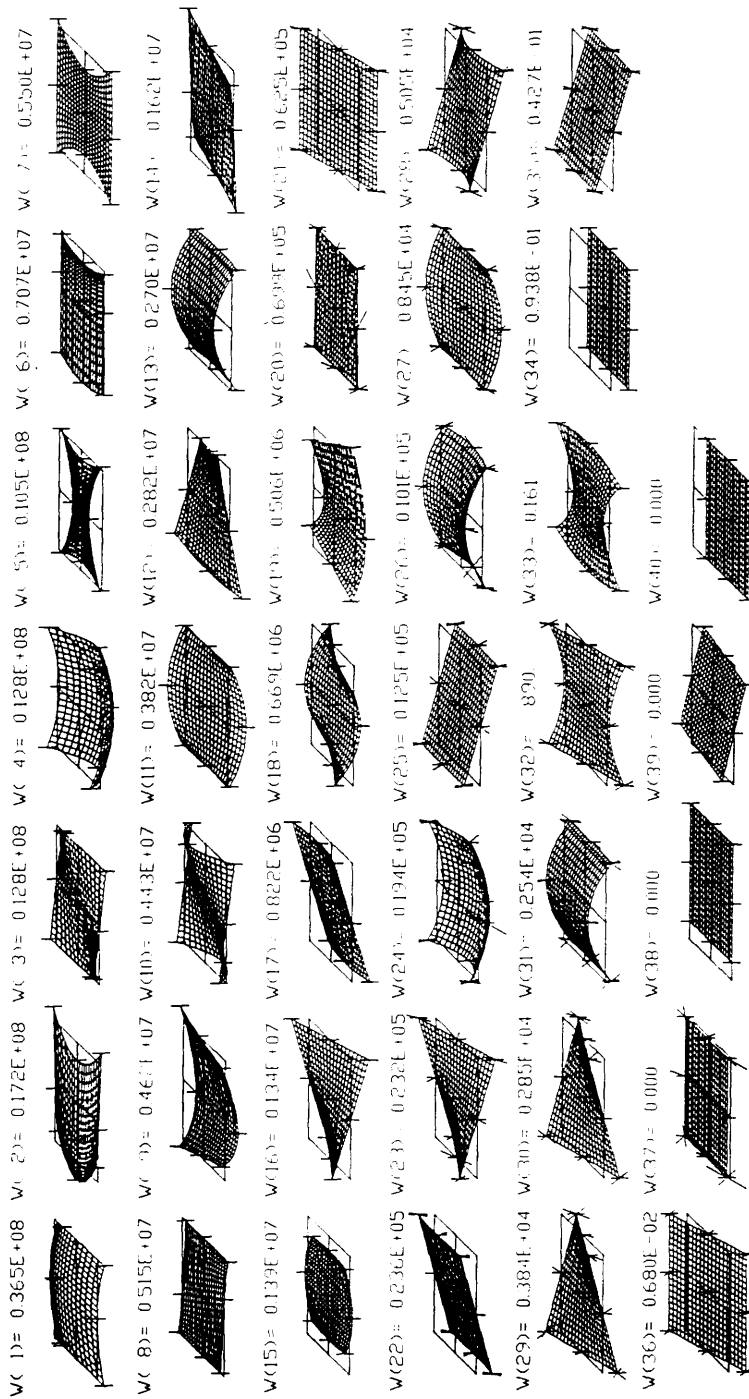


Fig. 5.18 Rank analysis of the Ahmad's element, the eigenmodes of the Serendipity approximation with the reduced rule.

The results are summarized in Tab. 5.4.

Displacement approximation	Integration rule								
	Full			Selective			Reduced		
Type of mode	B	M	T	B	M	T	B	M	T
Lagrangian	0	0	0	1	0	1	4	3	7
Heterosis	0	0	0	0	0	0	3	1	4
Serendipity	0	0	0	0	0	0	1	1	2


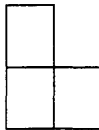

Legend: B = bending mode
M = membrane mode
T = total number

Tab. 5.4 Rank analysis of Ahmad's elements, number of spurious energy modes of one element.

From Fig. 5.10 to 5.18 it is apparent that the more integration points, the higher the associated energy with particular eigenmodes. The most important eigenmodes are those with low inherent energy. This is due to the fact that they have the most significant influence on the stability of the analysis of a structure. In other words they strongly influence the determinant of the global stiffness matrix. Furthermore comparing the example results for the Serendipity element with the Lagrangian approximation it is apparent that the "bubble" mode associated with the central ninth point is missing. Clearly, six zero energy modes are associated with rigid body motions of the element, three displacements in the x, y and z directions and three rotations with respect to the x, y and z axis. However it should be pointed out that some of them are fulfilled only in an integral form, see for example the vertical z displacement of Lagrangian element and reduced integration, i.e. mode no. 34. Obviously, using full 3x3 nodes Gaussian integration and full quadratic displacement approx-

ximation (Lagrangian element) all rigid body motions are exact.

Finally tests were made to determine the previously found spurious modes are communicable. The two, three and four element meshes depicted in Tab. 5.5 were analyzed. The material properties and geometry of the adopted element were the same as those for the cantilever, the only difference being that now the element length in the x direction was only 0.5m.

Number of element	2	3	4
Structure layout			

Tab. 5.5 Rank analysis of Ahmad's elements, their layout for the analysis of communicability of spurious energy modes.

As expected the number of spurious energy modes is the same for all three meshes and is summarized in Tab. 5.6.

Displacement approximation	Integration rule								
	Full			Selective			Reduced		
Type of mode	B	M	T	B	M	T	B	M	T
Lagrangian	0	0	0	1	0	1	4	3	7
Heterosis	0	0	0	0	0	0	3	0	3
Serendipity	0	0	0	0	0	0	0	0	0

Legend: B = bending mode
M = membrane mode
T = total number

Tab. 5.6 Rank analysis of Ahmad's element, number of spurious energy modes of meshes of two or more elements.

Comparing Tab. 5.4 with Tab. 5.6 it is obvious that both spurious energy modes of Serendipity element and reduced integration as well as the membrane spurious mode, the so called hour-glass mode of the Heterosis element and reduced integration, are non communicable and can be ignored for practical analysis, where many elements are used.

The influence of material nonlinearity.

The following part of this section is concerned with the influence of material nonlinearity on the rank of Ahmad's shell element stiffness matrix. Obviously any "releasing" of the material's internal bounds, which simulates either cracks or plastic flow, degrades the rigidity of the element and consequently also the stability of the solution of the problem's set of governing equations. However the question is to what extent this can happen. Based on the author's experiences with analysis of ordinary reinforced concrete shells which are usually very thin, the limiting factor of the bearing capacity of this type of structures is dependent upon material failure, and the best results were obtained with the Lagrangian approximation and full integration of the element. This type of element formulation will now be discussed.

The structure comprising two elements depicted in Fig. 5.9 was used again. However instead of loading by concentrated forces a longitudinal displacement at the free edge (opposite to the clamped end) was applied. Compression hardening was modeled by the Madrid parabola, (defined by (3.66), (3.67) in Chapter 3).

The additional material constants used were:

Compression strength $f'_c = 32\text{MPa}$

Tension strength $f_{tu} = 3.0\text{MPa}$

Maximum uniaxial strain beyond which full crushing is expected

$$\varepsilon_{m,c} = 0.006$$

Tension stiffening factor for stress normal to the crack $\alpha_2 = 0.5$

Shear retention factor for shear modulus $\beta_2 = 0.25$

The strain in the crack corresponding to zero normal strain in the crack

$$\alpha_1 \varepsilon_{cr} = 0.002$$

The strain in the crack corresponding to zero shear modulus in the crack

$$\beta_1 \varepsilon_{cr} = 0.004$$

Plasticity.

The structure was loaded by a longitudinal displacement at the free-end edge until plasticity occurred and the solution diverged. This took place at an average strain ε_x of approximately -0.0021. At this state the modal analysis of the stiffness matrix was carried out. The results are shown in Fig. 5.19. The least non-zero mode was 686kPa, which is approximately 28% of its original value (for the elastic condition). The same drop in the least non-zero eigenmode was found to be 26.5kPa for selective integration.

One can see that in spite of a substantial decrease of energy pertaining to bending and longitudinal membrane eigenmodes the rank of matrix remained correct. On the other hand the element rigid body modes are not simple movements or rotations with respect to particular coordinate axis.

Nevertheless it can be concluded that numerical collapse of the solution is caused by the independence of internal forces on displacements in the fully plastic state and not by a stiffness matrix singularity. When selective integration is used, in addition to one spurious mode pertinent to this formulation, the first non-zero eigenmode might become so small that numerical problems may arise. The eigenmode energies near failure for that element formulation are summarized in Tab. 5.7.

LAGRANGIAN APPROXIMATION, FULL INTEGRATION - PLASTIC MATERIAL

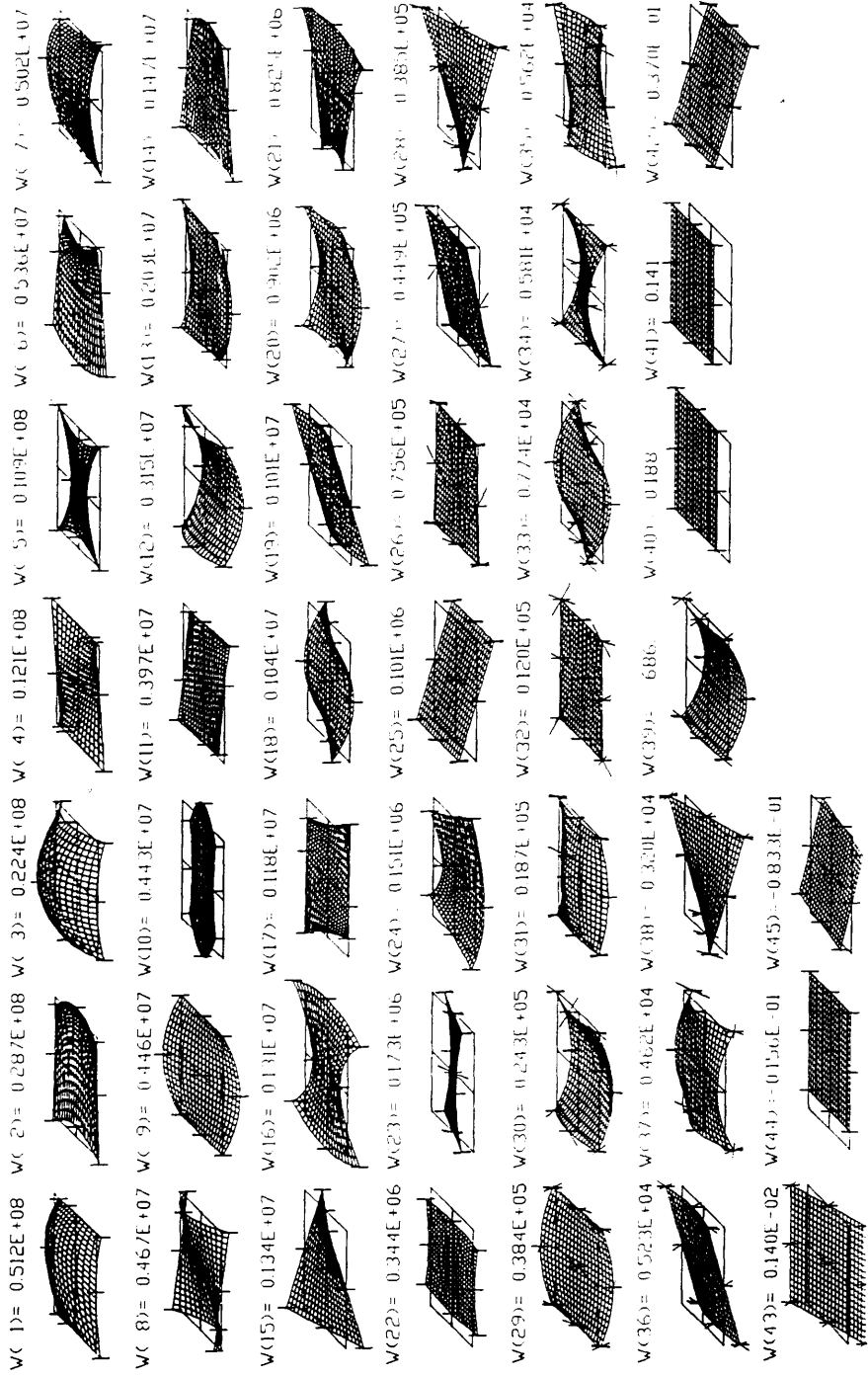


Fig. 5.19 Rank analysis of the Ahmad's element, the eigenmodes of the Lagrangian approximation, full integration - plastic material condition in the longitudinal direction.

No.	Energy	No.	Energy	No.	Energy
1	51197192.0000	16	1311029.7500	31	3749.0940
2	28691792.0000	17	1176385.3750	32	3082.9612
3	21580850.0000	18	969992.3750	33	2703.8564
4	12146729.0000	19	825307.6250	34	2422.1797
5	10944694.0000	20	689302.8750	35	2037.1451
6	5364164.5000	21	343558.1250	36	1410.8766
7	5017893.5000	22	151468.1563	37	630.5328
8	4449131.5000	23	82119.0625	38	265.3866
9	4427108.0000	24	68460.1328	39	0.1875
10	3968827.5000	25	34204.8633	40	-0.0040
11	3955486.7500	26	21930.3730	41	-0.0156
12	3009769.0000	27	20257.8301	42	-0.0255
13	2025495.6250	28	9795.6201	43	-0.0833
14	1468745.5000	29	9222.1240	44	-0.2347
15	1344603.1250	30	8172.1479	45	-0.2800

Table 5.7 Rank analysis of the Ahmad's element, the eigenmodes of the Lagrangian approximation, selective integration - plastic condition in the longitudinal direction.

Cracks.

In order to study influence of cracks on the rank of the stiffness matrix, the same structure was used again. As with the plastic case, the structure was loaded by a longitudinal displacement at the free edge up to failure. This occurred for an average strain, $\epsilon_x \cong 0.0012$. At this point the shear modulus G had reduced to 17% of its original value. For the calculation of the stiffness matrix Young's modulus perpendicular to the cracking is assumed to be, (see also material model b/ in Chapter 3, (3.36), (3.37)):

- 1 - zero, if the crack is in the process of opening, and,
- 2 - equal to the residual secant value, if the crack is in the

process of closing (i.e. the current strain is below the maximum value reached during previous iterations at that particular integration point). The residual Young's modulus is given by the line defined by the points $[0; \alpha_t E]$ and $[\epsilon_{m,t}, 0]$, i.e. for $\epsilon \geq \epsilon_{m,t}$ the value of Young's modulus is equal to zero. The full tension stiffening model is considered only for calculation of internal forces.

Fig. 5.20 presents the results of a modal analysis corresponding to the failure state. It should be noted that most of the integration points were in the process of closing when the stiffness matrix was calculated and Young's modulus used across the crack was about 3GPa. For the remaining points (about 10%) zero Young's modulus was used.

One can see that this time the least non-zero mode was only 166kPa and thus numerical stability of the solution has deteriorated more significantly than was the case for the plastic material. Using selective integration the situation is even worse. The eigenmode energies near failure for that element formulation are summarized in Tab. 5.8. In this case a plausible reason for the numerical failure of the solution seems to be the singularity which appears in the stiffness matrix, therefore a priori rank deficient element formulations seem to be less suitable.

LAGRANGIAN APPROXIMATION, FULL INTEGRATION - MATERIAL CRACKED

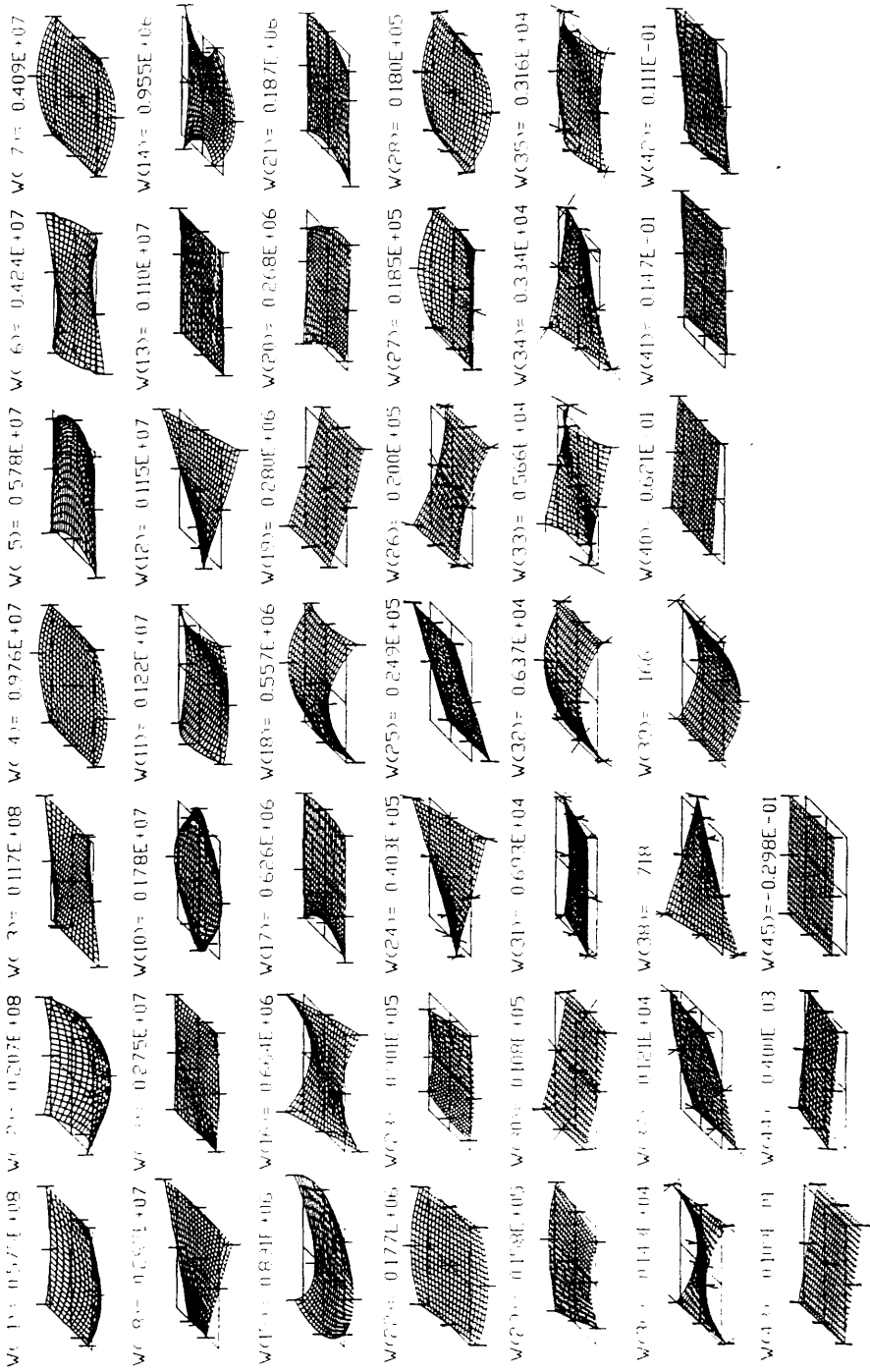


Fig. 5.20 Rank analysis of the Ahmad's element, the eigenmodes of the Lagrangian approximation, full integration - fully cracked material in the longitudinal direction.

No.	Energy	No.	Energy	No.	Energy
1	57526536.0000	16	629158.1875	31	1762.8800
2	20083550.0000	17	269158.3750	32	1632.5271
3	11726142.0000	18	266928.6250	33	1135.1084
4	9764140.0000	19	198896.0000	34	816.4446
5	5803756.5000	20	187466.2188	35	495.8130
6	4188461.2500	21	90720.9063	36	337.5460
7	3676849.5000	22	89170.3438	37	164.7204
8	2850331.0000	23	25611.5215	38	28.1272
9	2750403.0000	24	18042.3672	39	0.1456
10	1780067.7500	25	16290.3555	40	0.0364
11	1152568.3750	26	15856.6973	41	0.0236
12	1101694.3750	27	7409.3589	42	0.0121
13	958359.8750	28	5096.4927	43	0.0072
14	892333.6875	29	4931.7388	44	-0.0027
15	845440.3750	30	3294.0686	45	-0.1149

Table 5.8 Rank analysis of the Ahmad's element, the eigenmodes of the Lagrangian approximation, selective integration - fully cracked material in the longitudinal direction.

It can be concluded that some earlier published data on this topic do not agree with the present results even for the elastic material condition. Furthermore it was found that in spite of the fact that neither plastic nor cracked material conditions didn't change the rank of the stiffness matrix, (due to the small residual shear considered), numerical problems could arise as a consequence of very small least non-zero eigenvalues. The cracks in the material are more difficult to treat numerically than plasticity. Despite other recommendations pertaining to the elastic regime [56], for nonelastic material conditions the element formulation with correct rank is highly preferable. It should be also noted that the same material conditions is assumed within the whole area of the integration point. Hence, more integration

points result in a more gradual failure. From that point of view it may be justified to integrate at more sampling points than required for exact integration under elastic material conditions.

Note that the simplest case was assumed, that is the same type of failure occurred at all integration points. However it is reasonable to presume the element behavior in a more general case would be similar.

6. NUMERICAL METHOD FOR SOLUTION OF NONLINEAR EQUATIONS.

The finite element formulation and discretization procedures result in a set of equations which characterize the response of the structure due to loading. The dimension of the problem is generally equal to the number of structural degrees of freedom. For real structures this can be very large.

In linear analysis the set of equations is obviously linear and can be solved directly using, for instance, Gauss elimination procedures, the Cholesky method or some iterative method such as Gauss-Siedel, Jordan methods etc. These procedures are quite well known and their usage causes no serious problems.

If the structural behavior is nonlinear the solution is much more difficult. A direct or "closed" solution for practical examples is impossible and we have to use some iterative procedure. This brings problems with, for example, convergence, numerical stability, uniqueness etc. Therefore we must pay careful attention to this phase of the analysis.

In general it is not possible to suddenly load a structure with its full loading and instead we must apply step-by-step incremental loading. For each load level the response of the structure is computed. This corresponds to the simplifications (the linearization of deformation increment) made during the approximation of the virtual work increment. It is apparent, however, that the time cost of nonlinear analysis is very high and hence it is crucially important to establish the minimum number of increments which are required to preserve convergence.

The main objective of this chapter is to review some well established methods for the solution of a set of nonlinear equations resulting from nonlinear structural analysis and to present an improved solution scheme. The numerical results pertaining to the particular algorithms are discussed in Chapter 8.

6.1 Newton-Raphson method.

Using the concept of incremental step by step analysis we obtain the following set of nonlinear equations:

$$\mathbf{K}(\underline{p}) \Delta \underline{p} = \underline{q} - \underline{f}(\underline{p}) \quad /6.1/$$

where \underline{q} is the vector of total applied joint loads ,

$\underline{f}(\underline{p})$ is the vector of internal joint forces,

$\Delta \underline{p}$ is the deformation increment due to loading increment,

\underline{p} are the deformations of structure prior to load increment,

$\mathbf{K}(\underline{p})$ is the stiffness matrix, relating loading increments to deformation increments.

The R.H.S. of /6.1/ represents out-of-balance forces during a load increment, i.e. the total load level after applying the loading increment minus internal forces before additional loading. Generally, the stiffness matrix is deformation dependent, i.e. a function of \underline{p} , but this is usually neglected within a load increment in order to preserve linearity. In this case the stiffness matrix is calculated based on the value of \underline{p} pertaining to the level prior the load increment.

The set of equations /6.1/ is nonlinear because of the nonlinearity of the internal forces:

$$\underline{f}(k\underline{p}) \neq k \underline{f}(\underline{p}), \text{ where } k \text{ is an arbitrary constant}$$

$$\mathbf{K}(\underline{p}) \neq \mathbf{K}(\underline{p} + \Delta \underline{p}) \quad /6.2/$$

and hence the necessity of a nonlinear solution scheme.

The set of equations represent the mathematical description of structural behavior during one step of the solution. Rewriting

equations /6.1/ for the i -th iteration within a distinct loading increment we obtain:

$$K(p_{i-1}) \Delta p_i = q - f(p_{i-1}) \quad /6.3/$$

All the quantities for the $i-1$ iteration have already been calculated during previous solution steps and solved for p_i at load level q , which corresponds to loading at this step:

$$p_i = p_{i-1} + \Delta p_i \quad /6.4/$$

As pointed out earlier, equation /6.3/ is nonlinear and therefore it is necessary to iterate until some convergence criterion is satisfied. There are many possibilities for defining the convergence criterion. Two of the most widely used are given by:

$$\frac{\Delta p_i^T \Delta p_i}{p_i^T p_i} \leq \varepsilon^2 \quad /6.5/$$

and

$$\frac{(q - f(p_{i-1}))^T (q - f(p_{i-1}))}{q^T q} \leq \varepsilon', 2$$

respectively.

The first one checks the norm of deformation changes during the last iteration whereas the second one checks the norm of the out-of-balance forces. In both cases the acceptable error ε and ε' are defined in relative terms in order to avoid dependence on units, dimensions of structure etc. Usually the value of ε and ε' are of order of 0.01.

The above solution can also be understood from the following abbreviate point of view: The main equations can be re-written

as:

$$\underline{f}(\underline{p}) = \underline{q} \quad /6.6/$$

where $\underline{f}(\underline{p})$ is the vector of internal nodal forces that correspond to deformation \underline{p} and \underline{q} is the vector of applied loads. Then using Taylor's theorem equations /6.6/ can be written for the j -th equation by (using only constant and linear terms):

$$f_j(\underline{p}) = f_j(\underline{p}_{i-1}) + \frac{\partial f_j(\underline{p}_{i-1})}{\partial p_k} \Delta p_k + \dots = q_j \quad /6.7/$$

where j ranges from 1 to n , k is the summation index, i is the iteration number, i.e. $i=1,2,\dots$

Comparing /6.7/ and /6.3/ it is obvious that both expressions are identical, the notation only being different.

The concept of the incremental loading strategy is depicted in Fig. 6.1.

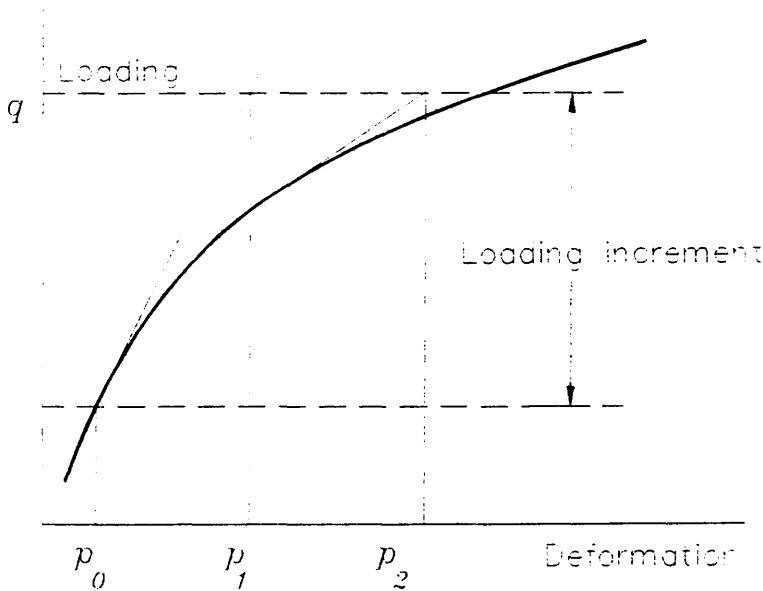


Fig. 6.1 Newton-Raphson method.

6.2 Modified Newton-Raphson method.

The most time consuming part of solution /6.3/ is recomputing the stiffness matrix $K(p_{i-1})$ for each iteration. In many cases this is not necessary and we can use matrix $K(p_0)$ from the first iteration of the step. This is the basic idea of the so-called Modified Newton-Raphson method. It produces very significant time saving, but on the other hand, it also causes worse convergence of the solution procedure.

Therefore this solution scheme is suitable for structures and loading far enough from some local extreme, bifurcation point etc., where there are difficulties to deal with. An additional simplification is the so-called Initial stiffness method in which the matrix K is computed only for the first loading step and iteration, and thereafter is kept constant for all following solution steps.

The simplification adopted in the Modified Newton-Raphson method can be mathematically expressed by:

$$K(p_{i-1}) \approx K(p_0) \quad /6.8/$$

The modified Newton-Raphson method is shown in Fig. 6.2. Comparing Fig. 6.1 and 6.2 it is apparent that the Modified Newton-Raphson method converges more slowly than the original Newton-Raphson method. On the other hand one iteration costs less time because it is necessary to assemble and eliminate the stiffness matrix only once. In practice a careful balance of the two methods is usually adopted in order to produce the best performance for a particular case. Usually we start a solution with the Modified Newton-Raphson method and later, i.e. near extreme points, switch to the original procedure to avoid divergence.

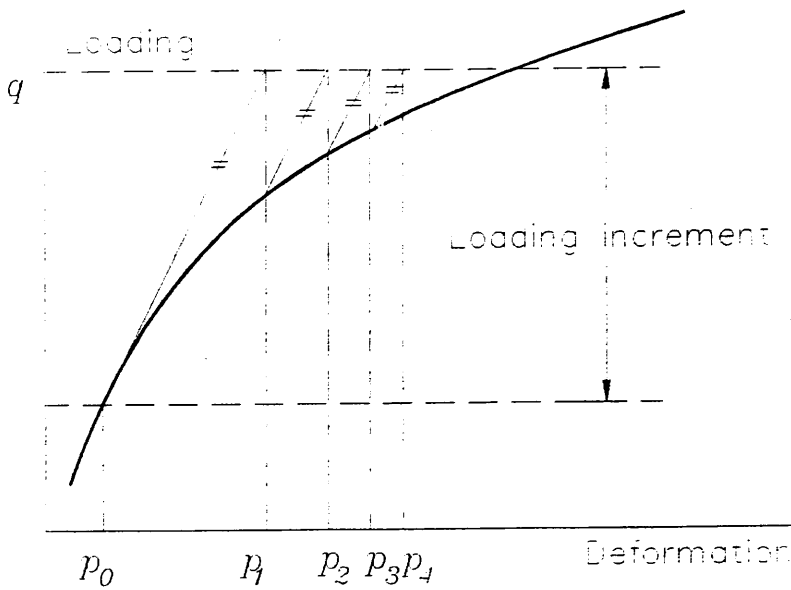


Fig. 6.2 Modified Newton-Raphson method.

6.3 Quasi-Newton method.

The Quasi-Newton method is very similar to the above methods and can be understood as a compromise between time cost and convergence performance. The basic idea is to modify the stiffness matrix $K(p_{i-1})$ for every iteration based not on the mechanical nature of the problem, but on the convergence behavior in previous iterations. For most cases the solution converges much better compared to the Modified Newton-Raphson method and at the same time the recomputation and redecomposition of K pertaining to the original Newton-Raphson method is avoided. The crucial importance is the way K is modified.

Equation /6.3/ can be re-written by:

$$D_i \Delta p_i = q - \underline{f}(p_{i-1}) \quad /6.9/$$

where the matrix D_i is based on the equation behavior at two successive points p_{i-1} and p_i :

$$D_{i-1} (p_i - p_{i-1}) = \underline{f}(p_i) - \underline{f}(p_{i-1}) + \Delta \underline{r} \quad /6.10/$$

Then for $p_i \Rightarrow p_{i-1}$, $\underline{f}(p_i) \Rightarrow \underline{f}(p_{i-1})$ and $\Delta \underline{r} \Rightarrow \underline{0}$.

$$\quad \quad \quad /6.11/$$

Suitable candidates for matrix D must satisfy equations /6.10/ and /6.11/ and in addition their evaluation based on D_{i-1} , $\Delta p_i = p_i - p_{i-1}$ (displacement increment) and $\Delta \underline{f}_i = \underline{f}(p_i) - \underline{f}(p_{i-1}) = -\underline{g}_i$ (out-of-balance forces) must be easy.

The simplest way to modify matrix D_{i-1} to D_i is given by the first order change:

$$D_i = D_{i-1} + \frac{[\Delta \underline{f}_i - D_{i-1} \Delta p_i] \underline{u}^T}{\underline{u}^T \Delta p_i} \quad /6.12/$$

where \underline{u} is arbitrary vector to be chosen, and $\underline{u}^T \Delta p_i \neq 0$.

There are many choices for \underline{u} and two of the most widely used are summarized as follows:

$$\underline{u} = \Delta p_i \quad \dots\dots\dots \text{Broyden method (B),}$$

$$\underline{u} = (\Delta \underline{f}_i - D_{i-1} \Delta p_i) \quad \dots\dots \text{Davidson method (D)} \quad /6.13/$$

Substituting /6.13/ into /6.12/ it is possible to modify the matrix D for every iteration, which actually serves as a replacement of the original stiffness matrix $K(p_{i-1})$ in /6.3/.

The most used second order modification of the matrix D are: (where E is the identity matrix):

Davidson-Fletcher-Powell method (DFP):

$$D_i = \left[\begin{array}{cc} E & -\frac{\Delta \underline{f}_i \Delta \underline{p}_i^T}{\Delta \underline{f}_i^T \Delta \underline{p}_i} \end{array} \right] D_{i-1} \left[\begin{array}{cc} E & -\frac{\Delta \underline{p}_i \Delta \underline{f}_i^T}{\Delta \underline{p}_i^T \Delta \underline{f}_i} \end{array} \right] + \frac{\Delta \underline{f}_i \Delta \underline{f}_i^T}{\Delta \underline{p}_i^T \Delta \underline{f}_i} \quad /6.14/$$

or Broyden-Fletcher-Goldfarb-Shanno method (BFGS):

$$D_i = D_{i-1} + \frac{\Delta \underline{f}_i \Delta \underline{f}_i^T}{\Delta \underline{p}_i^T \Delta \underline{f}_i} - \frac{D_{i-1} \Delta \underline{f}_i \Delta \underline{f}_i^T D_{i-1}^T}{\Delta \underline{p}_i^T D_{i-1} \underline{p}_i}$$

Unfortunately there is one essential drawback common to all Quasi-Newton procedures and it is the fact that they destroy the sparse character of the stiffness matrix. In practice we work with very large systems of equations and hence the sparse character of matrix K has a crucial importance. In addition, the stiffness matrix is symmetric and this property is also employed. Using this method, the above advantages are lost. Only Davidson and BFGS methods preserve symmetry, but the penalty is a worse convergence performance.

Therefore instead of /6.9/ we usually rewrite the problem in the form:

$$\Delta \underline{p}_i = D_i^{-1} \left[\underline{q} - \underline{f}(\underline{p}_{i-1}) \right] \quad /6.15/$$

and matrix D_i is inverted only once, i.e. for the first iteration. Then during the following solution one of the previous modifications of matrix D are applied directly on D_i^{-1} , i.e. we compute directly $\Delta \underline{p}_i$ without any decomposition of D .

In the case of the second order modifications it is necessary to change /6.15/ appropriately¹. The sparse character of structural matrices is lost in any case and it is worthwhile to note that the inversion of D is also very laborious.

Advantages are gained by using the first order modification in which case the matrix D_i^{-1} can be written in form:

$$D_i^{-1} = D_0^{-1} + \sum_{k=0}^i \beta_k \frac{v_k}{v_k} \frac{v_k^T}{v_k^T} \quad /6.16/$$

The expressions for the scalar β_k and vector \underline{v}_k can be set by comparing /6.16/ with the inverted expressions for /6.13/ through /6.15/.

Hence using /6.16/ it is not necessary to invert matrix D_0 , because we can write directly:

$$\Delta p_1 = \Delta p_1 + \sum_{k=0}^i \beta_k \frac{v_k}{v_k} \frac{v_k^T}{v_k^T} \left[\underline{q} - \underline{f}(p_{1-1}) \right] \quad /6.18/$$

and Δp_1 is computed directly by Gauss elimination similar

Note:

¹To invert the matrix from /6.14/ and /6.15/ the following formulae are used:

$$\left(A + \alpha \underline{u} \underline{v}^T \right)^{-1} = A^{-1} - \beta \underline{x} \underline{z}^T$$

$$\underline{x} = A^{-1} \underline{u}$$

$$\underline{z} = A^{-1} \underline{v}$$

$$\beta = \alpha \left(1 + \alpha \underline{v}^T A^{-1} \underline{u} \right)^{-1} \quad /6.17/$$

to the Modified Newton Raphson method using matrix $K(p_0)$.

Unfortunately this method of solution can be used only in the case of the first order modifications of D . Its use is relatively simple because it involves storing only a couple of vectors v_k (in slow memory) and evaluating their scalar product. For $k \geq 4$ it is usually better to assemble a new matrix K and to start the Quasi-Newton method from the beginning again, i.e.:

$$D_0 = K(p_0) \quad /6.19/$$

Quasi-Newton methods represent a significant improvement over the Modified Newton-Raphson method in terms of convergence performance and time cost but is worse than the full Newton Raphson scheme in terms of convergence, but not in time. Good experience has been obtained especially with the BFGS modification and it can be said that for many years it was the only procedure suitable for the solution of more difficult large problems. In these cases the Modified Newton-Raphson method diverged and the original Newton-Raphson method was unacceptable because of solution time cost. In recent times, the importance of this method has diminished because of the discovery of Arc-length methods, which are more reliable and robust and at the same time not as expensive. Nevertheless some authors combine the Arc-length and Quasi-Newton methods into one solution scheme and claim very good results in the case of the first order modifications in the form /6.16/.

More information about Quasi-Newton methods can be found in numerous references, e.g. [24].

6.4 Arc-length method.

Next to the Modified Newton-Raphson method, the most widely used method is beginning to be the Arc-length method. This method was first employed about fifteen years ago to solve geometrically nonlinear structures. Because of its excellent performance, it is now quite well established for geometric nonlinearity and for material nonlinearity as well. Many workers have been interested in using and improving Arc-length procedures. The work of Riks [28] and Crisfield [25], [26], [27], [29] are important, but there is still much to do.

The main reason for the popularity of this method is its robustness and computational efficiency which assures good results even in cases where traditional Newton-Raphson methods fail. Using an Arc-length method stability problems such as snap back and snap through phenomena can be studied as well as materially nonlinear problems with unsmooth or discontinuous stress-strain diagrams. This is possible due to the changing load conditions during iterations within an increment.

The main idea of this method is well explained by its name, arc-length. The primary task is to observe complete load-displacement relationship and not to apply a constant loading increment which is defined throughout the load step as in the Newton-Raphson method. Hence this method fixes not only the loading but also the displacement conditions at the end of a step. There are many ways of fixing these, but one of the most common is to establish the length of the loading vector and displacement changes within the step. Hence the name of the procedure, because all admissible solutions of one loading increment must lay on an arc.

From the mathematical point of view it means that we must introduce an additional degree of freedom associated with the loading level (i.e. a problem has n displacement degrees of freedom and one for loading) and in addition a constraint for the new unknown variable must be introduced. The new degree of freedom is usually named λ . There are many possibilities for defining

constraints on λ and some of these are briefly reviewed in the following.

To derive the Arc-length method we rewrite the set of equations /6.1/ in form of /6.20/, where λ defines the new loading factor:

$$K(\underline{p}) \Delta \underline{p} = \lambda \underline{q} - \underline{f}(\underline{p}) \quad /6.20/$$

Now re-writting /6.20/ in a form suitable for iterative solution then:

$$K(\underline{p}) \Delta \underline{p}_1 = \lambda \underline{q} - \underline{f}(\underline{p}_{1-1}) = \lambda \underline{q} - \underline{f}_{1-1} \quad /6.21/$$

$$\underline{p}_1 = \underline{p}_{1-1} + \Delta \underline{p}_1 = \underline{p}_{1-1} + \eta_{1-1} \underline{\delta}_{1-1} \quad /6.22/$$

$$\Delta \underline{p}_1 = \Delta \underline{p}_{1-1} + \eta_{1-1} \underline{\delta}_{1-1}$$

$$\lambda_1 = \lambda_{1-1} + \Delta \lambda_{1-1} \quad /6.23/$$

The notation is explained in Fig. 6.3. The matrix K can be recomputed for every iteration (similar to original Newton-Raphson method) or it can be fixed within one step for all iterations (Modified Newton Raphson method) or it can be replaced by matrix D as in the Quasi-Newton methods. The vector \underline{q} does not mean in this case the total loading at the end of the step but only a reference loading "type". The actual loading level is a multiple of this.

The scalar η_{1-1} is an additional artificial variable which is used to accelerate solutions in cases of well behaved load-deformation relationships or to damp it near bifurcation and extreme points.

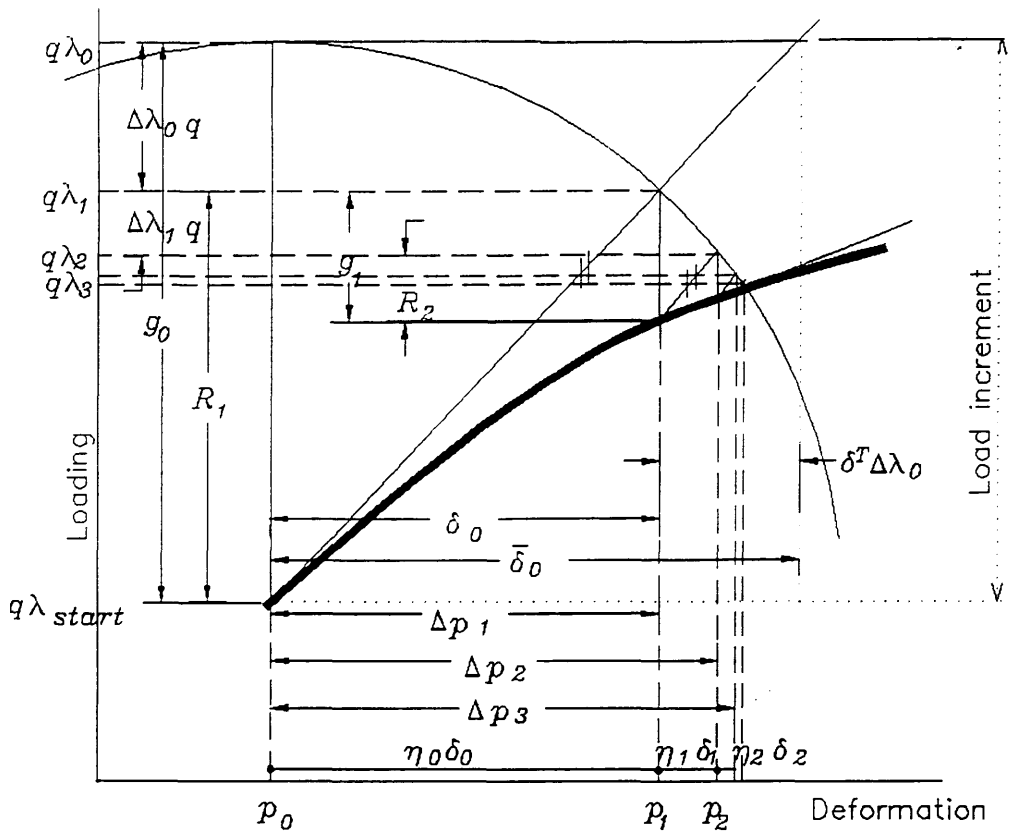


Fig. 6.3 The Arc-length method notation and convergence performance.

Additional notation is defined as follows:

Out-of-balance forces in i -th iteration:

$$\mathbf{g}(\mathbf{p}_i) = \mathbf{g}_i = \mathbf{f}_i - \lambda_i \mathbf{q} = \mathbf{f}_i - (\lambda_{i-1} + \Delta\lambda_{i-1}) \mathbf{q} \quad /6.24/$$

R.H.S vector in i -th iteration:

$$\underline{\text{RHS}}_i = \lambda_i \mathbf{q} - \mathbf{f}_{i-1} = \Delta\lambda_{i-1} \mathbf{q} - \mathbf{g}_{i-1} \quad /6.25/$$

Using /6.22/ through /6.25/ into /6.21/ the deformation increment δ_{-1-1} can be calculated from:

$$K \delta_{-1-1} = \underline{RHS}_{-1-1} = \Delta\lambda_{-1-1} \underline{q} - \underline{g}_{-1-1} \quad /6.26/$$

Hence:

$$\delta_{-1-1} = \bar{\delta}_{-1-1} + \Delta\lambda_{-1-1-T} \delta_{-T}$$

where

$$\bar{\delta}_{-1-1} = -K^{-1} \underline{g}_{-1-1} \quad \text{and} \quad \delta_{-T} = K^{-1} \underline{q}$$

It remains only to set the additional constraint for $\Delta\lambda_{-1-1}$ and η_{-1-1} and the whole algorithm is defined. Thus compared to the Newton-Raphson methods in which we solve n dimensional nonlinear problem, we now need to solve a $(n + 2)$ dimensional problem, where the first n unknowns correspond to deformations and the last two to $\Delta\lambda_{-1-1}$ and η .

If we set $\eta_{-1-1} = 1$ then we deal with an $(n + 1)$ dimensional problem. Else an additional constraint must be introduced, usually by the Line search method. This is discussed later. Also $\bar{\delta}_{-1-1}$, δ_{-T} and δ_{-1-1} are of order $(n + 1)$, and the $(n + 1)$ -th coordinate, which corresponds to the loading dimension λ , is set to zero.

Now let us introduce two new vectors \underline{t}_{-1-1} and $\bar{\eta}_{-1-1}$ as shown in Fig. 6.4. There are defined by:

$$\underline{t}_{-1-1} = \Delta p_{-1-1} + \beta (\lambda_{-1-1} - \lambda_{-s} \text{ t art}) \quad /6.27/$$

and

$$\underline{n}_{-1-1} = \eta \delta_{-1-1} + \beta \Delta\lambda_{-1-1} \quad /6.28/$$

where:

β is scalar that relates dimensions of λ and deformation space,
 λ_{i-1} is a $(n + 1)$ dimensional vector with its first n coordinates set to zero (deformation space) and its $(n + 1)$ -th coordinate equal to λ_{i-1} ,
 λ_{start} is a $(n + 1)$ dimensional vector with its first n coordinates set to zero (deformation space) and its $(n+1)$ -th coordinate set to λ_{start} , i.e. the load level prior to the current loading increment was applied,
 Δp_{i-1} is a deformation vector (The 1-st through n -th coordinates are nonzero, $(n + 1)$ -th coordinate equals zero)

The entities \underline{t}_{i-1} and \underline{n}_{i-1} are understandable from Figure 6.4:

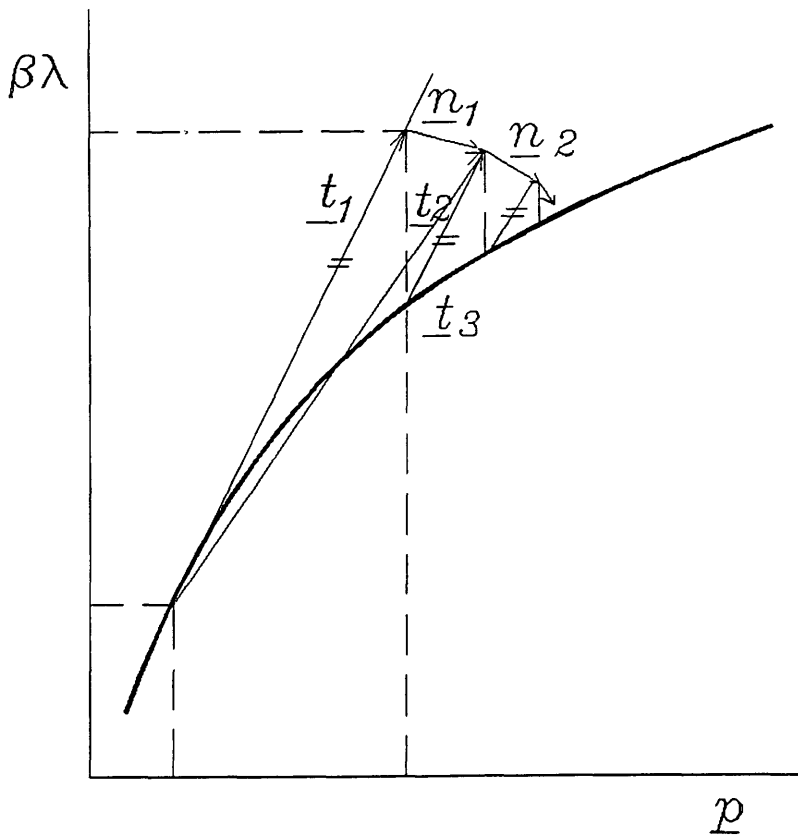


Fig. 6.4 The vectors \underline{t}_i , \underline{n}_i and scalar β .

It is then obvious that

$$\underline{t}_1 = \underline{t}_{1-1} + \underline{n}_{1-1} \quad /6.29/$$

Also the residual R_{1-1} is defined by:

$$R_{1-1} = \underline{t}_{1-1} \underline{n}_{1-1} \quad /6.30/$$

Equations /6.26/ through /6.30/ lead to the final expression for the unknown $\Delta\lambda_{1-1}$ (noting that $\Delta p_{1-1}^T \Delta\lambda_{1-1} = p_{1-1}^T * \lambda_{1-1} = 0$):

$$\Delta\lambda_{1-1} = \frac{R_{1-1} - \Delta p_{1-1}^T \bar{\delta}_{1-1}}{\eta \Delta p_{1-1}^T \bar{\delta}_{1-1} + \beta^2 (\lambda_{1-1} - \lambda_{\text{start}})} \quad /6.31/$$

To obtain $\Delta\lambda_{1-1}$ using /6.31/, the main problem is how to compute the residual R_{1-1} . Some of these are now briefly listed.

6.4.1 Vector \underline{n}_1 lies in the plane normal to \underline{t}_1 (Normal update plane method):

In this particular case $R_{1-1} = \underline{t}_{1-1}^T \underline{n}_{1-1} = 0$ and thus /6.30/ leads to :

$$\Delta\lambda_{1-1} = \frac{\Delta p_{1-1}^T \bar{\delta}_{1-1}}{\eta \Delta p_{1-1}^T \bar{\delta}_{1-1} + \beta^2 (\lambda_{1-1} - \lambda_{\text{start}})} \quad / 6.32/$$

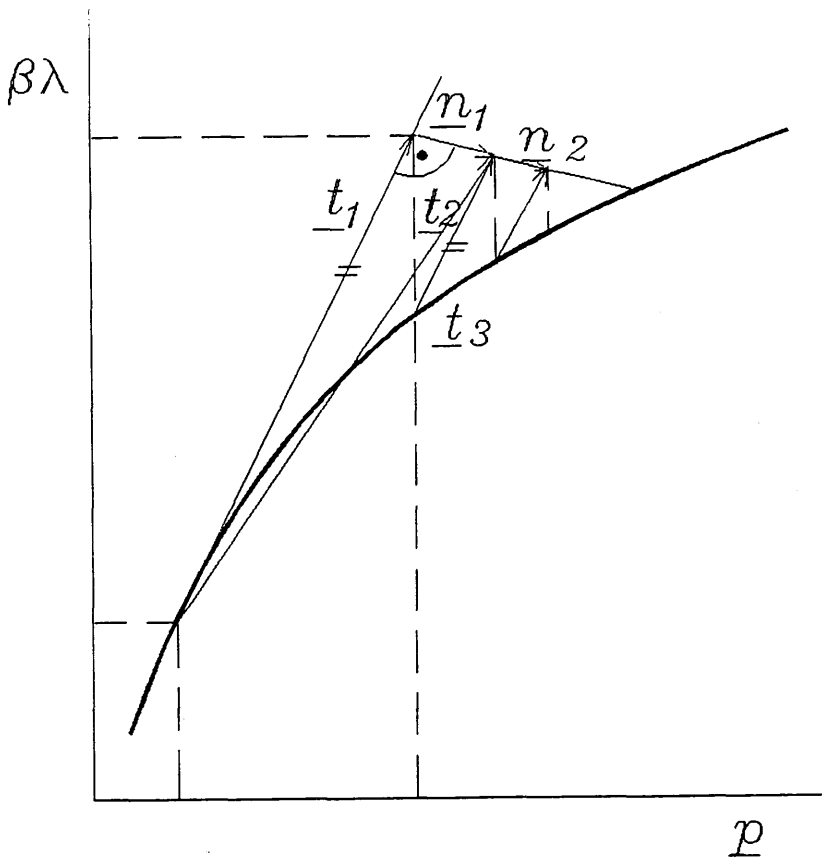


Fig. 6.5 Normal update plane for solution $\Delta\lambda_{i-1}$.

The main advantage of this method is its simplicity. The Normal update plane is relatively reliable, but it can fail if the λ - p diagram suddenly changes its slope or turns back or down (snap back and snap through). Nevertheless if these special conditions are treated by this method then a very significant reduction in step length is unavoidable.

6.4.2 Consistently linearized method:

The residual R_{i-1} is defined in this case by

$$\begin{aligned}
 R_{i-1} &= \underline{t}_{i-1}^T \underline{n}_{i-1} = |\underline{t}_{i-1}| |\underline{n}_{i-1}| \cos\alpha = \\
 &= -|\underline{t}_{i-1}| (|\underline{t}_{i-1}| - s) \quad /6.33/
 \end{aligned}$$

The step length s and angle α are depicted in Fig. 6.6. The norm of the vector $|\underline{t}_{i-1}|$ is calculated using /6.27/ :

$$|\underline{t}_{i-1}|^2 = \Delta p_{i-1}^T \Delta p_{i-1} + \beta^2 (\lambda_{i-1} - \lambda_{\text{start}})^2 \quad /6.34/$$

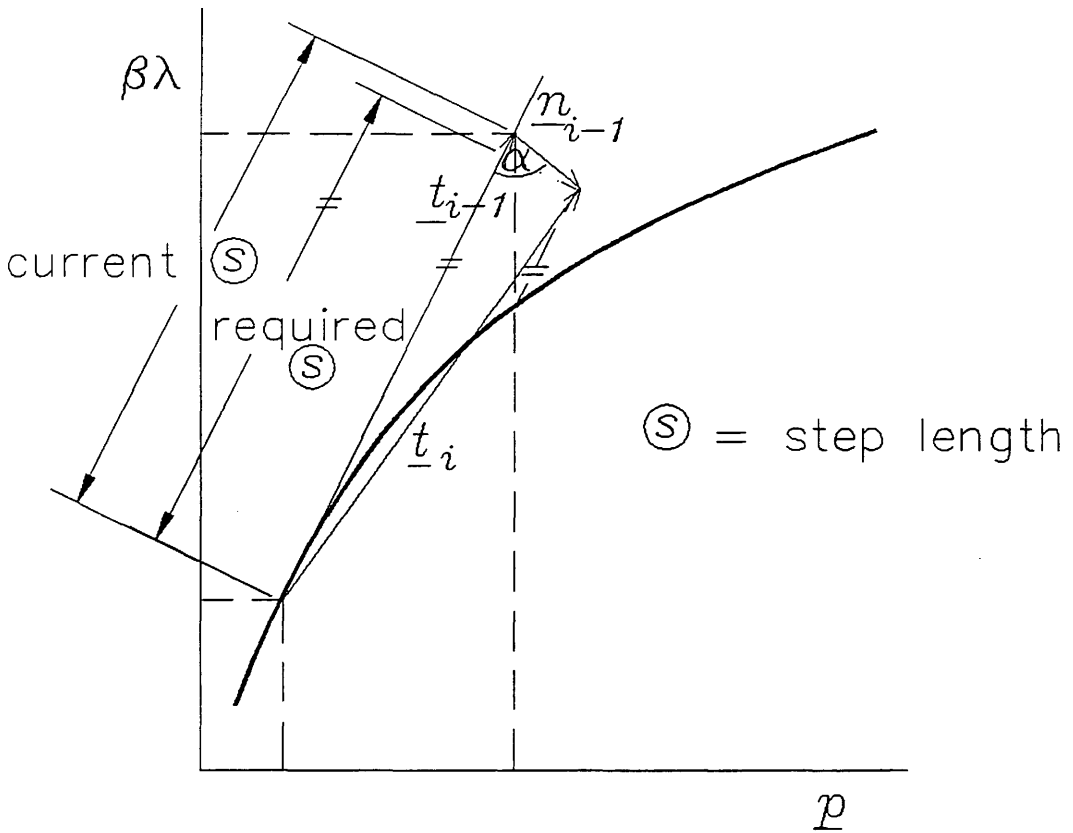


Fig. 6.6 Consistently linearized method for $\Delta\lambda_{i-1}$.

Substituting /6.33/ and /6.34/ in /6.3/ we obtain the final expression for $\Delta\lambda_{i-1}$. It should be noted that the scalar s is set 'a priori' and governs the actual step length. Of course, the proper choice of this parameter is essential for the solution and therefore it will be discussed later in more detail.

This method is especially suitable for solutions which embrace λ - p diagrams with sudden breaks and discontinuities. Thus it is employed especially for materially nonlinear problems.

6.4.3 Explicit orthogonal method.

The basic constraint for $\Delta\lambda_{i-1}$ in this case is that $|\underline{t}_{i-1}| = |\underline{t}_1| = s =$ is some distinct 'a priori' set step length. Similar to the previous method we also have to evaluate the residual R_{i-1} :

$$\begin{aligned} R_{i-1} &= \underline{t}_{i-1} \underline{n}_{i-1} = |\underline{t}_{i-1}| |\underline{n}_{i-1}| \cos\alpha \\ &= -|\underline{t}_{i-1}| |\underline{r}_{i-1}| \end{aligned} \quad /6.35/$$

Based on the similar triangles, the following can be derived:

$$\frac{|\underline{r}_{i-1}|}{|\underline{t}'_{i-1}| - s} = \frac{|\underline{t}_{i-1}|}{|\underline{t}'_1|}$$

i.e.:

$$|\underline{r}_{i-1}| = \frac{|\underline{t}_{i-1}|}{|\underline{t}'_1|} (|\underline{t}'_{i-1}| - s) \quad /6.36/$$

After some tedious manipulation of /6.35/ and /6.36/ we obtain:

$$R_{i-1} = \frac{-s^2(|\underline{t}'_1| - s)}{|\underline{t}'_1|}$$

where /6.37/

$$\underline{t}'_1 = \underline{t}_{i-1} + \underline{n}'_{i-1}$$

The entities \underline{t}'_1 and \underline{n}'_{i-1} pertain to the solution using the Normal update plane method. Without any additional derivation let us present the expression for $|\underline{t}'_1|$:

$$|\underline{t}'_i|^2 = |\underline{t}'_{i-1}|^2 + \beta^2 \Delta\lambda_{i-1}^2 + \eta^2 |\delta_{i-1}|^2 \quad /6.38/$$

The vector $|\underline{t}'_{i-1}|$ is calculated using /6.34/. By substituting the above equations into /6.31/ we obtain the final expression for $\Delta\lambda_{i-1}$.

From the above derivation it is clear that in practice we at first employ the method 6.4.1 to solve for \underline{t}'_i and \underline{n}'_{i-1} and thereafter we correct the $\Delta\lambda_{i-1}$ in order to satisfy the constraint $|\underline{t}'_i| = |\underline{t}'_{i-1}| = s$.

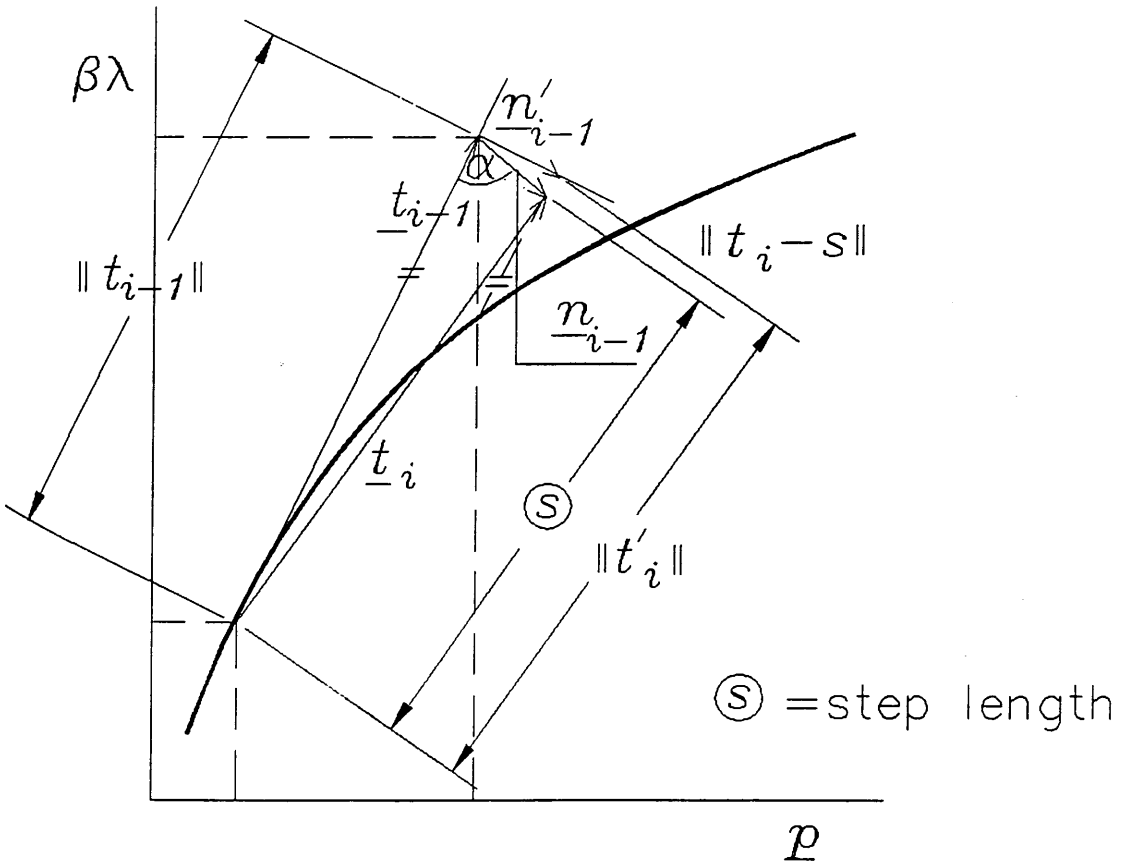


Fig. 6.7 Explicit orthogonal method for $\Delta\lambda_{i-1}$.

This method is usually utilized to analyze geometrically nonlinear structures, particularly stability problems. Its main feature is robustness and compared with the "classical" Crisfield cylinder method [29] it avoids the problem of the choice of the proper $\Delta\lambda_{i-1}$ root (the condition $\underline{t}_i = \underline{t}_{i-1}$). It is reached by applying geometrically similar triangles (see Fig. 6.7) rather than

direct evaluation of the step length \underline{t}_1 (which leads to quadratic equations).

As regards convergence, the method is comparable to method 6.4.1, but has the advantage that it preserves the step length.

6.4.4 The Crisfield method.

The Crisfield method is derived directly from the constraint of constant step length $|\underline{t}_1| = |\underline{t}_{1-1}| = s$. The residual R_{1-1} is not used in this case and we substitute equations /6.21/ through /6.29/ straight into the above constraint. It leads to the following equation for $\Delta\lambda_{1-1}$:

$$a_1 \Delta\lambda_{1-1}^2 + a_2 \Delta\lambda_{1-1} + a_3 = 0 \quad /6.39/$$

where for the case of an arbitrary iteration:

$$a_1 = \eta \delta_{-T}^T \delta_{-T} + \frac{\beta^2}{\eta}$$

$$a_2 = 2 \left(\Delta p_{1-1}^T \delta_{-T} + \eta \bar{\delta}_{-1-1}^T \delta_{-T} + \beta^2 \frac{\lambda_{1-1} - \lambda_{\text{start}}}{\eta} \right)$$

$$a_3 = 2 \Delta p_{1-1} \bar{\delta}_{-1-1} + \eta \bar{\delta}_{-1-1}^T \bar{\delta}_{-1-1}$$

and for the first iteration:

$$a_1 = \beta^2 + \eta^2 \delta_{-T}^T \delta_{-T}$$

$$a_2 = 2\beta^2 (\lambda_{1-1} - \lambda_{\text{start}}) + 2\delta_{-T}^T \bar{\delta}_{-1-1} \eta^2$$

$$a_3 = \beta^2 (\lambda_{1-1} - \lambda_{\text{start}})^2 + \eta^2 \bar{\delta}_{-1-1}^T \bar{\delta}_{-1-1} - s^2$$

The use of different equations to solve for $\Delta\lambda_1$ in the first iteration and in all additional ones is justified by the improvement of numerical stability. For the first iteration we simply employ the basic constraint for this method, i.e. $|\underline{t}_1| = s$. For all additional iterations, it is much more numerically stable to constrain $\Delta\lambda$ by $|\underline{t}_1 - \underline{t}_{1-1}| = 0$ rather than $|\underline{t}_1| = s$, which is in fact the identical equation.

Equation /6.39/ has generally two roots $\Delta\lambda_{1-1}$ and hence we must decide which of them to use. Obviously two values of $\Delta\lambda_{1-1}$

are accompanied by two vectors \underline{n}_{i-1} (see eq. 6.28 and 6.29). The situation is shown in Figure 6.8 :

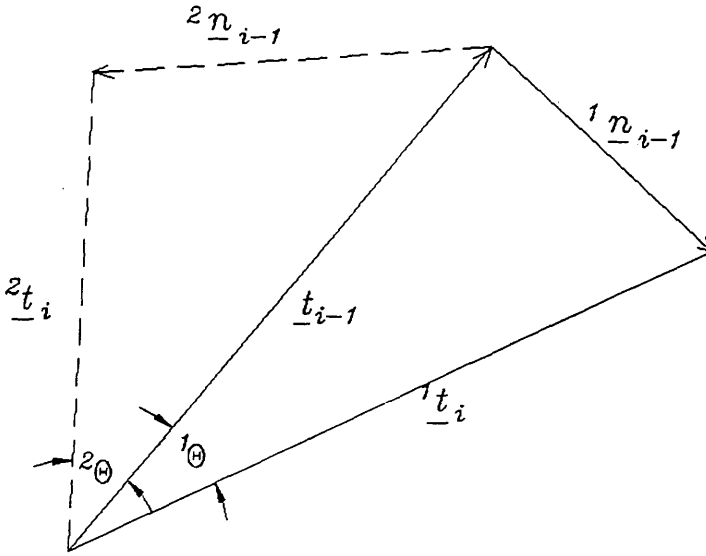


Fig. 6.8 The choice of the proper $\Delta\lambda_{i-1}$ root.

Several recommendations are available on how to choose the suitable $\Delta\lambda_{i-1}$ root. These are generally based on the path of previous deformations. Some of these were checked in this work and the most reliable was found to be when $\Delta\lambda_{i-1}$ was chosen so that $\cos\Theta$ is positive (for Θ , see Fig. 6.8). In other words the requirement is that the angle between \underline{t}_i and \underline{t}_{i-1} is acute or that their scalar product is positive.

Unfortunately it can sometimes happen that the above condition is satisfied either for both roots or neither.

In the former case, the better choice is usually the root which is most close to the linear solution, i.e.

$$\Delta\lambda_{i-1, \text{lin}} = - \frac{a_3}{a_2} \quad /6.40/$$

In the latter case it is recommended that the root closest to the acute angle constraint is chosen. It should be noted, however that this case is very rare and usually signals that there is something wrong (solution out of the convergence, numerical difficulties, violation of some general mechanical principle etc.). In this situation, the reliable remedy is usually to decrease the step length.

The step length s .

The proper step length is of essential importance for good execution performance. It directly influences the convergence radius on the one hand and the number of required steps on the other. Hence if s is too big, the solution diverges, if it is too small the computational cost is excessive because the diagram λ - p is traced in unnecessary detail. Hence much care must be paid in setting a value for s .

The literature provides numerous ways for estimating s . These are usually based on previous convergence performance and on the value of Bergan's stiffness parameter [18]. Unfortunately none of these are 100 per cent reliable and thus it is better to entrust more to the professional judgment of the analyst using the Arc-length method.

Based on the author's experience it is a good idea to set s so that the analysis of the structure exhibits some λ - p diagram difficulties after approximately 3 - 4 solution steps. This approach to the problem is of course also not totally satisfactory but may be better than the blind following of some unsuitable formulae.

During execution it is also important to know at what particular part of a λ - p diagram the solution is and to change s accordingly.

In practice the following sequence is usually recommended:

1/ Set loading vector q and thus define the type of loading.

2/ Compute λ_0 so that after 3 - 4 load increments $\lambda_0 \underline{q}$ the "dangerous" part of λ - \underline{q} diagram can be expected. The step length is then given by:

$$s = \lambda_0 \begin{matrix} \delta \\ -T \end{matrix} \begin{matrix} \delta \\ -T \end{matrix} \quad /6.41/$$

where the expression /6.41/ is derived from /6.26/ for $|\bar{\delta}_0| = 0$, i.e. it is assumed that at the beginning of step the structure is in equilibrium.

The step length can be fixed for all steps or preferably it can be adjusted for every new step with respect to the previous convergence performance. Some of the possibilities are as follows:

$$a/ \quad s_i = \sqrt{\frac{n_{i-1}}{n}} \quad s_{i-1}$$

$$b/ \quad s_i = \sqrt[4]{\frac{n_{i-1}}{n}} \quad s_{i-1} \quad /6.42/$$

$$c/ \quad s_i = \sqrt{\frac{n}{n_{i-1}}} \quad s_{i-1}$$

where:

s_i and s_{i-1} are new and last step length s ,

n_{i-1} is number of iteration required to reach convergence in last step, corresponding to s_{i-1} ,

n is desired number of iterations per step, usually 5 to 6.

It is apparent that expressions a/ and b/ tend to keep fixed loading increments. For poor convergence and many iterations, the $\Delta\lambda$ factor decreases and hence to eliminate this, it is necessary to increase the initial step length. This causes a larger initial

$\Delta\lambda$, but because of the above, it decreases during iterations and at the end of iterating, a good value of $\Delta\lambda$ is obtained.

The strategy for the last expression c/ has quite the opposite character. If there are difficulties with convergence, i.e. the value of n_{i-1} is increasing, the step length is decreased. Hence it maintains a nearly constant deformation increment rather than load increments as in a/ and b/. Based on practical experience the last expression seems to be the best one (apart from some special cases). Decreasing s improves convergence and it seems quite reasonable that in the case of problems with convergence one should try to improve it by decreasing s . On the other hand it should be noted that expression a/ and b/ can sometimes help in passing some extreme points etc.

It remains to add that the result of using 6.4.3 and 6.4.4 constraints for $\Delta\lambda$ provides identical solutions. The Crisfield method is slightly more robust but costs more time and one has to deal with the difficulties of choosing the proper $\Delta\lambda$ root.

6.5 Line search method

This method can be used either quite independently (i.e. in conjunction with some Newton-Raphson method) or simultaneously with the above Arc-length method. In this case the parameter λ is constant during all Line search iterations.

The objective of this method is to calculate the parameter η that was used in previous expressions and which previously was assumed for the sake of simplicity to be equal to one.

The primary reason for introducing a new parameter in the equations is to accelerate or to damp the speed of analysis of the load-displacement relationship. The secondary reason is that it can be used as a very advantageous criterion to trace the convergence properties of analyzed steps.

The basic idea used to derive the η value is minimization of the work done by out-of-balance forces on the displacement increment. This work can be used as a criterion to evaluate convergence qualities. If it is small, then the solution converges well, if the work is nearly the same as it was before the current iteration or even larger, it signals that something is wrong and we can execute the appropriate actions to improve convergence.

Let us assume that we have already solved two points \underline{p}_0 and $\underline{p}_0 + \eta' \underline{\delta}$, and thus we have also calculated out-of-balance forces $\underline{g}(\underline{p}_0)$ and $\underline{g}(\underline{p}_0 + \eta' \underline{\delta})$ at these points. The aim of this method is to set the parameter η so that the work being done by out-of-balance forces at point $\underline{p} = \underline{p}_0 + \eta \underline{\delta}$ is minimal.

For the work of out-of-balance forces we can write the following expression:

$$\Phi(\underline{p}) = \Phi(\underline{p}_0) + \int_{\underline{p}_0}^{\underline{p}} \underline{g}(\underline{p})^T d\underline{p} = \text{minimum} \quad /6.43/$$

The given constraint for η leads to:

$$\frac{\partial \Phi(\underline{p})}{\partial \eta} = 0 + \frac{\partial}{\partial \underline{p}} \left(\int_{\underline{p}_0}^{\underline{p}} \underline{g}(\underline{p})^T d\underline{p} \right)^T \frac{\partial \underline{p}}{\partial \eta} = \underline{g}(\underline{p})^T \frac{\partial \underline{p}}{\partial \eta} = 0$$

/6.44/

Now let us linearly interpolate the out-of-balance forces \underline{g} between points \underline{p}_0 and $\underline{p}_0 + \eta' \underline{\delta}$:

$$\begin{aligned} \underline{g}(\underline{p}_0 + \eta' \underline{\delta}) &= \underline{g}(\underline{p}_0) + \left(\frac{\underline{g}(\underline{p}_0 + \eta' \underline{\delta}) - \underline{g}(\underline{p}_0)}{|\underline{p}_0 + \eta' \underline{\delta} - \underline{p}_0|} \right) |\underline{p}_0 + \eta' \underline{\delta} - \underline{p}_0| = \\ &= \underline{g}(\underline{p}_0) + \frac{\underline{g}(\underline{p}_0 + \eta' \underline{\delta}) - \underline{g}(\underline{p}_0)}{\eta'} \eta \end{aligned}$$

/6.45/

In addition:

$$\underline{p} = \underline{p}_0 + \eta' \underline{\delta}$$

and

$$\frac{\partial \underline{p}}{\partial \eta} = \underline{\delta} \quad /6.46/$$

Substituting /6.46/ in /6.45/ and /6.44/ the final form for the calculation of parameter η can be derived:

$$\frac{\eta}{\eta'} = \frac{\underline{g}(\underline{p}_0)^T \underline{\delta}}{\underline{g}(\underline{p}_0)^T \underline{\delta} - \underline{g}(\underline{p}_0 + \eta' \underline{\delta})^T \underline{\delta}} \quad /6.47/$$

Hence, using the Line search method the algorithm of the solution is as follows:

- Use any of the preceding methods to calculate displacement increment $\underline{\delta}$ (i.e. the total displacement of the structure changes from \underline{p}_0 to $\underline{p}_0 + \eta' \underline{\delta}$). In this phase, parameter η' can be set from the last Line search iteration or simply set equal one.

- For both points calculate out-of-balance forces, i.e. $g(\underline{p}_0)$ and $g(\underline{p}_0 + \eta' \underline{\delta})$.

- Using formula /6.47/ calculate new η parameter.

- Due to our simplification (linear regression of out-of-balance forces g) equation /6.44/ may not be satisfied accurately and it might be necessary to repeat the above steps. Hence /6.44/ is checked and if the desired convergence is reached a new displacement of the structure $\underline{p}_0 + \eta \underline{\delta}$ can be calculated.

- If not, the whole procedure must be repeated. For the two initial points the current solution, i.e. point $\underline{p}_0 + \eta \underline{\delta}$ and either point \underline{p}_0 or $\underline{p}_0 + \eta' \underline{\delta}$, (usually \underline{p}_0) are used. According to this choice it is necessary to modify /6.47/ (which is written for point \underline{p}_0).

The exact satisfaction of /6.44/ is very difficult and therefore a suitable criterion must be derived to cut off Line search iterations. If the method is used separately, then the work of the out-of-balance forces can be related to the work due to the external loading. If the method is used in conjunction with the Arc-length method, it is recommended that the Line-search iterating is finished if $\frac{|g(\underline{p}_0 + \eta \underline{\delta})|}{g(\underline{p}_0)} < 0.6 - 0.8$, i.e. there is approximately a 40% decrease in the work being done by the out-of-balance forces during the current iteration. Thereafter execution control is returned to the Arc-length solution scheme.

Practical experience suggests that the value of parameter η should be limited within a given range. Good results have been achieved using:

$$\eta \in < 0.1 ; 10.>$$

/6.48/

Sometimes difficulties are experienced with convergence of the Line search and thus it is useful to support this possibility in the solution algorithm so that the Line search is executed only for one iteration or is used only to evaluate the overall convergence rate.

6.6 Parameter β .

As already mentioned, the parameter β scales the deformation space \underline{p} to the loading dimension λ . The sense of the parameter β can be demonstrated on the Crisfield constraint for $\Delta\lambda$.

If $\beta = 0$, the solution for $\Delta\lambda$ is searched for on the area of a cylindrical shape of radius s (the step length) and the axis normal to the \underline{p} (deformation) space. The solution is the point of intersection of this area and the line, defined by the energy gradients of structure and by the applied load at point \underline{p}_0 .

If $\beta = 1$, the shape of the cylindrical area is changed to an ellipsoid (or in special cases to a sphere).

Based on the author's experience for the case when $\beta = 0$ the $\lambda - \underline{p}$ diagram is analyzed more coarsely than if β is large. This is quite apparent if one realizes that for $\beta = 0$ the size of changes in the loading space is neglected and thus the user defined step length s is fully available for changes in deformation space.

If the parameter β is too big, the "weight factor" of changes in loading space is so high that they can't be achieved. Thus the Arc-length method degenerates to the Newton-Raphson method.

A suitable choice of β and its changes during the execution are now discussed. Unlike the case of the Arc-length method, there is a lack of available information for dealing with the β parameter. There are some recommendations usually based on the value of Bergan's stiffness parameter, but these are applicable only for very simple systems (e.g. structures created by elastic springs etc.). All the following suggestions are based on the author's practical experience in solving numerous test problems. Therefore in the algorithm presented in the next section, there is also the possibility of adjusting the β parameter manually.

Best results were observed if the size of deformation space was approximately the same as the size of the loading dimension. Hence the parameter β is estimated by:

$$\beta = \beta_{\text{ref}} = \frac{\Delta\lambda_0 |\delta_{-T}|}{\Delta\lambda_0} \quad /6.49/$$

i.e. β is based on the assumptions that at the first loading step the norm of the displacement increments and "λ change" (i.e. $\Delta\lambda_0$) are identical.

During the subsequent steps the parameter β is adjusted as follows:

$$\beta = \frac{\beta_{\text{ref}}}{|\Delta p_{i-1}|} \Delta\lambda_{i-1} \quad /6.50/$$

where $|\Delta p_{i-1}|$ and $\Delta\lambda_{i-1}$ are changes in deformations and loading due to the previous loading increment respectively. This ensures approximately the same scale for the subsequent load increments.

6.7 The new solution algorithm.

The new algorithm, which will be now presented, combines all the methods already discussed to create a solution scheme which facilitates all of their particular advantages. In comparison with other similar sets of solution schemes the present algorithm incorporates the influence of the loading space dimension (λ coordinate) and new suggestions for the best adjustment of β factor.

These were developed in Fortran 77 program codes for the cases of the frontal solution technique and for band solution technique with variable sky line. A more detailed description of all codes will be given later, here the theoretical background and the flow chart will be presented. Practical demonstrations and Benchmark tests are also discussed later.

The main idea of the scheme is to combine different methods to provide a solution procedure which on run-time basis chooses automatically the most effective solution strategy. The decision is based on the convergence behavior from previous steps. It also optimizes the step length, β scale factor and η parameter.

It is apparent that no recommendation for adjusting of the execution parameters, which are usually based on empirical formulae, are applicable for every case. Hence great care was given in programming this method to enable user adjustments during the execution. The simplest example is the setting of maximum number of iterations per loading step. If it is seen that the convergence criterion is nearly satisfied but the maximum number of iterations is already reached, then it is better to increase the threshold for the number of iterations and let execution successfully finish (and for example slightly decrease the step length for the next loading steps) than to terminate the whole solution and repeat everything once again. Many run-time changes are therefore incorporated in both solvers frontal and band strategy.

It should be also noted that unlike the original Newton-Raphson methods, a problem of $n + 2$ dimensions is solved. Some authors suggest incorporating the additional two equations directly in the stiffness matrix (e.g. Riks) but in the present work the n deformation degrees of freedom are solved first and thereafter one equation for λ parameter and one equation for η parameter are solved separately. This technique is employed e.g. by Crisfield etc.

It is known that the former approach gives better results. However this is counterbalanced by a slightly more complicated flow chart of the solution and the fact that it causes violation of symmetry of the problem (which is much more serious).

The best way to understand the developed solution scheme is to follow the flow chart in Fig. 6.9:

The following notation is used:

$$c_1 = \delta_{-T}^T \delta_T$$

$$c_2 = -\delta_{-T}^T \underline{q}$$

$$d_1 = \Delta p_{1-1}^T \delta_{-T}$$

$$d_2 = \bar{\delta}_{-1-1}^T \delta_{-T}$$

$$d_3 = \bar{\delta}_{-1-1}^T \bar{\delta}_{-1-1}$$

$$d_4 = \Delta p_{1-1}^T \bar{\delta}_{-1-1}$$

$$d_5 = -\underline{q}^T \bar{\delta}_{-1-1}$$

$$d_6 = \underline{f}_{1-1}^T \bar{\delta}_{-1-1}$$

$$d_7 = \underline{f}_{1-1}^T \delta_{-T}$$

$$d_8 = \Delta p_{1-1}^T \Delta p_{1-1}$$

$$e_1 = \frac{f_1^T}{f_1} \bar{\delta}_{1-1}$$

$$e_2 = \frac{f_1^T}{f_1} \delta_{-T}$$

The above constants are used to calculate the new λ and η parameters. The detailed expressions to compute λ , η and Δp_{1-1} were given in the previous sections.

The present method provides much better convergence than the Newton-Raphson family of procedures, and is also better than the solution schemes based on a single Arc-length because it is possible to employ the most suitable form of constraint for $\Delta\lambda$.

Also, matrix K can be calculated and its triangulation performed for the first step and iteration only (i.e. the Initial stiffness method), at the beginning of every load increment (i.e. the Modified Newton-Raphson method) or at every iteration (i.e. the original Newton-Raphson method). In addition it is also possible to recompute K every second iteration and in the case of structural unloading (i.e. at the point of probable difficulties).

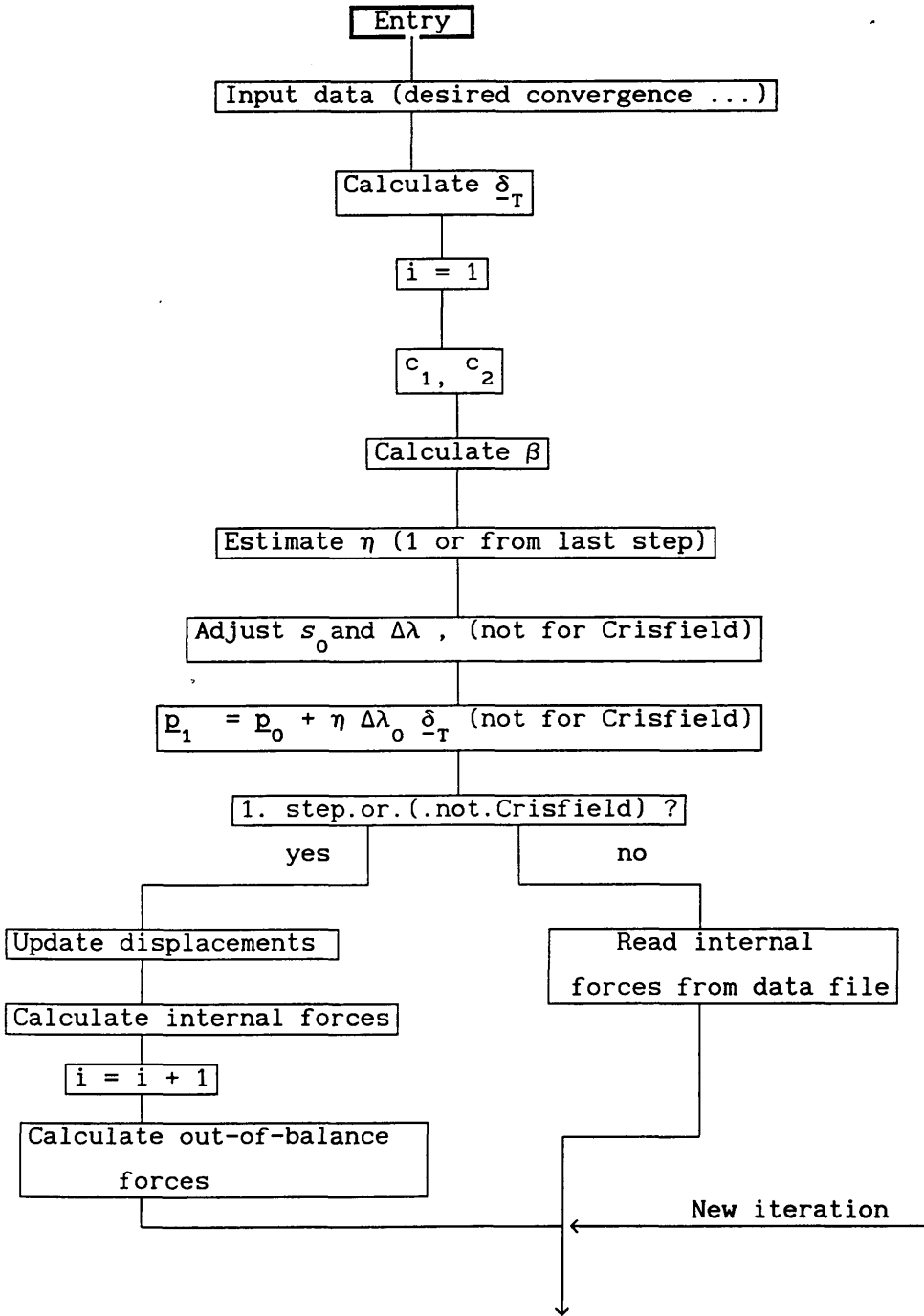


Fig. 6.9 Solution flow chart (part 1)

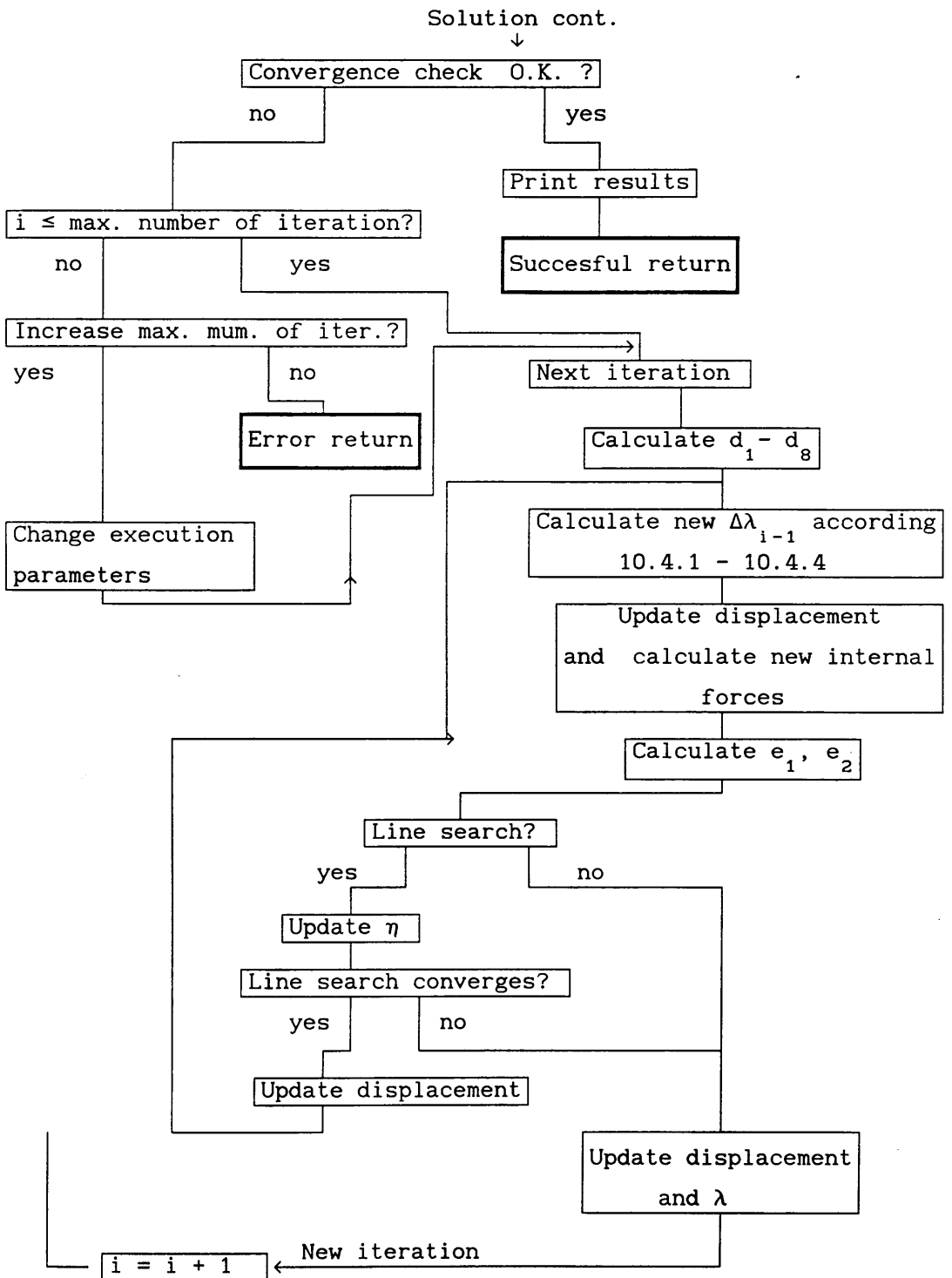


Fig. 6.9 Solution flow chart (part 2).

6.8 Final remarks on nonlinear solution schemes.

Finally it is necessary to discuss one of the most difficult problems which is unfortunately common to all nonlinear procedures, i.e. uniqueness of results and the guarantee that the least energy solution has been found.

It is unfortunate that in very complicated situations there is no guarantee that the least energy path has been found and what is worse there is no theoretical check or proof to evaluate the quality of computed results. On the other hand it must be noted that for the vast majority of problems we really do find what we are looking for. The main difficulties occur especially in materially nonlinear structures with strong discontinuities in the material stress-strain diagram and in the case of geometrically nonlinear structures near bifurcation points (or even multiple bifurcation points).

In both cases we usually have problems with convergence. One possibility is to obtain some information about the state of the observed structure by computing the eigenvectors and eigenmodes, or even to study the class of all possible virtual displacements at the point (usually using Taylor series with base functions equal to eigenmodes). This is the main idea of the perturbation method. But again it is emphasized that it is only information, not proof.

An additional problem is to find the real failure point of the structure and not the failure point of the numerical solution, as is often the case. Here, usually, it is better to forget about mathematical aspects and to focus attention more on the mechanics of the problem.

All nonlinear computations are in most cases only "extrapolation" of linear solutions. However what is applicable for a linear solution need not be applicable for a nonlinear solution. It is always a good idea not to rely 100 per cent on the computed results, but to use in principle a different method to check the results.

7. ANALYSIS OF STRUCTURES SUBJECT TO SHORT-TERM LOADING.

This chapter presents a series of short-term loading analyses using the proposed theoretical methods and the developed software. Advantages and shortcomings of particular solution techniques are discussed at the end of the examples and where appropriate recommendations towards their use are given.

It is difficult to categorize the analyses because one structure is often used to investigate more than one aspect of the modeling and solution procedures. However analyses are presented with a statement at the beginning as to what is being examined in that example, and why the analysis was carried out. A short summary of the analyses and the aspects examined follows:

Anal.	Structure	Problems:	Program:
7.1	2 trusses, elastic	NS, GN	PI-1
7.2	Ramm's shell, elastic	NS, GN, FE-2	PI-2
7.3	Ramm's shell, R/C	NS, CE-2, GN	PI-2
7.4	Slabs A, B, R/C	NS, FE-2	PI-2
7.5	Slab C, R/C	GN, CE-2, NS	PI-2
7.6	Shell [67], R/C	FE-2, GN, CE-2	PI-2

where:

CE-1 = Constitutive equations for 2D analysis,

CE-2 = Constitutive equations for shell analysis,

FE-1 = Finite element for 2D analysis,

FE-2 = Finite element for shell analysis,

GN = Effect of geometrical nonlinearity,

NS = New algorithm to solve nonlinear structural governing equations,

PI-1 = 2D program

PI-2 = Shell program

It should be emphasized that the present work deals with so many aspects of an analysis, e.g. geometric nonlinearity, nonlinear material law comprising several parameters, different tech-

niques for solving nonlinear equations etc. that only a few of them could be addressed here.

Last but not the least this chapter demonstrates that the developed software works satisfactorily and thus one of the tasks of this work, namely to create PC computer based environment for general nonlinear analyses of 2D and shell R/C structures was satisfactorily accomplished.

7.1 Simple two truss element structure.

A. Aim of the analysis:

- comparison of various Arc-length techniques to solve structural nonlinear governing equations,
- to prove that the present solution algorithm is able to deal with "snap-back" phenomenon,
- to show the importance of geometrical nonlinearity,
- to test the newly developed nonlinear equation solver with sky-line data housekeeping.

B. Description of analyses and results:

A simple structure was chosen for this analysis so that the calculated load-displacement relationship could also be checked manually. The other advantage of this structure being used is that during the solution the stiffness matrix is at first positive definite, then nearly singular, thereafter negative definite and finally positive definite again. Hence the algorithm is tested for very difficult structural conditions. The symmetry of the structure helps to trace numerical accuracy and stability of the solution.

The analyzed structure is depicted in Figure 7.1. It is an assemblage of two truss elements (no bending or torsion are accounted for) with two degrees of freedom. However, due to symmetry, only the vertical displacement is nonzero. The horizontal displacement shows only numerical stability near extreme points of structure.

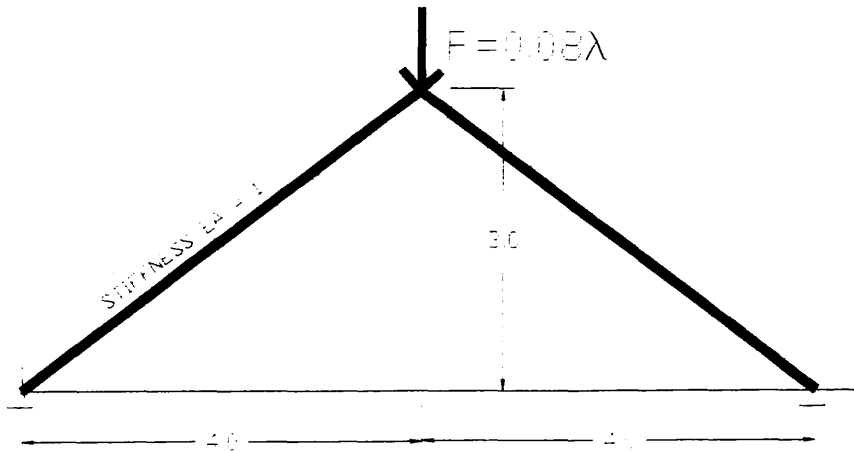


Fig. 7.1 Structure and loading condition to test nonlinear solver.

A linear elastic constitutive model was assumed. The analysis was formulated in the Total Lagrangian coordinates. The structure was loaded vertically at the top by the local force $P = 0.08\lambda$.

The Arc-length methods have been combined with the Modified Newton-Raphson method. If a Line search was incorporated, the solution always converged to the closest extreme point irrespective of whether we started from a point lying before or behind this extreme. Hence the Line search method is more suitable for finding the extreme points rather than tracing the whole working diagram of the structure. The results of analyses, i.e. the relationship between load and vertical displacement for various modifications of solution scheme (procedure parameters), is depicted in Fig. 7.2 and Tab. 7.1.

Both step length and β parameter modified

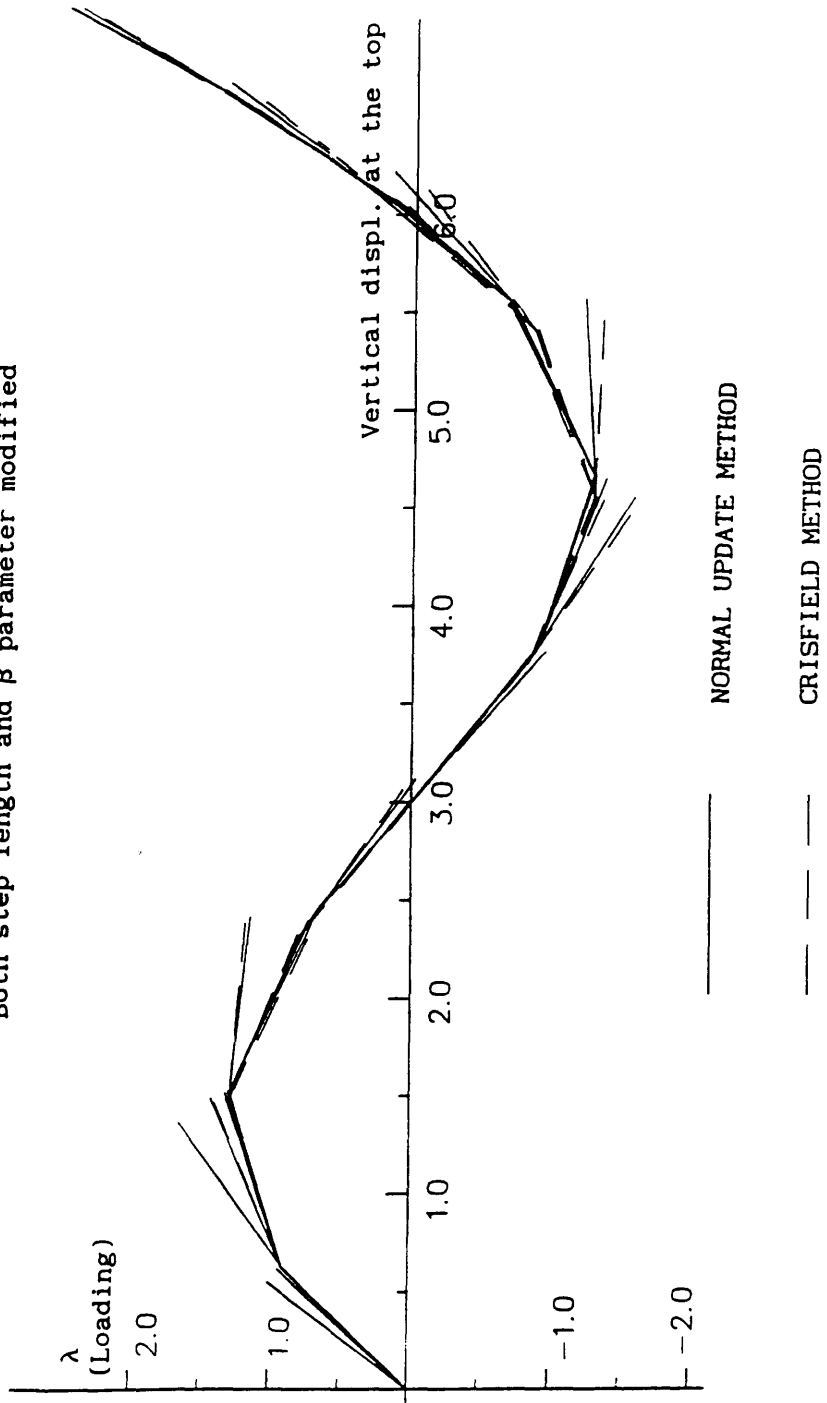
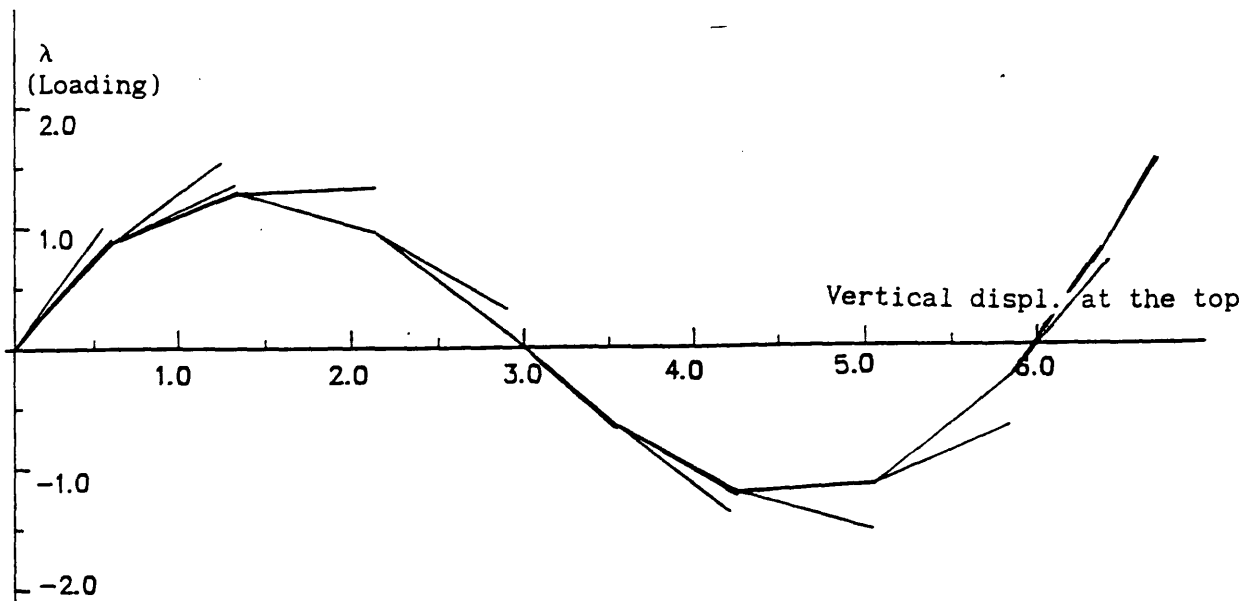


Fig. 7.2 Load vs. displacement relationship of the truss structure to test the nonlinear solver.

CRISFIELD METHOD, β modified, step length constant



CRISFIELD METHOD, $\beta = 0.707$, step length const.

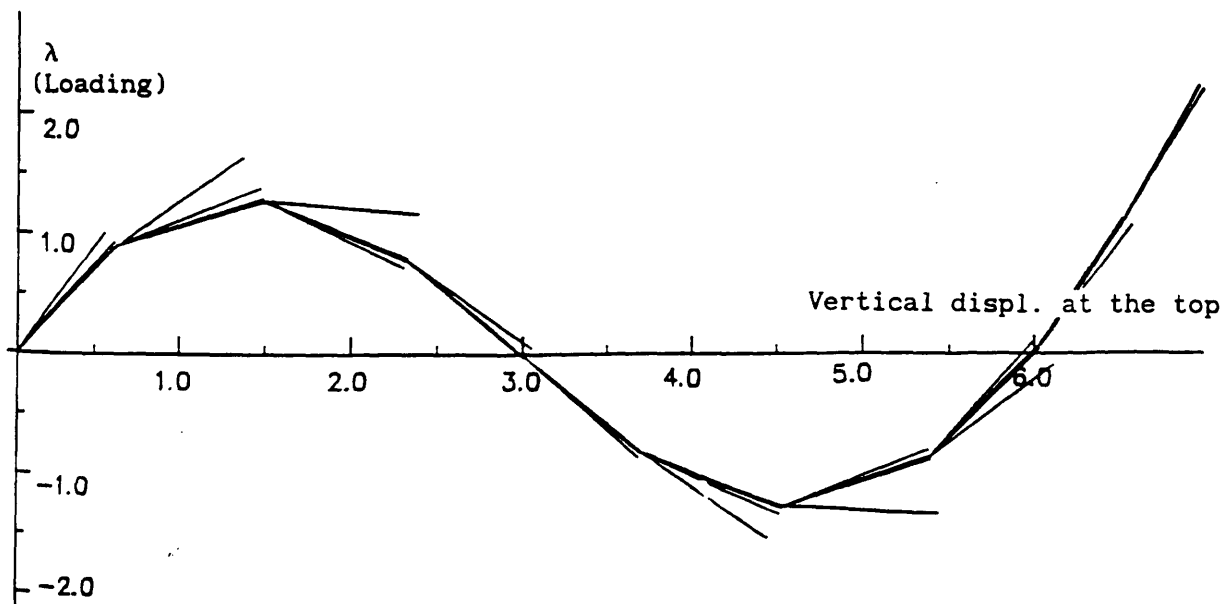


Fig. 7.2 Load vs. displacement relationship of the truss structure to test the nonlinear solver (cont.).

RESULTS OF ANALYSIS $\beta=0.707$, step length const.															
Loading Increment	Normal update plane				Consistently li- near. method				Explicit ortho- gonal method				Crisfield method		
	λ	Displ.	Number of iter.		λ	Displ.	Number of iter.		λ	Displ.	Number of iter.		λ	Displ.	Number of iter.
1	0.90308	-6.3867	6		0.89974	-6.3551	6		0.89979	-0.63547	6		0.89980	-0.6355	6
2	1.27451	-1.52629	7		1.278591	-1.49392	6		1.279077	-1.49379	7		1.27909	-1.4938	7
3	0.71734	-2.39213	6		0.78734	-2.3234	7		0.787531	-2.323149	6		0.78672	-2.3229	7
4	-0.1024	-3.0825	4		-0.0214	-3.0174	4		-0.02139	-3.01703	5		-0.0216	-3.0172	5
5	-0.8926	-3.7883	5		-0.8243	-3.7148	4		-0.82411	-3.71449	4		-0.82425	-3.71464	4
6	-1.2829	-4.6634	6		-1.2853	-4.5533	5		-1.28371	-4.55296	6		-1.2837	-4.5531	6
7	-0.6935	-5.5495	7		-0.8611	-5.40152	9		-0.86150	-5.40120	6		-0.86065	-5.4012	7
8	-0.2769	-6.1467	7		0.05137	-6.0279	7		0.051006	-6.02754	7		0.05089	-6.0282	8
9	1.35203	-6.6308	5		1.10714	-6.52925	5		1.106263	-6.5294	6		1.10663	-6.5296	6
10	2.47487	-7.0542	5		2.22086	-6.9634	5		2.220267	-6.9630	5		2.22065	-6.9632	5

Tab. 7.1 Results of truss analysis testing the nonlinear solver.

The results can be summarized as follows:

1/ The algorithm is capable of analyzing structures with negative definite stiffness matrix and can be used to trace "snap through" phenomenon.

2/ There is no significant difference between the results provided by particular Arc-length constraints. The exception might be in zones which are especially difficult to handle, e.g. near structural failure and bifurcation points.

3/ Near extremes and on the descending part of force-displacement diagram no problems were experienced with stability and convergence of the solution algorithm. No special increase in the number of iteration was necessary.

4/ The horizontal displacement at the top of the structure was always nearly zero even in cases when convergence had not yet been reached. This proves the high numerical stability of the adopted double precision arithmetic.

5/ It is not ^{the} intention of this analysis to test an influence of the β factor on convergence properties of the solution procedure. This is investigated in analysis 7.2. Here β is considered in order to check if the program works correctly.

When $\beta = 0$ (i.e. the load dimension is ignored in calculations of the step length) convergence was reached within two iterations. The first iteration always calculated the displacement according to the current tangent stiffness matrix and in the second iteration the current deformation, (i.e. the deformation after the first iteration), remained unchanged and only the load level, (i.e. λ), was adjusted to satisfy the structural nonlinear behavior. This is in agreement with theory and shows that no inaccuracy was introduced due to the horizontal degree of freedom. If the $\beta \neq 0$ more iterations are necessary.

6/ A comparison with the standard Newton-Raphson method was impossible because this method diverged beyond the first extreme of the load-displacement curve.

7.2 Ramm's shell.

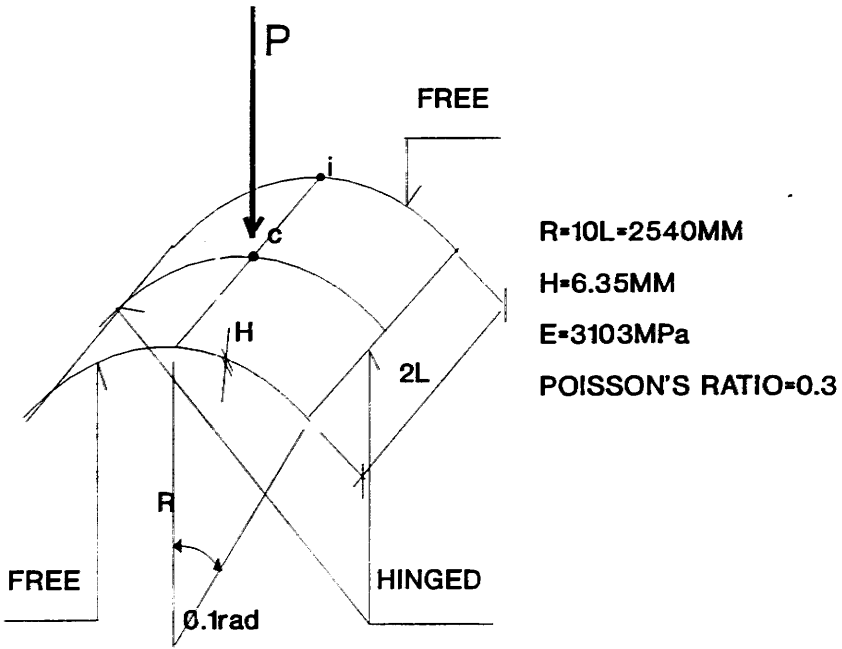
A. Aim of the analysis:

- to check that the present solution algorithm is able to deal with "snap-back" and "snap through" phenomena in the case of a more complicated structure,
- to show the importance of geometrical nonlinearity,
- to tests the new nonlinear equation solver with a frontal data housekeeping strategy,
- comparison of Arc-length techniques with and without parameter β ,
- to study various mesh sizes and their influence on the results.

B. Description of analyses and results:

In this analysis Ramm's cylindrical shell [69] has been examined. This structure was chosen because its behavior has also been studied by other authors, e.g. Ramm, Riks [70], Sabir and Lock [71] etc. and therefore the results can be compared with independent sources.

The geometry and material properties of the structure are depicted in Fig. 7.3. A quarter of the shell was modeled by 4 shell elements using 9-noded Lagrangian biquadratic approximation of displacement integrated at 9 integration points, (i.e. full integration). Geometrical nonlinearity was accounted for whereas a linear elastic isotropic material was assumed. The shell was loaded at its mid-point by concentrated force.



DEFLECTION AT POINT c

DEFLECTION AT POINT i

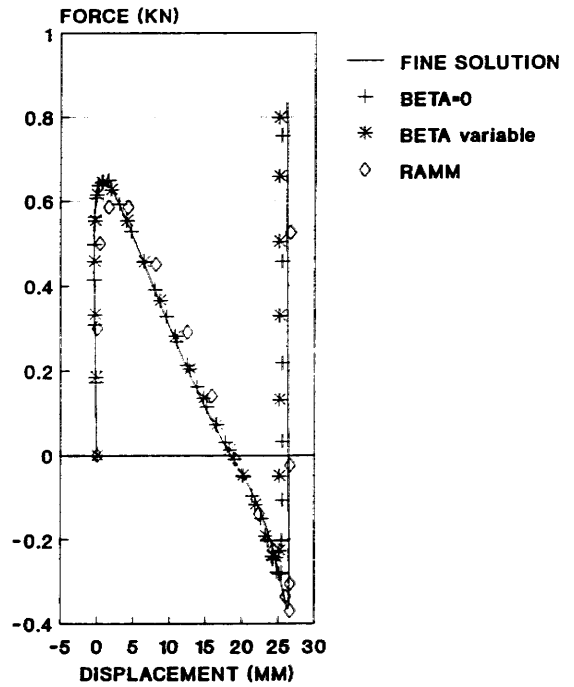
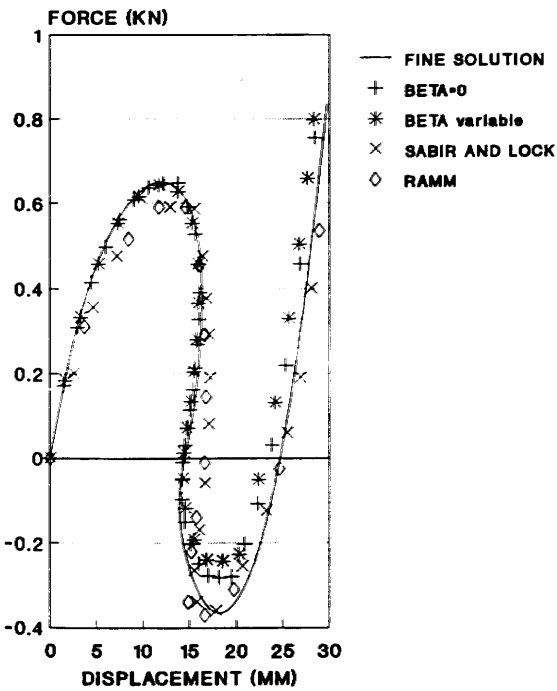


Fig. 7.3 Ramm's shell; geometry, loading and deflections at points c, i.

The Crisfield variant of the Arc-length method combined with full Newton-Raphson method was employed to solve the problem because we believe it to be the most robust solution scheme. Line search was not activated. Three analyses has been carried out. In the first one β parameter was zero during the whole analysis and the structure was loaded in very small loading increments. In the second solution β parameter was again zero but much larger loading increments were applied. The third variant was the same as the second one except β was variable, adjusted at the beginning of every load increment by the proposed algorithm (see Chapter 6). Resulting displacements at central point c and at mid-point i of the free shell edge are compared with other authors in Fig. 7.3. The norm of displacements changes due to iteration over the norm of total displacement is less then 0.001.

The following observation can be deduced from the results:

- No special problems with convergence were experienced in any of the analyses. The first analysis converged within 2-3 iterations per loading increment whilst the other analyses needed about 3-5 iterations per per loading increment to meet the convergence criterion. Loading increments used in the particular analysis are depicted in Fig. 7.3.
- The solution procedure managed to deal with snap back as well as snap through phenomena.
- There is little difference between these results and those of the other authors, (Ramm used the same geometry of structural discretization but with bicubic elements).
- For the loading part of the force-displacement diagrams load increment size had little influence on the results, however in the unstable phase, i.e. for negative force P , some differences appeared. These are probably due to the fact that a fully incremental solution scheme is adopted in which the starting point for every iteration is the final result from the previous iteration. Some other authors always prefer to start from the converged structural conditions, i.e. from the end of the last step. In

other words a secant approach must be used within the load increment. However this is contradictory to the hypoelastic constitutive equations used and involves the necessity of much finer loading increments.

-If parameter β was non-zero, points on the load-deformation relationship were spread more evenly than for $\beta = 0$. Hence the variable $\beta \neq 0$ option is preferable.

In order to study the importance of geometrical nonlinearity and mesh size dependence 6 additional analyses were carried out. A quarter of the structure modeled by 4, 9 and by 16 elements were compared. One set of solutions did not account for geometric nonlinearity whilst the other did. Deflections at points *c* and *i*, (Fig. 7.3), are presented in Fig. 7.4 and 7.5. Throughout these analyses $\beta = 0$ was assumed.

DEFLECTION AT POINT c

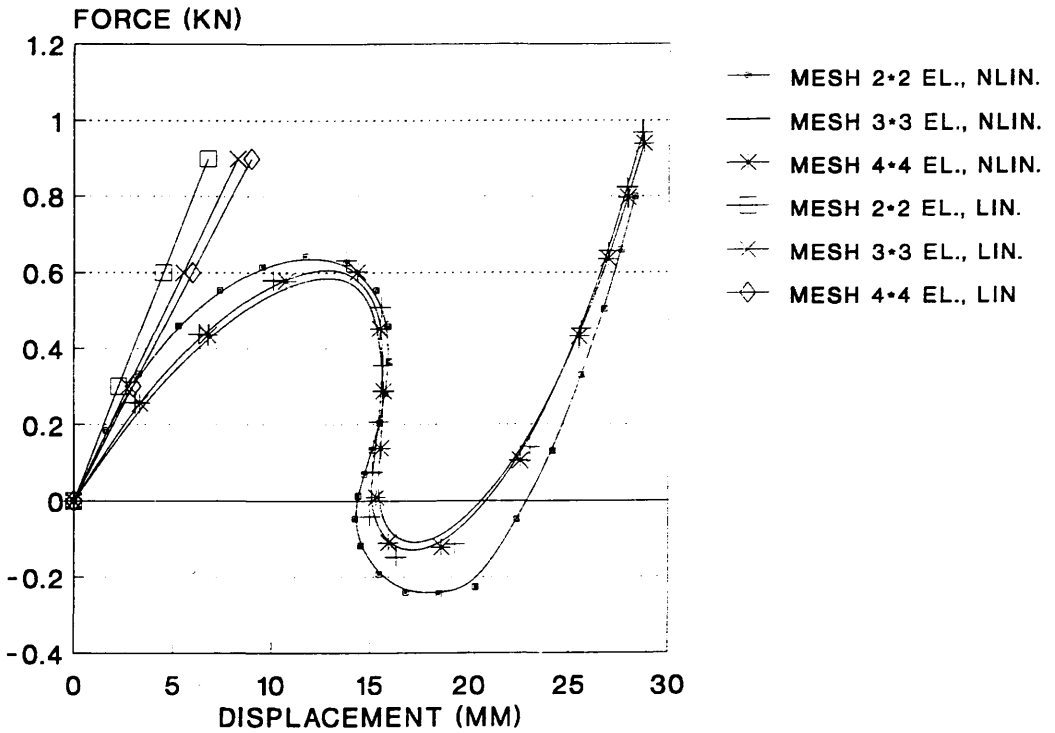


Fig. 7.4 Deflection at point c of Ramm's shell; different meshes, with and without geometrical nonlinearity.

DEFLECTION AT POINT *i*

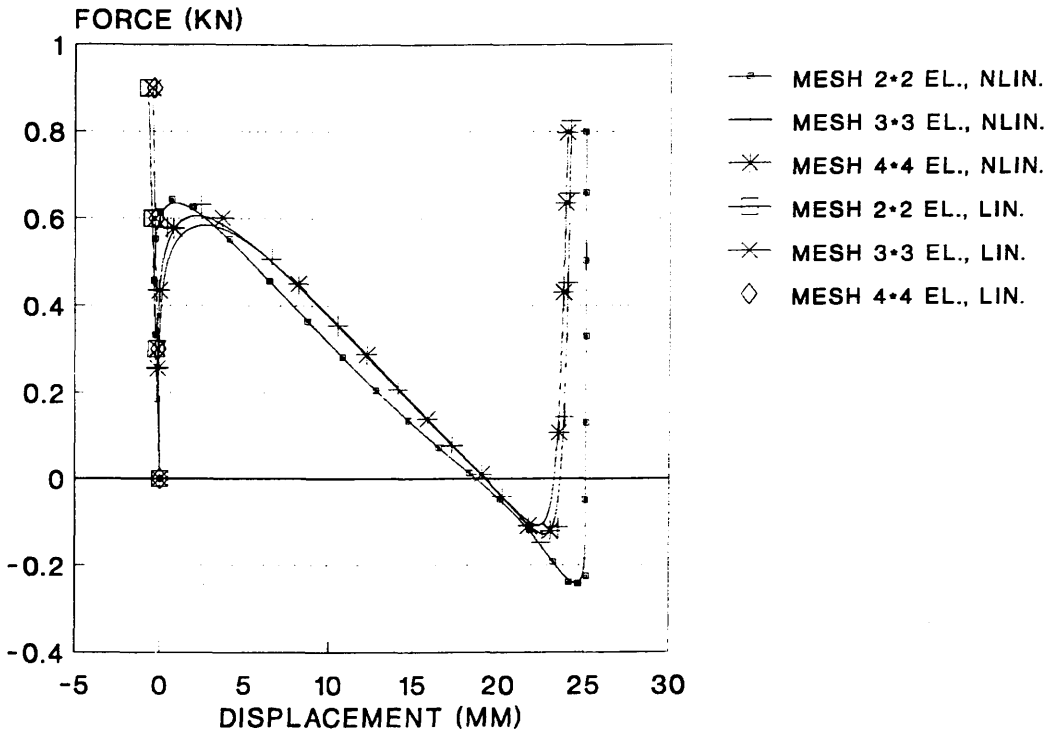


Fig. 7.5 Deflection at point *i* of Ramm's shell; different meshes, with and without geometrical nonlinearity.

It can be concluded from these results that:

- 4 element mesh results did not differ substantially from those for finer meshes, hence a 4 element mesh is acceptable,
- the effect of geometrical nonlinearity is important from an early loading stage and its consideration is essential for stability problems similar to the present one,
- the same problems as those in the previous analysis has been experienced in the unstable phase of force-displacement diagrams. They have already been discussed in the previous section.

7.3 Ramm's shell in reinforced concrete.

A. Aim of the analysis:

- to test the new nonlinear equations solver with frontal data housekeeping strategy,
- to compare of the full nonlinear solution, (i.e. geometrical and material) with the full linear solution and materially only nonlinear solution.

B. Description of analyses and results:

The same shell as that from analysis 7.2 is investigated here again, however the structure is now of reinforced concrete. The shell is reinforced in its bottom and top surfaces by 1% reinforcement meshes in each direction. Loading and boundary conditions were not changed. The following material constants were considered:

Concrete: Young's modulus = 33 GPa

Poisson's ratio = 0.18

Strength in tension = 3.8 MPa

Strength in compression = 38 MPa

Max. compression strain = 0.003 (beyond which complete loss of material rigidity is assumed)

Max. tensile strain = 0.002 (beyond which no strain stiffening is considered).

Steel: Young's modulus = 200 GPa

Poisson's ratio = 0.2

Yield strength = 294 MPa

The same mathematical model as used in analysis 7.2 (with 4 elements) was used again.

Load vs. deflections are presented in Fig. 7.6. For compari-

son, the figure also includes results from analyses, where geometrical nonlinearity was neglected and results for a linear elastic material condition where both the linear elastic Young's modulus and the loading force were considered to have values 10 times higher than those in analysis 7.2. Thus Young's modulus of concrete and Young's modulus of elastic material become comparable as well as deformations for both structures being comparable.

Fig. 7.6 shows that the R/C structure collapsed due to material properties, rather than due to loss of stability. The ultimate loads for geometrical linear and nonlinear analyses, (with nonlinear material law) nearly equal each other despite the difference in corresponding deformations. Reinforced concrete can not sustain high structural deformations, which are necessary to activate geometric nonlinearity, and thus a structure usually collapses due to material failure. It emphasizes the importance of material nonlinearity and that a materially linear solution can only serve as some very rough first estimate.

The solution algorithm used (i.e. the Arc-length method with Crisfield's constraint and $\beta = 0$) did not manage to trace the descending branch of the loading-deflection diagram because of the too sudden drop of structural stiffness after peak load. It will be shown later that a Line search can be of great help in this phase.

DEFLECTION AT POINT c

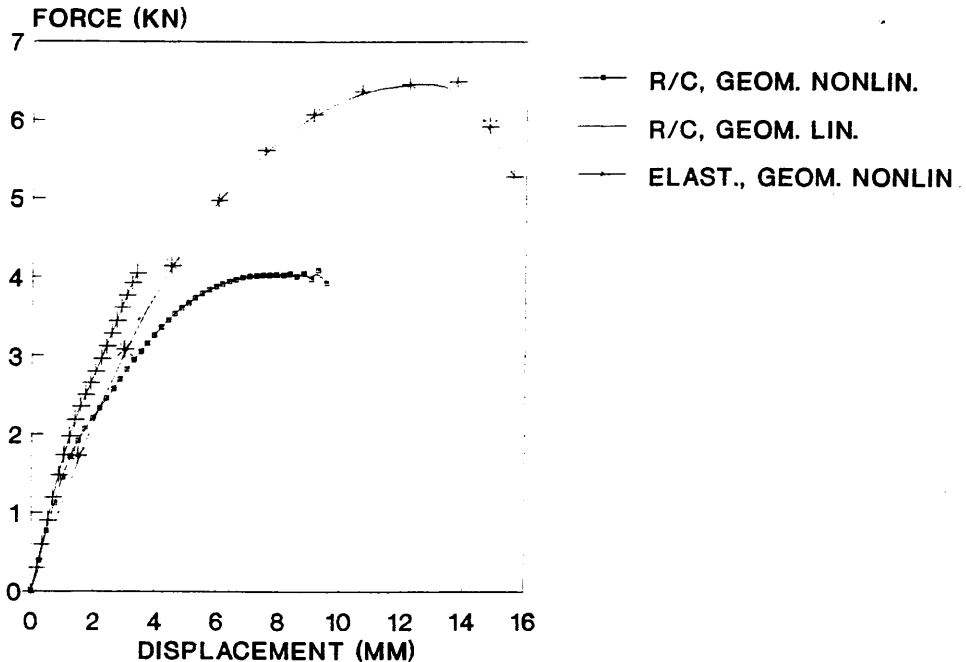


Fig. 7.6 Ramm's shell from reinforced concrete.

7.4 R/C slabs A and B.

A. Aim of the analysis:

- to examine the performance of the shell element formulation for the analysis of R/C slabs,
- comparison of converged behavior of different techniques to solve structural nonlinear governing equations,
- influence of step length during solution on results accuracy,
- comparison of results using selective and reduced integration,
- influence of mesh size on results accuracy,
- element accuracy subject to pure bending and bending and twisting actions, (2 different boundary conditions).

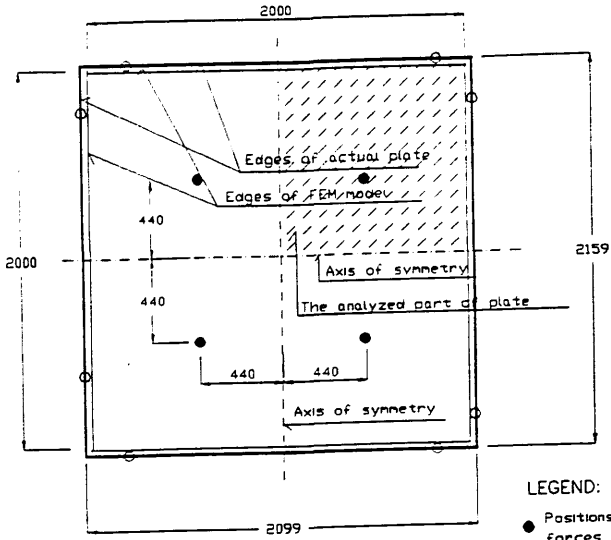
B. Description of analyses and results:

Two R/C plates are analyzed, one with simple boundary conditions, (plate *A*) where only element bending behavior is important and the other one with a pin support at one corner, (plate *B*) in which element twisting also matters.

Plate A.

The reinforced concrete square plate is shown in Fig. 7.7. Nine Heterosis elements, (see Fig. 7.8) with selective and reduced integrations were used to model a quarter of the plate. The geometry and reinforcement are depicted in Figure 7.7. The plate thickness is 10 cm.

GEOMETRY



LEGEND:

- Positions of loading forces 50 kN
- 'Roller' type boundary conditions
- All reinforcement bars are 8mm ϕ

REINFORCEMENT

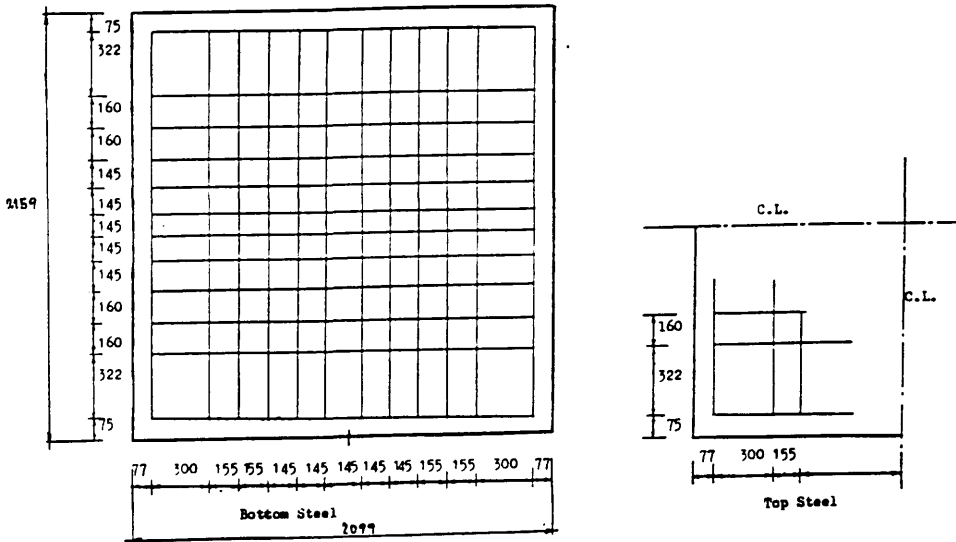


Fig. 7.7 Plate A: geometry, reinforcement, loading and boundary conditions.

The structure is supported along its boundary by rollers and loading is applied at four points by vertical forces of 50λ kN.

Because of the relatively coarse finite element mesh each force of 50λ kN was replaced by eight forces acting at element nodes. Their values are given in table 7.2.

Points	Force (kN)
14	-6.3629λ
15	29.5850λ
16	-10.853λ
21	13.8270λ
27	-8.7545λ
26	13.8270λ
25	-10.853λ
28	29.5850λ

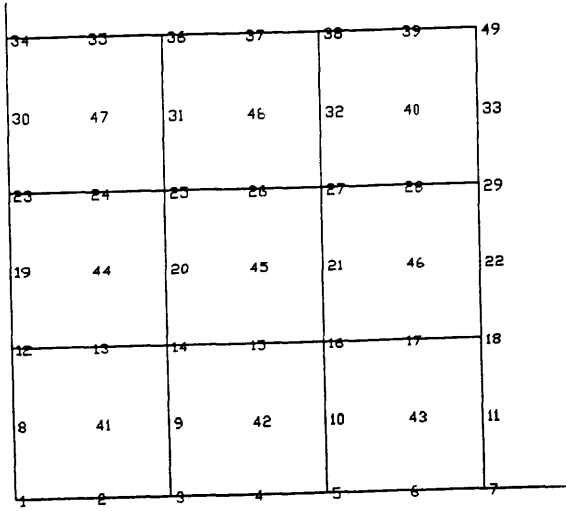
Tab. 7.2 Plate A: joint loading for 9 element mesh.

The material constants defining concrete and steel material are as follows:

Concrete:	Young's modulus E_c	21.5 GPa
	Poisson's ratio μ	0.18
	Tension strength f_t	3.4 MPa
	Compression strength f'_c	46.1 Mpa
	Ultimate compress. strain ϵ_m	0.0060
	Max. tension strain ($=\alpha_1 \epsilon_{cr}$)	0.002
	Tension stiff. parameter α_2	0.5
	Shear param. β_1	0.25
	Shear param. β_2	0
	Shear param β_3	$0.004/\epsilon_{cr}$
Steel:	Young's modulus E_{st}	214 GPa
	Young's modulus (hardening) E'_{st}	16 GPa
	Yields strength f_{st}	473 MPa

where ϵ_{cr} is strain the across the crack and $\beta_1, \beta_2, \beta_3$ and α_1, α_2 are shear retention and tension stiffening parameters. Ref. [46], where experimental data for this slab is available provides neither these parameters nor a value for ultimate compression strain ϵ_m . However Ref. [42] deals with a similar analysis and thus data from this was used.

SIMPLY SUPPORTED SQUARE PLATE -45- UDL (SI UNITS) TEST NO.1



UNDEFORMED SHAPE

APRIL 20, 1990 11:10

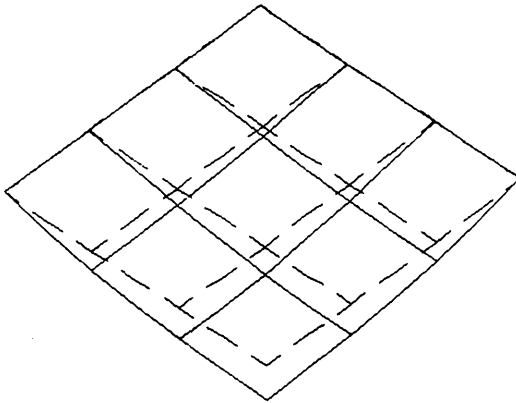
IAXIS= 2

ALPHA= 0.000

BETA= 0.000



SIMPLY SUPPORTED SQUARE PLATE -45- UDL (SI UNITS) TEST NO.1



LOAD CASE 2

TIME 1 INCR 2

FACTOR 0.25000

APRIL 20, 1990 11:10

IAXIS= 3

ALPHA= -45.000

BETA= 45.000

DEFLECTION SCALE FACTOR=

56307.9



Fig.7.8 Plate A: finite element mesh and structural deformations.

The actual 8 mm reinforcing bars were replaced by a continuous steel layer with the same reinforcement area for both directions.

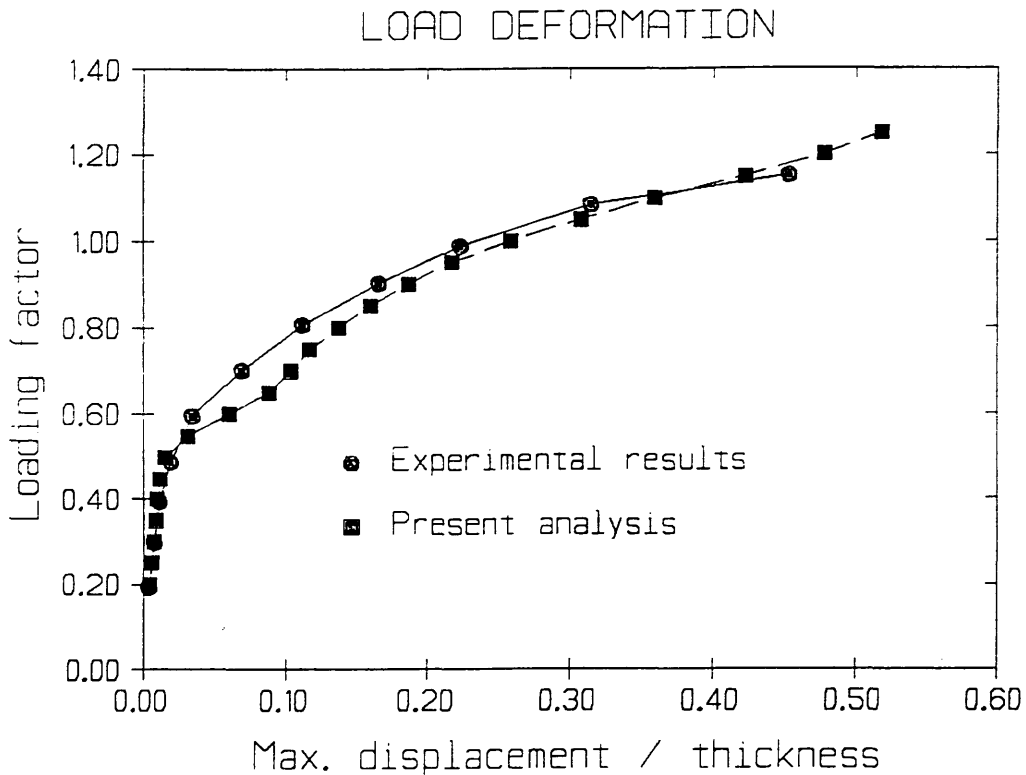


Fig. 7.9 Plate A: load-deformation diagram.

A layer model was used with two steel layers and ten concrete layers (two of them, near the plate top and bottom, had half the thickness of the others for better approximation of areas with the highest stresses).

The resulting maximum structural deformations, i.e. at the center, are compared with experimental data [46] in Figure 7.9; structural deformation is depicted in Figure 7.8.

The nonlinear equations were solved by a Newton-Raphson iteration scheme where the stiffness matrix was recomputed every second iteration.

Good agreement between the experimental results and the present analysis has been reached. This is partially due to the fact that the tension stiffening parameters used were adjusted in [42] for a very similar structural shape, loading and boundary conditions.

In order to study the solution behavior of nonlinear solvers, the same slab was also computed by Arc-length methods with normal update constraint and variable step length, Crisfield constraint with variable large step length and Crisfield constraint with fixed small step length. The results were compared with Newton-Raphson analysis with large load increments and small load increments in Fig. 7.10. Note that every plot mark corresponds to a converged loading increment.

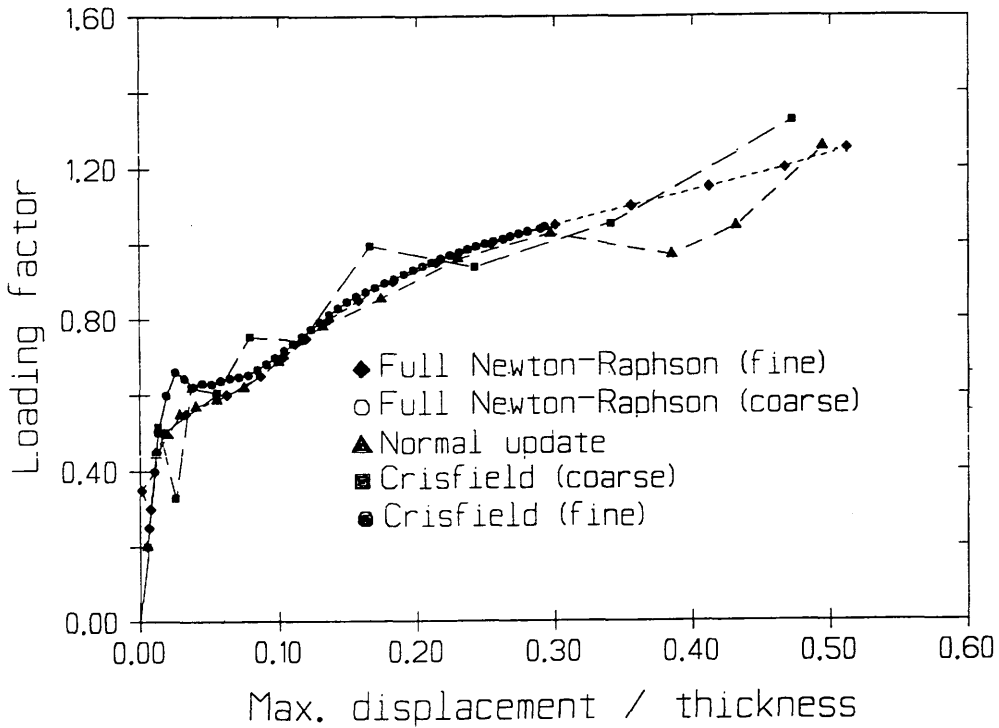


Fig. 7.10 Plate A: comparison of the nonlinear solvers.

From the above results it can be summarized:

-All tested nonlinear schemes are able to trace the load-displacement relationships.

-Newton-Raphson method can be used only if very small loading increments are applied. In the case of larger loading increments the solution diverges at a load level about $\lambda = 0.6$, i.e. the load level corresponding to the beginning of crack creation. At the same time the Newton-Raphson method is not able to trace any sudden drops (snaps through) of a working diagram of structure and the method converges always onto an stable energy part of the

load-displacement diagram.

-Arc-length method, even for big loading steps, converged satisfactorily. The "waving" of the curve is caused by the fact that the present material model (elastic-plastic) uses a linear stiffness matrix for the unloading condition. This situation occurs practically in every iteration, because during iterations the Arc-length usually tends to decrease λ load factor. This restricts the maximum acceptable step length of a solution. If used with hyperelastic constitutive equations this phenomenon disappears.

-Fig. 7.10 also shows the importance of using a variable step length in the Arc-length method. If a fixed length is employed then near structural failure the load-displacement diagram is traced in too much detail whilst at the beginning the solution is coarse and could miss some essential points.

-Good computation performances has been reached also by Normal update and other modifications of the Arc-length method.

-The time necessary for analysis using Newton Raphson method was approximately 3 - 4 times longer then using Arc-length method (for approximately the same density of points on the load-displacement diagram). This was due to the fact that Newton Raphson used about two times more iterations to reach convergence. Convergence was especially difficult (about 15 iterations!) at the beginning of cracking. Arc-length solved this situation by simply reducing the load factor λ during three iterations only.

-All Arc-length modifications traced without any problems sudden drops in the structure due to crack initiation.

In order to test the possibility of saving computation time, the structure was also analyzed using reduced integration only. The results are shown in Fig 7.11 (Newton-Raphson solver). It is obvious that the results are nearly identical and hence integration in two by two sampling points is permissible in this case.

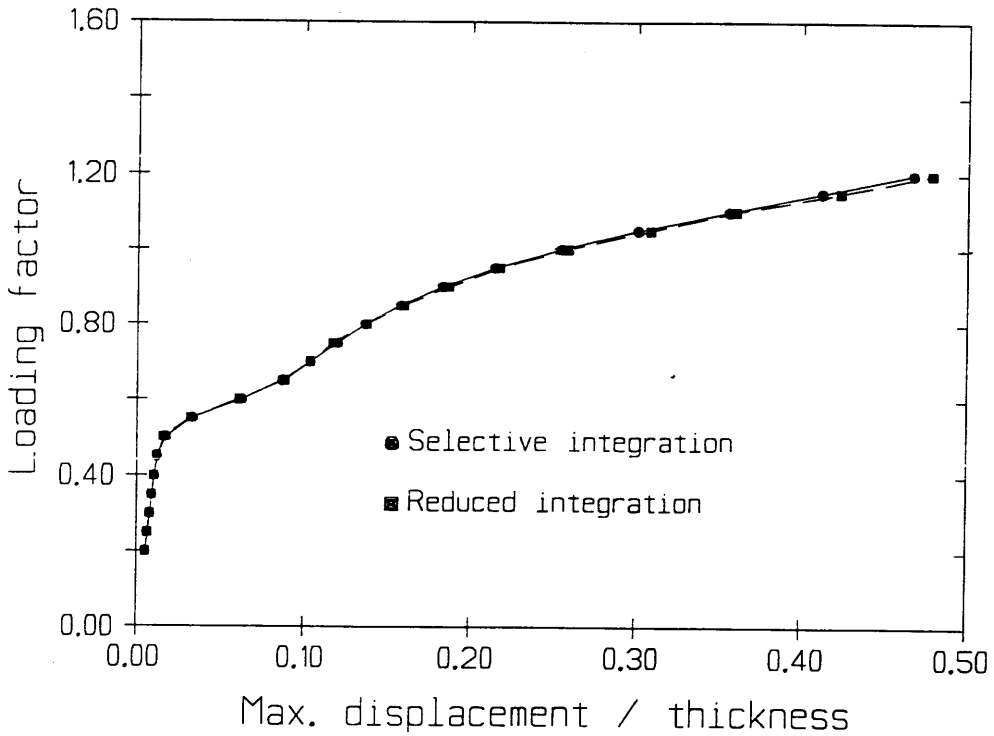


Fig. 7.11 Plate A: comparison of results for reduced and selective integration scheme.

Finally attention was focused on the sensitivity of results to the finite element mesh density. The same plate was computed by finite element mesh comprising six by six elements (Fig. 7.12). Mesh no. 1 was distorted near the loads in order to ensure a finite element node at the place of a force and to examine the influence of mesh distortion. Mesh no. 2 was quite regular and loading forces was again replaced by the eight nodal forces listed in Tab. 7.3.

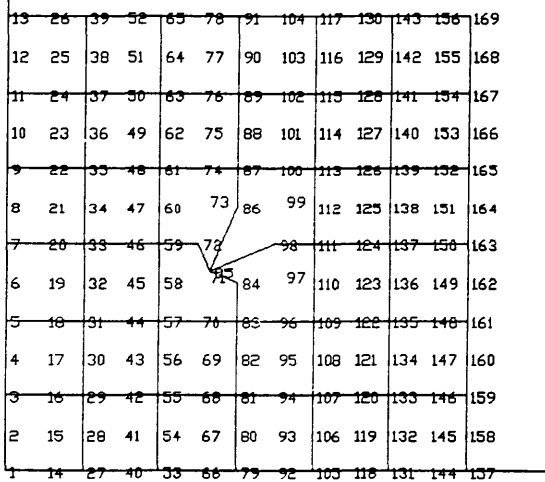
Points	Force (kN)
57	-10.088 λ
70	16.5890 λ
83	-11.520 λ
84	29.4912 λ
85	-9.0110 λ
72	29.4910 λ
59	-11.520 λ
58	16.5800 λ

Tab. 7.3 Plate A: joint loading for 36 element mesh.

The results for six loading increments for mesh no. 1 are shown in Figure 7.13.

MESH 1

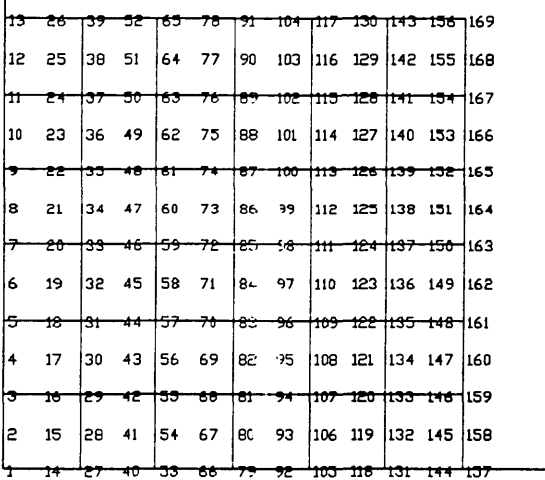
Simply supported square, 36 elements, loading 44 cm from center



UNDEFORMED SHAPE
 APRIL 21, 1990 906
 IAXIS= 2
 ALPHA= 0.000
 BETA= 0.000

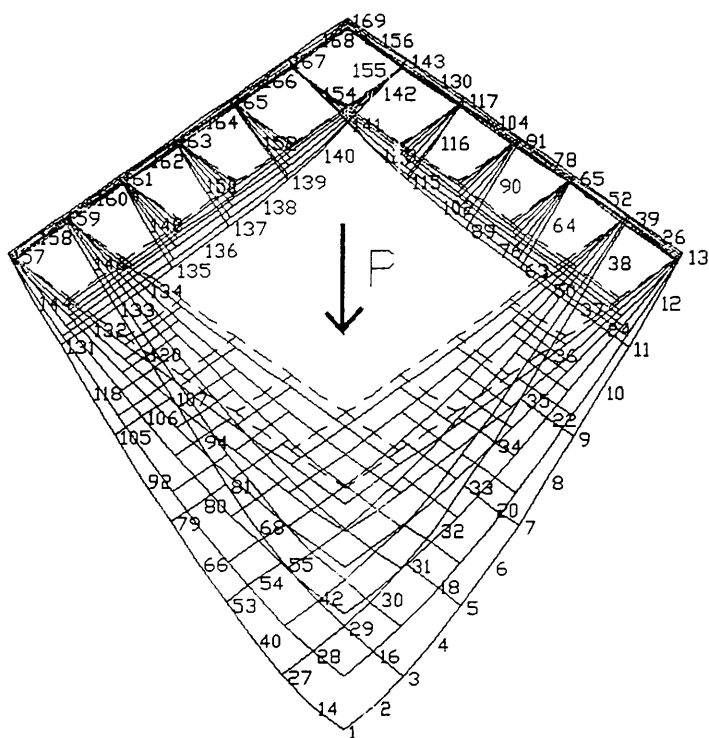
MESH 2

Simply supported square, 36 elements, loading 44 cm from center MESH 2



UNDEFORMED SHAPE
 APRIL 21, 1990 903
 IAXIS= 2
 ALPHA= 0.000
 BETA= 0.000

Fig 7.12 Plate A: mesh no. 1 and mesh no. 2.



LOADING 1 THROUGH 6

APRIL 21, 1990 9:19

IAXIS= 3

ALPHA= -45.000

BETA= 45.000

DEFLECTION SCALE FACTOR=

11613.1

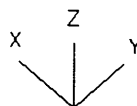


Fig 7.13 Plate A: mesh no. 1, loading 1 to 6.

The maximum displacements with respect to loading level are similar to the results for the 3 by 3 elements mesh depicted in Fig. 7.14. The results for mesh no. 1 and mesh no. 2 are nearly the same and it suggests that replacing one loading force by eight nodal forces according to table 7.3 works correctly. The results compared with experimental results illustrate that the 36 elements model is by about 10 percent less stiff and that the structural collapse corresponds to a lower loading level. This is due to the well known fact that material parameters (tension stiffening) are directly dependent on element mesh size and may be adjusted by fracture energy theory. In addition, the 36 element finite element model is itself slightly less stiff than 9 element model due to better approximations of geometry and displacements.

36 ELEMENTS, MESH 1 AND 2

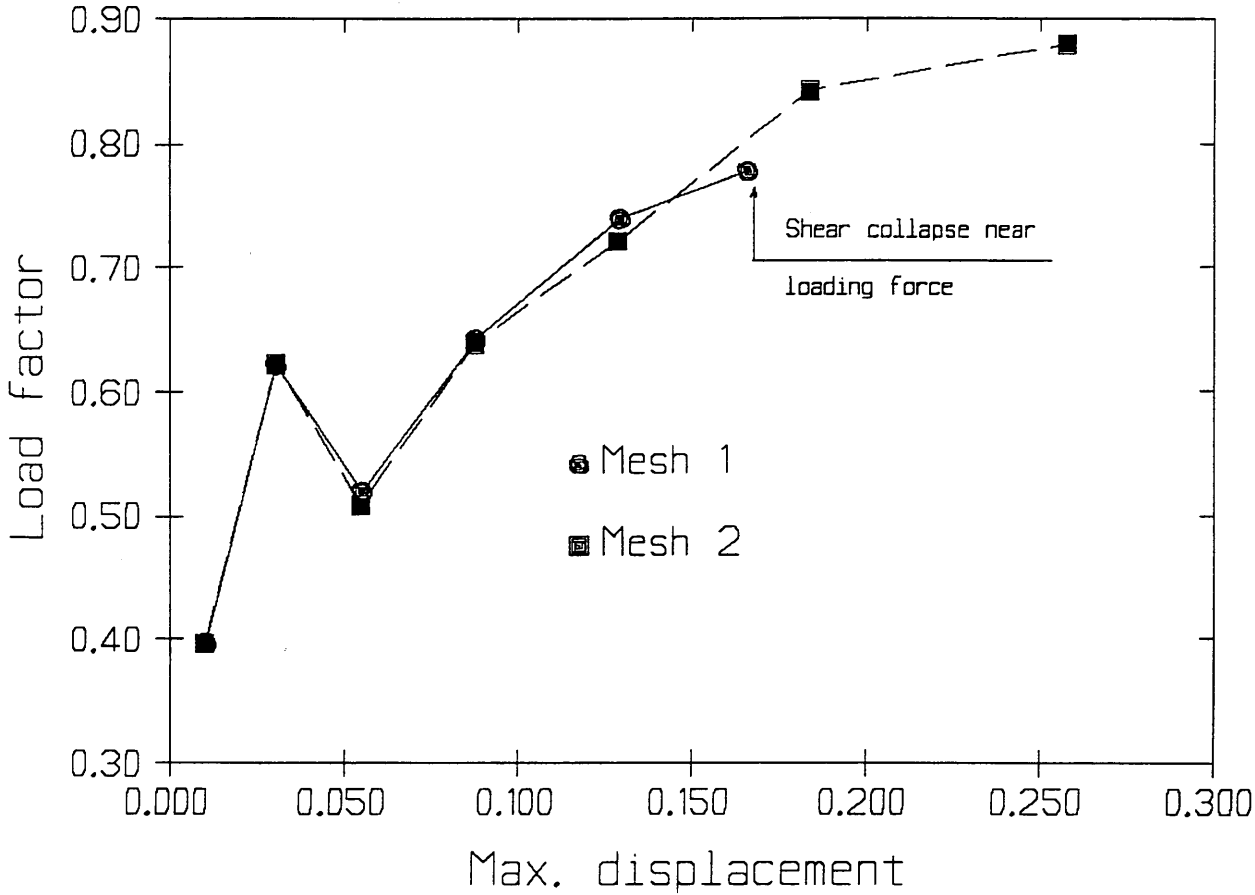


Fig. 7.14 Plate A: results for mesh no. 1 and no. 2.

Fig. 7.14 also demonstrates an other important problem in nonlinear analysis which is to distinguish between local and global collapses of structure. The global failure of 36 elements model corresponds to loading level about $\lambda = 0.9$. The analysis using mesh no. 1 however failed at a loading level $\lambda = 0.8$ due to local collapse in which the shear strength was exceeded near the applied loads rather than bending failure at mid plate (global collapse mode). Thus the mesh no. 1 "hid" a local shear failure mode of the slab.

Plate B.

In order to examine the solution performance for more difficult conditions, a nearly square plate *B* similar to the previous example has been analyzed. However this plate was supported by 'roller' longitudinal supports at the two adjacent edges and by a pin support at the corner opposite to the intersection of the longitudinal supports. An experimental test of the slab was carried out by [46]. Loading was applied by the two forces in a distance of 200mm from the plate center. The geometry of the structure is drawn in Figure 7.15 and reinforcement at bottom and top of the plate is depicted in Fig 7.16.

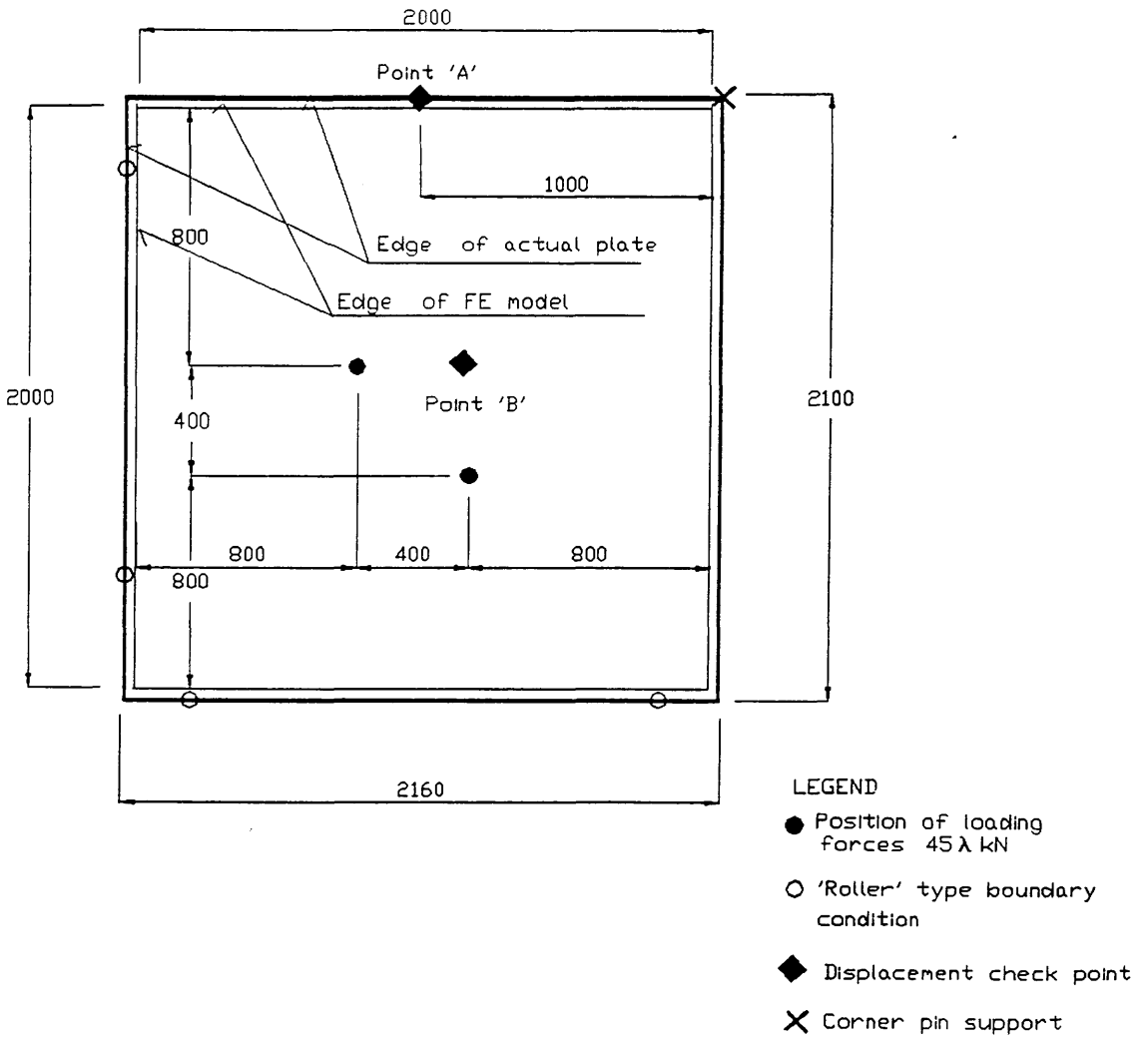
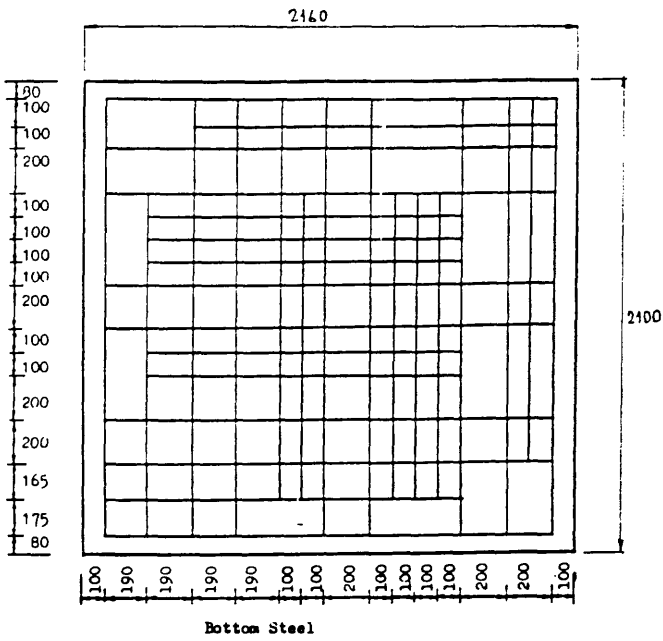


Fig. 7.15 Plate B: geometry, loading and boundary conditions.



LEGEND

All Bars Are 8mm ϕ

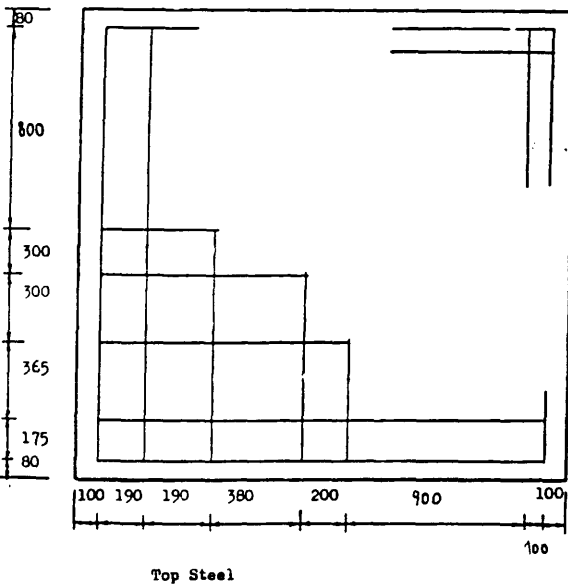
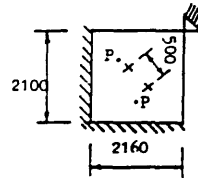


Fig 7.16 Plate B: reinforcement near top and bottom.

Simply supported square, 36 elements, loading 44 cm from center

13	26	39	52	65	78	91	104	117	130	143	156	169
12	25	38	51	64	77	90	103	116	129	142	155	168
11	24	37	50	63	76	89	102	115	128	141	154	167
10	23	36	49	62	75	88	101	114	127	140	153	166
9	22	35	48	61	74	87	100	113	126	139	152	165
8	21	34	47	60	73	86	99	112	125	138	151	164
7	20	33	46	59	72	85	98	111	124	137	150	163
6	19	32	45	58	71	84	97	110	123	136	149	162
5	18	31	44	57	70	83	96	109	122	135	148	161
4	17	30	43	56	69	82	95	108	121	134	147	160
3	16	29	42	55	68	81	94	107	120	133	146	159
2	15	28	41	54	67	80	93	106	119	132	145	158
1	14	27	40	53	66	79	92	105	118	131	144	157

UNDEFORMED SHAPE

APRIL 22, 1990 12: 7

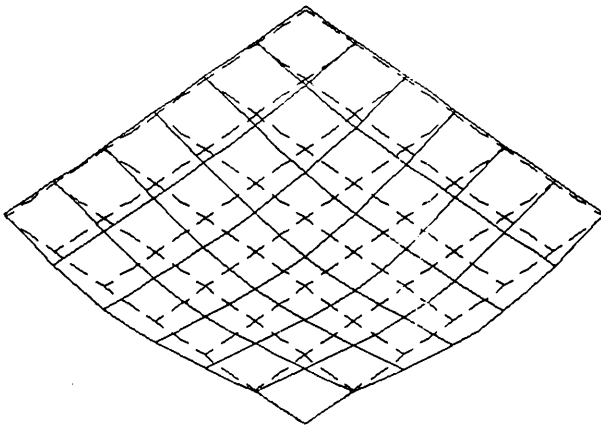
IAXIS= 2

ALPHA= 0.000

BETA= 0.000



Simply supported square, 36 elements, loading 44 cm from center



LOAD CASE 3

TIME 1 INCR 3

FACTOR 0.00000

APRIL 22, 1990 12: 7

IAXIS= 3

ALPHA= -45.000

BETA= 45.000

DEFLECTION SCALE FACTOR=

2518.55



Fig. 7.17 Plate B: finite element mesh and deformations for the third load increment.

The structure was modeled by 36 elements and the two local forces 45λ kN were replaced by eight nodal forces as shown in Tab. 7.4.:

Points	Force (kN)	Points	Force (kN)
59	-21.600λ	83	-21.605λ
72	34.5600λ	96	51.8400λ
85	-20.160λ	109	-19.440λ
86	34.5600λ	110	51.8400λ
87	-21.610λ	111	-21.605λ
74	51.8410λ	98	34.5600λ
61	-19.440λ	85	-20.160λ
60	51.8400λ	84	34.5600λ

Tab. 7.4 Plate B: nodal loading forces.

The finite element mesh used and displacement shape is presented in Figure 7.17.

The following material constant were used:

Concrete:	Young's modulus E_c	$2.04 \cdot 10^7$ kPa
	Poisson's ratio μ	0.18
	Tension strength f_t	2970 kPa
	Compression strength f'_c	37.3 Mpa
	Ultimate compres. strain ϵ_m	0.0060
	Max. tension strain ($=\alpha_1 \epsilon_{cr}$)	0.002
	Tension stiff. parameter α_2	0.5
	Shear param. β_1	0.0025
	Shear param. β_2	0
	Shear param β_3	$0.004/\epsilon_{cr}$
Steel:	Young's modulus E_{st}	$2.14 \cdot 10^8$ kPa
	Young's modulus (plast.) E'_{st}	$1.60 \cdot 10^7$ kPa
	Strength f_{st}	473 Mpa

where ϵ_{cr} is the strain across the crack. The tension stiffening parameters correspond to model b/ described in Chapter 3 and again values recommended in [42] were used.

The deflections at points 'A' and 'B', (see Figure 7.15) are compared with the experimental results [46] in Figures 7.18 and 7.19.

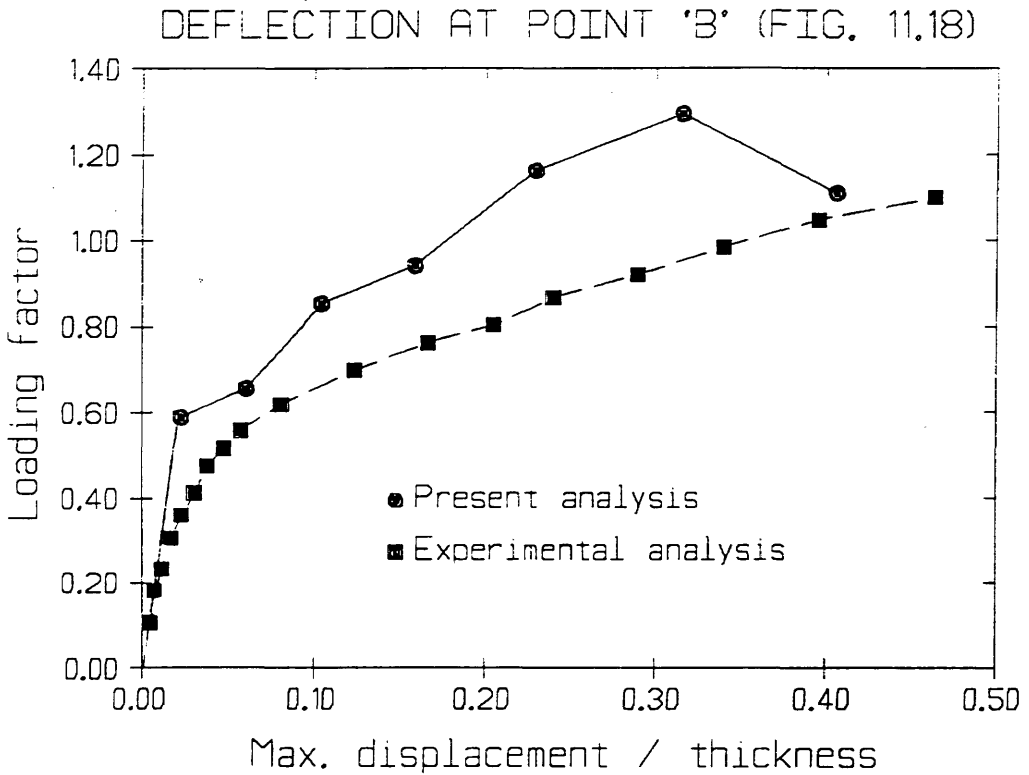


Fig. 7.18 Plate B: the deflection near the plate center (at point 'B').

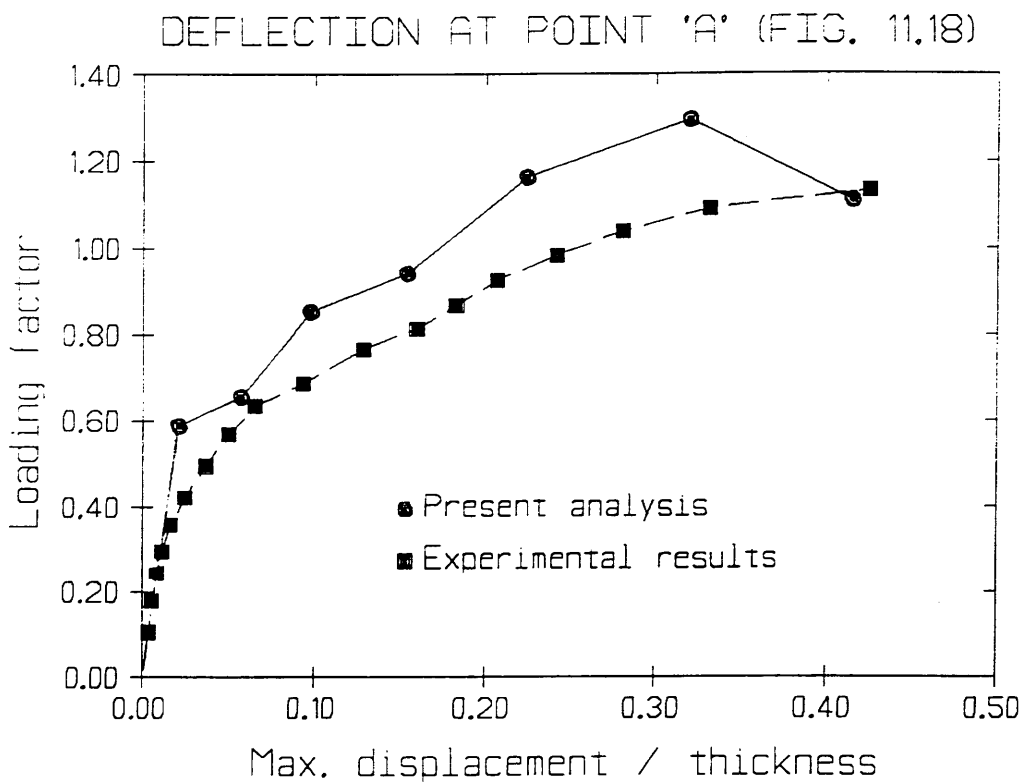


Fig. 7.19 Plate B: the deflection at the mid of free plate edge (at point 'A').

The results are less accurate than for the plate A. The structural stiffness is overestimated, especially for higher loading levels (by about 15%). The remedy could be to use a finer element mesh or elements with higher order approximations. Of course, adjustments of the material constants for this particular structure would also be feasible (using experimental results); however no general advice for improving their values is known.

The analysis was done by Arc-length method with implicit linearized step length and $\beta = 0$. The level of loading at structural failure was calculated by Line search method. As it is apparent from Fig. 7.18 and 7.19, a relatively large length of analysis steps was used and again no problems with convergence were found.

7.5 R/C slab C.

A. Aim of the analysis:

- to investigate the effect of geometrical nonlinearity for R/C slab *c*,
- to examine the post-failure behavior of the structure, and particularly to test the Line search .

B. Description of analyses and results:

The R/C plate *C*, similar to the plate *A* from analysis 7.5 is investigated. The dimensions, reinforcement and material properties are the same as those for the plate *A*. The plate is supported by hinges at its boundary, i.e. compared to plate *A*, displacements normal to the plate edges are also restrained. The structure was loaded by uniform loading and, again, 9 Heterosis elements with selective integration have been used to model one quarter of the plate.

Three solutions have been carried out: geometrically linear, geometrically nonlinear, both solved by Arc-length method with $\beta = 0$ and suppressed Line search method, and geometrically nonlinear solution using $\beta = 0$ and Line search method. Material nonlinearity was always considered. Resulting maximum displacements, (at the center) vs. loading levels are depicted in Fig. 7.20.

R/C SLAB

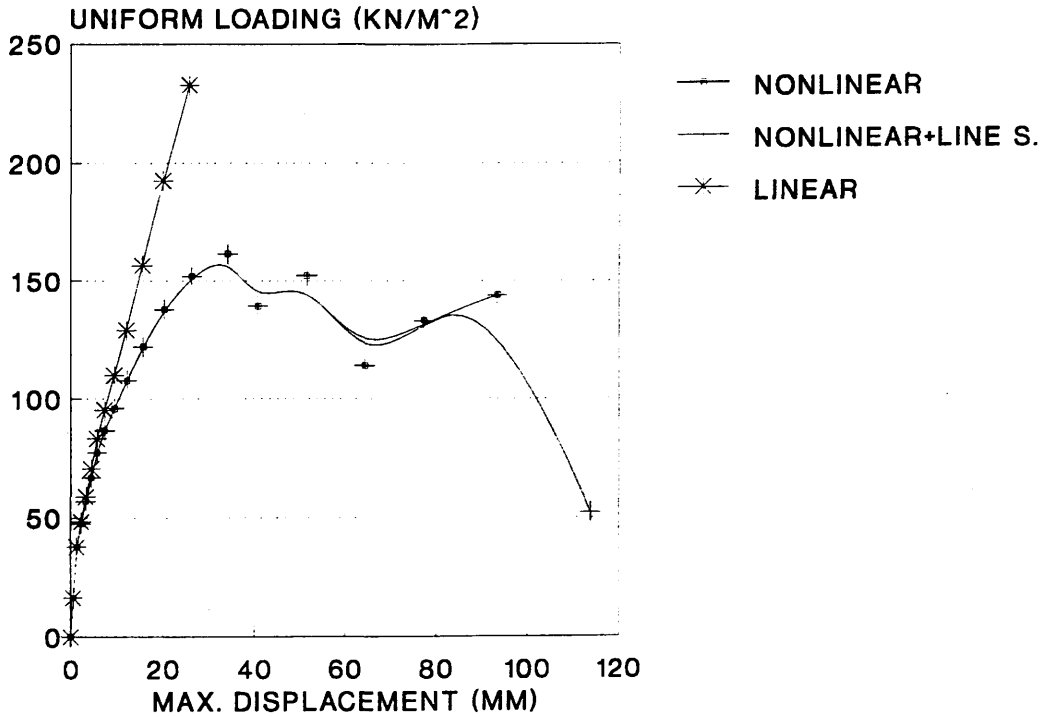


Fig. 7.20 Plate C: load-displacement relationships.

The analysis emphasizes the importance of geometrical non-linearity to be able to account for membrane action in the plate. Obviously if rollers rather than hinged boundary conditions are assumed, geometrical nonlinearity become much less significant.

Comparing results for suppressing and incorporating the Line search in the equation solver, the positive effect of the Line search is clear. However the present material model for concrete does not exhibit high accuracy for sudden unloading, (from high stress levels), so that the descending branch in Fig. 7.20 is disputable. Of course, for geometrical nonlinear and materially linear analyses the situation is different. The point here is that the proposed solver is able to deal even with such complex structural behavior.

7.6 Cylindrical R/C shell [67].

A. Aim of the analysis:

- to examine the results deterioration in results due to incorrect modeling of shell-edge beam interface,
- to examine the influence of geometrical nonlinearity on behavior,
- to investigate effect of incorporation compression hardening and compression strain softening into concrete material model,
- to provide much information about structural behavior and thus to the study finite element properties. These will include figures of deformations, stresses, failure zones etc. for various loading levels.

B. Description of analyses and results:

The cylindrical shell examined here was first experimentally investigated in [67], and analytical results are also available [41], [66].

The geometry and reinforcement of the structure are depicted in Fig. 7.21. Note that ref. [67] presents five alternatives of edge beam reinforcement. The reported results did not differ significantly and therefore, in the present analysis only variant No. 2 is analyzed.

The shell has a span of 3.36m, width of 1.305m and a height of 0.339m including 0.1m deep edge beams. The shell is supported along its more distant ends where bracing walls are mounted. The structure is loaded by the self-weight and by vertical surface loading which is also self-weight proportional. Therefore, in the present analysis loading is defined as a λ multiple of the structural self-weight.

Material properties are summarized in Table 7.5. Some discrepancies in reported material properties used by refs. [66], [41] and [67] were found. Although in refs. [66] and [41] the

authors state they have used the values from ref. [67], their values differ significantly. Because of the fact that we refer also to their results, Tab. 7.5 also includes their values.

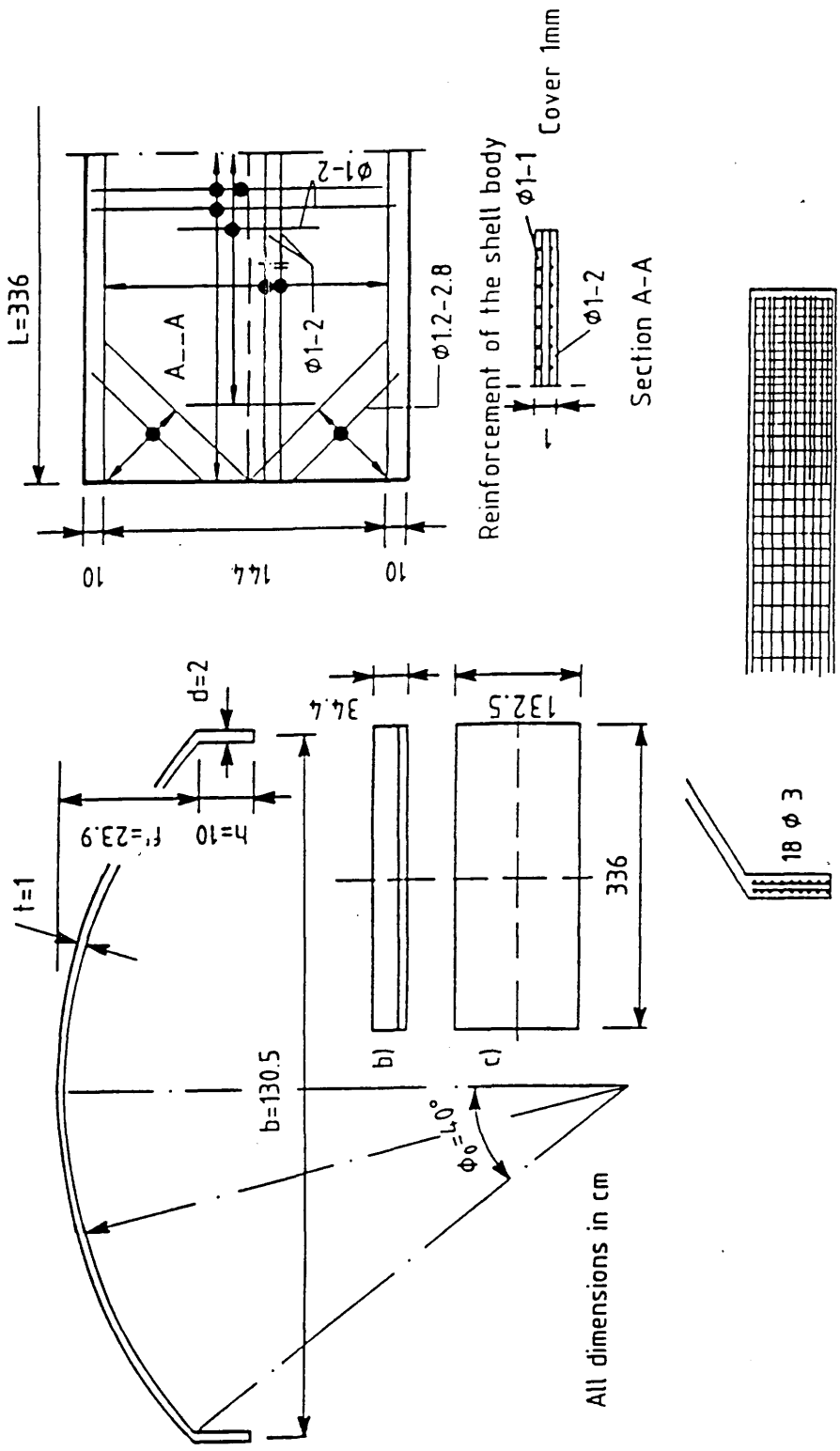


Fig. 7.21 Geometry and reinforcement details of the cylindrical shell.

	Pres. anal.	[67]	[41]	[66]
Concrete:				
Young's modulus[GPa]	33	33	30	29.4
Poisson's ratio	0.18	*	0.2	0.2
Ult. comp. stress[MPa]	38	38	30	29.4
Ult. tens. stress[MPa]	3.8	*	1.67	1.64
Ult. comp. strain	0.003	*	0.0027	var.
Tens. stiff. coef. α	0.5	*	0.5	*
Tens. stiff. coef. ϵ_m	0.002	*	0.0015	*
Shear ret. factor β	0.5	*	*	*
Strain for $\tau_{cr} = 0.$	0.004	*	*	*
Steel:				
Young's modulus[GPa]	200	*	196.	206.
Young's m. (plast)[GPa]	20.	*	20.	19.6
Yield stress [MPa] (shell)	294.	289.	295.	295.
Yield stress [MPa] (edge beam)	294.	274.6	280.	274.6

Legend: * = value not given

Tab.7.5 Material properties for shell analysis.

To test the consequence of incorrect modeling of the shell-beam interface, two models have been used. In the first (Fig. 7.22) the edge beams were modeled by vertical shell elements, i.e. the real position. Because of doubts about shell behavior in the area near the shell-beam connection, (due to local coordinates system, which does not allow in-plane rotations, rotation degrees of freedom on shell-beam edge are constrained), another model was also used, where edge beams were replaced by a smooth continuation of the shell (Fig. 7.23). This "artificially" created part was designed so that the total depth of the shell is not changed, the cross section area of edge beams does not differ and also the amount of reinforcement is identical with the original shell.

Due to symmetry only a quarter of the structure was analyzed. In both models the shell was discretized by 4 x 5 elements (5 in longitudinal direction) and edge beams by 2 x 5 elements. For elements modeling the shell part of the structure 8 equally deep layers were used whilst elements for edge beams comprised only 4 equally deep layers.

SHELL ANALYSIS - MODEL NO. 1

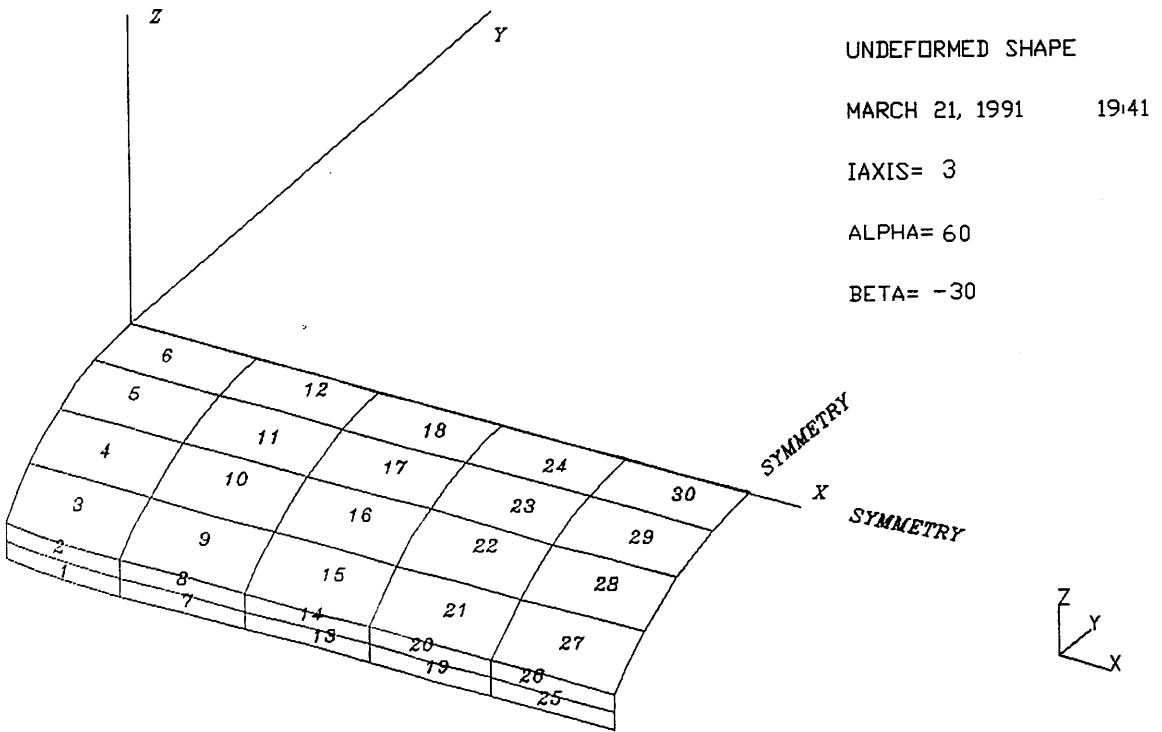


Fig. 7.22 Shell, model No. 1.

SHELL ANALYSIS - MODEL NO. 2

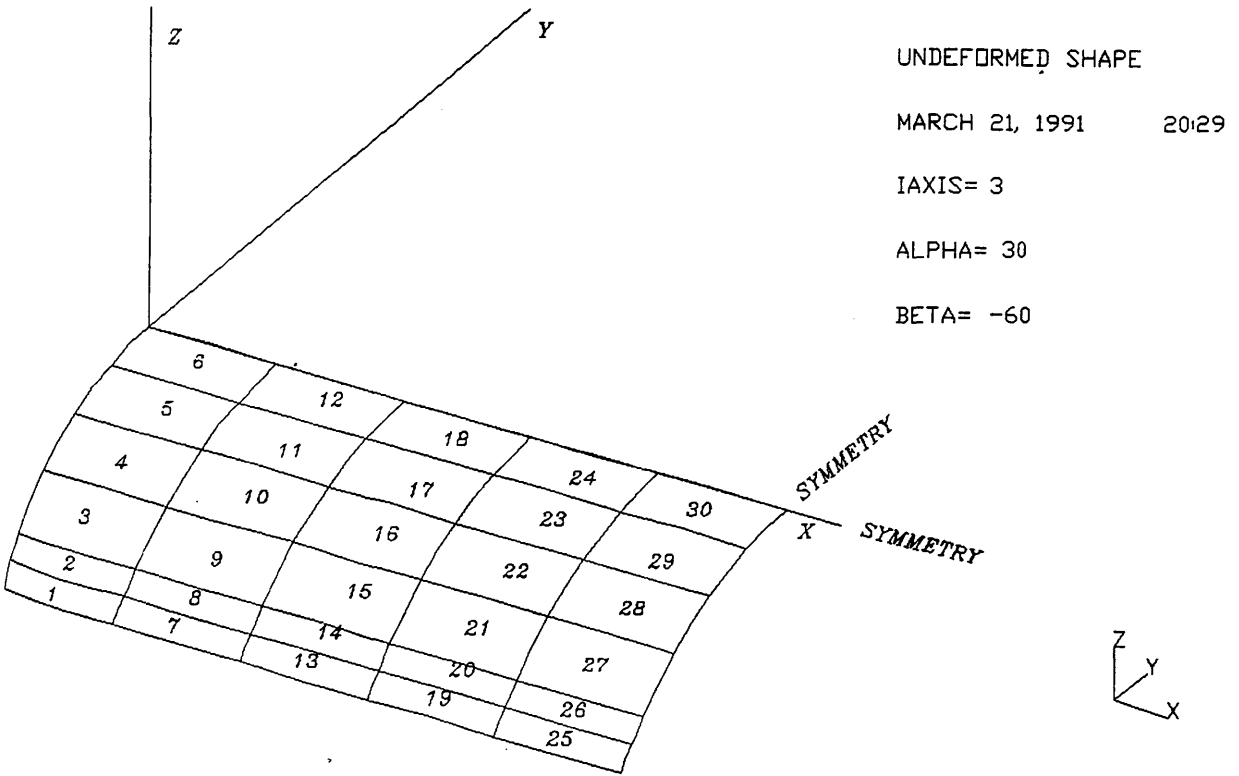


Fig. 7.23 Shell, model No. 2.

All reinforcement was smeared into steel layers. Only normal rigidity of reinforcement is accounted for, i.e. dowel action in the steel bars is not considered.

A full nonlinear solution, including the effect of geometric nonlinearity using the Von Karman assumptions, and compression hardening for concrete, was carried out by the Arc-length method with the Crisfield equal step length constraint for λ parameter. The Line search was inhibited and $\beta = 0$.

The mid-span vertical displacements of edge beams, (maximum deflection) vs. loading levels are shown in Fig. 7.24. The results are compared with those given by [66], [41] and [67]. The model No.1 matched the experimental data very well, better than

[66] or [41]. The stiffness reduction in model No. 2, (due to removing the sudden change of element slope between shell and beam) caused higher structural deformations. Model No.1 is clearly superior to model No.2.

MID-SPAN DISPLACEMENT (EDGE BEAM)

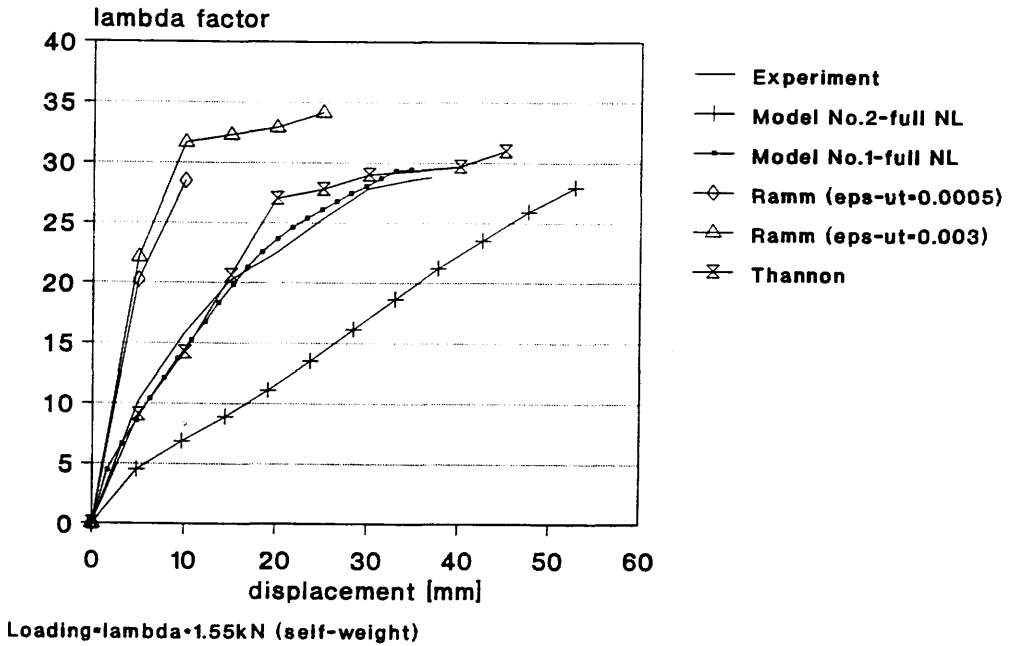


Fig. 7.24 Mid-span displacement of shell edge beams.

Deformations corresponding to $\lambda = 10.3$ for the model No. 1 and model No. 2 are depicted in Fig. 7.25 and Fig. 7.26.

SHELL ANALYSIS - MODEL NO. 1

LOAD CASE

TIME 19:41

FACTOR 10.15

MARCH 21, 1991

IAXIS= 3

ALPHA= 30.

BETA= -60.

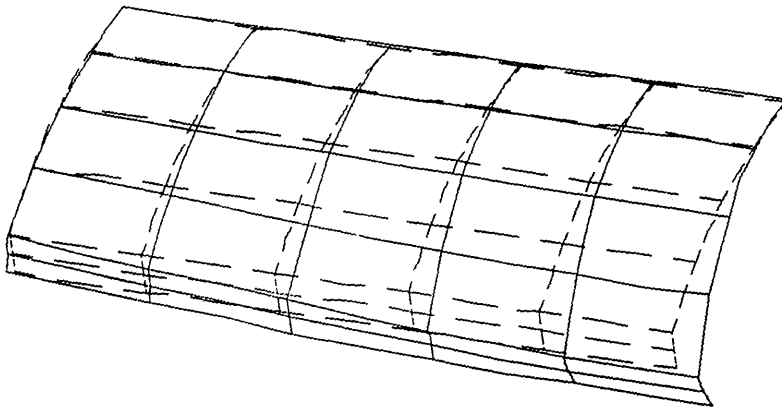


Fig.7.25 Shell deformation for $\lambda = 10.3$ model No. 1.

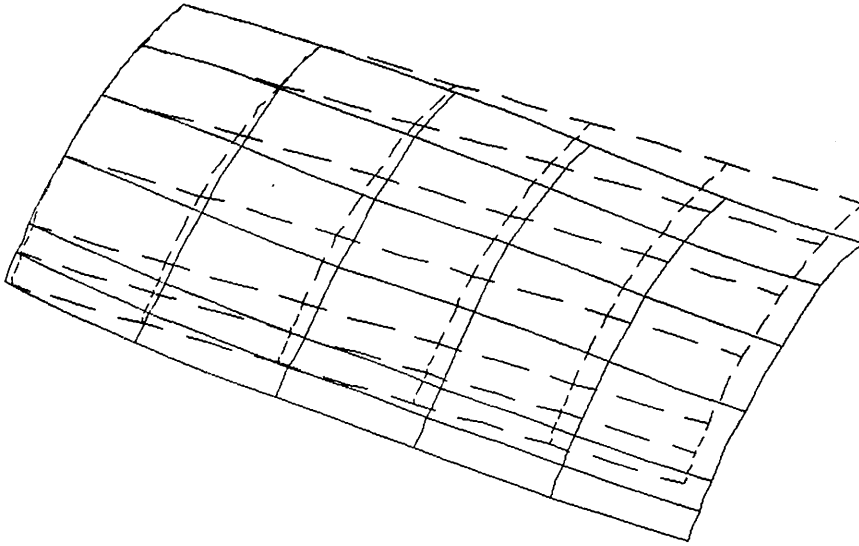


Fig. 7.26 Shell deformation for $\lambda = 10.3$, model No. 2.

Failure development in model No.1. is shown in Fig 7.27. Near loading level $\lambda \cong 5$, first cracks have been created. At $\lambda \cong 10$ the process of first cracks propagation seemed to settle and at about $\lambda \cong 20$ the first plastic areas develop and reinforcement yielding first occurred. At ultimate loading, ($\lambda = 29.23$) nearly the whole structure was beyond material elasticity, including longitudinal reinforcement at mid-span of the edge beams. Here also first crushing of structure occurred. Beyond this loading a spontaneous crushing near midspan and near supports happened resulting in a structural singularity and consequently numerical collapse.

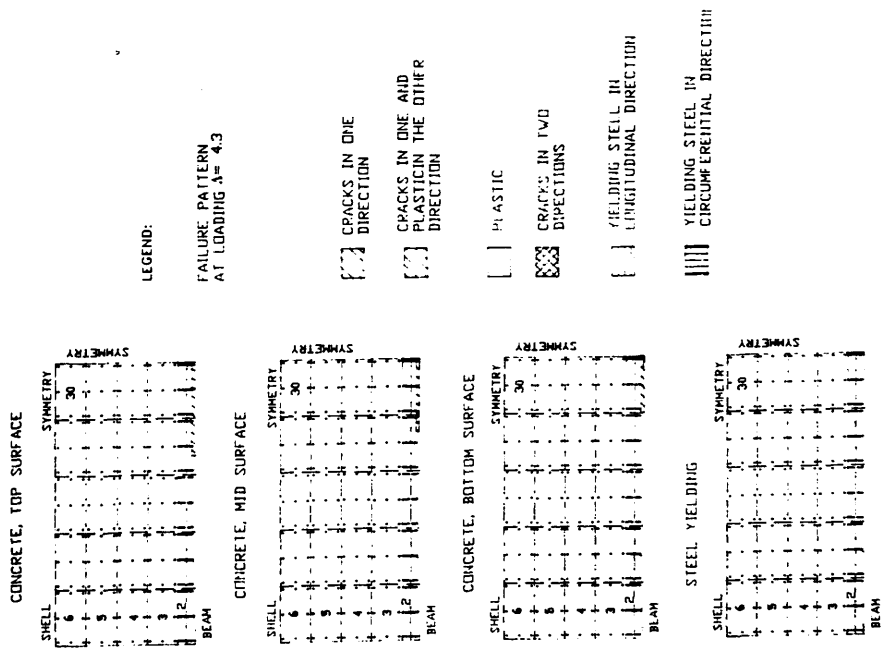
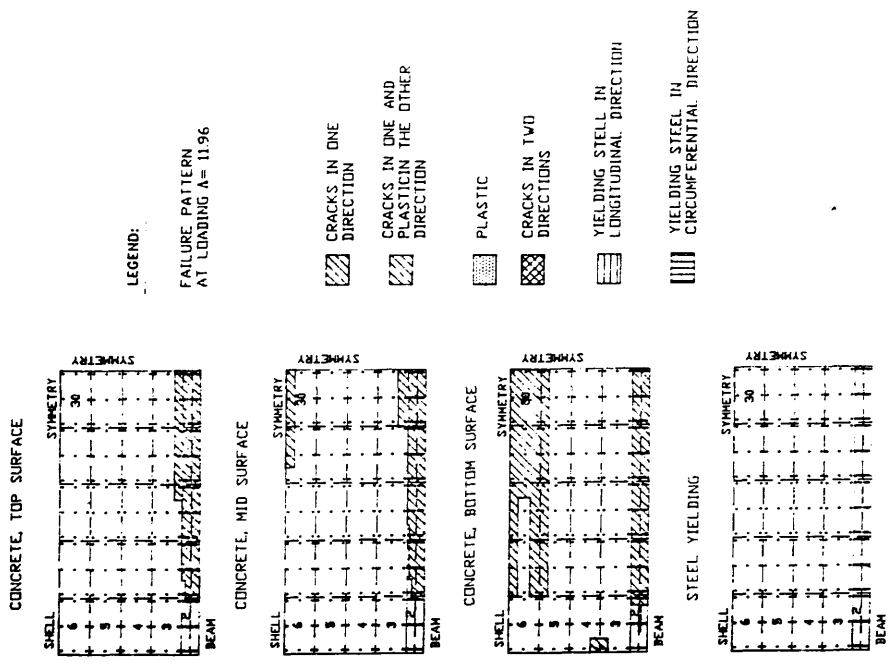


Fig. 7.27 Shell , model No.1, failure zone progression.

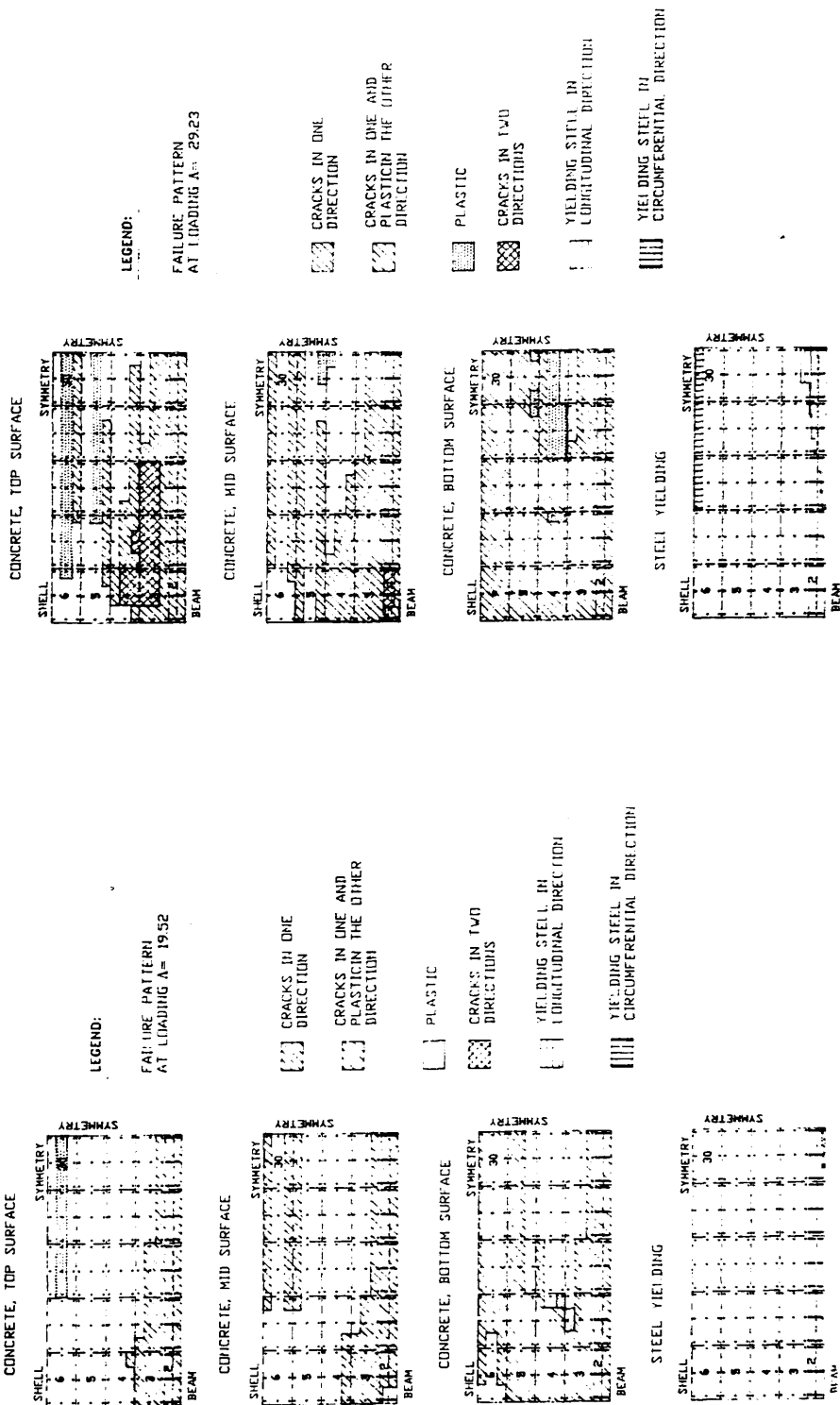


Fig. 7.27 Shell , model No.1, failure zone progression (cont.).

Contours of internal forces for $\lambda = 4.3, 11.96, 19.52$ and 29.23 , (model No.1) are given in Fig 7.28 through Fig. 7.31. They show how the internal forces move from midspan area of beam, (in longitudinal direction) and shell, (in circumferential direction) to less exploited neighbouring areas, up to the ultimate load where no further force redistribution is possible and the structure collapses.

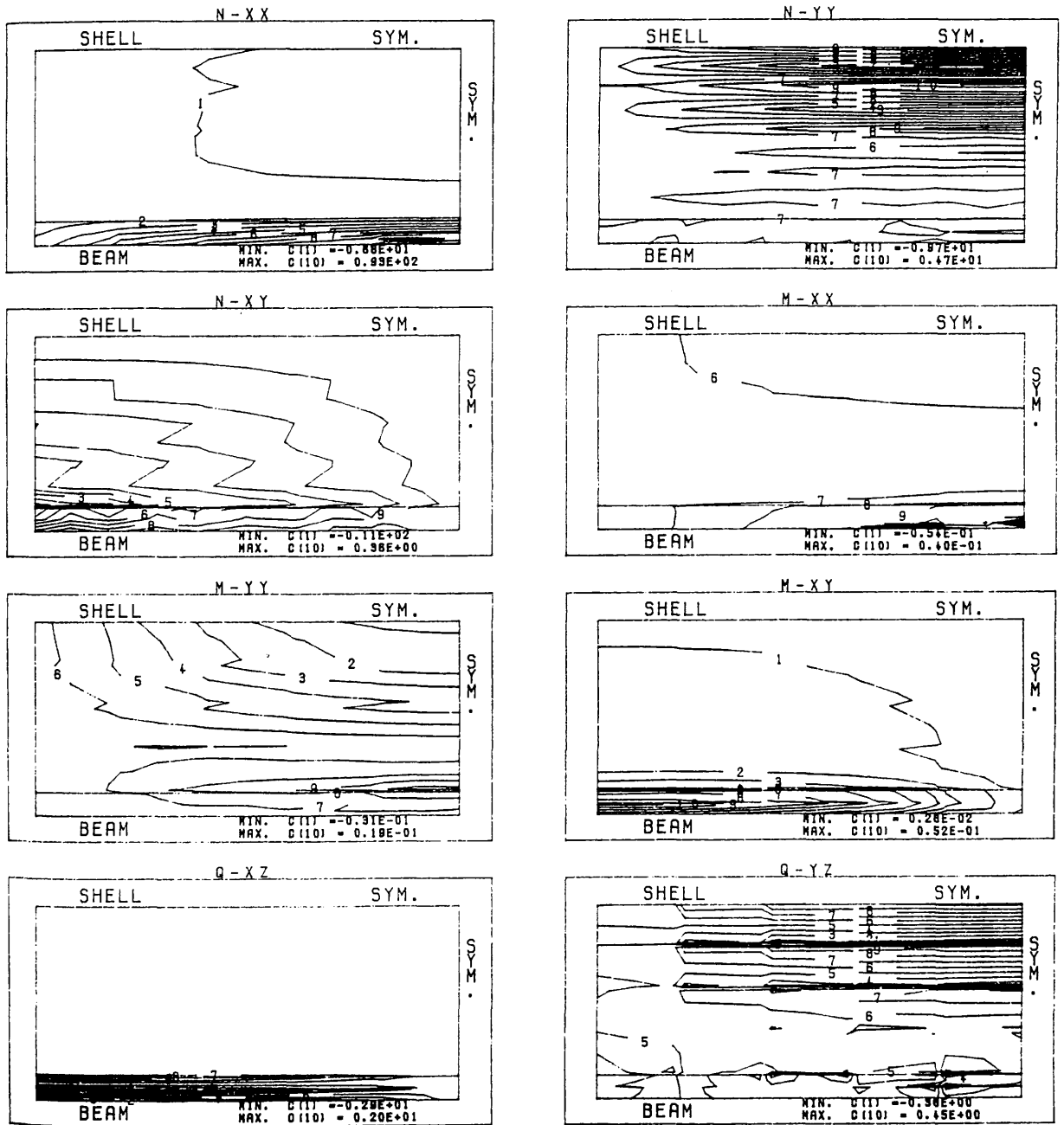


Fig. 7.28 Shell internal forces for $\lambda = 4.3$, model No. 1.

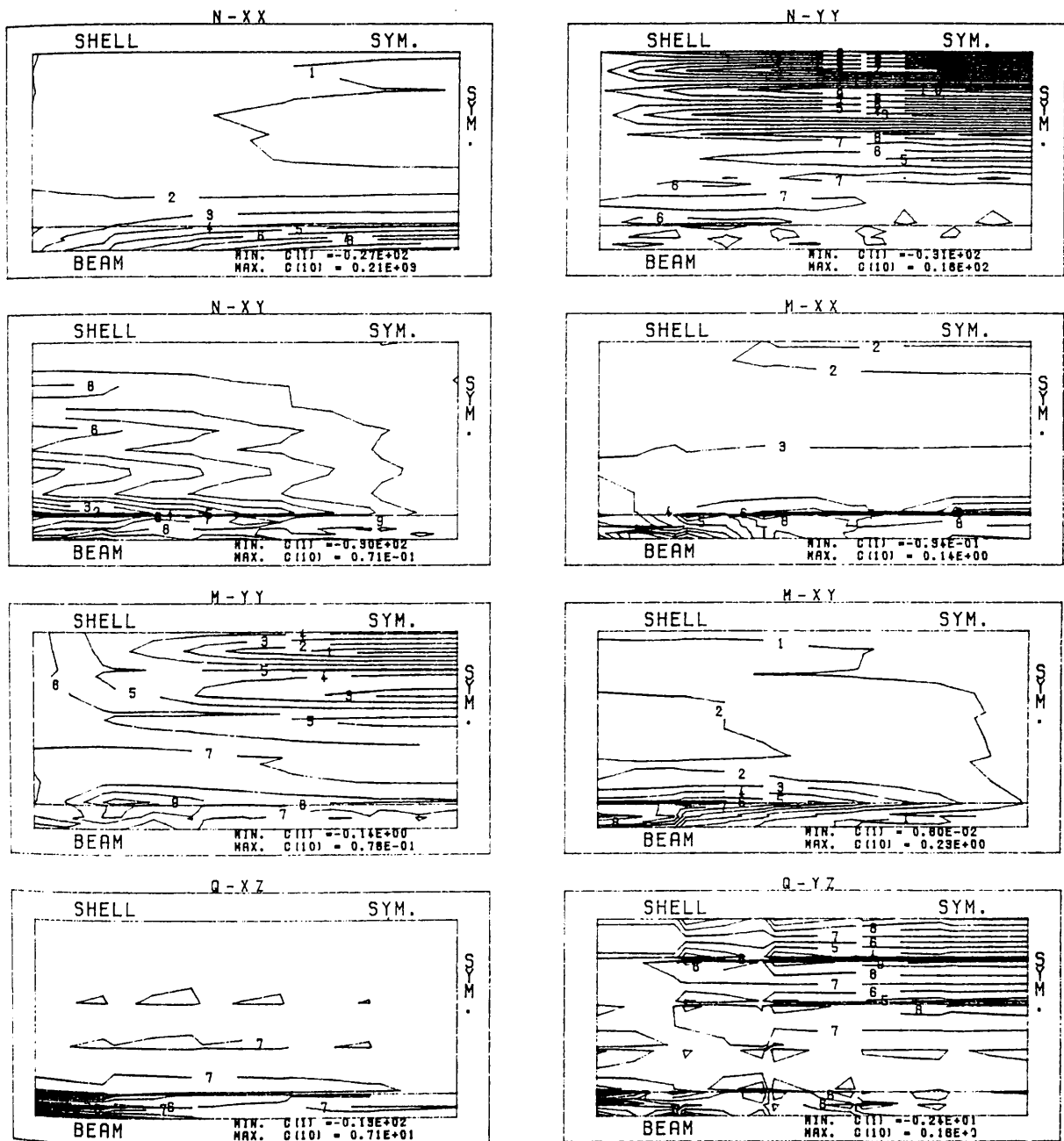


Fig. 7.29 Shell internal forces for $\lambda = 11.96$, model No. 1.

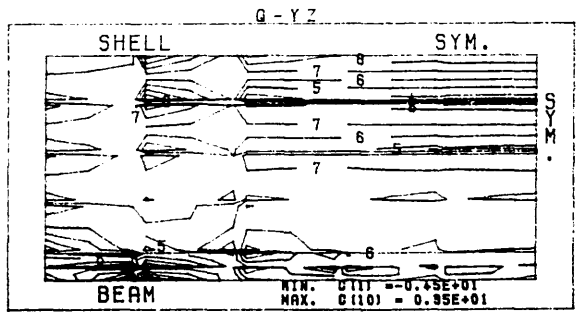
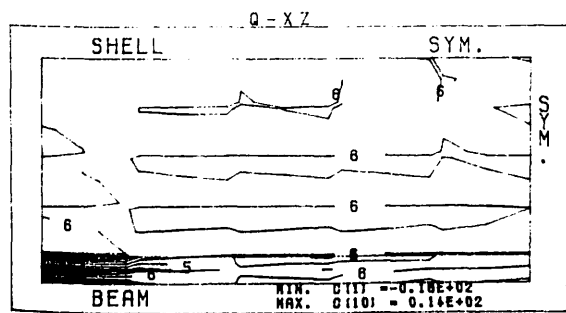
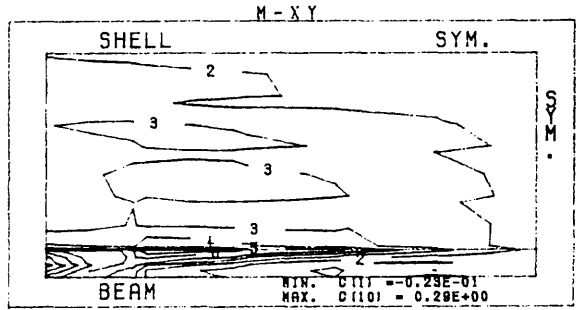
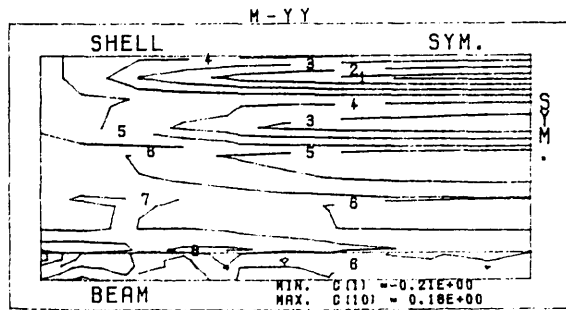
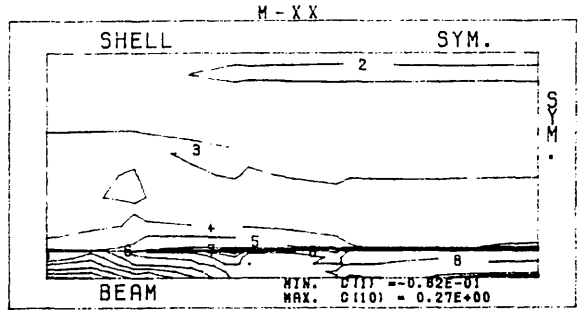
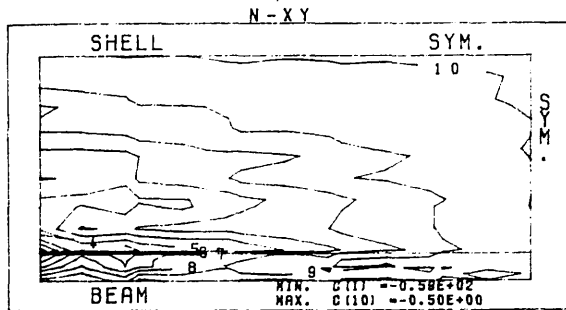
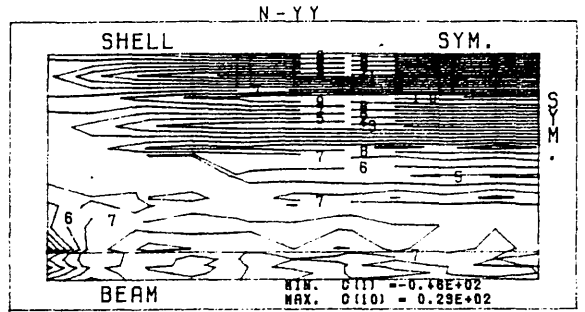
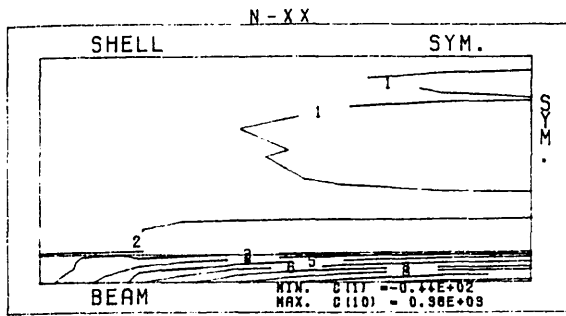


Fig. 7.30 Shell internal forces for $\lambda = 19.52$, model No. 1.

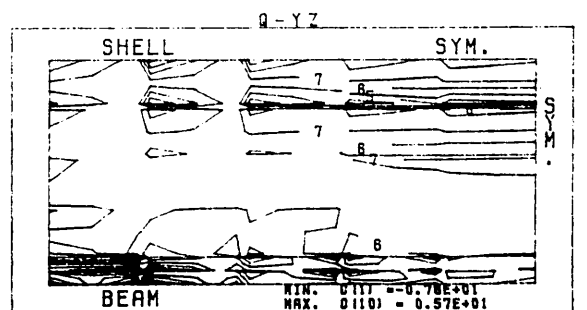
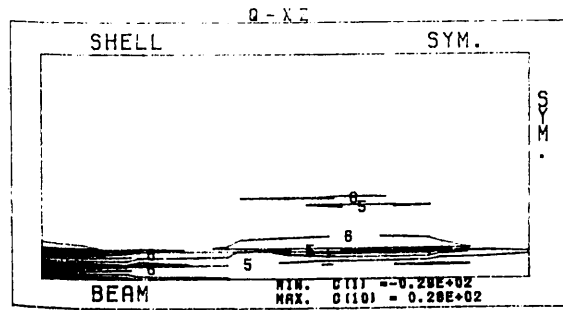
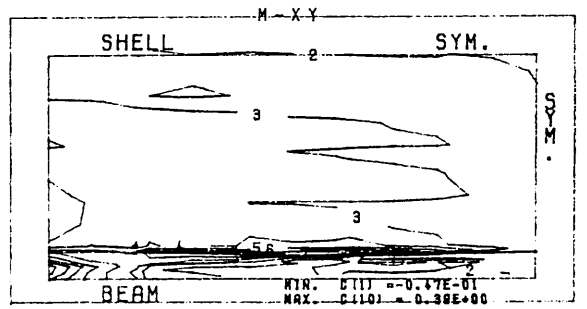
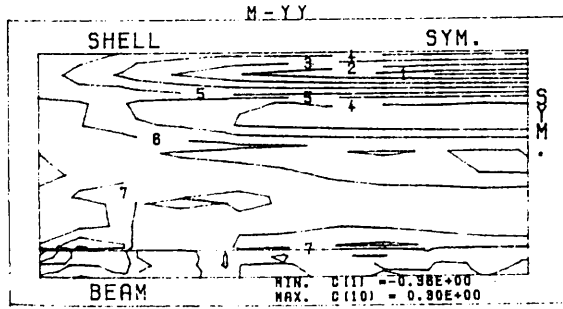
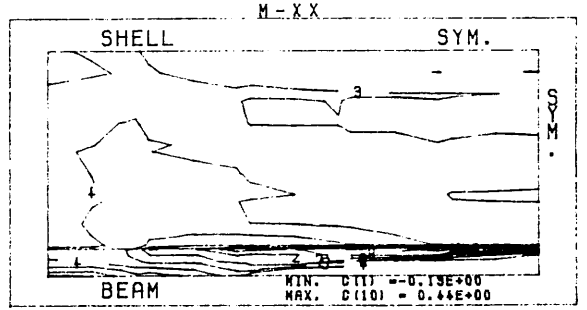
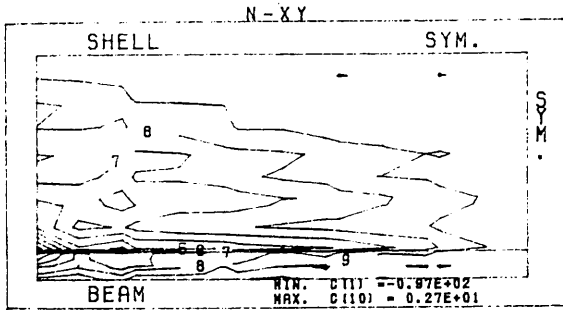
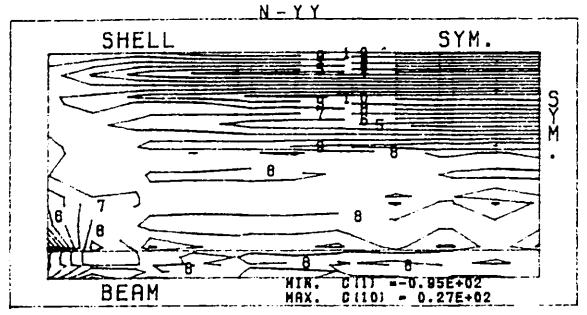
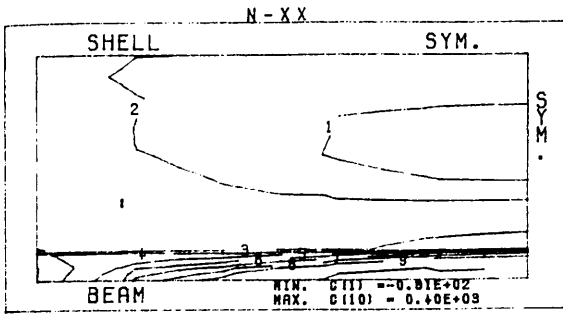


Fig. 7.31 Shell internal forces for $\lambda = 29.23$, model No. 1.

Structural collapse according to the experiment occurred due to punching in the area near shell center. It is very difficult to identify collapse mode from the present analysis, because we used smooth material laws reducing continuously material resistance~~down~~ to zero value. Hence the structural failure, not numerical failure, lies already somewhere below ultimate value $\lambda = 29.23$. Some estimates could be drawn by a closer examination of figures 7.27 - 7.31.

In the following interest is focused on the effect of the degree of nonlinearities considered on analysis accuracy. Model No. 1 is investigated. Structural load-maximum displacement relationship is recalculated for the following cases:

a/ full nonlinearity is considered, compression hardening of concrete neglected. This leads to elastic-perfect plastic constitutive equations in compression, (tension regime is unaffected). Beyond ultimate compression strain, (assumed to be a value of 0.003) a sudden drop of material rigidity to zero occurs,

b/ The improved version of concrete material model in used, i.e. with compression hardening and the softening branch, however geometrical nonlinearity is neglected.

The results are compared with the previous, fully nonlinear solution in Fig. 7.32.

MID-SPAN DISPLACEMENT (EDGE BEAM)

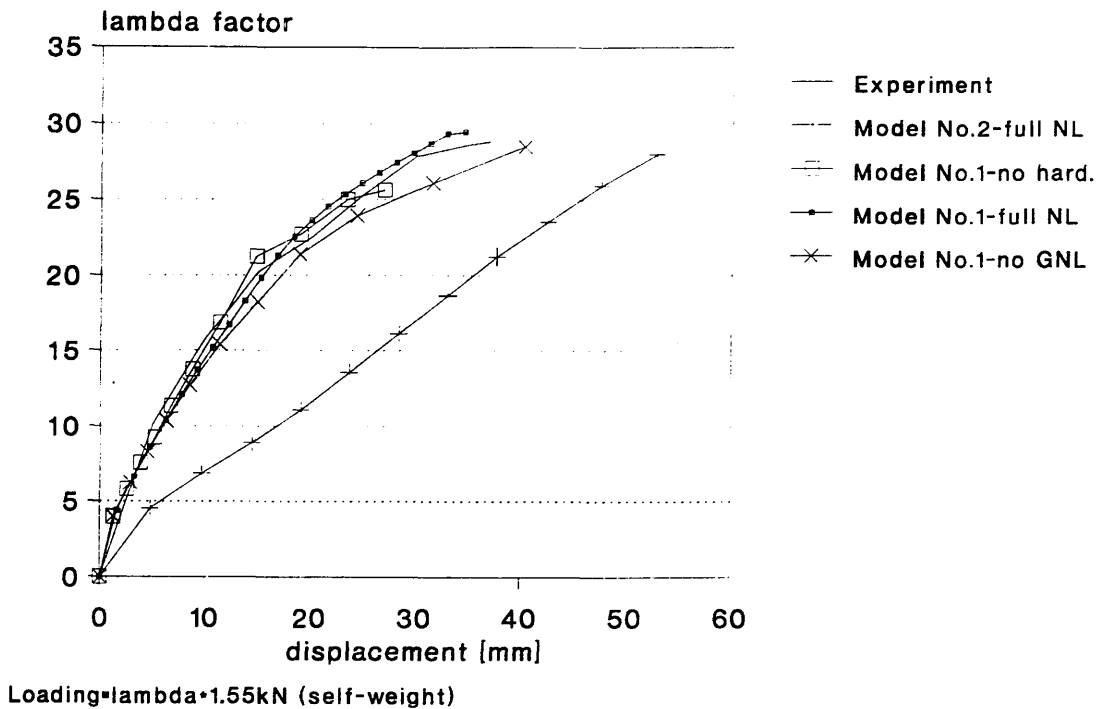


Fig. 7.32 Influence of geometrical nonlinearity and various modeling of concrete compression on the shell behavior, model No.1.

Fig. 7.32 includes also results for fully nonlinear solution using model No.2. Apparently a proper structural model is the first requirement for accurate analysis.

In summary:

- good agreement between experimental and the present analysis has been reached,
- model No. 1 provides more accurate results than model No. 2 and consequently constraining of rotations along shell-beam edge does not influence the accuracy too much,
- neglecting geometrical nonlinearity resulted in less structural stiffness, (about 10%),
- the improvements of concrete material model enable higher analysis accuracy and reduce numerical problems near the limit point.

Notice also that ultimate load itself was calculated more accurately.

7.7 Summary.

It is beyond the scope of this work to investigate all aspects involved in the presented analyses. Therefore we concentrated on providing some evidence to support the theoretical developments.

Introducing compression hardening and softening into the elastic-plastic constitutive equations for concrete improved both the accuracy and the numerical behavior of the model.

The new nonlinear solution algorithm can handle complicated situations of structural behavior, e.g. snap back and snap through phenomena. If the governing equations of a structure suffer from discontinuities (e.g. due to cracking), the Line search may be of great help, otherwise its use is debatable. It is, however, always useful for checking the overall convergence of the algorithm.

All analyses were carried out on a standard personal computer thus meeting one of the objectives of this work.

8. CREEP AND SHRINKAGE ANALYSIS.

When a concrete specimen is loaded, the specimen first shows an instantaneous deformation which is then followed by a slow increase of further deformation. This slow increase of deformation, originally discovered at the beginning of the 20th century, is called creep. A concrete specimen deforms in time even if no loading is applied. These deformations are called shrinkage (apart from temperature deformations).

It is known that the physical nature of creep has its source in the hardening of cement paste and in failure of the paste-aggregate bond. The cement gel contains about 40 to 55% of capillary pores in volume, has an enormous pore surface (about $500 \text{ m}^2/\text{cm}^3$) and is made up of sheets of colloidal dimensions. Because the pores of cement gel are micropores of subcapillary dimensions they cannot contain evaporable water, which is strongly held by solid surfaces and may be regarded as absorbed water or inter-layer water. This water can exert on the pore walls a significant pressure called the disjoining pressure. The bonds between the colloidal sheets in cement are very disordered and unstable. Hence creep is caused by changes in solid structure. The precise mechanism of creep is still a subject of discussion. Bonding and rebonding process similar to movement of dislocations may be involved and it is also possible that various solid particles migrate from the zones with a high stress to unstressed zones with larger pores. Due to disjoining pressure the presence of water causes a weakening of bonds. This is the reason why after drying the creep is less. On the other hand during drying the creep is higher than in sealed specimens. It has probably two main sources: stresses and microcracks produced by drying in the specimen as a whole and the fact that water diffusing out of the loaded gel micropores creates disorder and migration of solid particles.

Because the solid particles migrate out of the highly stressed regions, their load is gradually relaxed and is transferred to more stable part of the microstructure. Therefore the creep rate decreases in time. The second reason for creep reduction in time is increasing volume of cement gel at the expense

of capillary pores due to the hydration process.

The main cause of shrinkage is the increase of solid surface tension and capillary tension due to drying and also the decline of disjoining pressure in the gel.

In recent times there has been increasing interest in the analysis of reinforced concrete structures which accounts for shrinkage and creep. It is well known, that in the deformation of ordinary structures or even in case of some special structures, e.g. nuclear reactors and pressure vessels, both creep and shrinkage are very important and cannot be neglected. They are also very important in the behavior of composite structures, where, for example, high stress levels can be caused by different shrinkage of two adjacent layers. On the other hand it should be noted that to compute only stresses in ordinary structures time entities are not usually very important.

Creep and shrinkage in structures may have the following effects:

- 1/ redistribution of internal forces due to external loading,
- 2/ reduction of initial stresses and
- 3/ reduction of strength due to deformations

The influence of shrinkage is often reduced by creep of the material and for that reason its effect is not so important. But, there are structures where a more accurate solution is necessary.

Creep effects can be very significant if the limiting factor is the deformation of a structure. It is quite well known that the short-term Young's modulus for concrete can be two times higher than long-term Young's modulus which takes creep into account.

The study of creep and shrinkage of reinforced concrete consists of two main topics. The first is the study of creep and shrinkage at the material level in order to identify the controlling parameters and to produce laboratory measurements from which suitable mathematical models can be developed.

The second topic is the development of numerical methods and solution schemes which enable us to use these material models in

the analysis and design of concrete structures.

The main concern of this chapter is to review some of the most widely used material models and thereafter to focus attention on how to use these in practical examples. Some results of practical implementation will be presented in Chapter 9.

Special interest will be paid to a comparison of ACI-78 [32], CEB-FIP 78 [31], [32] and Bazant-Panula's model I and II [31], [48] for creep and shrinkage prediction and to their use with the recursive step-by-step iterative procedure for geometrically and materially nonlinear structures.

It should be pointed out that there is usually a very intimate interrelationship between the creep function used for creep prediction and the creep analysis itself. However this is not the case for the Recursive step-by-step solution scheme, because the original creep function is approximated by a special function based on a degenerated kernel (to be discussed later). There are many other significant advantages of this method, but its "independence" of the function for creep modeling was an important factor contributing to its choice.

As for shrinkage the situation is much more simple than with creep. Usually it is accounted for by introducing an initial strain only. Hence the situation is very similar, for example, to accounting for temperature effects only.

8.1 Models of creep and shrinkage prediction.

In previous years a high interest in creep and shrinkage modeling of concrete can be found. Unfortunately the presented results are not unique and sometimes there are also significant differences in the adopted terminology. For instance the "Young's modulus" is sometimes based on immediate elastic strains whilst other times it covers also short-term delayed strains (also recoverable), which are in the former models treated in a separate term. Therefore a complete definition of a particular creep and shrinkage model should be used.

There are two basic ways for dealing with creep of concrete. The first attempts to represent the experimentally obtained creep surfaces of virgin concrete as a product of an age and duration function, usually in the form of one or two power law functions. This leads to a general form for creep function $\Phi(t, t')$:

$$\Phi(t, t') = \frac{1}{E(t')} [1 + K_0 f_1(t') g_1(t - t')] \quad /8.1/$$

where t is at the time of our interest of structural behavior,
 t' is the time when the structure was loaded,
 f_1 and g_1 are functions given by the model,
 K_0 is constant
 $E(t')$ is Young's modulus at time t' .

The creep function $\Phi(t, t')$ defines strains in material at time t subject to loading by the unity stresses at time t' . The decomposition of the time function $f(t, t')$ to $f(t') g(t - t')$ has been found quite acceptable and has been used by many authors (Bazant, Osman [35], [37], [38], [41] etc.). It was also applied in creating CEB 1964 and ACI-78 standards for creep prediction.

The second approach is to compose the total creep function as the sum of two or more creep components, namely an elastic (recoverable) component, a delayed recoverable component and irrecoverable flow. An important feature is that the delayed elastic component is independent of time t' and similar to /8.1/ the flow component is dependent on the loading duration $(t - t')$.

This simplification leads to creep functions of the following form:

$$\Phi(t, t') = \frac{1}{E(t')} + K_1 f_2(t - t') + K_2 [g_2(t) - g_2(t')] \quad /8.2/$$

where K_1 and K_2 are constant. This type of creep law is used in the model CEB-FIP 78 standard.

In the following, descriptions of ACI 78, CEB-FIP 78 and Ba-

zant-Panula's model II are given. Further details are available in refs. [31], [32], [38] and [43]. The Bazant-Panula's model I is too sophisticated to present it here but is described in detail in [48].

These models were implemented into a material preprocessor called MATERIAL which provides appropriate input for the time-dependent finite element analysis (programs CONCRETE and NONSAP). The following sections provide a theoretical description of the creep and shrinkage modeling in the developed software. Using interactive program facilities the user can conveniently compare the generated creep and shrinkage functions for a particular case, choose the best of these models and if necessary to modify the input data to obtain the desired functional shape. In addition the preprocessor can also accept direct experimental data.

8.1.1 American Concrete Institute (ACI) 1978 model.

Creep function.

In this method the creep coefficient is the ratio of creep at any age t after application of loading at time t' , to the elastic strain at the age at application of load t' .

$$\phi(t, t') = C(t, t') E_c(t') \quad /8.3/$$

where $\phi(t, t')$ is the creep coefficient

$C(t, t')$ is creep per unit of stress, i.e. specific stress

$E_c(t')$ is the modulus of elasticity at time t' .

The proposed form for the creep coefficient $\phi(t, t')$ is expressed by:

$$\phi(t, t') = \frac{(t - t')^{0.6}}{10 + (t - t')^{0.6}} \phi_{\infty}(t') \quad /8.4/$$

where $(t - t')$ is the time since load application (in days)
 and $\phi_{\infty}(t')$ is the creep coefficient at $t = \infty$
 (ultimate).

The expression for $\phi_{\infty}(t')$ has the form:

$$\phi_{\infty}(t') = 2.35 k'_2 k'_1 k'_4 k'_3 k'_6 k'_7 \quad /8.5/$$

k'_1 is the coefficient accounting for environmental humidity:

$$k'_1 = 1.27 - 0.0067 h$$

where h is humidity (in %), $h \geq 40$.

k'_2 can be estimated by:

$$k'_2 = 1.25 t'^{(-0.118)} \quad \text{for moist curing or}$$

/8.6/

$$k'_2 = 1.25 t'^{(-0.095)} \quad \text{for steam curing}$$

and accounts for the age of loading. It should be noted, that /8.6/ are applicable only if $t' \geq 7$ days or $t' \geq 3$ days for moist and steam curing respectively.

The coefficients which allow for the composition of concrete are k'_3 , k'_6 and k'_7 :

$$k'_3 = 0.82 + 0.00264 s_f \quad /8.7/$$

where s_f is the slump of fresh concrete (in mm).

The coefficient k'_6 is used to account for fine aggregate/total aggregate ratio $\frac{s}{a}$ (in %):

$$k'_6 = 0.88 + 0.0024 \frac{s}{a} \quad /8.8/$$

and the coefficient k'_7 :

$$k'_7 = 0.46 + 0.09 A \geq 1. \quad /8.9/$$

where A is air content (in %).

The coefficient k'_4 accounts for the influence of thickness:

a/ If average thickness is less than 150 mm then ACI 78 provides creep coefficients as presented in Table 8.1.

Average member thickness	Creep coefficient k'_4
50 mm	1.30
75 mm	1.17
100 mm	1.11
125 mm	1.04
150 mm	1.00

Table 8.1. ACI 78 model, creep coefficient k'_4 .

In the preprocessor program MATERIAL these values are approximated by a 4th order spline to compute intermediate values.

/b For average thickness d between 150 and 380 mm then

$$k'_4 = 1.14 - 0.00091 d, \text{ for } (t - t') \leq 1 \text{ year}$$

and /8.10/

$$k'_4 = 1.14 - 0.00067 d, \text{ for } (t - t') > 1 \text{ year}$$

c/ For average thickness $d \geq 380$ mm then ACI 78 recommends:

$$k'_4 = \frac{2}{3} [1 + 1.13 \exp(-0.0212 \frac{V}{S})] \quad /8.11/$$

where $\frac{V}{S}$ is volume/surface ratio (in mm).

Table 8.2 summarizes the expressions for computing the

effective (theoretical) thickness, volume/surface ratio and average thickness for common shapes of cross sections:

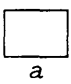
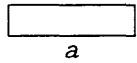
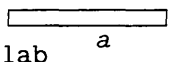
Cross section	Effective thick.	Volume/surface	Average thick.
 a	$\frac{a}{2}$	$\frac{a}{4}$	a
 b	$\frac{a b}{a + b}$	$\frac{a b}{2(a + b)}$	$\frac{2a b}{a + b}$
 t slab a	$\frac{a t}{a + t}$	$\frac{a t}{2(a + t)}$	$\frac{2a t}{a + t}$
annular section of thickness t	t	$\frac{t}{2}$	2t
cylinder of diameter d	$\frac{d}{2}$	$\frac{d}{4}$	d

Table 8.2 Definition of average and effective thicknesses.

The total deformation under a unit stress (i.e. elastic strain plus creep) can be computed by:

$$\Phi(t, t') = \frac{1}{E_c(t')} [1 + \phi(t, t')] \quad /8.12/$$

where the modulus of elasticity at the age of load application t' is given by:

$$E_c(t') = 42.8 * 10^{-6} [\rho^3 f_{cyl}(t')] \left(\frac{1}{2}\right) \quad /8.13/$$

and

$$f_{cyl}(t') = \frac{t'}{A + B t'} f_{cyl28} \quad /8.14/$$

Hence the modulus $E_c(t')$ is related to the 28-day compressive strength f_{cyl28} . Units are GPa for $E_c(t')$, MPa for f_{cyl28} and kg/m^3 for the density of concrete. The constants A and

B are function of the type of cement and curing conditions. These are given in Table 8.3.

Type of cement	Curing condition	Constant A	Constant B
I	Moist	4.00	0.85
	Steam	1.00	0.95
III	Moist	2.30	0.92
	Steam	0.70	0.98

Table 8.3 ACI78 model, constants A and B .

Shrinkage.

Shrinkage is measured with respect to the time t'_{sh} , since the start of the drying process.

Two expressions are recommended, depending on the type of curing:

$$\epsilon_{sh}(t, t'_{sh}) = \frac{(t - t'_{sh})}{35 + (t - t'_{sh})} \epsilon_{sh00} \quad \text{for moist curing and}$$

/8.15/

$$\epsilon_{sh}(t, t'_{sh}) = \frac{(t - t'_{sh})}{55 + (t - t'_{sh})} \epsilon_{sh00} \quad \text{for steam curing.}$$

In /8.15/ $\epsilon_{sh}(t, t'_{sh})$ is the shrinkage strain (in 10^{-6}) and the ultimate shrinkage ϵ_{sh00} is defined by:

$$\epsilon_{sh00} = 780 \cdot 10^{-6} q'_5 q'_1 q'_4 q'_3 q'_6 q'_8 q'_7 \quad \text{/8.16/}$$

For evaluating the coefficients $q'_5, q'_1, q'_4, q'_3, q'_6, q'_8$ and q'_7 ACI 78 provides the following expressions:

The humidity coefficient q'_1 is:

$$q'_1 = 1.4 - 0.01 h, \quad \text{for } 40 \leq h \leq 80$$

/8.17/

$$q'_1 = 3.0 - 0.03 h, \quad \text{for } 80 \leq h \leq 100,$$

where h is humidity (in %).

The coefficients which allow for the composition of the concrete are q'_3 , q'_6 , q'_7 and q'_8 .

$$q'_3 = 0.89 + 0.00264 s_f \quad /8.18/$$

where s_f is the slump of fresh concrete (in mm),

$$q'_6 = 0.30 + 0.014 F \quad \text{for } F \leq 50, \quad /8.19/$$

$$q'_6 = 0.90 + 0.002 F \quad \text{for } F > 50$$

where F is the fine aggregate/ total aggregate ratio by weight (in %).

$$q'_7 = 0.95 + 0.008 A, \quad /8.20/$$

where A is air the content (in %) and finally:

$$q'_8 = 0.75 + 0.00061 \gamma, \quad /8.21/$$

where γ is the cement content (in kg/m^3).

The coefficient q'_4 is a function of average thickness d for d from 150mm to 380 mm:

$$q'_4 = 1.23 - 0.0015 d \quad \text{for } (t - t'_{sh}) \leq 1 \text{ year}, \quad /8.23/$$

$$q'_4 = 1.17 - 0.0015 d \quad \text{for } (t - t'_{sh}) > 1 \text{ year}.$$

or is given by /8.24/ if $d > 380$ mm:

$$q'_4 = 1.2 \exp(-0.00473 \frac{V}{S})$$

/8.24/

where V/S is volume/surface ratio. For the effective thickness d less than 150 mm the value of q'_4 is given by Table 8.4:

Average member thickness	Shrinkage coeff. q'_4
50 mm	1.35
75 mm	1.25
100 mm	1.17
125 mm	1.08
150 mm	1.00

Table 8.4 ACI 78 model, coefficient q'_4 .

Similar to the creep coefficient k'_4 , the preprocessor MATERIAL computes intermediate values using a 4th order spline.

The last coefficient q'_5 accounts for curing times which are different from 7 days. For moist cured concrete, values are given in Table 8.5. For steam curing $q'_5 = 1$ for a period of 1 to 3 days.

Period of moist curing (in days)	Shrinkage age coefficient q'_5
1	1.2
3	1.1
7	1.0
14	0.93
28	0.86
90	0.75

Table 8.5 ACI 78 model, shrinkage age coefficient q'_5 .

In this case it is not possible to use a high order spline approximation and therefore simple linear interpolation is employed.

8.1.2 CEB - FIP 1978 model.

Here the models for creep and shrinkage developed by Comité Européen du Béton (CEB - FIP), 1978 are presented. There are based on the CEB - FIP models from 1970.

Creep function.

The creep function is split into the following additive components (compare with (8.30)):

$$\frac{1}{E_c(t')} = \frac{\beta_1(t')}{E_{c28}} = \text{initial elastic strain (30-60 sec),}$$

/8.25/

$$\frac{\beta_a(t')}{E_{c28}} = \text{fast initial strain in the first day after load application,}$$

$$\frac{\varphi_d \beta_d(t - t')}{E_{c28}} = \text{delayed elastic strain,}$$

and

$$\frac{\varphi_f [\beta_f(t) - \beta_f(t')]}{E_{c28}} = \text{irrecoverable time dependent strain (flow, delayed plastic strain).}$$

The value of the initial deformation modulus $E_c(t')$ is defined using the term corresponding to initial strain only, i.e. at $t' = 28$ days:

$$E_{c28}^{-1} = \Phi(t, t') \text{ where } \Delta t = t - t' \cong 0.5 \cdot 10^{-3} \text{ days.}$$

If experimental results are not available, it is possible to

use the CEB - FIP Model Code which recommends for E_{c28} :

$$E_{c28} = 1.25 * 9500 \sqrt[3]{f_{cm28}} \quad /8.26/$$

where f_{cm28} is cylinder mean compressive strength (in Mpa),
 E_{c28} is initial deformation modulus at $t' = 28$ days
(in MPa),
and 1.25 is coefficient increasing the original
code recommendation by 25% [32].

It is apparent that all entities are based on a loading
time of $t' = 28$ days. For other times /8.27/ can be used:

$$\beta_c(t') = \frac{f_{cm}(t')}{f_{cm\infty}} \quad (\text{see /8.29/}) \quad /8.27/$$

where $f_{cm}(t')$ and $f_{cm\infty}$ are mean cylinder compressive
strengths at time t' and ∞ . If 28-day data is available, then
/8.28/ can be used instead:

$$\beta_1^{-3}(t') = \frac{f_{cm}(t')}{f_{cm28}} \quad /8.28/$$

Similarly for the deformation modulus:

$$\frac{1}{E_c(t')} = \beta_1(t') \frac{1}{E_{c28}} = \sqrt[3]{\beta_c(t')} \frac{1}{E_{c\infty}} \quad /8.29/$$

The nondimensional creep function is of the form:

$$E_{c28} \Phi(t, t') = \beta_1(t') + \beta_a(t') + \varphi_d \beta_d(t - t') + \\
+ \varphi_f [\beta_f(t) - \beta_f(t')] \quad /8.30/$$

Functions $\beta_1(t')$, $\beta_a(t')$, φ_d , $\beta_d(t - t')$, φ_f , $\beta_f(t)$ as well
as $\beta_1(t')$ and $\beta_c(t')$ are given mostly in the form of diagrams in
order to simplify their use. Nevertheless to encourage engineers
to develop computer codes they are also provided in analytical

form (in CEB-FIP) and some authors have also developed their own approximations.

In the following the recommended functions from the appendix of CEB-FIP 1978 are given and these are compared with functions derived by Neville et al. [32].

The adopted notation is as follows:

t = the age of concrete (of our interest) (in days),

t' = the age of load application (in days),

$humid$ = environment humidity (in %),

f_{cyl28} = mean cylindric strength in compression (in MPa)

h_0 = effective (nominal) thickness (in cm).

For numerical comparisons the following data were used:

final time $t = 110$ days,

time at loading $t' = 50$ days,

humidity $humid = 50\%$,

the effective thickness $h_0 = 40$ cm,

compressive strength $f_{cyl28} = 32$ MPa.

It is clear that any comparisons of the presented models can not be based on the one example only. However the numerical evaluations of these expressions provides some verification for their use.

The expressions and their numerical values for the above data are summarized in Table 8.6. From the total result (Table 8.7) it is apparent that differences between them are negligible. The only important difference is the increase of E_{c28} by 25 per cent (see /8.26/) which is recommended in the CEB - FIP Code. Therefore for the sake of compatibility this 25 per cent addition was not used in either model.

CEB - FIP expression:	Neville at al. expression:
$\beta_i(t') = 0.875 \left(\frac{t' + 47}{t'} \right)^{\frac{1}{7.35}}$ $\beta_i(50) = 0.958$	$\beta_i(t') = \left(\frac{4.2 + 0.85 t'}{t'} \right)^{0.5}$ $\beta_i(50) = 0.966$
$\beta_a(t') = 0.8 \left(1 - \frac{t'}{t' + 47} \right)^{\frac{1}{2.45}}$ $\beta_a(50) = 0.189$	$\beta_a(t') = 0.8 \left[1 - \frac{1}{1.276} * \right.$ $\left. * \left(\frac{t'}{4.2 + 0.85 t'} \right)^{\frac{3}{2}} \right]$ $\beta_a(50) = 0.105$
$\varphi_d = 0.4 = \text{const.}$	$\varphi_d = 0.4 = \text{const.}$
$\beta_d(t-t') = \left(\frac{t - t'}{t - t' + 328} \right)^{\frac{1}{4.2}}$ $\beta_d(60) = 0.641$	$\beta_d(t-t') = 0.73 \left(1 - \right.$ $\left. - \exp[-0.01(t-t')] \right) + 0.27$ $\beta_d(60) = 0.599$
$\varphi_f = \varphi_{f1} \varphi_{f2}$	$\varphi_f = \varphi_{f1} \varphi_{f2}$
$\varphi_{f1}(\text{humid}) = 4.45 - 0.035 \text{ humid}$ $\varphi_{f1}(50) = 2.7$	$\varphi_{f1}(\text{humid}) \dots \text{ see table 12.2}$ in ref. [100] $\varphi_{f1}(50) = 2.66$

Table 8.6 Expressions for CEB-FIP model for creep predictions.

$\varphi_{f2}(h_0) = \exp \left[4.4 \cdot 10^{-5} h_0 - \frac{0.357}{h_0} - \ln \left(\frac{h_0^{0.1667}}{2.6} \right) \right]$ $\varphi_{f2}(40) = 1.3957$	$\varphi_{f2}(h_0) \dots \text{ see diagram 12.}$ <p style="text-align: right;">in ref. [100]</p> $\varphi_{f2}(40) = 1.4$
$\beta_f(t, h_0) = \left(\frac{t}{t + K_1(h_0)} \right)^{K_2(h_0)}$ $K_1(h_0) = \exp \left[\frac{5.02}{h_0} + \ln(6.95 h_0^{1.25}) \right]$ $K_2(h_0) = \exp \left[0.00144 h_0 - \frac{1.1}{h_0} - \ln \left(1.005 h_0^{0.2954} \right) \right]$ $\beta_f(110, 40) = 0.4837$ $\beta_f(50, 40) = 0.377$	$\beta_f(t, h_0) = \left(\frac{t}{t + H_f} \right)^{\frac{1}{3}} - \left(\frac{t'}{t' + H_f} \right)^{\frac{1}{3}}$ $H_f(h_0) \dots \text{ see table 12.3}$ <p style="text-align: right;">in ref. [32]</p> $\beta_f(110, 40) = 0.482$ $\beta_f(50, 40) = 0.379$

Table 8.6 Expressions for CEB-FIP model for creep predictions (cont.).

<u>CEB - FIP results</u>	<u>Neville at al. results</u>
$E_{c28} = 37.7 \text{ GPa}$	$E_{c28} = 37.7 \text{ GPa}$
$\Phi(110, 50) = 0.487 \cdot 10^{-7}$	$\Phi(110, 50) = 0.449 \cdot 10^{-7}$
$f_{cyl}(50) = 36.39 \text{ MPa}$	$f_{cyl}(50) = 35.43 \text{ MPa}$

Table 8.7 Comparison of total results of creep prediction using CEB - FIP approximation expressions and Neville at al. functions.

Shrinkage.

In the following the CEB-FIP 1978 expressions for shrinkage evaluation are given. As in the case of creep the expressions are also presented both in the form of diagrams and as analytical approximations.

They are given in Table 8.8 simultaneously with Neville at al's. approximate functions [32]. To compare both sets, numerical results for a particular example have also been computed and are included in Table 8.8. This data is the same as that used for creep prediction with the addition of $t'_{sh} = 7$ days (time at which drying starts):

The strain due to shrinkage which occurs in a time interval of $(t - t'_{sh})$ is given by:

$$\epsilon_{sh}(t, t'_{sh}) = \epsilon_{sh,0}(humid, h_0) [\beta_{sh}(t, h_0) - \beta_{sh}(t'_{sh}, h_0)]$$

/8.31/

where t is the age of concrete,

t'_{sh} is the time when the drying started,

$\epsilon_{sh,0}$ = basic shrinkage,

β_{sh} is the function for the development of shrinkage.

CEB - FIP expressions	Neville expressions
$K_3(h_0) = 11.8 h_0 + 16$ $K_4(h_0) = \exp\left[0.00257h_0 - \frac{0.32}{h_0} + \ln\left(0.22 h_0^{0.4}\right)\right]$	not used
$\epsilon_{sh}(t, t') = \epsilon_{sh1}(humid) \epsilon_{sh2}(h_0)$	$\epsilon_{sh}(t, t') = \epsilon_{sh1}(humid) * \epsilon_{sh2}(h_0)$
$\epsilon_{sh1}(humid) = (0.00075 humid^3 - 0.156 * humid^2 + 11.0325 humid - 303.25) 10^{-5}$ $\epsilon_{sh1}(50) = -460 10^{-6}$	$\epsilon_{sh1}(humid) \dots \text{see table 12.2 in ref. [100]}$ $\epsilon_{sh1}(50) = -453 10^{-6}$
$\epsilon_{sh2}(h_0) = \exp\left[0.00174 h_0 - \frac{0.32}{h_0} - \ln\left(\frac{h_0^{0.254}}{1.9}\right)\right]$ $\epsilon_{sh2}(50) = 0.7917$	$\epsilon_{sh2}(h_0) \dots \text{see table 12.5 in ref. [100]}$ $\epsilon_{sh2}(50) = 0.80$
$\beta_{sh}(t) = \left(\frac{t}{t + K_3(h_0)}\right)^{K_4(h_0)}$ $\beta_{sh}(110, 40) = 0.227$ $\beta_{sh}(7, 40) = 0.024$	$\beta_{sh}(t) \dots \text{see figure 12.5 in ref. [100]}$ $\beta_{sh}(110, 40) = 0.26$ $\beta_{sh}(7, 40) = 0.04$
<p>Total shrinkage:</p> $\epsilon_{sh}(110, 7) = -7.47 10^{-5}$	<p>Total shrinkage:</p> $\epsilon_{sh}(110, 7) = -7.97 10^{-5}$

Table 8.8 Expressions for CEB-FIP model for shrinkage predictions

8.1.3 Bazant and Panula's model II, 1978.

In the following the Bazant and Panula's model [32] for creep and shrinkage prediction is given. All expressions are provided in brief form and the reader is referred to the original source for more details. It should be noted that Bazant and Panula have also developed a more accurate version of this model which accounts better for temperature influence, method of curing etc. [33], [48]. Nevertheless the present model is often used, has a good reputation and requires only two material properties, the mean compressive strength $f_{cm}(t')$ and the concrete unit weight ρ .

Shrinkage.

The general expression to compute shrinkage in the time interval t'_{sh} to t is:

$$\varepsilon_{sh}(t, t'_{sh}) = k_1 \varepsilon_{sh, \infty} \left(\frac{(t - t'_{sh})}{t_{(1/2)sh} + (t - t'_{sh})} \right)^{\frac{1}{2}} \quad /8.32/$$

where t is the age of concrete (in days),

t'_{sh} is the age at beginning of drying (in days).

The coefficient k_1 is a function of the ambient relative humidity h (in %) and is defined by:

$$k_1 = 1 - 10^{-6} h^3 \quad \text{for } h \leq 98\%, \quad /8.33/$$

$$k_1 = -0.2 \quad \text{for } h = 100\%.$$

The interval $98\% < h < 100\%$ is not covered in ref [32] and thus linear interpolation was used.

The ultimate shrinkage $\varepsilon_{sh, \infty}$ is related to the mix parame-

ters by the following expressions:

$$\varepsilon_{sh,\infty} = 1330 - 970 y$$

$$y = (390 z^{-4} + 1)^{-1}$$

$$z = 0.381 \sqrt{f_{cy128}} \left[1.25 \sqrt{\frac{a}{\gamma}} + 0.5 \left(\frac{g}{s} \right) \right] \left[\frac{1 + \frac{s}{\gamma}}{\frac{w}{\gamma}} \right]^{\frac{1}{3}} - 12$$

and:

/8.34/

$$z \geq 0$$

In the above expression:

$\frac{a}{\gamma}$ is the ratio total aggregate / cement,

$\frac{g}{s}$ is the fine aggregate / cement ratio,

$\frac{w}{\gamma}$ is the water / cement ratio.

All ratios are proportional by weight and the 28 day cylinder strength in compression f_{cy128} is in MPa. The fine aggregate is assumed to be aggregate of maximum size 4.77 mm, the rest is coarse.

The value of $t_{(1/2)sh}$ is defined by

$$t_{(1/2)sh} = 4 \left(k' \frac{V}{S} \right)^2 \frac{1}{D(t'_{sh})} \quad /8.35/$$

where $\frac{V}{S}$ is volume/surface ratio in mm,

k' is the shape factor = 1. for a slab,
 = 1.15 for a cylinder
 = 1.25 for a square prism,
 = 1.3 for a sphere,
 = 1.55 for a cube.

$D(t'_{sh})$ is drying diffusivity defined by:

$$D(t'_{sh}) = 2.4 + \frac{120}{\sqrt{t'_{sh}}} \quad /8.36/$$

Creep.

The total creep is considered separately from basic creep by introducing a drying creep term in the creep function. The basic creep is a function of elastic strain and the basic creep strain caused by unit stress applied at time t' and measured at time t :

$$\Phi_b(t, t') = \frac{1}{E'} [1 + \phi'_b(t, t')] \quad /8.37/$$

where $\Phi_b(t, t')$ is the basic creep function (in GPa^{-1}) and

$$\phi'_b(t, t') = B [(t')^{-m} + 0.05] (t - t')^n \quad /8.38/$$

The parameters E' , m , n and B are all functions of 28 - day strength:

$$E' = \left(0.01306 + 3.203 \frac{1}{\sqrt{f_{\text{cyl28}}}} \right)^{-1} \quad (\text{in GPa}) \quad /8.39/$$

$$B = 0.3 + 152.2 f_{\text{cyl28}}^{-1.2} \quad /8.40/$$

$$m = 0.28 + 47.54 f_{\text{cyl28}}^{-2} \quad /8.41/$$

$$n = 0.115 + 0.183 \cdot 10^{-6} f_{\text{cyl28}}^{3.4} \quad /8.42/$$

where f_{cyl28} is in MPa.

The static modulus at time t' can be calculated using /8.39/ through /8.42/:

$$E_c(t') = \left\{ \frac{1}{E'} [1 + B [t'^{-m} + 0.05) 10^{-n}] \right\}^{-1} \quad /8.43/$$

The total creep function $\Phi(t, t')$ in GPa^{-1} is expressed as follows:

$$\Phi(t, t') = \Phi_b(t, t') + \frac{\phi'_d(t, t', t'_{sh})}{E'} \quad /8.44/$$

where $\Phi_b(t, t')$ is the basic creep function /8.37/ and the drying creep coefficient $\phi'_d(t, t', t'_{sh})$ is given by the following equation:

$$\phi'_d(t, t', t'_{sh}) = B'_d k'_1 (t')^{-\frac{m}{2}} \left(1 + \frac{3 t_{(1/2)sh}}{t - t'} \right)^{-0.35} \quad /8.45/$$

$$B'_d = \left(1 + \frac{t - t'_{sh}}{10 t_{(1/2)sh}} \right)^{-\frac{1}{2}} B_d \epsilon_{sh\infty} \quad /8.46/$$

$$B_d = 0.0056 + \frac{0.0189}{1 + 0.7r^{-1.4}} \quad /8.47/$$

$$r = 0.56 \left[\left(\frac{s}{a} \right) f_{cyl28} \right]^{0.3} \left(\frac{g}{s} \right)^{1.3} \left[1610 \frac{\left(\frac{w}{\gamma} \right)}{\epsilon_{sh, \infty}} \right]^{1.5} - 0.85 \quad /8.48/$$

If $r \leq 0$, then $B_d = 0.0056$. Finally

$$k'_1 = 1 - 10^{-3} h^{1.5} \quad /8.49/$$

where h is again the relative ambient humidity (in %).

It should be noted that for all expressions of this model the time t' is assumed to be greater than time t'_{sh} . The opposite case is not covered by this method.

It is emphasized that the aim of Sections 8.1.1 to 8.1.3 was not to study the problem of creating the creep and shrinkage functions. This is beyond the scope of this work. The main interest is on the solution procedures of the whole structure, which is the content of the next section.

8.2 Methods of creep and shrinkage analysis.

There are many different methods to account for creep and shrinkage phenomena in an analysis. These range from the simplest in which creep is evaluated by decreasing Young's modulus only and shrinkage is neglected, to very sophisticated nonlinear methods, which account for nonlinear aging of concrete, the whole loading history of the structure etc. To the author's knowledge all methods used in practice assume that within an infinitesimal increment creep and stresses vary linearly and obey Boltzmann's principle of superposition. More advanced methods are rarely used for real structures due to their complexity.

The principle of superposition means that the total strain of concrete at time t subjected to varying stress is calculated by summing the strain caused by each stress increment (or decrement), $\Delta\sigma(t')$ applied at t' . Or in other words the strain increments due to stress increments applied at time t' is quite independent on the stress history in times $t < t'$.

Mathematically this can be written:

$$\varepsilon(t) = \sum_t^t \Delta\sigma(t') \Phi(t, t') \quad /8.50/$$

For the case of a variable stress history it is necessary to replace the sum operator in /8.50/ by an integral operator:

$$\varepsilon(t) = \int_t^t \Phi(t, t') \frac{\partial\sigma}{\partial\tau'} d\tau' \quad /8.51/$$

The integral /8.51/ is sometimes called Stieltejs integral and incorporates the general assumption for all methods, which will be discussed later. It greatly simplifies the problem of creep and shrinkage analysis and based on experimental evidence the inaccuracy due to its use is negligible.

8.2.1 Effective modulus method (EM method).

The EM method is one of the simplest methods and

incorporates creep in an analysis by an appropriate reduction of Young's modulus. Hence instead of using a current modulus at the time of loading t' , a so called effective modulus is used, given by:

$$E_{\text{eff}} = \frac{E(t')}{1 + \phi(t, t')} = \frac{E(t')}{\Phi(t, t')} \quad /8.52/$$

This method gives good results if the stress does not vary very much. This is due to the fact that for all stress histories only one creep function $\Phi(t, t')$ is used which is defined with respect to time t' , i.e. the time to the first loading. For later loading creep is underestimated.

Despite this deficiency the method is still extensively used because of its simplicity and because of the fact that it is adopted in many codes for the analysis of reinforced concrete structures.

Shrinkage is incorporated in the analysis in the form of initial strains with values equal to the total shrinkage during the time interval $t - t'_{\text{sh}}$, i.e. the period of concrete drying. This is of course also a very simplified approach which can be adopted only in linear analysis (i.e. when the stiffness of the structure is assumed independent of load and deformation level).

8.2.2 Rate of creep method (RC method).

The basic assumption of this method is that the rate of creep is independent of time t' when the load is applied. This method was first presented by Glanville [35] and Whitney [36] but its real practical implementation to structural problems was done by Dischinger [37]. Mathematically the basic idea of RC method can be written:

$$\frac{d\varepsilon}{dt} = \frac{\sigma(t)}{E(t')} \frac{d\phi}{dt} + \frac{1}{E(t)} \frac{d\sigma}{dt} + \frac{d\varepsilon_{\text{sh}}}{dt} \quad /8.53/$$

The assumption of creep rate independence of time t' leads to an affinity of creep curves (see Fig. 8.1) which is contrary

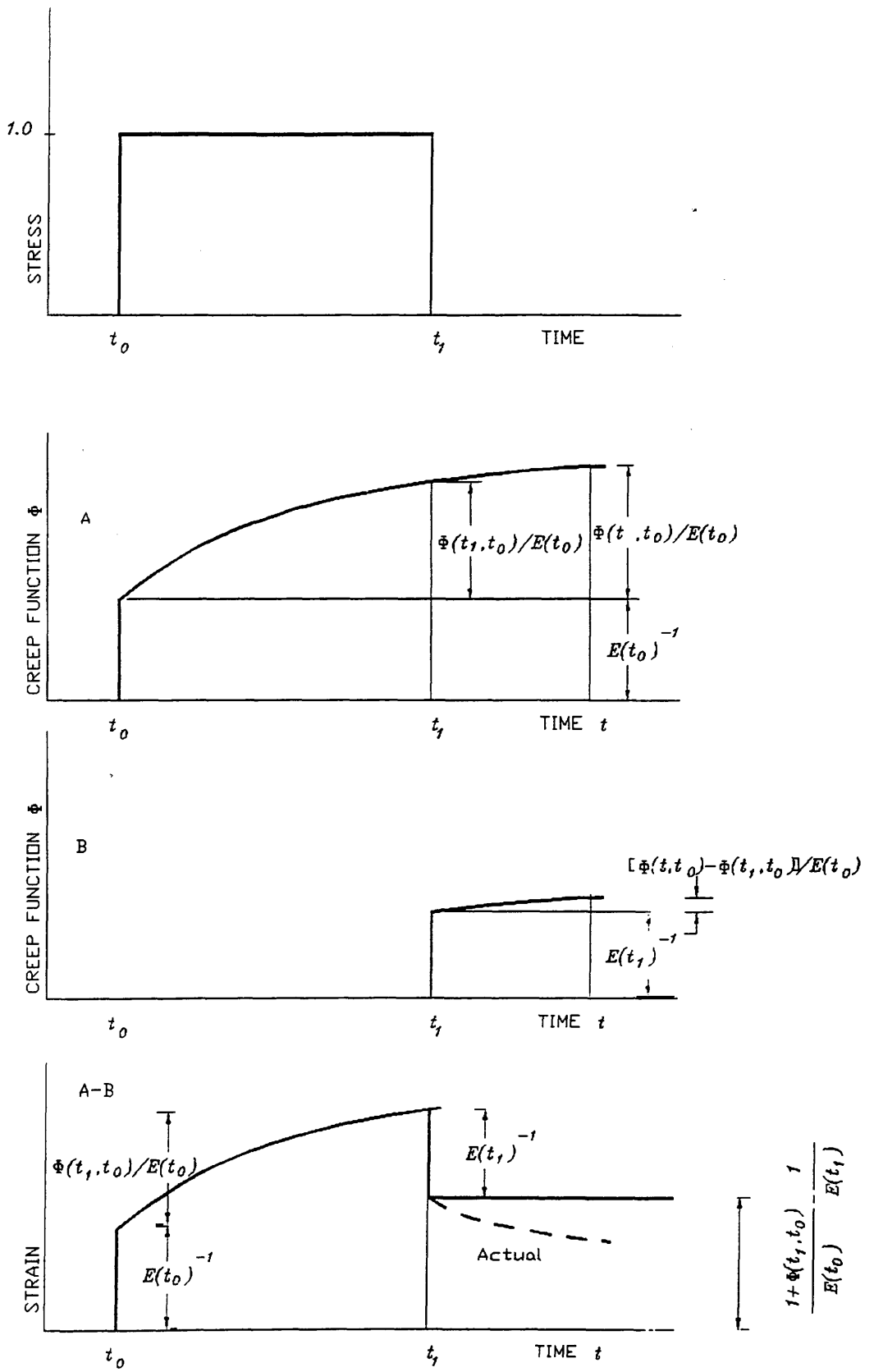


Fig. 8.1 RC method.

to experimental evidence. It causes an overestimation or underestimation of creep if the load decreases or increases later on.

8.2.3 Rate of flow method (RF method).

The essential assumption in this method is that the total strain at time t is composed from the elastic strain, the recoverable delayed elastic strain and from irrecoverable strain flow. It was justified by the experimental evidence that the delayed elastic strain is independent of time of loading t' . Strain flow is treated similarly to the RC method.

The results based on RF method are better than in case of RC method, but the use of a constant creep curve for strain flow is in contradiction to experimental results and the nature of the problem itself. The strain-time relation is depicted in Fig. 8.2.

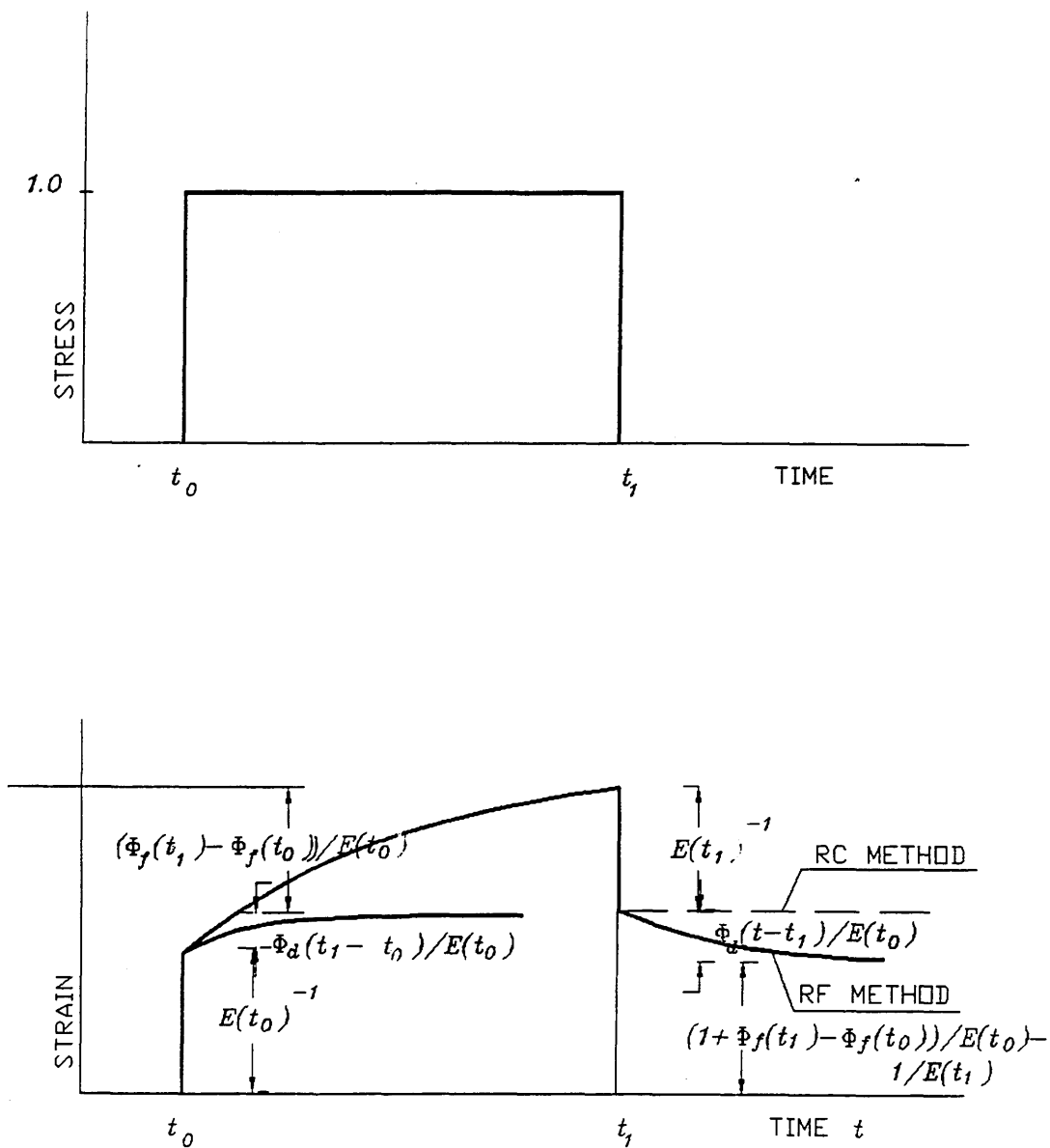


Fig. 8.2 RF method.

8.2.4 Improved Dischinger method (ID method).

This method is very similar to RF method. The only difference is that the elastic and delayed elastic strains from RF method are treated as one term. This simplification can be adopted because the time which is necessary for all the delayed

elastic strain to occur is much smaller than the time which is necessary for the total strain flow to occur (which is in fact infinite). Hence the creep function can be written:

$$\phi(t, t') = \frac{1}{E_d} + \frac{\phi_f(t) - \phi_f(t')}{E(t')} \quad /8.54/$$

where E_d is defined by:

$$E_d = E(t') / (1 + \phi_d) \quad /8.55/$$

The term E_d serves as a secant Young's modulus for the structure at the age when both elastic strain parts occurred. Hence it is not a suitable modulus for calculating the immediate response of the structure after applying the loading. For ϕ_d the value 1/3 is recommended [33] and hence $E_d = 0.75 E(t')$.

Although the above assumption does not provide accurate results for the case of very small $(t - t')$, the ID method was adopted in the CEB - FIP 1978 code for $(t - t') >$ three months and the results are good.

The ID method is very simple and can be understood as a hybrid of the EM and RC methods. Adjusting the time of loading t' to 28 days, the mathematical equation for strain - stress relation has the form:

$$\frac{d\varepsilon}{dt} = \frac{\sigma(t)}{E_{28}} \frac{d\phi_f}{dt} + \frac{1 + \phi_d}{E_{28}} \frac{d\sigma}{dt} + \frac{d\varepsilon_{sh}}{dt} \quad /8.56/$$

The strain - time relationship for this method is depicted in Fig. 8.3.

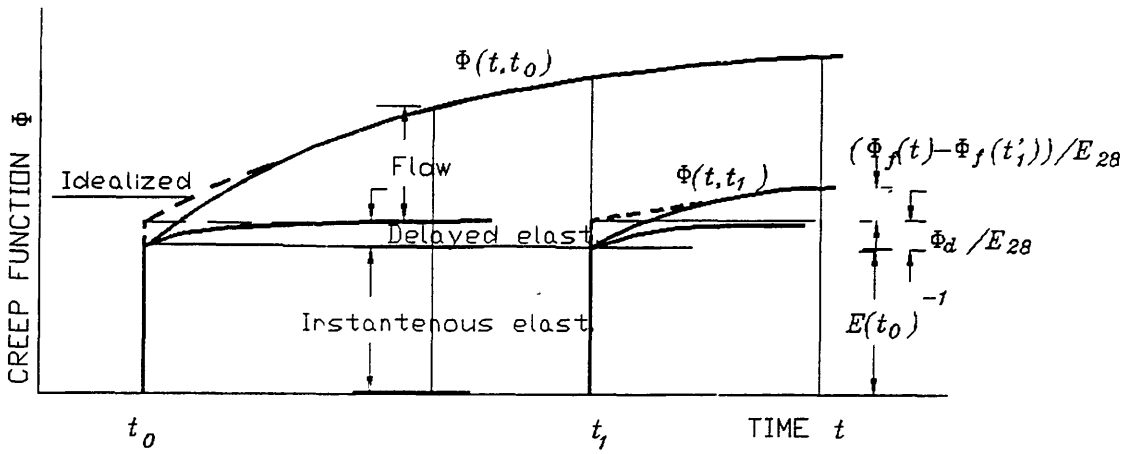


Fig. 8.3 ID method.

8.2.5. Rheological models (RM method).

To date many different types of rheological models have been developed and this is still a popular way of modeling concrete creep. Unfortunately this is not due to their excellent properties but because of their simplicity. Some these models are based purely on mathematical fitting of experimental data, the others are designed to reflect directly the processes in concrete. Nevertheless the final results are identical.

The common feature of all rheological models is that they consist only of spring and dashpot elements connected in parallel or series.

The essential definition of a spring element is that:

$$d\sigma = k d\varepsilon$$

while for a dashpot element:

$$d\sigma = \nu d\left(\frac{\partial\varepsilon}{\partial t}\right)$$

In other words, the spring element stress increment is dependent on the strain increment and the dashpot stress increment is dependent on the rate of strain increment. Both types can be either linear, i.e. $k = \text{const.}$ and $\nu = \text{const.}$ or

nonlinear, in which case the value of k and ν depends on particular values of strain and rates of strain in the element.

It can be proved that any combination of springs and dashpots can be replaced by groups of parallel springs and dashpots connected in series (Maxwell chains) or by a series of parallel connected groups consisting of serial springs and dashpots (Kelvin chains). Hence the comment about identical results in the above paragraph.

One of the most successful of these models for the prediction of creep in concrete was designed by Burger [33]. The model is schematically depicted in Fig. 8.4 and its analytical representation is given by:

$$\Phi(t, t') = \frac{1}{E(t')} + [f_3(t) - f_3(t')] + A(t') \left[1 - \exp\left(-\frac{t-t'}{h(t')}\right) \right]$$

/8.57/

where $f_3(t)$ represents the irreversible creep of a dashpot at time t and parameters $A(t')$ and $h(t')$ apply to the Kelvin unit (see Fig 8.4). If we want to account for the effect of temperature and humidity, it is necessary to correct accordingly the irreversible part of /8.57/ (the second term) by introducing a function $\psi(T)$ for temperature and a function $\rho(H)$ for humidity. The delayed elastic part is not affected (the third term of /8.57/).

More information about this model and additional simplifications are given in [33], where the final expressions are also presented. These can be solved easily using Laplace transformation.

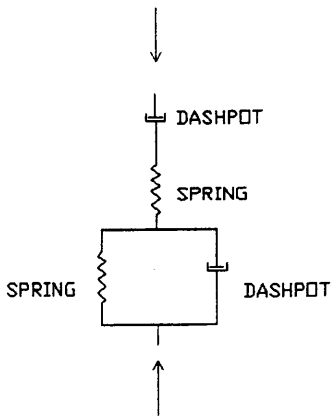


Fig. 8.4. Burger's model.

8.2.6 Step by step method.

This method is actually completely general. It can deal with any type of creep function and any prescribed history of stress and strain. It is based on the principle of superposition or mathematically on Stieltjes integral (see Fig. 8.5):

$$\epsilon(t) - \epsilon^0(t) = \int_0^t \phi(t, t') d\sigma(t') \quad /8.58/$$

where $\epsilon^0(t)$ are initial strains at time $t=0$.

As stated before the practical consequence of this assumption is that strain produced at any time t by a stress increment applied at time $t' < t$ is independent of the effect of any stress applied earlier or later.

Contrary to the previous methods here it is possible to use creep curves of general shape. The accuracy of results depend on the accuracy of the numerical integration scheme of /8.58./ and on the accuracy of the creep and shrinkage model.

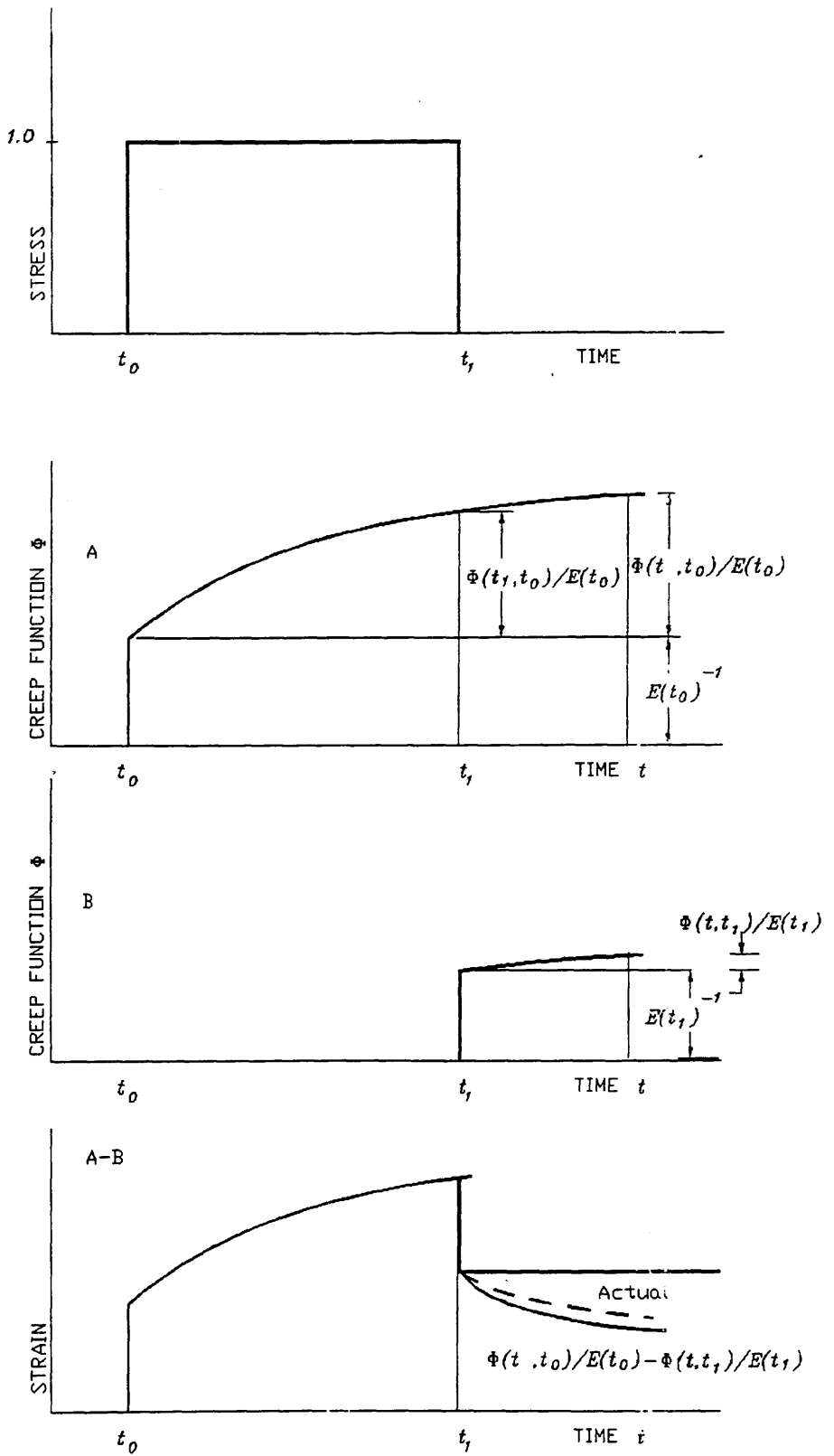


Fig. 8.5 Superposition of virgin creep curves.

Rewriting equation /8.58/ for the case when initial strains are zero we obtain:

$$\varepsilon(t) = \frac{\sigma_0}{E(t')} [1 + \phi(t, t')] + \int_{t'}^t \Phi(t, \tau) d\sigma(\tau) \quad /8.59/$$

where t is the time of our interest (the age of structure),
 t' is the time from which variable loading is applied,
 ϕ , and Φ are functions defining creep,
 $E(t')$ is Young's modulus at t' .
 σ_0 is stress at time t' .

Note that $(1 + \phi(t, t')) = \Phi(t, t')$ and that the term $\frac{\sigma_0}{E(t')} [1 + \phi(t, t')]$ represents the strain at time t due to loading at t' . The second term of /8.59/ accounts for strain changes due to subsequent stress history (i.e. time from t' to t).

Closed integration of /8.59/ is not possible and therefore numerical integration is used. The time t' through t is divided into a number of time intervals and there are several methods which can be used to integrate /8.59/. This problem is addressed in Section 8.3 where description of the step-by-step solution scheme using a recursive formulation is given.

The step by step method will be now briefly presented. The notation used is presented in Fig. 8.6.

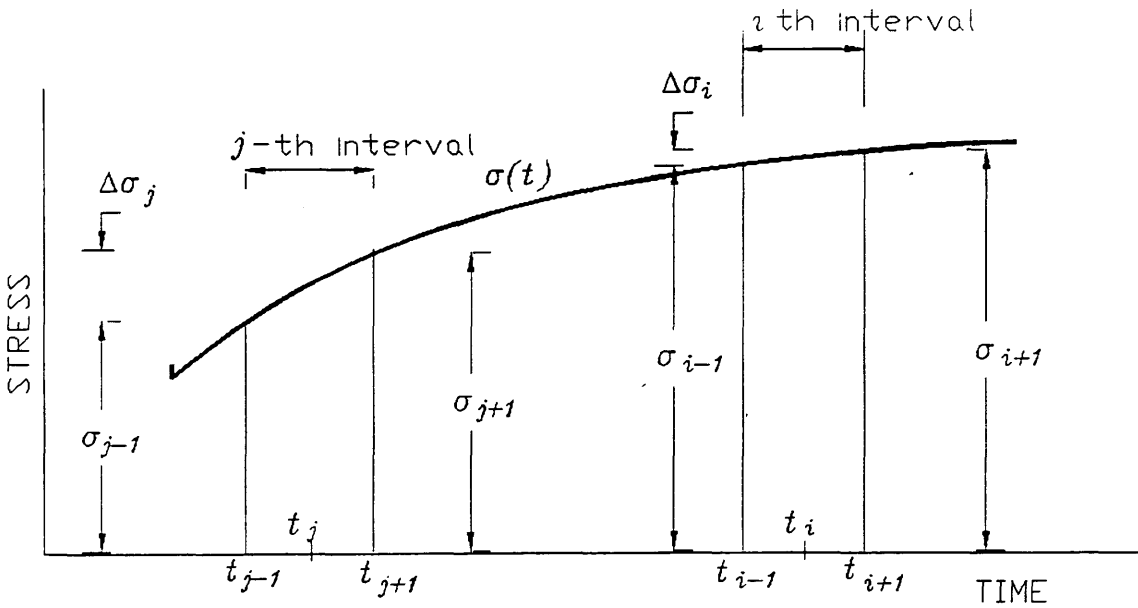


Fig 8.6 Notation adopted in step-by-step procedure.

Using a trapezoidal integration scheme the second term of equation /8.59/ can be written in the form (at the end of j -th interval due to $\Delta\sigma_j$):

$$\Delta\varepsilon_j(t_{j+1}) = \Delta\sigma(t_{j+1}, t_j) \Phi(t_{j+1}, t_j) = \frac{\Delta\sigma_j}{E(t_j)} [1 + \phi(t_{j+1}, t_j)]$$

/8.60/

For time t_{i+1} (i.e. interval i) the strain due to $\Delta\sigma_j$ is:

$$\Delta\varepsilon_j(t_{i+1}) = \Delta\sigma(t_{j+1}, t_j) \Phi(t_{i+1}, t_j) = \frac{\Delta\sigma_j}{E(t_j)} [1 + \phi(t_{i+1}, t_j)]$$

/8.61/

The total strains at time t_{i+1} can be calculated by summing all $\Delta\varepsilon_j(t_{i+1})$ corresponding to all stress changes $\Delta\sigma_j$ ($j \leq i$).

$$\varepsilon(t_{i+1}) = \sum_{j=1}^i \Delta\varepsilon_j(t_{i+1}) = \sum_{j=1}^i \left\{ \frac{\Delta\sigma_j}{E(t_j)} [1 + \phi(t_{i+1}, t_j)] \right\}$$

/8.62/

or using abbreviated notation:

$$\varepsilon_{i+1} = \sum_{j=1}^i \Delta\varepsilon_j = \sum_{j=1}^i \left\{ \frac{\Delta\sigma_j}{E_j} [1 + \phi_{ij}] \right\} \quad /8.63/$$

Note that $\phi_{ij} = \phi(t_{i+1}, t_j)$. Equations /8.60/ to /8.63/ are used to compute the stress at time $i+1$. Thus:

$$\Delta\varepsilon_j = \frac{\sigma_{i+1} - \sigma_{i-1}}{E_i} [1 + \phi_{ii}] + \sum_{j=1}^{i-1} \frac{\sigma_{j+1} - \sigma_{j-1}}{E_j} [1 + \phi_{ij}] \quad /8.64/$$

and after some rearranging the final expression for stress σ at the end of interval i is obtained as:

$$\sigma_{i+1} = \sigma_{i-1} + \frac{E_i}{1 + \phi_{ii}} \left(\sum_{j=1}^i \Delta\varepsilon_j - \sum_{j=1}^{i-1} (\sigma_{j+1} - \sigma_{j-1}) \frac{1 + \phi_{ij}}{E_j} \right) \quad /8.65/$$

It should be noted that $\Delta\varepsilon_j$ contains all strain changes, i.e. it also accounts for shrinkage, swelling etc.

As already pointed out, the method is quite general and this is its important advantage. However to compute stresses σ_{i+1} it is necessary to store the complete previous stress and strain history. This drawback is avoided by using a creep function in the form of a degenerated kernel discussed in Section 8.3.

8.2.7 The Trost - Bazant method (TB method).

The Trost - Bazant method is a practical tool which enables an engineer to obtain a direct solution of strain for variable stress history. It can be computed manually (i.e. without computer support, which is necessary for the previous method) using only some pre-prepared graphs. It introduces the concept of an

aging coefficient χ to account for the time factor.

The sense of coefficient χ can be explained if we write the equation for the total strain at time t as:

$$\varepsilon(t) = \frac{\sigma_0}{E(t')} [1 + \phi(t, t')] + \int_{t'}^t \Phi(t, \tau) / E(\tau) d\sigma(\tau) \quad /8.66/$$

The stress differential can be computed by:

$$d\sigma = \frac{\partial \sigma}{\partial \tau} d\tau \quad /8.67/$$

and hence

$$\Delta\sigma(t) = \int_{t'}^t \frac{\partial \sigma}{\partial \tau} d\tau = \sigma(t) - \sigma(t') \quad /8.68/$$

where t , t' are again the age of concrete and the time at first loading.

Substituting /8.68/ into /8.66/ we obtain the final equation for evaluation of strains at time t :

$$\varepsilon(t) = \frac{\sigma_0}{E(t')} [1 + \phi(t, t')] \frac{\sigma(t) - \sigma(t')}{E(t')} [1 + \chi(t, t')\phi(t, t')] \quad /8.69/$$

where $\chi(t, t')$ is the aging coefficient which accounts for aging on the ultimate value of creep for stress increments or decrements occurring gradually after the application of the original load.

The main problem using the Trost-Bazant method is, of course, the evaluation of the aging coefficients. An exact mathematical expression can be found by comparing /8.66/ and /8.69/. These were first calculated by Trost using the assumption that the strain variation is affine to the creep-time function. Later Bazant recalculated them using the assumption that they vary according to a relaxation function.

For relaxation, $\varepsilon(t)$ is constant and equal to $\frac{\sigma(t')}{E(t')}$ and we can write:

$$\chi(t, t') = \frac{\sigma(t')}{\sigma(t') - \sigma(t)} - \frac{1}{\phi(t, t')} \quad /8.70/$$

or for unit stress:

$$\chi(t, t') = \frac{E(t')}{E(t') - E(t)} - \frac{1}{\phi(t, t')} \quad /8.71/$$

The aging coefficient must be defined for all combinations of loading, the age of concrete, environmental condition, structural shape etc. and this is the biggest drawback of the method. The only small simplification possible is not to create $\chi(t, t')$ for every structural thickness because it was found that they vary little with the thickness.

This method is quite well established in practice and χ coefficients are provided for all material models described in Section 8.1.1 to 8.1.3.

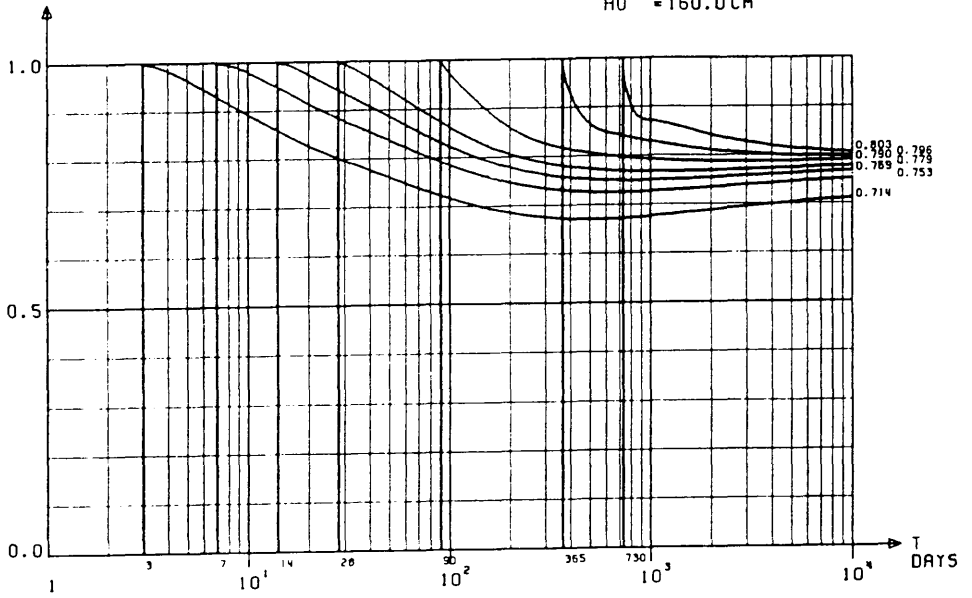
As an example, the diagrams for $\chi(t, t')$ provided in CEB - FIP 1978 are illustrated in Fig. 8.7 [31].

AGING COEFFICIENT $\chi(t, t_0)$

FF1 = 3.00

EPFL-CEBAP
JULIN 1978/79

HO = 160.0 CM



AGING COEFFICIENT $\chi(t, t_0)$

FF1 = 1.00

EPFL-CEBAP
JULIN 1978/79

HO = 20.0 CM

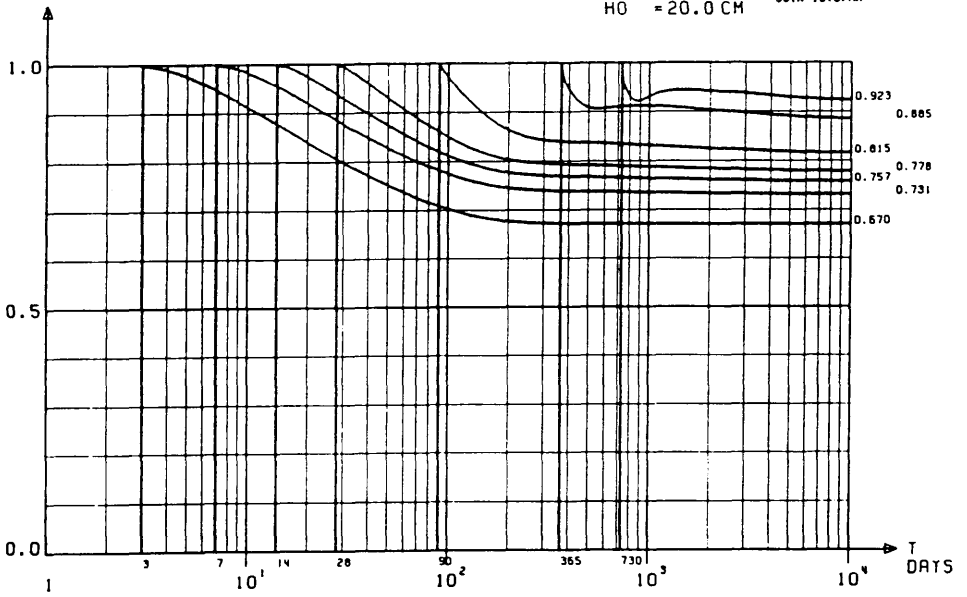


Fig. 8.7 Examples of $\chi(t, t')$ diagram (CEB - FIP).

8.3 Step-by-step procedure using Dirichlet series creep function.

Finally the most powerful method of creep and shrinkage analysis is presented. It is a modification of the previously discussed Step-by-step method but requires much less computer storage than its original formulation. As already mentioned, this method is a completely general solution procedure allowing any shape of creep and shrinkage functions. Its main disadvantage, i.e. its relatively high complexity, is not now such a limiting factor as it is possible to use very efficient computer techniques.

The above properties are the reason why this solution method is nowadays becoming more popular and some of the earlier widely used schemes, as discussed in previous sections are gradually being superceded. This is also the reason why this method has been chosen for further investigation in the present work.

The main drawback of the original version of Step-by-step method is the necessity to store the whole stress and strain history of the structure. Supposing the real structure is discretized by the Finite element method and requires about twenty time intervals, it is not difficult to realize that this is excessive even for modern computers. (It would be necessary to analyze twenty structures together).

To avoid this Bazant [38] developed a new procedure which preserves all the generality of the original Step-by-step procedure but at the same time reduces very significantly the demands on data storage.

In fact the complete strain and stress history of the structure is replaced by several "internal" variables from the previous time step. The key to this drastic improvement is the approximation of the original form of the creep function by a Dirichlet series creep function.

Some time after the method was published it appeared that although theoretically everything works perfectly, in practice it is not so easy. The main difficulty is the numerical stability of the integration of Stieltjes integral and also the approximation of the arbitrary creep function by Dirichlet series itself. Ba-

zant [38] commented that '... a good numerical approximation of the integral ... with regard to the exponential term is imperative.' In some later work [33], [34] he made some suggestions but nevertheless the problem remained open ..

The main objective of this section is first, to describe the Step-by-step method using the approximation by the Dirichlet series and, second, to deal with the numerical difficulties of this procedure. In addition, the original formulation for linear short-term constitutive equations is extended to fully nonlinear solutions. However it should be noted at this point that although geometric and short-term constitutive equations are incorporated in nonlinear form, the implementation of the aging creep law itself still remains linear, as apparent from Stieltjes integral /8.73/ and the creep models (see Section 8.1). This restricts the use of this method to serviceability conditions only.

The practical use of this method, particularly its combination with geometric and material nonlinearities, is presented in Chapter 9, where also various solution parameters and other aspects are discussed.

The essential idea of the method is the approximation of the creep function by a Dirichlet series of the form:

$$\Phi(t, t') = \frac{1}{E(t')} + \sum_{\mu=1}^n \frac{1}{E'_{\mu}(t')} \left(1 - \exp\left[-\frac{t - t'}{\tau_{\mu}}\right] \right)$$

/8.72/

where τ_{μ} are so called retardation constants,

$E'_{\mu}(t')$ are constants of the Dirichlet series (in dimension of stress unit),

$E(t')$ is the instantaneous elastic modulus ($=\Phi(t', t')$).

Inserting the creep function /8.72/ into Stieltjes integral and extending to 3D conditions:

$$\underline{\varepsilon}(t) = \int_{t'}^t \Phi(t, \tau) \mathbf{B}(\underline{\sigma}) \frac{\partial \underline{\sigma}}{\partial \tau} d\tau \quad /8.73/$$

leads, after some rearranging, to:

$$\begin{aligned} \underline{\varepsilon}(t) = \int_{t'}^t \left(\frac{1}{E(\tau)} + \sum_{\mu=1}^n \frac{1}{E'_{\mu}(\tau)} \right) \mathbf{B}(\underline{\sigma}) \frac{\partial \underline{\sigma}}{\partial \tau} d\tau \\ - \sum_{\mu=1}^n \underline{\varepsilon}_{-\mu}^*(t) + \underline{\varepsilon}^0(t) \end{aligned} \quad /8.74/$$

where $\mathbf{B}(\underline{\sigma})$ is a material compliance matrix multiplied by $E(\tau)$, $\underline{\varepsilon}^0(t)$ is a stress independent strain vector comprising shrinkage and thermal dilatation and the $\underline{\varepsilon}_{-\mu}^*(t)$ vector may be viewed as hidden material variables which characterize the past history. These are defined by:

$$\underline{\varepsilon}_{-\mu}^*(t) = \exp\left(-\frac{t}{\tau_{\mu}}\right) \int_{t'}^t \exp\left(\frac{t'}{\tau_{\mu}}\right) \frac{1}{E'_{\mu}(\tau)} \mathbf{B}(\underline{\sigma}) \frac{\partial \underline{\sigma}}{\partial \tau} d\tau \quad /8.75/$$

where $\mu = 1, 2, 3, \dots, n$.

Now, similar to the original step-by-step solution scheme, numerical integration is employed here also. To achieve this, let us divide time t into discrete times $t_0, t_1, t_2, \dots, t_N$ ($t_0 = t', t_N = t$). Note, that the total number is N and not n , the number of retardation times.

The time increment is:

$$\Delta t_r = t_t - t_{r-1} \quad /8.76/$$

The proper setting of times t_r and retardation times τ_{μ} is very important and will be discussed later.

Now assuming that $\frac{1}{E'_{\mu}(\tau)}$ and $\frac{\partial \underline{\sigma}}{\partial \tau} d\tau$ are constant within a time step, equation /8.76/ can be replaced by numerical inte-

gration as follows:

$$\varepsilon_{-\mu}^*(t_r) = \exp\left(-\frac{t_r}{\tau_\mu}\right) \sum_{s=1}^r \frac{1}{E'_{\mu}(t_{s-1/2})} B(\underline{\sigma}) \frac{d\underline{\sigma}(t_{s-1/2})}{dt}$$

$$* \int_{t_{s-1}}^{t_s} \exp\left(-\frac{t'}{\tau_\mu}\right) dt'$$

/8.77/

In the following we will use notation as follows:

Subscript r for time t , i.e. t_r ,

$$\varepsilon_{-\mu_r}^* = \varepsilon_{-\mu}^*(t_r),$$

$$\Delta\sigma_s = \sigma(t_s) - \sigma(t_{s-1}) \text{ and}$$

$s - 1/2$ subscript refers to the average value within interval s , e.g. $E'_{\mu_{s-1/2}} = \frac{1}{2} (E'_{\mu_s} + E'_{\mu_{s-1}})$.

$B_s = B(\underline{\sigma})$ in interval Δt_s , i.e. from σ_{s-1} to σ_s .

This notation is also depicted in Fig. 8.8.

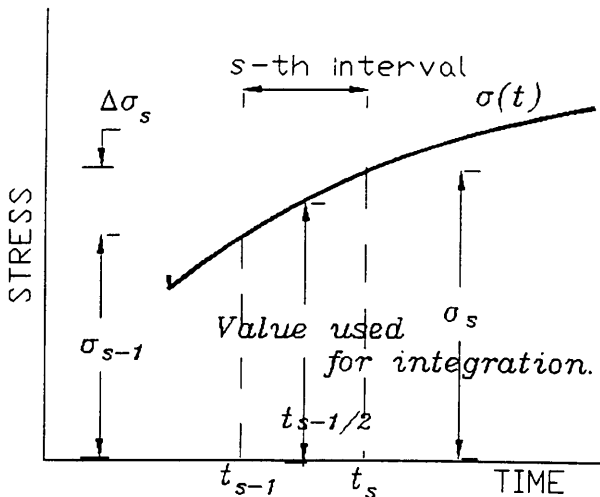


Fig. 8.8 Notation for Step-by-step procedure using Dirichlet series approximation of creep function.

The last term of /8.77/ can be integrated exactly and leads to:

$$\varepsilon_{-\mu_r}^* = \exp\left(-\frac{t_r}{\tau_\mu}\right) \sum_{s=1}^r \frac{\lambda_{\mu_s} \Delta\sigma_{-s}}{E'_{\mu_{s-1/2}}} B_s \exp\left(\frac{t_s}{\tau_\mu}\right) \quad /8.78/$$

The λ_{μ_s} constant can be evaluated using:

$$\lambda_{\mu_s} = \left[1 - \exp\left(-\frac{\Delta t_s}{\tau_\mu}\right) \right] \frac{\tau_\mu}{\Delta t_s} \quad /8.79/$$

The usefulness of the above expression is apparent if we subtract equation /8.78/ written for time t_r , from the same equation written for time t_{r-1} :

$$\varepsilon_{-\mu_r}^* = \exp\left(-\frac{\Delta t_r}{\tau_\mu}\right) \varepsilon_{-\mu_{r-1}}^* + \frac{\lambda_{\mu_r} B_r \Delta\sigma_{-r}}{E'_{\mu_{r-1/2}}} \quad /8.80/$$

where $\mu = 1, 2, \dots, n$.

Hence instead of all the previous stress and strain history of the structure, we need to store only n internal variables from the previous time step ($r - 1$).

Assuming again that $\frac{1}{E'_{\mu}(\tau)}$ and $\frac{\partial\sigma}{\partial\tau} d\tau$ are constant within the time step, equation /8.74/ may be rewritten for time interval r :

$$\Delta\varepsilon_{-r} = \left(\frac{1}{E_{r-1/2}} + \sum_{\mu=1}^n \frac{1}{E'_{\mu_{r-1/2}}} \right) B_r \Delta\sigma_{-r} - \sum_{\mu=1}^n \Delta\varepsilon_{-\mu_r}^* + \Delta\varepsilon_{-r}^0 \quad /8.81/$$

which uses $\Delta \underline{\varepsilon}_{-r} = \underline{\varepsilon}_{-r} - \underline{\varepsilon}_{-r-1}$ and a similar definition for $\Delta \varepsilon_{\mu_r}$.

The final expression of this method is then:

$$\Delta \underline{\varepsilon}_{-r} = \mathbf{B}_r \frac{\Delta \underline{\sigma}_{-r}}{E'_r} + \Delta \underline{\varepsilon}'', \quad /8.82/$$

$$\text{where } \frac{1}{E'_r} = \frac{1}{E_{r-1/2}} + \sum_{\mu=1}^n \frac{1 - \lambda_{\mu_r}}{E'_{\mu_{r-1/2}}} \quad \text{and}$$

$$\Delta \underline{\varepsilon}'', = \sum_{\mu=1}^n \left[1 - \exp\left(-\frac{\Delta t_r}{\tau_{\mu}} \right) \right] \underline{\varepsilon}_{\mu}^*(t_{r-1}) + \Delta \underline{\varepsilon}^0(t_r)$$

The set of equations /8.80/, /8.82/ and /8.79/ represent the complete definition of the method. The algorithm can be relatively simply incorporated into finite element programs because it is necessary only to repeat an ordinary analysis for every time interval and to call quite independent routines to calculate the "current" material modulus E'_r and initial strain $\Delta \underline{\varepsilon}''$ before and after each interval.

In most nonlinear finite element software, matrix \mathbf{B} is not available. Either the material rigidity matrix is used or constitutive relationships are evaluated directly. This causes no problem in equation /8.82/ because it is used in its inverse form; however difficulties arise in calculating the $\mathbf{B}_r \Delta \underline{\sigma}_{-r}$ term in equation /8.80/. The simplest solution is to modify equation /8.80/ using equation /8.82/ as follows:

$$\underline{\varepsilon}_{\mu_r}^* = \exp\left(-\frac{\Delta t_r}{\tau_{\mu}} \right) \underline{\varepsilon}_{\mu_{r-1}}^* + \frac{E'_r (\Delta \underline{\varepsilon}_{-r} - \Delta \underline{\varepsilon}'') \lambda_{\mu_r}}{E'_{\mu_{r-1/2}}} \quad /8.80' /$$

This is conveniently evaluated because the strain increment $\Delta \underline{\varepsilon}_{-r}$ is known from equation /8.82/ prior to computing equation /8.80/, and will automatically include material nonlinear effects.

The choice of retardation times.

The suitable choice of retardation times τ_{μ} can be explained in Fig. 8.9. If we plot $(t - t')$ on logarithmic scale the individual exponential terms $\left(1 - \exp\left[-\frac{t - t'}{\tau_{\mu}}\right] \right)$ of /8.72/ look like step functions with the step spread over one unit of $\log(t-t')$ and outside this interval they are nearly constant and horizontal. The retardation time τ_{μ} is located near the center of function rise. Hence the approximation of the original creep function can be understood as an overlaying of the original creep by a set of horizontal strips, each of them corresponding to one retardation time τ_{μ} . From this graphical construction some salient properties become evident (τ_{μ} is located in center of functional step).

This approximation is not unique because of the variable number of strips possible in the approximation. However, based on collective experience, it is recommended that τ_{μ} is spread uniformly on a logarithmic scale and at least one τ_{μ} for every unit of $\log(\tau)$ should be used, i.e. $m \geq 1$ [34]. Hence:

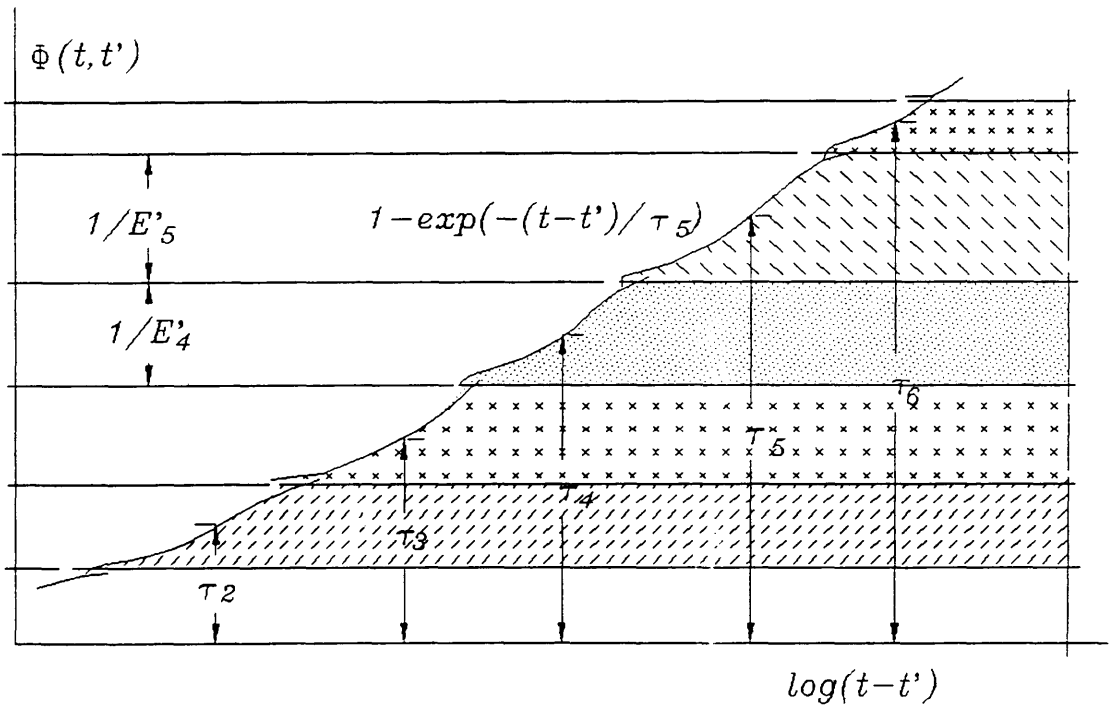
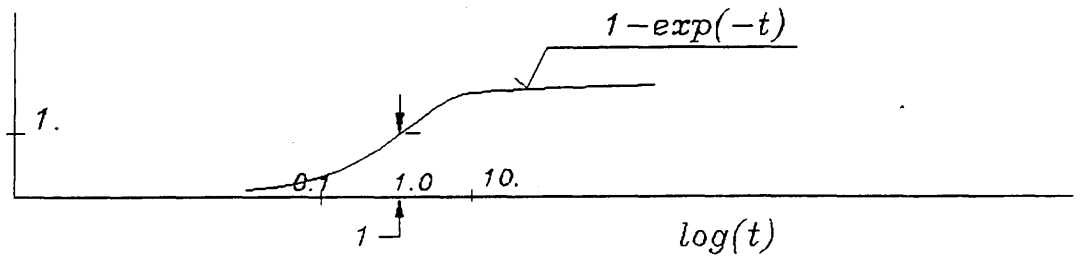


Fig. 8.9 Representation of Dirichlet series.

$$\tau_{\mu} = 10^{\frac{\mu-1}{m}} \tau_1, \quad /8.83/$$

where $\mu = 1, 2, \dots, n$ and τ_1 must be small enough to account for the aging of concrete. In addition, the values of τ_{μ} must cover the whole time of interest. Thus:

$$\tau_n \approx \frac{t}{2}$$

and

/8.84/

$$(\tau_1 \leq 2 t') \wedge (\tau_1 \leq 0.1 t'_0)$$

where t'_0 is the age of loading. Obviously, the first condition is more rigorous. t is the total age of structure.

The choice of integration times.

The choice of integration times, i.e. time interval for numerical integration of /8.74/ is very similar to the situation with retardation times τ_μ . However, for the sake of accuracy, it is better to place more integration intervals per one decade (at least two) [34]. Thus:

$$t_r = 10^{\frac{r-1}{l}} (t_1 - t') \quad /8.85/$$

where t' is time of sudden loading, $t_1 \approx t' + 0.1$ day and l is number of integration intervals unit of $\log(t)$, usually $l = 2$. Subscript r ranges from 1 to N , where $t_N \geq t$ (the age of the structure).

The expression /8.85/ is written for the case when structure is loaded at time t' and thereafter there are only small changes in loading condition.

If a structure is suddenly significantly loaded or unloaded after t' , then it is necessary to start again with small time intervals.

Approximation of creep function using Dirichlet series.

Minimizing the error between the specified creep function $\Phi(t, t')$ and the Dirichlet series $\Phi'(t, t')$ leads to sets of coefficients E_r and E'_{μ_r} of the Dirichlet series for specified values of retardation times τ_{μ_r} and integration times t_r , (one set per each $t' = t_r$). For example, using the least squares method,

$$\int_{t_r}^t (\Phi(\tau, t_r) - \Phi'(\tau, t_r))^2 d\tau = \text{minimum} \quad /8.86/$$

or re-writing in summation form:

$$\sum_{k=r}^N [\Phi(t_k, t_r) - \Phi'(t_k, t_r)]^2 = \text{minimum} \quad /8.87/$$

where $\Phi(t_k, t_r)$ are sampling points of the specified creep function and $\Phi'(t_k, t_r)$ are their equivalent values using the Dirichlet series.

Minimization leads to the final set of equations for every value of t_r from which the unknown material constants E_r and $(E'_\mu, \mu=1, n)$ are computed, i.e.

$$a_{11r} E_r^{-1} + \sum_{\mu=1}^n a_{i\mu r} E_\mu^{-1} = y_{1r} \quad /8.88/$$

where

$$a_{11r} = N - r + 1$$

$$a_{11r} = \sum_{k=r}^N \left[1 - \exp\left(-\frac{t_k - t'_r}{\tau_i}\right) \right]$$

$$a_{1\mu r} = \sum_{k=r}^N \left[1 - \exp\left(-\frac{t_k - t'_r}{\tau_\mu}\right) \right]$$

$$a_{i\mu r} = \sum_{k=r}^N \left[1 - \exp\left(-\frac{t_k - t'_r}{\tau_i}\right) \right] \left[1 - \exp\left(-\frac{t_k - t'_r}{\tau_\mu}\right) \right]$$

$$y_{1r} = \sum_{k=r}^N \Phi(t_k, t'_r)$$

$$y_{i_r} = \sum_{k=r}^N \Phi(t_k, t'_r) \left[1 - \exp\left(-\frac{t_k - t'_r}{\tau_i}\right) \right]$$

The coefficients a_{i1_r} , $a_{i\mu_r}$, $r = 1, n$ can be collected together to form a matrix **A** with $(n + 1)$ rows and columns. Hence index i ranges from 1 to $(n + 1)$ whilst μ ranges from 1 to n . Index k is a summation index through all creep data for $t' = t'_r$, i.e. from r to N .

Examination of equation /8.88/ suggests that matrix **A** might become ill-conditioned under certain circumstances. Large retardation times τ_i cause nearly zero exponential terms, irrespective of values t and t' whilst small values of τ_i (which are necessary to allow aging in the creep function), combined with a large time span, causes $\frac{t - t'}{\tau}$ to become too large, giving excessively high values of the exponential term. It is difficult to establish criteria, using mechanics principles, which forecast the stability of equation /8.88/ in general cases. Therefore a purely mathematical solution is proposed here.

Matrix **A** is first assembled as it stands. If any ill-conditioning exists, then determinant $|A|$ must be close to zero, which, in the context of a Dirichlet series, implies that two or more adjacent columns must be nearly parallel when viewed as vectors. Thus it suffices to examine the angle α between the vectors given by

$$\cos^2(\alpha) = \frac{\left[\sum_{j=1}^{n+1} \begin{pmatrix} a_{ji} & a_{j(i+1)} \end{pmatrix} \right]^2}{\sum_{j=1}^{n+1} \begin{pmatrix} a_{j(i+1)} & a_{j(i+1)} \end{pmatrix} \sum_{j=1}^{n+1} \begin{pmatrix} a_{ji} & a_{ji} \end{pmatrix}} \quad /8.89/$$

where i and $i + 1$ are the column numbers. Hence the algorithm is developed as follows:

- 1/ starting at column $i = 1$, calculate α for columns i and $(i + 1)$.
- 2/ if $\alpha \geq \alpha_s$ (a small specified value), increment i by 1 and return to step 1.
- 3/ if $\alpha < \alpha_s$, then calculate α successively for columns i and i

+ 2, $i + 3$...etc. until columns i and $i + s$ satisfy $\alpha \geq \alpha_s$
4/ columns $(i + 1)$ to $(i + s - 1)$ are then rejected by setting
the variables $E'_{\mu_{i+1}}$ to $E'_{\mu_{i+s-1}}$ to 0, thus deleting modes cor-
responding to retardation times $\tau = t_{i+1}$ to t_{i+s-1} from the Di-
richlet series.

5/ restart process at column $(i + s)$, return to step 1, and
continue until all columns have been scanned.

Chapter 9 presents some examples demonstrating the efficien-
cy of the algorithm.

9. ANALYSIS OF STRUCTURES SUBJECT TO LONG-TERM LOADING

This chapter presents long-term loading structural analyses performed by the modified Step-by-step procedure, (described in Section 8.3). It will be always restricted to serviceability structural conditions as implied by linear creep considerations only.

Generally there is a considerable lack of experimental as well as analytical evidence about the behavior of reinforced concrete structures subject to long-term loading conditions. Experimental data are available mostly for relatively short-term loading only and analytical solutions, for the sake of simplicity, usually neglect structural nonlinearities (geometric and constitutive equations).

The examples presented demonstrate that full analytical nonlinear analysis is nowadays feasible, even if only PC techniques are available. In addition, comparison of the results with those based on other sources is given, (i.e. from experimental analysis, solutions based on British Standard BS 8110, 1985 etc.), so that the accuracy of the solution can be ascertained.

A brief list of the long-term analyses with their objectives follows:

Anal.	Structure	Problems	Program
9.1	Beam [49], R/C	SBS, CM, TI, RT	PI-1
9.2	Beam [49], R/C	SBS	PI-2
9.3	Concrete samples [49]	SBS, TI	PI-3
9.4	Beam, slab, shell, R/C	SBS, NSBS	PI-2
9.5	Concrete samples	DS, SBS	PI-3

where:

CM = Comparison of creep models,

DS = Creep function approximation by Dirichlet's series,
excessive modes rejection,

NSBS = Other than SBS method for creep analysis,

PI-1 = 2D analysis,
PI-2 = Shell analysis
PI-3 = Material preprocessor Material,
RT = Influence of retardation time choice,
SBS = Step-by-step procedure for creep analysis,
TI = Influence of the choice of time integration steps.

9.1 Beam analysis subject to three years loading. 2D analysis.

A. Aim of the analysis:

- analysis of beam structure subject to three year uniform loading using 2D approach,
- comparison of two finite element meshes,
- comparison of creep models,
- nonlinearity effect of matrix B, (equations /8.80/ vs. 8.80'/),
- comparison of results using different time integration density,
- influence of retardation times on accuracy of results.

B. Description of analyses:

Experimental data from a typical precast R/C floor subject to three year loading were used [49].

The tested floor plate consists of beam elements, each with a rectangular cross section 0.46x0.23m and span and total length 6.14m and 6.30m respectively. The geometry and reinforcement of a typical floor component are depicted in Fig. 9.1. The floor specimen was designed in accordance with CP 114 for its dead load and superimposed load of 56 lbf/ft² (2.682 kN/m²) which corresponds to a live load of 40 lbf/ft² (1.92 kN/m²) and an allowance of 16 lbf/ft² (0.76 kN/m²) for partitions and finishes. A load factor of 2. was used in order to meet requirements of GLC London Building (constructional) By-laws.

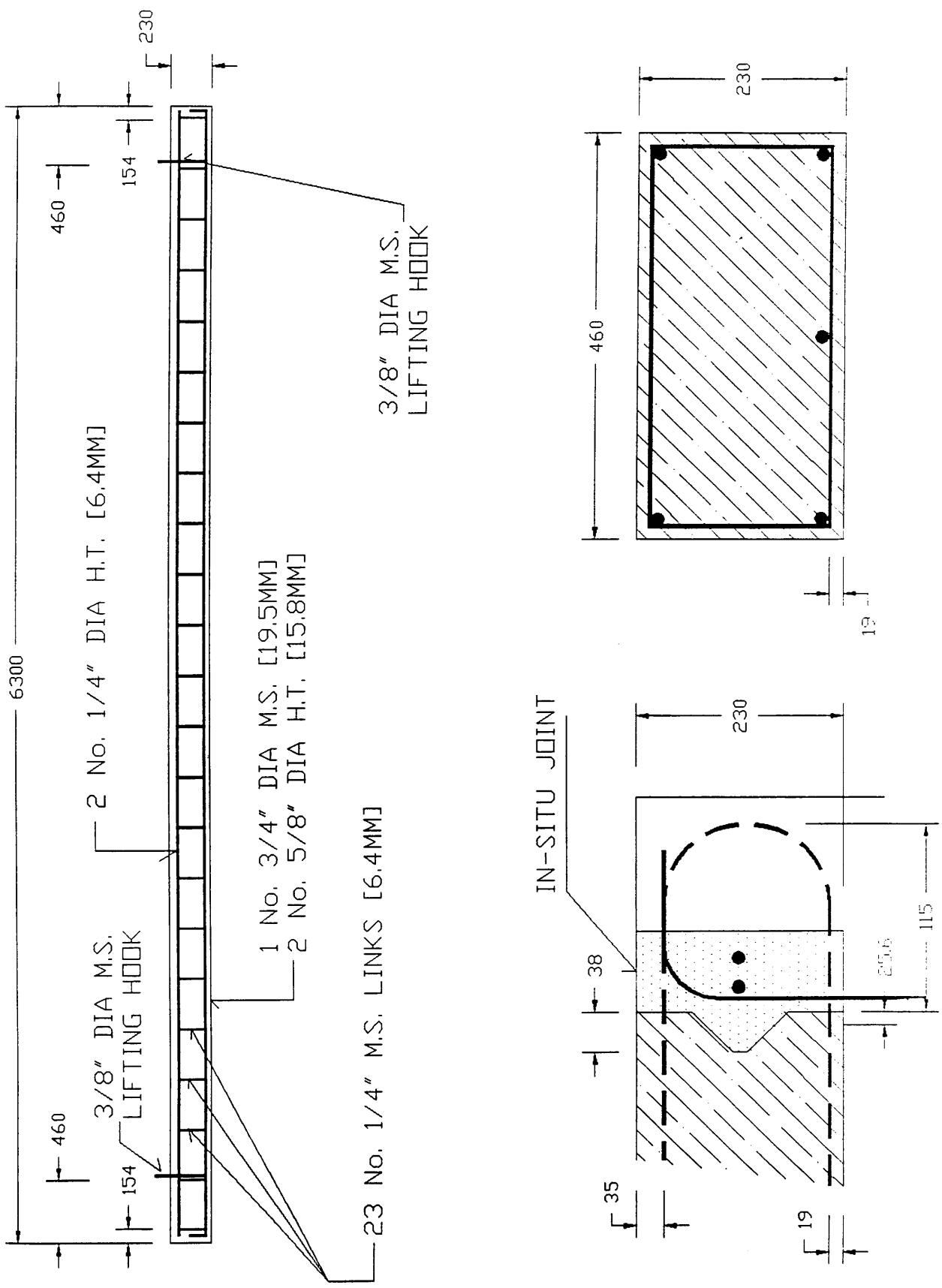


Fig. 9.1 Geometry and reinforcement of typical floor element.

A series of three floor specimens was cast using the following mix:

sand	863 kg/m ³
gravel	863 kg/m ³
portland cement	245 kg/m ³
water (0.63x460)	154 kg/m ³
total weight	2125 kg/m ³
compressive strength (28 days)	35.1 MPa
tension strength	3.41 Mpa
Young's modulus	30. GPa

Each beam was reinforced by two 5/8 in. diameter high tensile steel bars and one 3/4 in. diameter mild steel bar of the following properties:

3/4 in. diameter bar (19.2 mm):

Young's modulus (elastic)	208 Gpa
Young's modulus (plastic)	36.56 GPa
Yield stress	267 Mpa
Ultimate stress	468 Mpa

5/8 in. diameter bars (16 mm):

Young's modulus (elastic)	196 Gpa
Young's modulus (plastic)	31.2 GPa
Yield stress	427 Mpa
Ultimate stress	678 Mpa

All reinforcement was placed near the bottom of the beam (tension zone), the concrete cover being 3/4 in. (19.2 mm). The construction reinforcement, i.e. bars near the top, lifting hooks etc. was neglected. The total reinforcement area was 680.5 mm² which corresponded to 0.65% of total cross section area. The structure was simply supported near its ends.

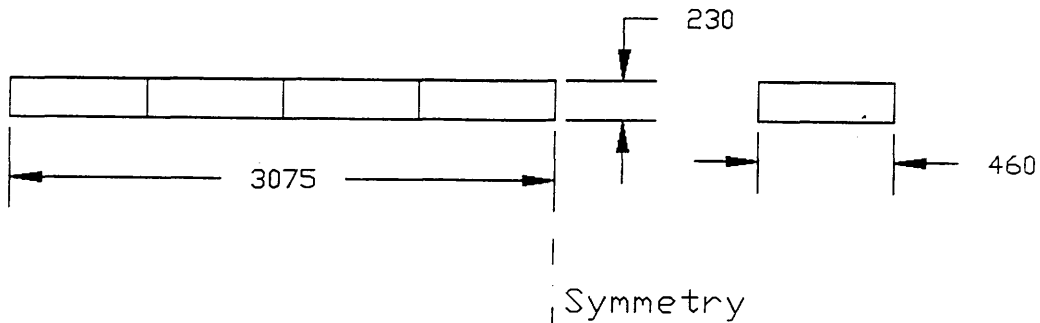
One day after the casting the specimens were removed from the moulds and then placed in curing tank, where they were water cured for seven days. At the age of fourteen days the beams were transported from precasting yard and erected on steel frames with rubber pads in the weather-proof test building with the average temperature and relative humidity about 15°C and 78%. The exact record of both temperature as well as relative humidity is provided in [49].

Dead load was applied at fourteen days and full loading was imposed at twenty eight days.

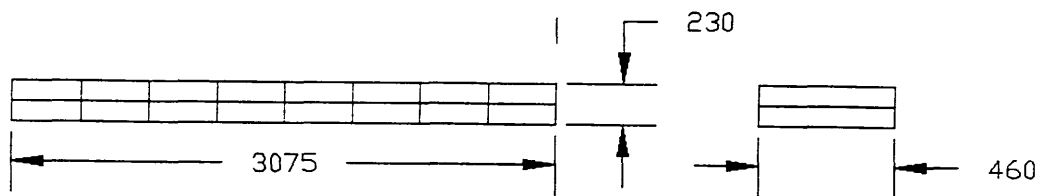
9.1.1 Comparison between element methods and integration rules.

Two finite element meshes were used to model the structure. The first one consists of 16 elements, i.e. 8 elements in longitudinal direction and 2 elements through the beam depth, and the second consists of 4 elements only, placed in the longitudinal direction (see Figure 9.2). Isoparametric quadratic elements were employed and were each integrated at 4, 9 or 16 Gaussian integration points. Creep and shrinkage were modeled by the Bazant-Panula model No. 1. The computed mid-span deflections are compared with experimental data [49] in Fig. 9.3. The legend indicates which particular mesh and integration was used, for example (16E/9I) means that the 16 element mesh was used and that each element was integrated by a 3 x 3 integration rule.

4-element model



16-element model



Support

Fig. 9.2 Geometry of the models used for 2D analysis.

Mid-span deflection Plane stress analysis

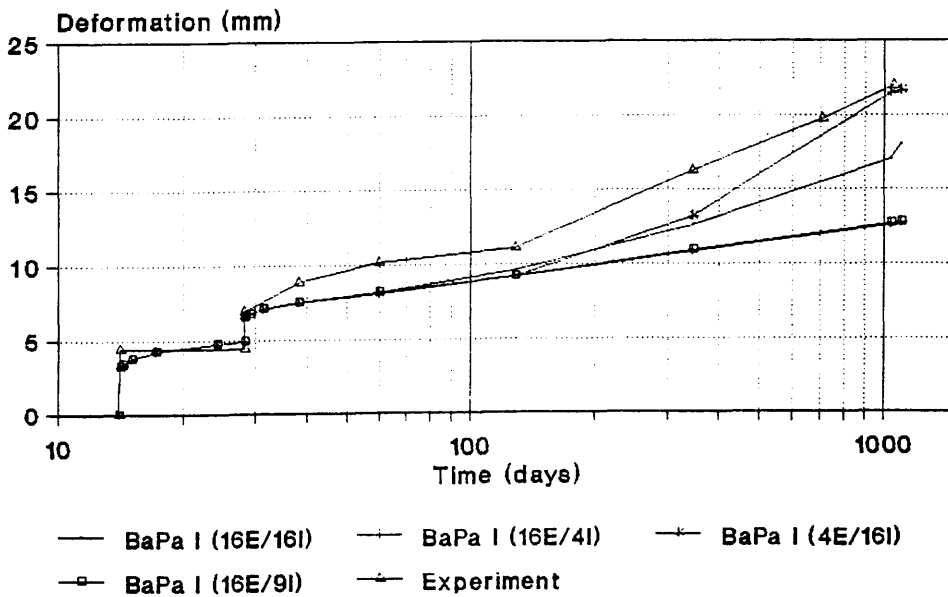


Fig. 9.3 Mid-span deflection of the beam, 2D analysis.

Discrepancies exist between the results. For the structural response up to about half a year the results for different meshes nearly coincide, however the final midspan deflections differ substantially, being similar for (16E/4I) and (16E/9I) meshes only. Hence for smaller deformations any of the above meshes can be used. For longer times and consequently for higher structural deformations the accuracy of the results is negatively influenced by the simplicity of the constitutive equations being used and a more sophisticated material model would be appropriate. Mesh densities and integration rules used influence rather the "speed" of progression of material failure than the accuracy of the results. The effect of creep and shrinkage model itself is subject of the next analysis.

9.1.2 Comparison between creep and shrinkage models.

The 16 element mesh with 16 integration points per element was used. Material properties were generated by ACI 78, CEB-FIP 78, Bazant-Panula No. 1 and No. 2 models. The mid-span deflections are depicted in Fig. 9.4.

A wide discrepancy exists between the code models, ACI 78 predicting a mid-span deflection approximately double that of CEB-FIP 78 at three years. The two Bazant-Panula models predicted fairly similar responses. These differences are mainly due to uncertainties in the basic material data and the use of averaged humidity, temperature and shrinkage data, rather than inadequacies in the creep function itself. In particular, the modulus of elasticity was computed using expressions inherent to each creep model, rather than its experimental value. This analysis emphasizes only the importance of using as accurate as possible material data for this type of analysis.

Crack development with time for the case of Bazant-Panula No.1 model is given in Fig. 9.5. Cracking first developed at 128 days and had almost doubled in extent by 344 days, after which it appears to have settled.

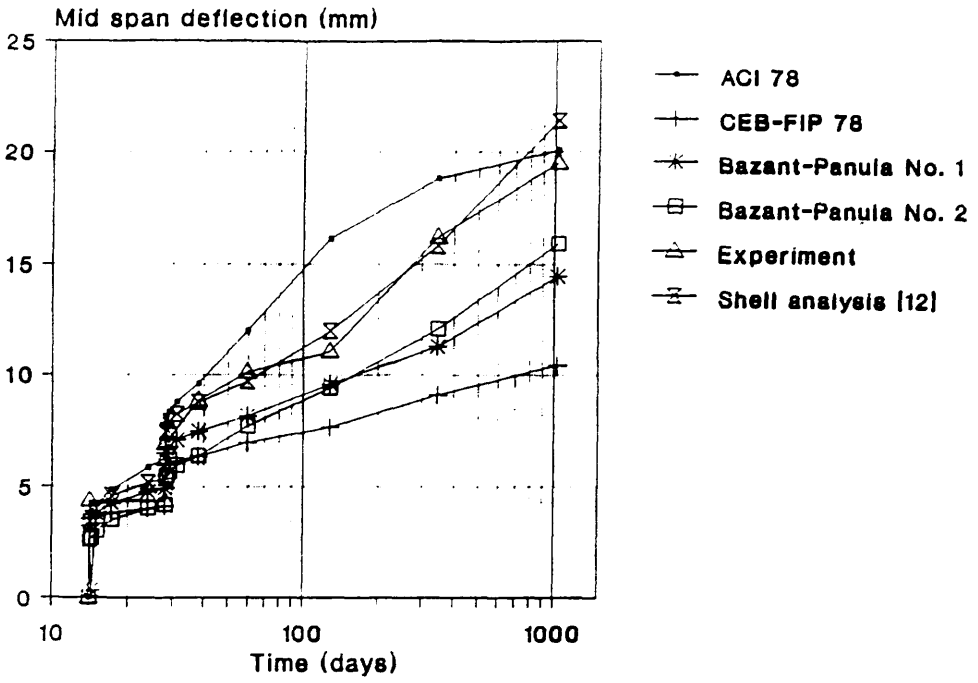


Fig. 9.4 Influence of different creep models on mid-span deflection, 2D analysis.

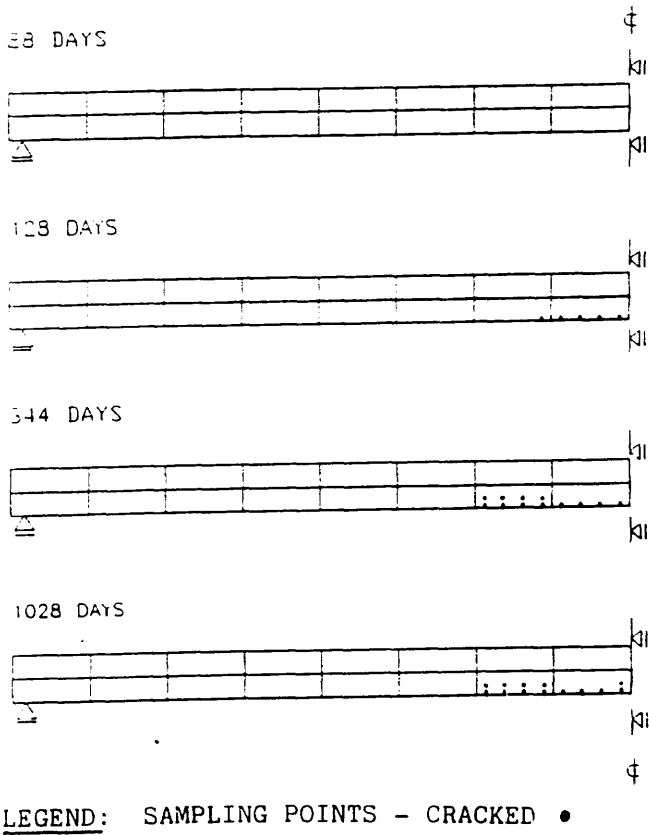


Fig. 9.5 Crack development with time, 2D analysis.

9.1.3 Effect of material non-linearity.

It was noted in the Chapter 8 that the internal variables $\varepsilon_{\mu_r}^*$ depend in part on matrix B. Equation /8.80' / was derived to automatically include nonlinear effects in B as time advances. A simpler alternative is to use the elastic, linear isotropic form of B in equation /8.80 / throughout. As can be seen from Fig 9.6 neglecting nonlinear effects causes a less stiff response after about 340 days. It indicates that material nonlinearity has developed and it is important to include its effects also in equation /8.80 /.

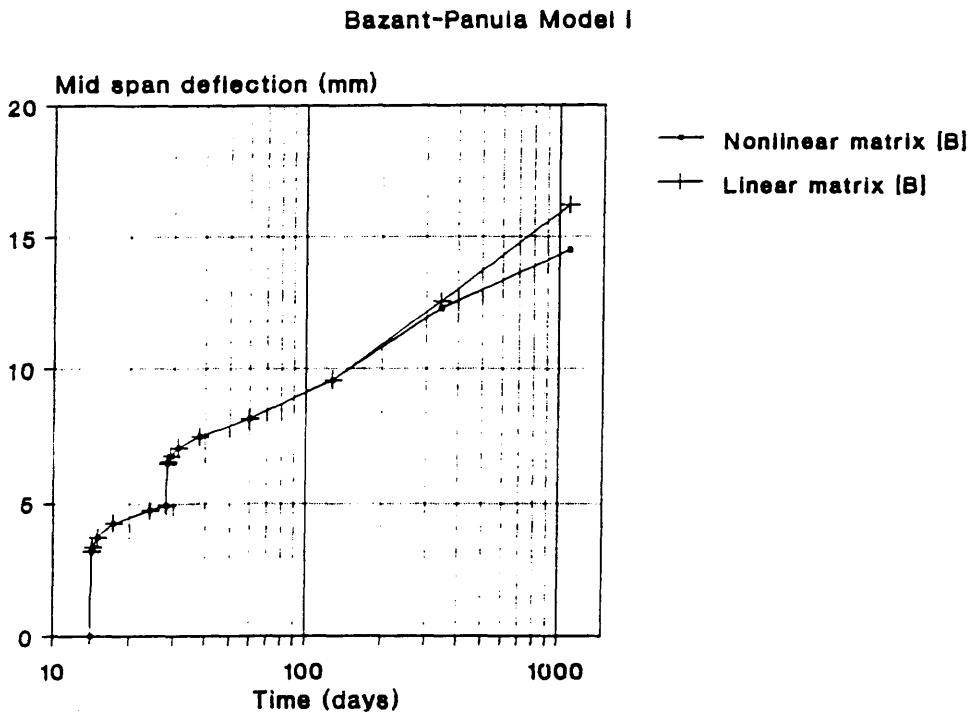


Fig. 9.6 Effect of matrix B on the mid-span deflection, 2D analysis.

9.1.4 Effect of time integration densities.

The influence of different time integration densities is demonstrated in this section. Again the 16 element mesh with 16 integration points per element was employed. Using small time steps again after the live load application at 28 days is also examined. Actual integration times are provided in Table 9.1. Four cases are presented:

1/ 6 time steps, $l = 1$ in equation /8.85/, no small time steps after 28 days.

2/ 10 time steps, $l = 2$, no small time steps after 28 days.

3/ 9 time steps, $l = 1$, small time steps applied after 28 days.

4/ 15 time steps, $l = 2$, small time steps applied after 28 days.

Case 4 corresponds to the recommended minimum values. Retardation times were generated by equation /8.83/ with parameter $m = 1$.

Not unexpectedly, differences in response exist immediately after 28 days, depending on whether small time steps are employed or not at this stage. Otherwise, there is little significant difference as time progresses, except at 1028 days for case 4 where a stiffer response starts to develop. Such differences, where they exist, are caused by slightly different progression of non-linear material behavior with different time advances. This suggests that the minimum recommendations /8.85/ are too cautious in this case.

Case	Integration times (days)
1	14.0, 14.1, 15.0, 24.0, 114.0, 1014.0, 1028.0
2	14.0, 14.1, 14.3, 15.0, 17.2, 24.0, 45.6, 114.0, 330.0, 1014.0, 1028.0
3	14.0, 14.1, 15.0, 24.0, 28.0, 28.1, 29.0, 38.0, 128.0, 1028.0
4	14.0, 14.1, 14.3, 15.0, 17.2, 24.0, 28.0, 28.1, 28.3, 29.0, 31.2, 38.0, 59.6, 128.0, 344.0, 1028.0

Table 9.1 Integration time steps.

Bazant-Panula Model I

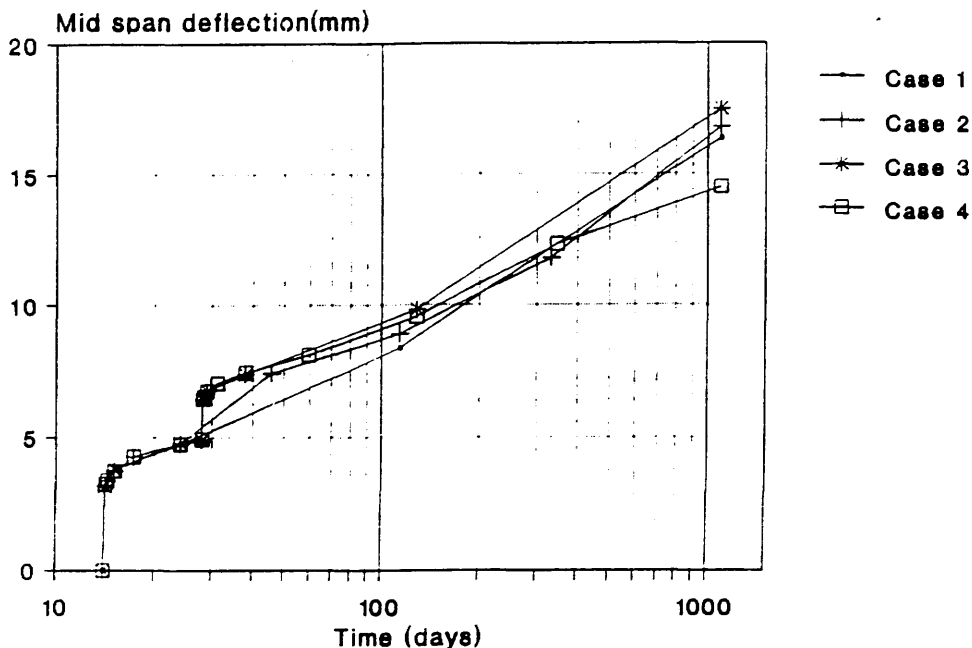


Fig. 9.7 Comparison between different integration time steps.

9.1.5 Effect of retardation times.

Finally interest is focused on the influence of retardation times. Three different retardation times sets were examined: for $m = 0.5$, case 1, $m = 1$, case 2 and $m = 2$, case 3 in equation /8.83/. Table 9.2 lists the actual values. The same time integration steps from case 4 in the previous analysis were adopted. The results are shown in Fig. 9.8.

Very little difference is observed in the deformation responses, suggesting again that the minimum recommendation, $m = 2$, is too strict.

Case	Retardation times (days)
1	1.4, 140.0, 547.5
2	1.4, 14.0, 140.0, 547.5
3	1.4, 4.4, 14.0, 44.3, 140.0, 442.7, 547.5

Table 9.2 Retardation time sets.

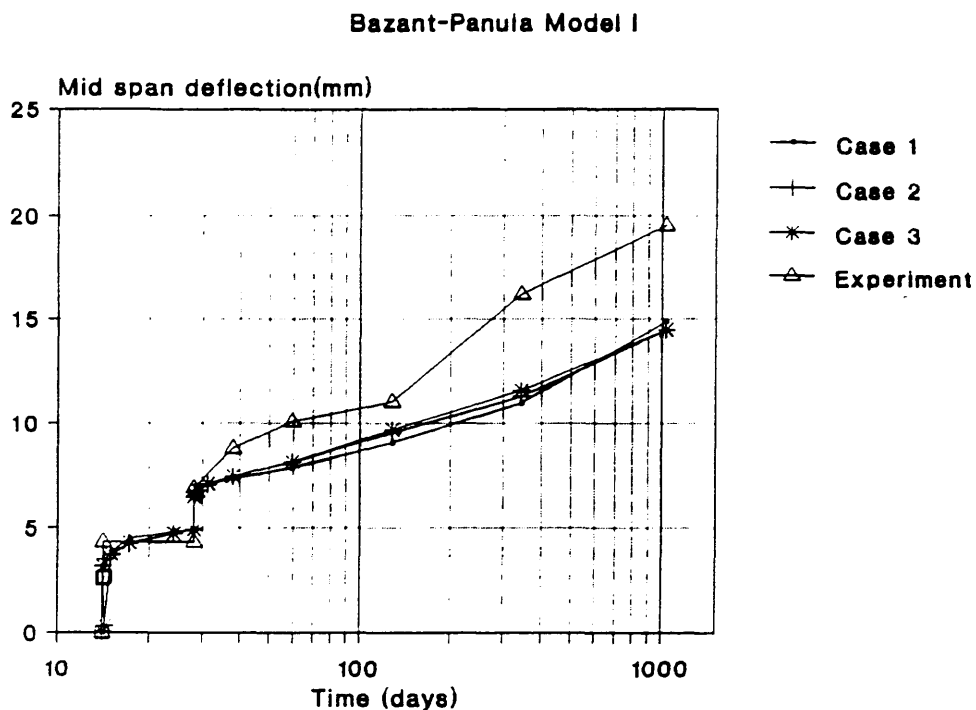


Fig. 9.8 Comparison between different retardation times, 2D analysis.

9.2 Beam analysis subject to three years loading.
shell analysis.

A. Aim of the analysis:

-analysis of beam structure subject to three year uniform

loading using shell approach
-comparison of creep models.

B. Description of analyses and results:

The same beam structure as the one analyzed in Section 9.1, is now examined using four shell elements with Heterosis displacement approximation.

For in-plane integration the Gaussian selective integration scheme were adopted whilst the third direction, i.e. through the thickness, was integrated by the trapezoidal integration algorithm. Ten equally thick concrete layers were spread through the beam depth and additional layers were created for reinforcement. The mathematical model of the structure is depicted in Fig. 9.9.

BEAM - Shell analysis

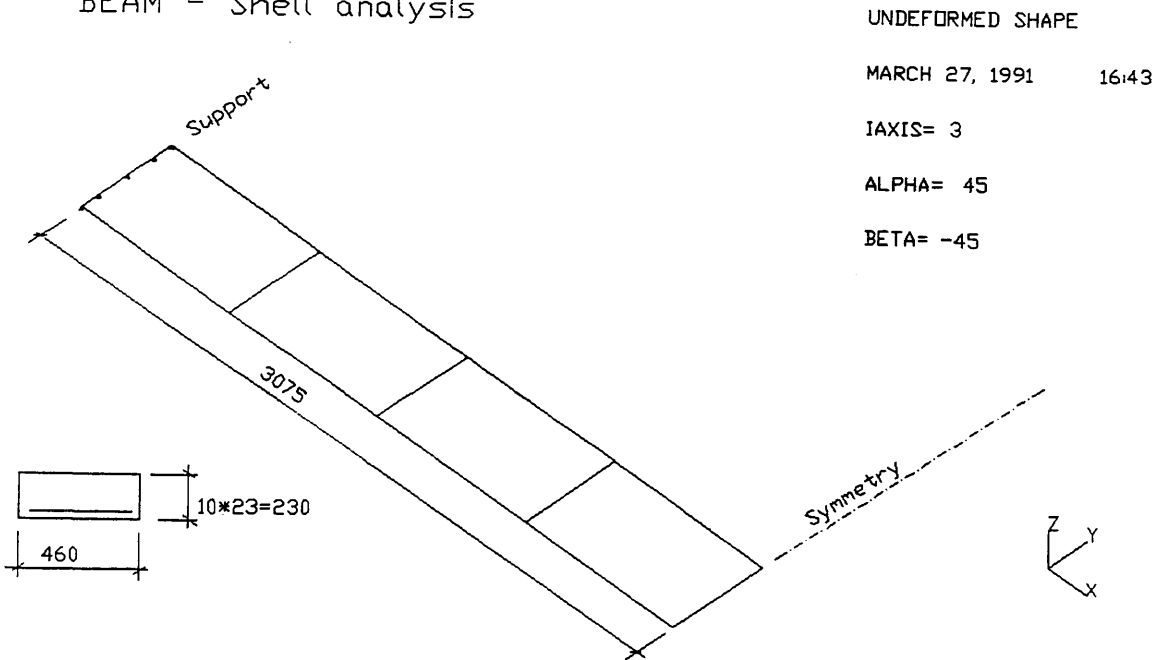


Fig. 9.9 Geometry of the model used for shell analysis.

9.2.1 Comparison between creep and shrinkage models.

The computed and experimental [49] results for mid-span displacement are compared in Fig. 9.10.

Mid-span deflection Shell analysis

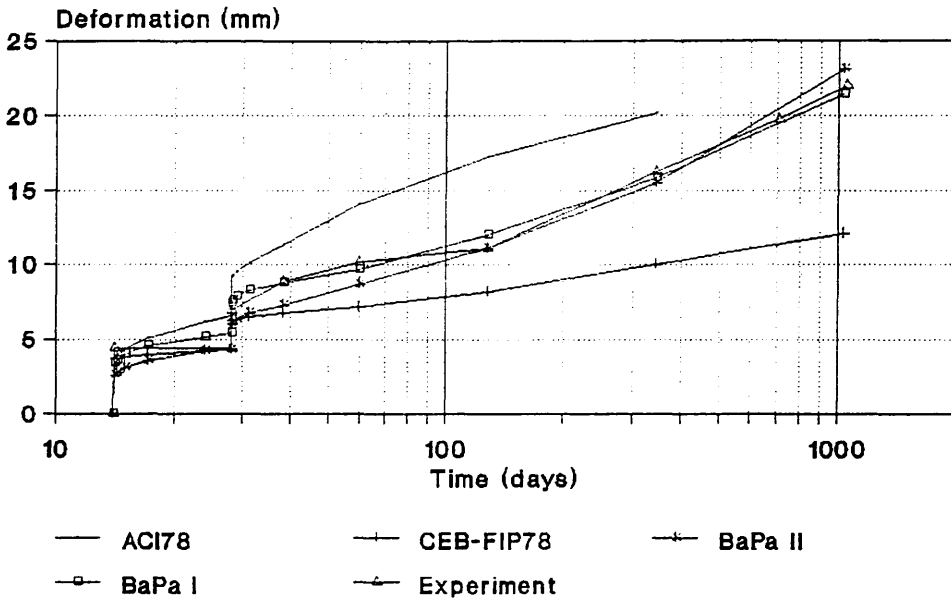


Fig. 9.10 The mid span deflection of the tested R/C beam, shell analysis.

Excellent agreement has been reached between the experimental and analytical results when the Bazant-Panula model I or model II was used. It should be noted that ref. [49] does not distinguish between short-term and long-term deformation till the age of 28 days. Hence there is no change in deformation from age 14 through 28 days. After 28 days ref. [49] presents a very detailed record of long-term deflections which enables the influence of other factors such as temperature, relative humidity etc. to be studied during aging of beam.

Using the ACI78 material model, a considerably bigger deflection has been computed. Looking for the cause of this scatter of accuracy it was found that this material model uses an empirical formulae to compute 28-days Young's modulus, which is based on the density and the 28-days compressive strength of concrete. Substituting the above data, Young's modulus is equal to 24.71 GPa. This value differs significantly from the one based on the experimental measurements, i.e. 30 GPa. If we use the ACI78 model with Young's modulus equal to 30 GPa, then the computed results would be more accurate. Note that the computed 28-days Young's modulus using the Bazant-Panula model I was 30.78 GPa, in the case of Bazant-Panula model II 29.9 GPa and using the CEB78 model it was 31.07 GPa.

The CEB-78 model provided the worst results. The model of the structure was too stiff, especially for longer ages. This is the penalty for its simplicity. However for relatively shorter loading conditions the accuracy of the results seems to be acceptable (half year or less). The predicted deflections for ages equal to a couple of days were excellent.

Thus we can summarize that for the present analysis the best results were calculated by the Bazant-Panula model I.

To be able to draw some general conclusions about creep and shrinkage material models much more analyses would be necessary. However a similar study, for structures with linear constitutive equations, has been done by Bazant et. al. [50] with conclusion favoring also the Bazant Panula model I.

9.3 Analysis of concrete samples.

A. Aim of the analysis:

-presentation of direct analysis by material preprocessor MATERIAL,

-comparison of shrinkage predictions by different material models,

-study of different time integrations for the case of simple

uniaxial concrete specimens with a linear short-term loading material law.

B. Description of analyses and results:

As already mentioned the material preprocessor can be also used for the direct analysis of concrete uniaxial specimens in which the short-term material law is assumed linear. This is now examined.

First, interest is focused on shrinkage and compressive strength of concrete within a three year period. The results provided by the creep and shrinkage material models are compared with experimental data from ref. [49].

Two series of sample specimens were tested, one with dimensions 70x70x280mm and the other 210x210x840mm. They were cast with the concrete mix defined in Section 9.1, but relative humidity and temperature were now kept constant at 65% and 20°C respectively.

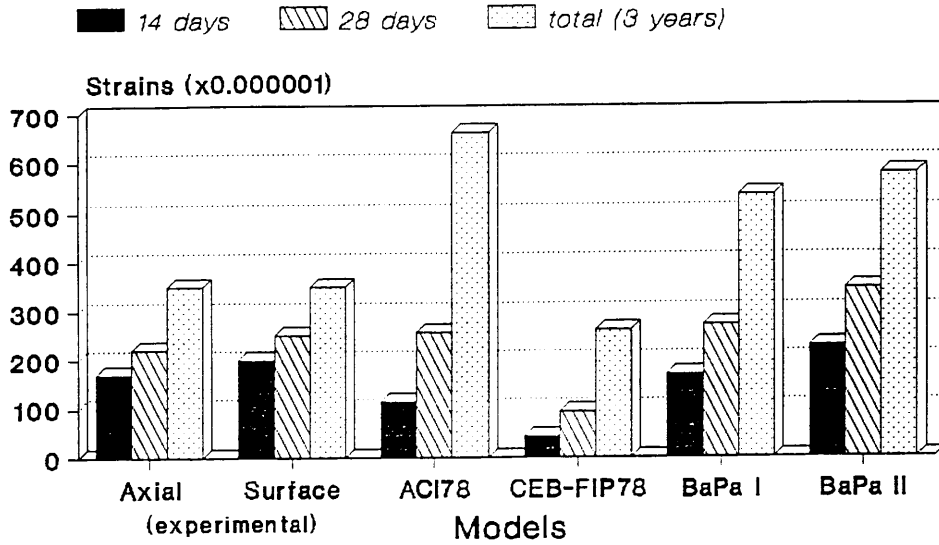
Figs. 9.11 and 9.12 compare the shrinkage and compressive strengths respectively. In the case of the experimental results, mean values are presented.

The shrinkage computed by Bazant-Panula model I and II matches relatively well the experimentally measured value. The ACI78 model overestimates it and the CEB-FIP78 underestimates it.

On the other side, the compressive strengths were better predicted by the CEB-FIP78 model. Note that the ACI78 and Bazant-Panula models I and II uses the same expression to evaluate compressive strength of concrete and therefore the corresponding curves in Fig. 9.12 coincide.

Shrinkage Comparison

Sample size 70x70x280mm



Shrinkage Comparison

Sample size 210x210x840mm

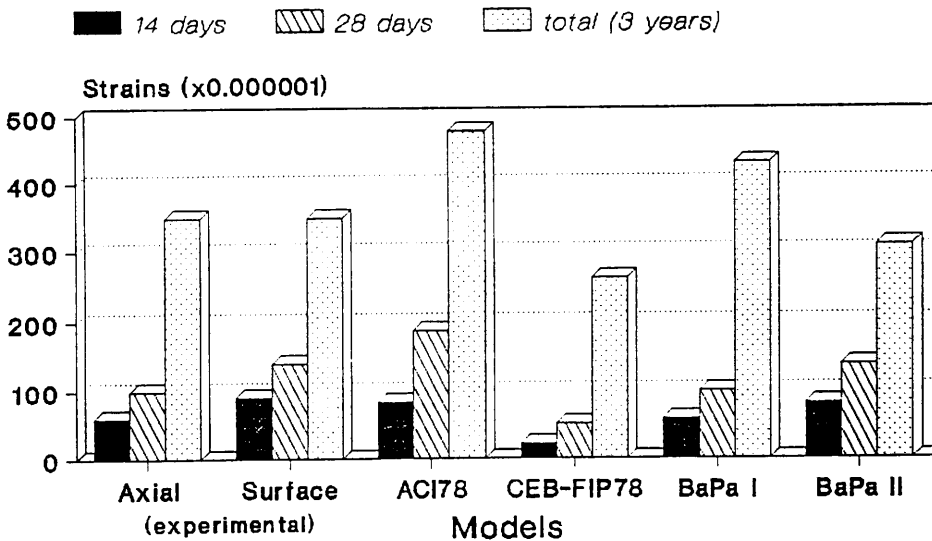


Fig. 9.11 Shrinkage of concrete samples.

Concrete compression strength

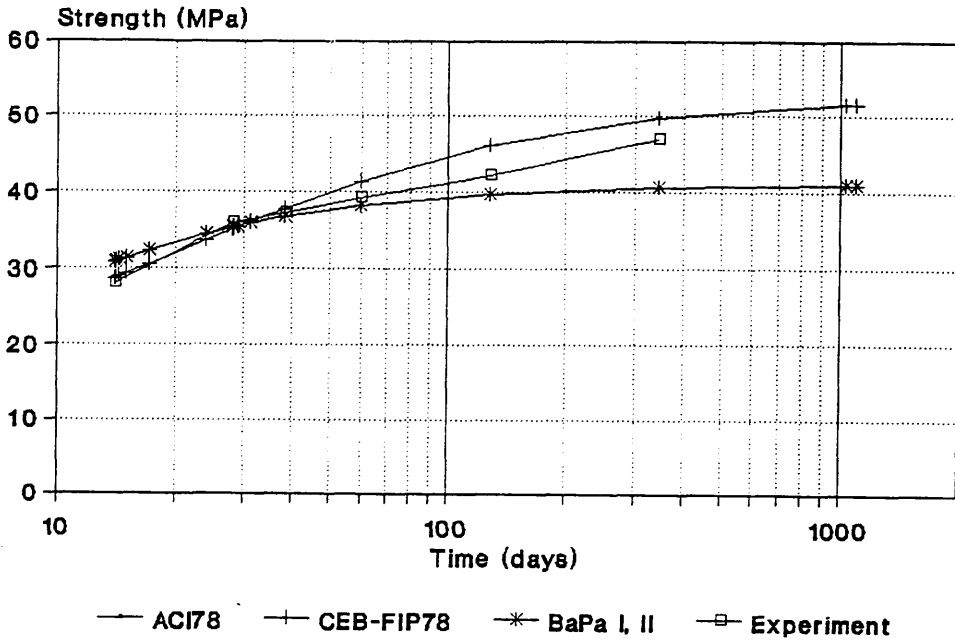
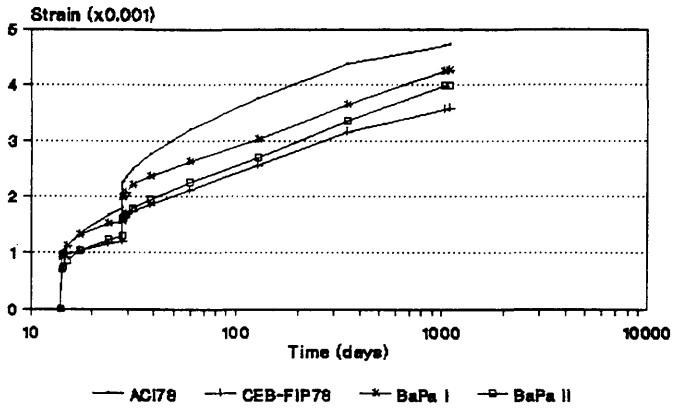


Fig. 9.12 Compressive strength of concrete samples.

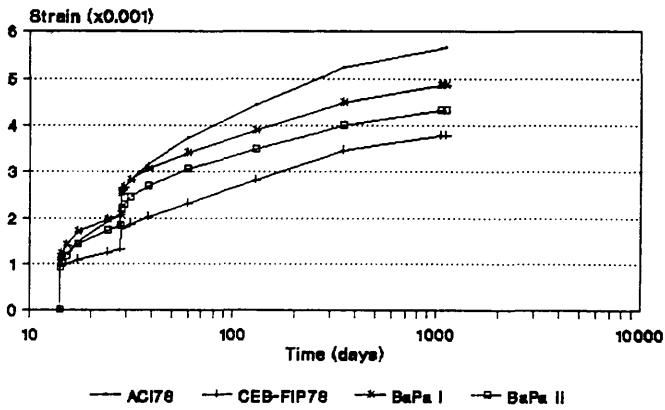
Deflections of the specimens under 3 years compression loading were also computed. The specimens were loaded at 14 days by a stress of 19.6 MPa and at 28 days by an additional stress of 10.4 MPa, i.e. by a total stress 30MPa. The loading time and ratio of loading correspond to that given in Section 9.1. Shrinkage was also accounted for. However short term material nonlinearity is neglected and thus time dependent aspects of structural behavior, i.e. the creep and shrinkage material models, are directly addressed.

The results of the analyses are shown in Fig. 9.13.

**Strain due to stress and shrinkage
Sample 210x210x840mm**



**Strain due to stress and shrinkage
Sample 70x70x280mm**



Stress history

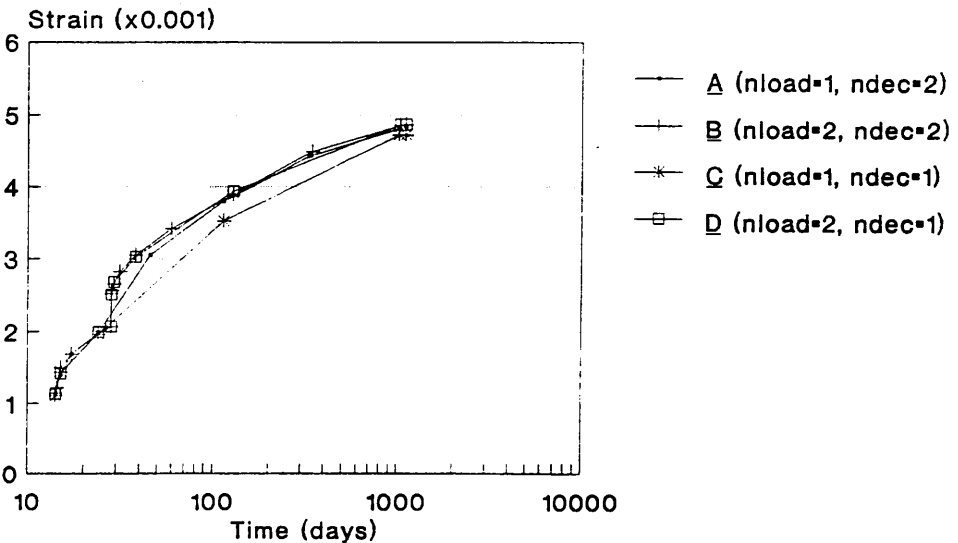
Time:	0	14	14.1	28	28.1	1095	(days)
Stress:	0	0	19.5	19.6	30.0	30.0	(MPa)

Fig. 9.13 Strain in sample bars due to stress and shrinkage.

Unfortunately no experimental data are available for comparison. However results differ significantly which proves again that creep and shrinkage analysis is a really challenging problem. In this case the only factor responsible for this scatter of accuracy is the creep and shrinkage model for concrete; time integration was practically exact (default settings, see analysis B in the following example).

Finally the 70x70x280 concrete sample was used to investigate different time integration. The loading was the same as in the previous example and Bazant Panula model I was used throughout.

Strain due to stress and shrinkage Sample 70x70x280mm Comparison of integration methods



nload = number of sudden loadings
ndec = number of integ. points / decade

Fig. 9.14 Different time integration methods to analyze uniaxial concrete specimen.

Four analyses were carried out:

In the first (curve A in Fig. 9.14) two integration points per unit of $\log(\text{time})$ were used whilst time integration was not refined after sudden reloading at time 28 days.

The second solution used two integration time points per unit of $\log(\text{time})$ and after every sudden loading (equal to 14 and 28 days) small time increments were used again (see curve B in Fig. 9.14).

The third solution was similar to the first one except that only one integration time per unit of $\log(\text{time})$ was considered (curve C in Fig. 9.14).

Finally, in the fourth analysis, the previous analysis B was modified so that one time point per unit of $\log(\text{time})$ was used.

Comparing the results (curves A through D) it is apparent that there is practically no difference between integrations using one or two time intervals per unit of $\log(\text{time})$ if after every sudden loading small time increments are used again.

Cases in which sudden reloading at 28 days was neglected (in integration) differ more significantly (for one and two points integration per unit of $\log(\text{time})$). However if we are interested in structural response at times far enough from reloading (say ten times the reloading time and later) the difference becomes marginal.

To be able^{to} draw some general conclusions many more examples would have to be performed. However it is again shown that the recommendations in ref. [50], i.e. two integration points per $\log(t)$ and integration refinement after every structural reloading are too cautious.

Ref. [50] also summarize results about reliability and accuracy of the material models incorporated in the MATERIAL preprocessor program. These have been tested for a huge material data base, (involving over 800 creep and shrinkage curves), in many laboratories. The 95% confidence limits (i.e. the relative deviations from the mean that are exceeded with a probability of 2.5% on the plus side and 2.5% on the minus side) were found for

Bazant-Panula model I to be $\pm 37\%$, for the ACI78 model $\pm 77\%$ and for the CEB-FIP model $\pm 92\%$. The effects which are ignored by the ACI and CEB-FIP models, such as temperature, were not included in the calculation of those statistics, although the Bazant-Panula model I describes them quite well. For the same reason the present results for the Bazant-Panula model I are applicable also for its simplified version, the Bazant-Panula model II.

9.4 Comparison of the present Step by step method with other solution techniques.

A. Aim of the analysis:

-comparison of different solution methods:

- 1/ the present Step by step method,
- 2/ nonlinear short-term solution based on 30-years Young's modulus, shrinkage considered, i.e. Effective modulus method,
- 3/ nonlinear short-term solution based on 30-years Young's modulus, shrinkage neglected,
- 4/ nonlinear short-term solution based of 28-days value of Young's modulus, shrinkage neglected,
- 5/ solution based on British Standard BS 8110 (1985), simplified method,
- 6/ solution based on British Standard BS 8110 (1985), more accurate method.

-comparison of short-term and long-term structural ultimate load behavior.

The above methods and ultimate loads are compared using sample beam, plate and shell structures. The influence of loading level and reinforcement level on the accuracy of the creep analysis methods is also investigated.

B. Description of analyses and results:

In order to compare results the following structures were investigated:

1/ Beam from Section 9.1. The 28-day compressive strength of concrete was taken as 38MPa. The beam was loaded at 28 days by 6.77kN/m^2 .

2/ Slab from Section 7.4. The structure was loaded by a uniform loading of 45kN/m^2 and the same concrete mix was assumed as for the above beam.

3/ Shell from Section 7.6. The above concrete was again used. Reinforcement was assumed to be 50% of the original value. The structure was loaded by a 6.3 multiple of its self-weight, i.e. $\lambda=6.3$.

The above structures were used as typical examples of 1D, 2D and shell structures. The reference loading level specified was derived from the assumption that mid-span deflection is approximately equal to the span over 250, the serviceability requirement in BS 8110. The reinforcement ratio is approximately 0.7% for beam, 0.6% for slab and 0.9% for shell (reinforcement in both directions considered).

Throughout each analysis the Bazant Panula model I was used. The results are presented for 30 years old structure, the age specified in BS 8110 for long-term loading condition.

Method 5 is based on recommendations from British Standard BS 8110. Linear elastic analysis is used to solve internal moments and forces in structure. These values are then used to calculate the structural deflection based on cracked cross sections conditions. Strains are derived from the assumptions:

-plane cross section remains plane,

-the reinforcement, whether in tension or in compression, is assumed to be elastic. Its modulus of elasticity was taken

to be 200GPa,

-the concrete in compression is assumed to be elastic. An effective modulus was taken by the value $E/(1+\phi)$, where ϕ is the appropriate creep coefficient specified by the creep and shrinkage model used,

-Stresses in concrete in tension are based on a triangular distribution, having a value of zero at the neutral axis and a value at the centroid of the tension steel of 550kPa.

The final mid-span deflection is calculated using:

$$Y_{\max} = K l^2 \frac{1}{r_b} \quad /9.1/$$

where K is a constant which depends on the shape of the bending moment diagram, specified in Table 3.1 of BS 8110. The value 0.104 was used in the present analyses. l is the structural span and $\frac{1}{r_b}$ is the curvature at mid span.

Method 6 is similar to method 5, the only difference being that, instead of equation /9.1/, structural deflections are obtained by direct numerical integration of equation /9.2/. In the present study we used four elements to model half of the beam (structure 1/) and half of the mid-span strip of the slab (structure 2/), (due to symmetry).

$$\frac{1}{r_x} = \frac{\partial^2 y}{\partial x^2} \quad /9.2/$$

where $y(x)$ is the structural deflection and $\frac{1}{r_x}$ is the curvature based on the same assumptions as those in the method 5.

The above specification for loading conditions and reinforcement are assumed to be a reference state, and in the following they are referred to as a case A.

To study the influence of the amount of reinforcement and loading on the accuracy of the methods three other cases were

considered:

case B: same as case A but only 70% loading,

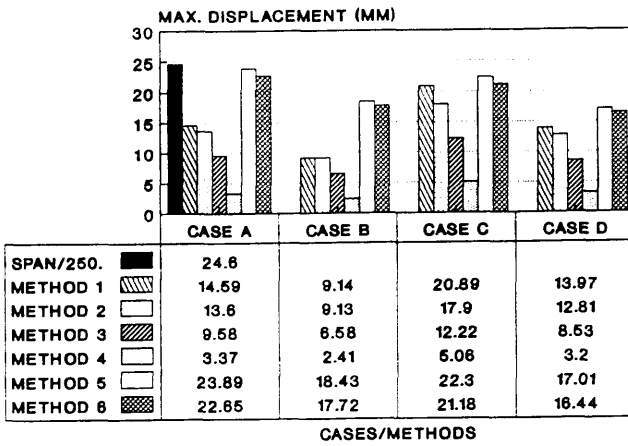
case C: same as case A but 200% reinforcement and 142% loading,

case D: same as A, but 200% reinforcing.

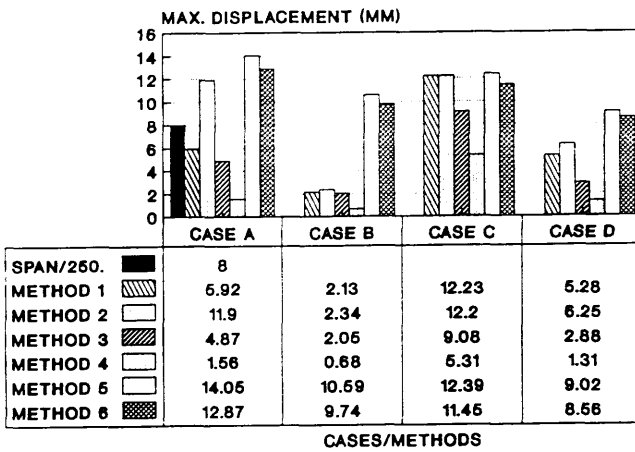
The above cases were defined to cover reasonable values for structural reinforcement and loading level.

The resulting maximum displacements are depicted in Fig. 9.15 in absolute values and as a percentage of the most accurate analysis, i.e. method 1, in Fig 9.16. The development of maximum structural deflections with time is shown in Fig. 9.17 using method 1.

BEAM



SLAB



SHELL

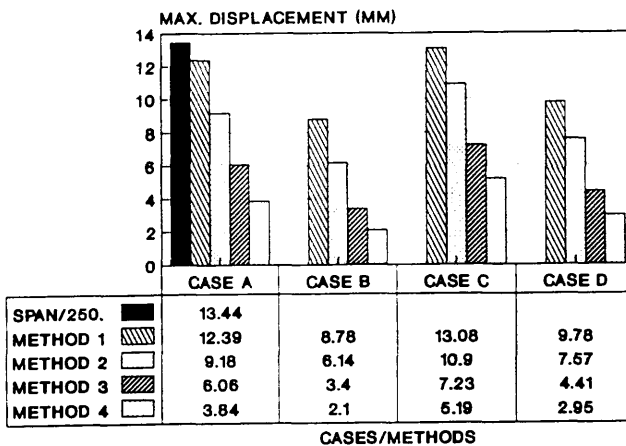
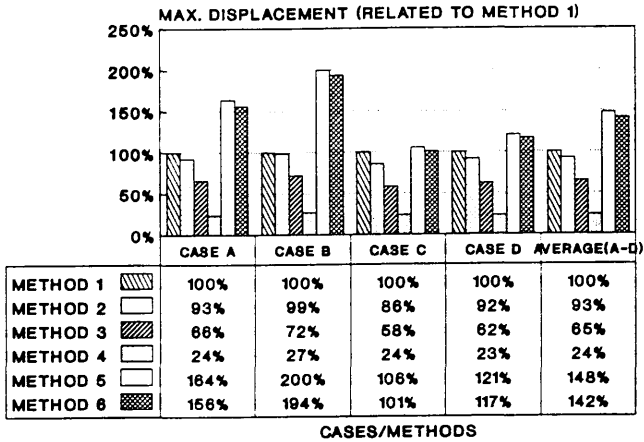
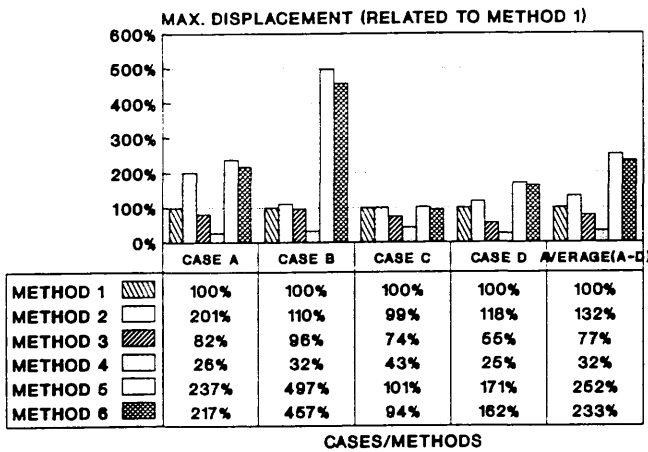


Fig 9.15 Maximum displacement of the structures, cases A-D.

BEAM



SLAB



SHELL

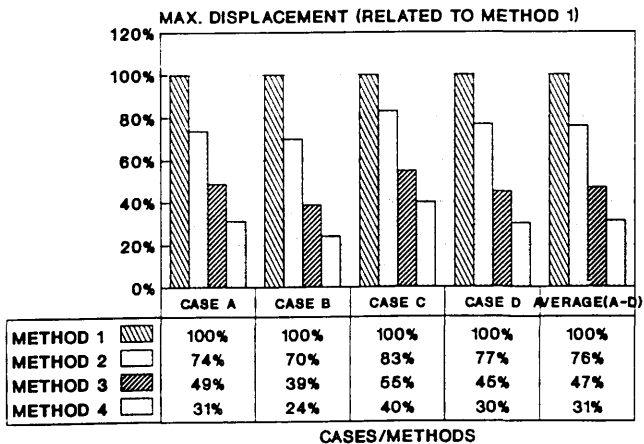
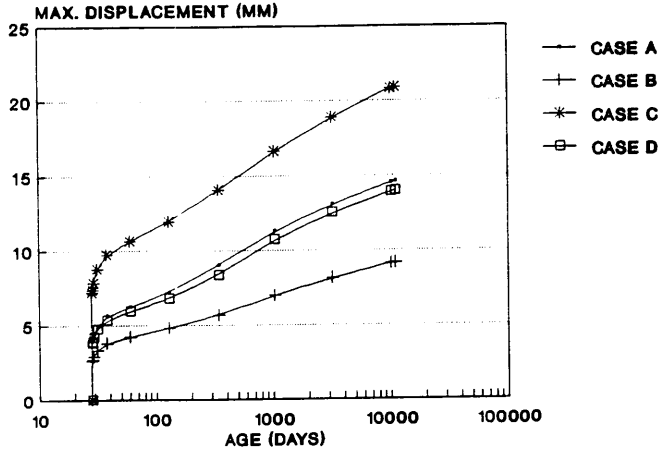
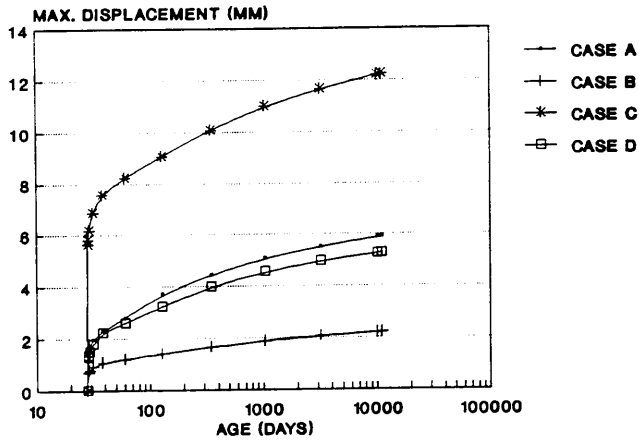


Fig 9.16 Maximum displacement of the structures, cases A-D, expressed in % of the results according to method 1.

BEAM



SLAB



SHELL

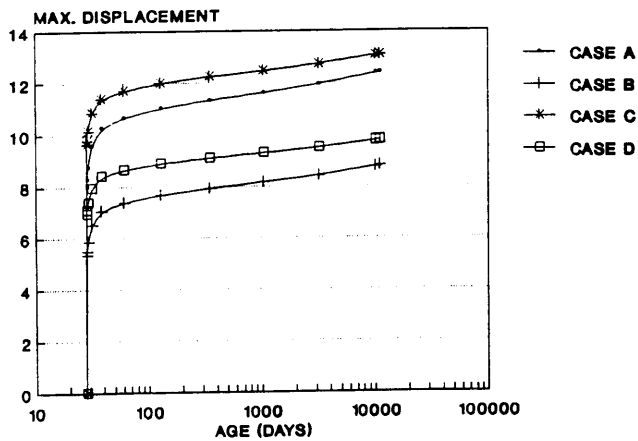


Fig 9.17 Maximum displacements development calculated by method 1.

The results can be summarized as follows:

- methods 5 and 6 in almost all cases highly overestimated the structural deformations,
- there are negligible differences between results by 5 and 6 methods. Considering the higher simplicity of method 5, this approach should be preferred were applicable,
- neither method 5 nor 6 allows calculation of deflections for more complicated structures, e.g. shells, particularly if structural membrane action is significant,
- the higher the reinforcement level, the closer are the results by methods 1 and 5, (resp. 6),
- the higher the loading level, the closer the results of methods 1 and 5 (resp. 6). This is probably due to the fact that the methods 5 and 6 are calibrated for higher reinforcement and higher loading levels,
- results provided by method 4 differ substantially and should not be used in practice,
- deflections provided by method 2 differ in most cases by about 5-20% from those by method 1. For geometrical and material linear solution they should match, however in a nonlinear solution the situation is more difficult. For example, higher concrete rigidity for short-term loading, i.e. early after load application, causes more loading to be sustained by concrete and less by reinforcing compared to direct application of long-term conditions, as is the case in method 2. It may result in the creation of more cracks and consequently higher structural deformations than method 2 predicts. The accuracy of method 2 is also affected by how shrinkage strains are accounted for. One extreme is that full shrinkage develops before applying loading, the other extreme is that structure is first loaded and thereafter shrinkage strains are accounted for. Moreover, it is difficult to predict whether the obtained results will lie on safe or unsafe side because each structure behaves differently. In the present analyses 4 load increment steps were always applied with the following loading in-

crements: 45%, 22%, 17% and 16% and shrinkage increments: 25%, 25%, 25% and 25%. It also matters whether the loading corresponds approximately to the level of crack and plasticity propagation or to structural "settled" conditions, i.e. elastic or already cracked/plastic ones. Obviously in the latter case method 2 gives better results because the structure is not so sensitive to its possible inaccuracy. As an example take the slab behavior in case A. The maximum deflection in step 3, i.e. for about 84% loading level was 5.16mm, being followed by spontaneous crack propagation in the next, i.e. the fourth step and resulting in a final deflection of 11.9mm. 19 iterations were necessary to reach convergence, whilst steps 1 through 3 needed at maximum 5 iterations. Nevertheless, use of this method is an option in cases when direct solution by method 1 is too costly.

-comparing the results of methods 2 and 3 shows the importance of shrinkage consideration in structural analysis. Moreover to account for it costs nearly nothing. The differences between results by methods 2 and 3 were about 25%.

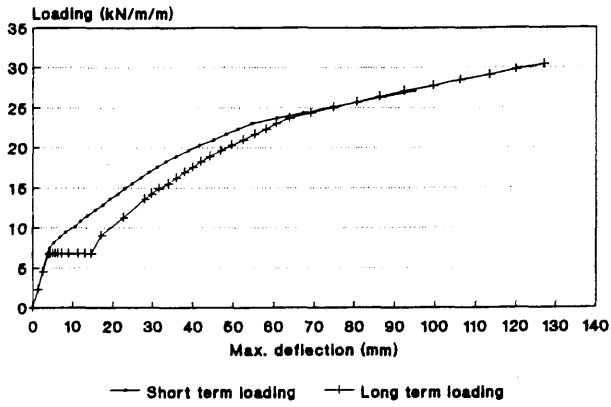
-method 1 is the most accurate one, but also the most expensive. It costs about 2.5 times more computation time than method 2. There is nearly no differences in computational costs of methods 2, 3 and 4 and methods 5 and 6 are obviously much cheaper, involving only a linear elastic solution and then some simple post-processing. Method 1 is the only one which is generally applicable, which allows for variable loading history, and which accounts for both geometric and material nonlinearities. Its present form is restricted to serviceability analyses due to linear aging creep law for concrete. Provided a more sophisticated nonlinear creep model is available, the method can be used for ultimate analyses, e.g. creep buckling analyses.

Finally the influence of structural age on the ultimate load was investigated. The previously analyzed reference beam, slab and shell, (i.e. the case A), were examined. Two loading conditions were imposed on each structure:

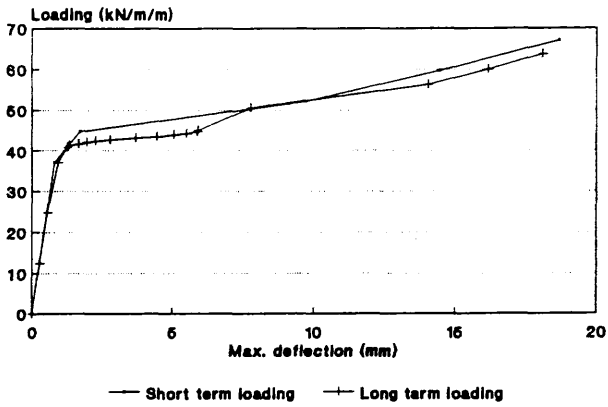
- 1/ short-term loading, i.e. loading up to ultimate value within 2.4 hours,
- 2/ long-term loading up to 30 years as in the previous creep analyses, followed by an additional short-term loading of 2.4 hours up to failure.

The resulting load-displacement diagrams are depicted in Fig. 9.18. It is apparent that the structural age did not affect the ultimate loads substantially. The curves for short-term and long-term loading nearly coincide for high loading/deformation levels. Note however that the deformations, for which the curves match each other are already far beyond the deformations which are acceptable from an engineering point of view. They correspond to the conditions in which the reinforced concrete contributes little to the structural stiffness, (due to failures), and the structure is suffering from several mechanisms. Hence it is difficult to distinguish between structural failure and the failure of the numerical technique used for the analysis and the calculated ultimate load levels have more or less informative significance only. For practical analyses the importance of creep is indisputable.

BEAM



SLAB



SHELL

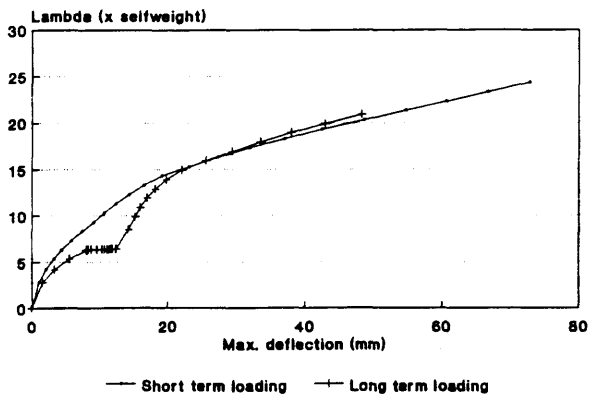


Fig. 9.18 Short term and long term load-displacement curves, (case A).

9.5 Approximation of creep function by Dirichlet's series, rejection of excessive modes.

A. Aim of the analysis:

- to test the mechanism rejecting excessive modes from the approximation by Dirichlet's series,
- to set the threshold value for the criterion which decides whether to keep or reject a mode function from the series,
- to provide simple example analyses for different values of the threshold value and compare results.

B. Description of analyses and results:

In Chapter 8 an algorithm was developed to remove excessive modes from the Dirichlet's series approximation of the original creep function and thus to remove ill-conditioning of this step of the solution. The purpose of section is to examine suitable values for $\cos^2(\alpha)$ in equation /8.89/.

A simple uniaxial plain concrete specimen, cast from the concrete mix defined in Section 9.1 is investigated. A short term linear stress-strain material relationship is assumed. The structure is loaded at 28 days by a compressive stress of 15MPa, linearly increasing to 16.5MPa at 30 years.

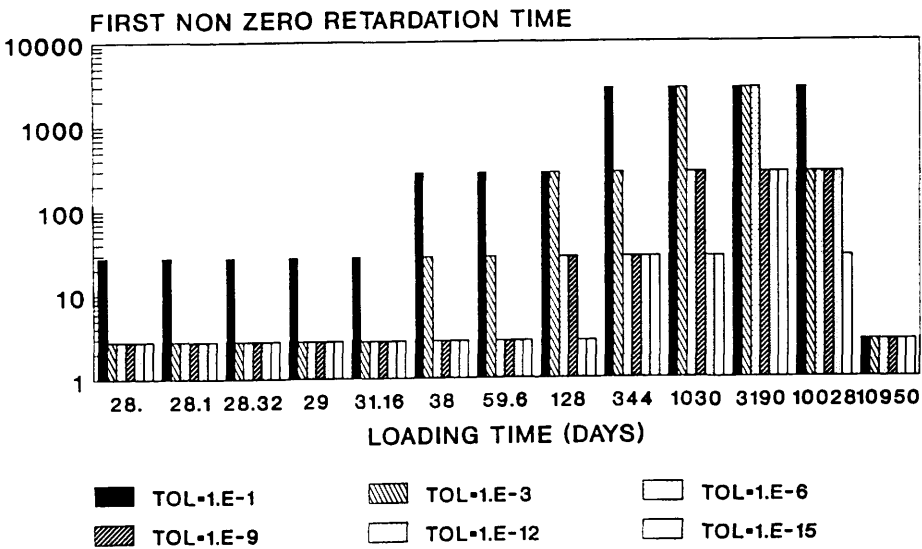
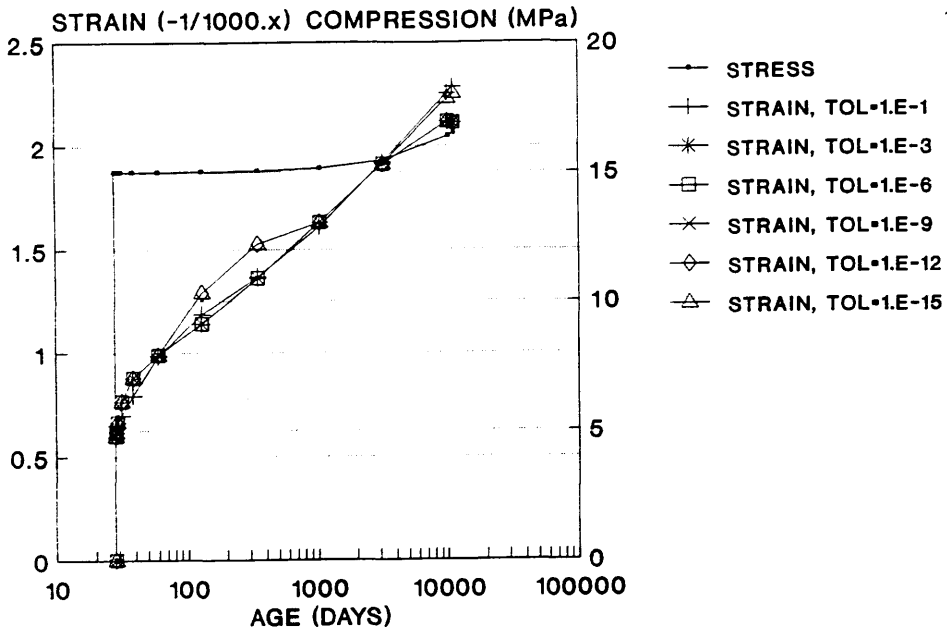
The resulting strain-time relationships for different values of tolerance $tol = \cos^2(\alpha)$ are presented in the first part of Fig. 9.19. The second part shows which particular modes were removed. For example in the approximation of the concrete compliance function $\Phi(t, t')$, $t' = 29$ days, $t \in \langle t', 30 \text{ years} \rangle$ for $tol = 0.1$ the mode corresponding to $\tau = 2.8$ was removed. For the other values of tol the full approximation spectrum is considered.

Analyzing the upper chart of Fig. 9.19 it is apparent that results pertaining to $tol \in \langle 0.001, 10^{-12} \rangle$ are identical. When $tol = 0.1$ some inaccuracy developed due to a too coarse functio-

nal spectrum of the approximation and at the other extreme, for $tol=10^{-15}$ the approximation procedure had already numerically failed.

It can be concluded that value $tol \approx 10^{-6}$ is the best choice and thus is set as the default in the developed software .

STRESS-STRAIN RELATIONSHIP FOR DIFFERENT VALUES OF PARAMETER "TOL"



RETARD. TIMES: 0;2.8;28.;280;2800.;5960
 INTEG. TIMES: 28.1;28.3;29;31.2;38;59.6;
 128;344;1030;3190;10000;10950

Fig. 9.19 Analysis of Dirichlet's series modal spectrum.

9.6 Summary.

Several long-time analyses have been presented in this chapter. The results of these can be summarized:

1/ The Step-by-step method should always be used if we are interested in structural deformations near the serviceability conditions.

2/ For well reinforced and relatively thin structures a simplified, short-term based analysis (e.g. the Effective modulus method, the BS 8110 recommendation etc.), can be used to investigate structural ultimate conditions.

3/ The Step-by-step method using Dirichlet's series for the approximation of creep functions of concrete works well in both 2D and shell implementations, especially after the algorithm which rejects excessive modal functions from Dirichlet's series has been incorporated.

4/ The density of retardation times and intervals for time integration recommended in ref. [50] has been found unnecessarily high for the present analyses. A coarser approach is acceptable.

5/ The Bazant-Panula model I is probably the best choice from the creep and shrinkage models implemented in the material preprocessor.

6/ All present analyses have been carried out on a standard personal computer. Time for any analysis did not exceed several hours. Hence also this objective of the work has been achieved.

10. USER'S AND PROGRAMMER'S CONSIDERATIONS OF THE DEVELOPED SOFTWARE IN A PC ENVIRONMENT.

An important stated aim of this work was to enable easy and convenient analysis of 2D and shell structures using only PC computers. To the author's knowledge, such software, (i.e. software for the analysis of R/C structures accounting for geometrical and material nonlinearities and at the same time also dealing with creep and shrinkage) is still rare. This chapter provides a brief description of the created PC environment and the performance of the software within it. Further information is available in refs. [42], [44] and [45].

10.1 General considerations.

The developed software has worked satisfactorily even on the simplest IBM XT compatible machine, making such analysis available for nearly everybody. It is not necessary to be connected to some computer center, it is not necessary to book a terminal one day in advance and to go somewhere else in the computer laboratory. Nowadays a PC machine is commonly available directly on a user's desk. The computational price of main frame and PC analyses should be also considered. Obviously the PC alternative is much cheaper in spite of the fact that the analysis itself takes a longer time.

One can object that for some solutions a simple PC computer is too slow and has disk and internal memory restrictions which significantly limit the problems that can be solved. That is true for an IBM XT and probably also for IBM AT compatible machines. However with the introduction of 32 bit technology these shortages are disappearing. These machines are delivered usually with at least a 100MByte hard disk (but also 300, 500MB and more) and if some smart system extender is used then the software can take advantage of virtual memory management and thus the internal program memory becomes, in fact, unlimited. In addition there are

other possibilities for "speeding" a PC computer such as using a disk cache, high speed memory cache, floating point instruction accelerator etc. Even if we buy the most deluxe PC model it is always far cheaper than any work station machine, (such as a SUN, Hewlett Packard, Apollo etc.) or indeed main frame.

Nowadays a hardware necessary to run the software developed in this work (with virtual memory etc.) can be bought for about £1000 (80386SX based machines). This availability was the main reason for choosing PC techniques for use in this work.

To compare analysis speed performance of programs CONCRETE and NONSAP, identical analyses were run on the IBM 3090, ICL 2957 main frame and PC computer Hewlett Packard Vectra RS25/C. Tests were carried out during ordinary working time and the time between start and stop of executions, (i.e. not CPU time) was measured. It was found that the IBM 3090 (even with a vector processor) was only about 30% faster than the Hewlett Packard PC computer and the ICL was nearly the same. Of course, such times are only informative in character and depend highly on how many users were currently utilizing the main frame service and on many other factors. Measurements during the weekend or at midnight would certainly be different. However this is not usually the time when designers work and hence generally we can conclude that the current 32 bit PC computer analyses are competitive with the traditional main frame performance.

10.2 Hardware requirements.

The developed software requires any PC IBM compatible computer with the MSDOS version 3.1 operating system or higher. Although a hard disk and numerical coprocessor are not strictly necessary, they are highly recommended. Without them the software is restricted only to very simple analyses.

The disk requirements essentially depends on the analyzed structure. Generally it can be said that about 10MB should be satisfactory for analyses with about 1000 degrees of freedom (pro-

vided the band width of the stiffness matrix is reasonable). The internal memory imposes no restrictions in the case of CONCRETE because it uses a frontal solution strategy. The NONSAP program uses a variable skyline data housekeeping system without "block by block" management. However analyses with about 1000 degrees of freedom still fit into the memory without problem. This was achieved by program segmentation which is discussed later.

Three versions of the software are available, one for real mode execution, i.e. for 8 and 16 bit machines, and two for 32 bit machines working in protected mode. These use the well established Eclipse DOS extender or the DEOS extender developed by Salford University in England. They both support virtual memory management so that the above memory restriction on NONSAP is no longer relevant. In this case extended memory of at least 1MB must be fitted (or expanded memory working under Virtual Control Program Interface (VCPI) protocol).

The software also provides graphic output for the geometry of the structure, eigenvalues and displacements. The supported graphic devices are CGA, EGA, VGA, MGA, SG4020 (ICL Quattro) video monitors and any Hewlett Packard Graphic Language (HPGL) compatible device (e.g. Hewlett Packard Laser Jet III or HP 7475 plotter). In addition it is possible to transfer the figures to an AUTOCAD program, (via the .DXF file interface), which supports nearly all available graphical peripherals.

If a 32 bit machine is used, programs can be run in a multi-tasking environment. The best choice is probably to use the well established DESQVIEW system (under VCPI protocol). The MS WINDOWS 3 is not suitable because it supports only multitasking of real-mode applications and hence only IBM XT and IBM AT versions could be run simultaneously.

10.3 User's considerations.

The environment consists of the following programs:

CONCRETE ... finite element solver for R/C shell structures,
NONSAP ... finite element solver for R/C 2D structures,
CONCRPLOT ... postprocessor for graphical output from
CONCRETE,
NSAPPLOT ... postprocessor for graphical output from NONSAP,
MATERIAL ... material preprocessor for creep and shrinkage
analyses by CONCRETE and NONSAP,
FORTRAN F77 graphical libraries (described in Section 10.4).

The CONCRETE and NONSAP programs reads data from an input file in the form defined in [42] and [44] respectively. In practice the data can be coded by any system editor such as EDLIN, BRIEF etc. or a simple program can be created to generate them automatically, (for example the nodal coordinates and element incidences).

All other software is "menu driven" and satisfactory data explanation is provided at run time. As an example, Fig. 10.1 shows the screen used to specify material parameters, (Bazant-Panula model 1), for the material preprocessor MATERIAL. Initially, the menu contains default values for all parameters, (see the right column). If the user wants to change any of these, first the cursor must point to the line containing the parameter to be changed, (e.g. ndec parameter in Fig. 10.1). Then selecting the letter 'E' the cursor jumps to the screen bottom prompting a new value. After the new value is specified, the cursor returns to the next parameter, i.e. the next line of the screen menu. In this way all non-default parameters can be modified and then by pressing 'R' start the material data generation. After the current material type is specified, generated and verified by the user, (from the immediate graphical output of the material characteristics onto the screen), a user can proceed to the next material type, i.e. a new menu appears.

--- BAZANT - PANULA GENERATOR FOR MATERIAL NO. 1 ---
 Enter "E", "R", "Esc" to Edit, Run or Escape the program.

```

Current data base:
type ... type of concrete (only type 1 and 3 supported) : 1
moist ... true/false = moist/steam curing : T
t ... last desired time of analysis : 0.110E+04
tsh ... time, when the curing of concrete is finished : 7.000
ndec ... number of tsamples per decade : 2
sfact ... =1/1.15/1.25/1.3/1.55-slab/cyl/square/sphere/cube: 0.125E+01
fcyl28 ... 28-day cylinder compression strength of concrete : 0.351E+05
thick ... =V/S, where V,S are volume and surface of element: 0.767E-01
humid ... environment humidity <0.4 - 1.) : 0.780000
ag ... =a/gama = total aggregate/cement ratio : 7.040000
gs ... =g/s = coarse/fine aggregate ratio : 1.000000
sg ... =s/gama = fine aggregate/cement ratio : 3.520000
wg ... =w/cement = water/cement ratio : 0.630000
sa ... =s/a = fine/total aggregate ratio : 0.500000
gama ... cement content(kg/m**3) : 0.250E+03
nt ... number of sudden loadings of structure : 1
tload ... times of sudden loadings : see below
          0.280E+02
  
```

Fig. 10.1 Menu to define material characteristics for Bazant-Panula model 1.

10.4 Programmer's considerations.

In this section a brief program description is presented. It contains a list of relevant subroutines and explanations of their functions. Also the general program layout will be discussed.

NONSAP:

The Figure 10.2 presents the general layout of this program in which two level segmentation is used. The first one corresponds to element type (1D, 2D and 3D element) and analysis phases, the second includes material models supported by the particular element formulation.

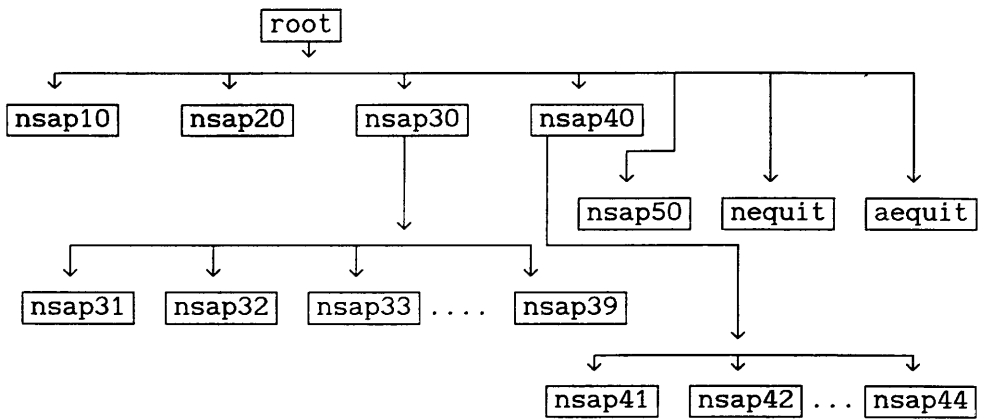


Fig. 10.2 NONSAP layout.

The above root and segments have the following function:

- root: The root portion of NONSAP comprises the data allocation strategy, system functions such as time, date etc. and also subroutines, which are called from higher segments (e.g. structural matrices assembly). It controls the whole analysis. The substantial part of these subroutines are in the nsap00 file.
- nsap10: This segment controls data input and also carries out some checks on the consistency of the geometry.
- nsap20: Segment supporting the element matrices and stress-strain calculations for the 1D truss element. Element material models are also included.
- nsap30: Segment supporting the element matrices and stress-strain calculations for the 2D truss element.
- nsap40: Segment supporting the element matrices and stress-strain calculations for the 3D truss element.

nsap50: Eigenvalue and eigenvector analysis, dynamic analyses.

nequit: The nonlinear equation solver based on the Newton-Raphson method.

aequit: Arc-length methods nonlinear solver, Line search method etc.

nsap31 - nsap39: Material models for 2D analyses

nsap41 - nsap44: Material models for 3D analyses.

The enhancement of NONSAP involved changes in the root, nsap10, nsap30, nsap36, nequit and aequit segments and therefore these are now discussed in more detailed.

nsap00:

This root segment consists of the following subroutines (their function are given in the brackets):

MAIN (main control over execution, data allocation etc.),

ADDBAN (add element structural matrices to global matrices),

ADDCM (similar to addban, deals with the mass matrix only),

ADDDI, ADDMA (similar to addban, deals with loading assembly, nonlinear contributions ...),

ADDRESS (addresses of diagonal elements in stiffness matrix (stored in vector form)),

CREEP (general control over creep analysis),

CREEP1 (calculation of "current" Young's modulus and initial strains),

CREEP2 (solution of internal constants E_{μ}),

COLHT (calculates the bandwidth of the stiffness matrix at particular degrees of freedom),

COLSOL (solution of linear equations and back substitution),

ELCAL (calls element dependent routines),

ELEMNT (cooperates with elcal, used also during iterations),

ERROR (checks data allocation requirements during analysis),
GETTIM (system get time function).
LOADDEF (calculation of effective loading for dynamic analyses),
MULT (system utility for matrix multiplication),
NEWDAV (used in dynamic analysis),
WRITE (write out the analysis results),
TTIME, STIME (provide time information of analysis).

This segment was modified to allow a new material model for 2D analysis, graphic output and nonlinear arc length solution. It also includes new programs supporting creep and shrinkage analyses.

nsap10:

The changes in this segment are only of minor importance. They comprise reading of additional data and saving of geometry for future plotting in the NONSPI subroutine.

nsap30:

The segment was modified to allow for new material models. Some bugs were also fixed.

DERIQ (solution of element structural matrices, derivatives etc.),
FUNCT2 (isoparametric interpolation functions, Jacobian of transformation ...),
INITWA (memory allocation for the material models),
MATRT2 (isotropic and orthotropic material linear models),
MAXMIN (principal stresses),
POSINV (matrix inversion)
QUADM (main routine to compute the element mass matrix)
QUADS (ditto for the stiffness matrix),
STSTL (linear isotropic and orthotropic material models),
STSTN (calls appropriate nonlinear material model),
TDFE (main control over evaluation of element entities),
TODMFE (memory allocation)

nsap36:

This segment is completely new. It comprises the material model for concrete including the new tension stiffening model.

ADSIGL (main control over calculation for unfailed material condition),
ADSIGC (ditto for failed material).
ELPAL9 (main control over material model computation),
ELT2D9 (similar to elpal9, uses data already allocated),
IELPAL9 (material initialization routine),
MOHR (Mohr-Coulomb and Rankine Cut off criterion),
PARAM (calculation of tension stiffness parameters),
STIFF (rigidity matrix for unfailed material),
RSTIFF (ditto for failed material),
TRANSF (rigidity matrix transformation).

nequit:

This segment consists of subroutines supporting the Newton-Raphson method. There were only minor changes to it.

aequit:

The function of this segment is to support the Arc-length nonlinear solvers. This segment is completely new.

AEQUIT (main control over nonlinear solution),
ARCLN1 (line search method),
BERGAN (evaluation of the β coefficient using Bergan's stiffness coefficient),
INFORC (evaluation of out of balance forces),
LAMBDA (calculation of the new λ factor)
MULT1 (system utility),
ORTHOG (cooperates with the LAMBDA routine to compute the λ factor for the Normal update, Explicit linear and Consistently linearized methods).

CONCRETE:

All routines of this program are placed directly in the root segment. All data are allocated in the main program via DIMENSION statements with variable lengths. These are defined in PARAMETER statements so that their readjustment is quite simple. The CONCRETE program consists of the following routines:

AEQUIT (main control over nonlinear solution),
ARCLN1 (line search method),
ALGOR (specifies whether the stiffness matrix should be recalculated in the current load increment),
ASSEMBLDR (assembles the global loading vector),
BERGAN (evaluation of the β coefficient using Bergan's stiffness coefficient),
BGMAT (calculates the strain-displacement B_0 and G matrices and stores them in the file No. 9),
CHECK1 (performs consistency check of input data),
CHECK2 (checks input data for loading, checks maximum front width),
CREEP1 (calculation of "current" Young's modulus and initial strains),
CREEP2 (solution of internal constants E_μ),
DIMEN (declares dimension of data arrays),
ECHO (echoes remaining input data after an error in the input data),
FLOWS (calculates entities for plastic flow in material, dependent on the used Yield function),
FRAME (system utility for vector and matrix arithmetic etc.),
FRONT (controls element assembly, stiffness matrix elimination and back substitution phases, it is the kernel of the program),
FUNC (calculates the strain-displacement matrix B and the Ja-

cobian of transformation from the global to natural coordinate system),
 GAUSSQ (specifies element sample points for integration),
 GEOME (adds the geometric stiffness matrix to the linear stiffness matrix),
 HARDEN (evaluates compression hardening factors),
 INCREM (adds the loading increments to the global loading, prepares the array for reactions for gaussian elimination),
 INPUT (inputs most input data and establishes internal data base),
 INVAR (evaluates the current value of the Yield function),
 INVA2 (calculates the uniaxial plastic strain corresponding to plastic strains),
 LAMBDA (calculation of the new λ factor)
 LCOMB (calculates loading combination for Arc-length methods),
 LDISP (calculate the second part of the strain-displacement matrix B_L and adds it to B_0),
 LOADS (subroutine to calculate node loads corresponding to the element internal loading),
 MATM (system utility for matrix calculations),
 MODUL (calculates material rigidity matrix),
 MODUL1 (used to compute shear moduli in creep analysis),
 MULT1 (system utility for matrix operations),
 MULT2 (system utility for matrix operations),
 NODEX (checks mid-node coordinates, if equals zero then interpolates them from corner element nodes),
 OUTPUT (prints displacements, reactions, strains etc.),
 ORTHOG (cooperates with the LAMBDA routine to compute the λ factor for the Normal update, Explicit linear and Consistently linearized methods).
 PRES (calculates the nodal equivalent of element distributed loading),
 PRIST (principal stresses evaluation),
 RESI1 (calculation of internal (nodal) forces from current strains for plastic concrete),

RESI2 (same as RESI1 but for cracked concrete),
RESI3 (same as RESI1 but for steel layers),
RESTR (global control over calculations of internal forces),
SFR1 (evaluation of isoparametric interpolation functions and
their derivatives),
SINGOP (system utility for matrix operations),
STIF (controls the calculation of element stiffness matrices),
TRANS (transforms material rigidity matrix),
VECT (system utility for vector operations),
WORKS (defines local node coordinates systems),
ZERO (analysis initialization routine).

CONCRPLOT:

The basic function of this program is to provide graphical output from the program CONCRETE. Plots of the geometry and/or loading deformations are possible. The program is menu driven and allows the choice of only some loading for drawing, or of only a part of the structure which is defined either by points or box (i.e. space limited by x, y and z boundaries) etc. It is also possible to define projection parameters. The input section is robust so that in the case of an error in the user input command there is still chance for remedy. The program works in the environment described in Sec. 10.2 and uses a graphical library which will be discussed further. There are no limitations on the size of drawn structures.

MAIN (main control over drawings, performs memory allocation,
includes code for interaction with the user),
ERROR (checks available computer memory for data and
generates error message in case of memory overflow),
BOX (supports boxing of a structure, i.e. checks which parts of
the structure are in the defined box and thus should be
drawn),
CLIP (routine for element clipping into specified box)

COED (checks if an element is inside the boundary limits of the window)

CPUTIM (system utility for CPU time),

DDATE (date and time information),

DEFORM (general control over drawing of deformed structure for one or more loading cases),

DELNOD (subroutine to support "deleting" of parts of structure connected to specified points),

DSHLIN (draws dashed lines),

GETDAT (system utility for current date),

GETTIM (system utility for current time),

GSCRON (switches between alphanumeric and graphic regimes of the video),

PLTADV (closes current drawing device/picture) and starts the new one),

PLTAXS (plots axis of coordinate system being used),

PLTEND (closes current drawing device/picture),

PLTFNM (draws floating point number of the specified format into the drawing),

PLTNUM (ditto as PLTFNM but for an integer number),

PLTLIN (plots lines),

PLTINT (open a new drawing device/picture),

PRNTPG (prints structural data including their 2D projection to output device (if required)),

ROLL (moves data pointer to the particular loading case),

SCALE (calculates scale of a drawing (for geometry only, deformations are scaled in DEFORM),

SETPG (sets an array comprising element numbers which are connected to nodes, checks for maximum allowed and eventually reallocates internal memory for more complex structures),

SORTPG (based on information from the SETPG routine it performs the optimization of drawings (each line is drawn only once)),

STPLOT (plots already scaled and projected geometry or one loading case of structure),

TITLE (plots header and footer of current drawing including

structure name, date, scale etc.),
UNDEF (master program to draw undeformed structure),
XP (function for node coordinate projection, conjugate to .YP),
YP (function for node coordinate projection, conjugate to XP),

NSAPLOT:

This program is very similar to the CONCRPLOT the only difference being that it works with a different data base (CONCRETE uses a different format for data housekeeping than NONSAP). Therefore all the above information is also relevant also for this program.

FORTRAN GRAPHICS:

A very simple graphic library has been created to enable direct access from the FORTRAN environment to a graphics device. The supported devices are listed in Sec. 10.3. For more complicated graphics it would be necessary to use some already available software package such as GKS (Graphic Kernel System), Hello, graphic supplement of NAG etc. The provided routines are very simple, fast and do not need to load the whole graphic kernel which supports hundreds of other facilities, none of which is used by the developed software.

In order to communicate with AUTOCAD, an additional pseudo-graphics device was created. All graphic data are in this case stored into disk file in a format compatible with the .DXF AUTOCAD transfer file. Via this interface the user can create a disk file with drawings and then modify them in the subsequent AUTOCAD session. This is very advantageous because all facilities provided by the CAD system need not be programmed in the user's program environment (which is virtually impossible). The additional advantages of AUTOCAD support is that this software supports

nearly all possible graphic devices.

The following table summarizes the routines name according to function and graphics device:

Function / Device	Video	HP-GL	SC4020	ACAD
open graphic device	IFRAMEV	HPLOTS	FRAMEV	ASTART
close graphic device	PLOT	HPLOT	GSCROF	AEND
draw line	ILINEV	HPLOT	LINEV	ALINEV
draw real number	IPRINTV	NUMBER	PRINTV	APRINTV
draw real number (cont. texts)	IPRINTVC	----	PRINTVC	APRINTVC
draw text	ILABLV	SYMBOL	LABLV	ALABLV
draw text (cont. texts)	ILABLVC	----	LABLVC	ALABLVC

MATERIAL:

This program generates material properties and some another data necessary for creep and shrinkage analysis by the CONCRETE and NONSAP programs. They use an identical format for material data so that only one version of MATERIAL is necessary.

The program supports CEB-FIP 78, ACI78, Bazant-Panula Model I and Bazant-Panula Model II creep and shrinkage models. Experimental data can be also dealt with.

The results of the execution are three data files which are then used by CONCRETE or NONSAP for the Step-by-step analysis described in Chapter 8.

In addition a direct analysis of linear elastic truss element is available. This is very useful because it gives the user an idea about the quality of the material model approximation, time step length and retardation time influences etc.

The program runs in a menu driven regime and provides immediate graphics results for the user's convenience.

ACI78 (generates compliance and shrinkage functions according to the ACI78 Code of Practice),
BAPA1 (generates compliance and shrinkage functions according to the Bazant-Panula model I),
BAPA2 (generates compliance and shrinkage functions according to the Bazant-Panula model II),
CEB78 (generates compliance and shrinkage functions according to the CEB-FIP Code of Practice),
EQUAT (linear equation solver),
DEGKER (generates already approximated concrete compliances for graphic output),
INPUT (main input data menu),
INPUT1 (input data routine for the ACI78 and CEB-FIP78 models),
INPUT2 (input data routine for the Bazant-Panula models I, II),
INTERPOL (system utility for polynomial interpolations),
LINEREG (system utility for linear interpolations),
MATERO (routine for the concrete truss sample analysis)
OUTPRN (prints results to disc file),
PLTFI (draws desired results, it follows the PLTSTR routine),
PLTSTR (starts graphic output of the results (e.g. shrinkage, concrete compliance function etc.), draws heading and footing of pictures),
SBR (strain-stress relationships routine for the truss analysis),
TIMGEN (generates retardation and integration times for the Step-by-step analysis),

The graphic output can either be drawn on the supported video monitor (see Sec. 10.2) or the AUTOCAD pseudo-graphics device can be used.

It should be noted that the present programs layout is subject to small changes due to different FORTRAN environments for real and protected modes software versions.

11. CONCLUSION AND SUMMARY

The work deals with the analysis of reinforced concrete structures. Both material and geometric nonlinear behavior were considered. Attention focused on plane stress structures as well as on general degenerated three dimensional shell structures. In addition to static loading, special emphasis was paid to the influence of time phenomena, i.e. shrinkage and creep.

The nonlinear governing equations were derived using the principle of virtual displacements which is formulated for arbitrary loading increments applied to the structure. Stresses and strains were treated in the form of the 2nd Piola-Kirchhoff tensor and the Green-Lagrange tensor respectively. Using the Updated Lagrangian formulation for 2D problems the above tensors can be alternatively replaced by the Cauchy stresses and the Almansi strains. The constitutive equations were defined in invariant form with the exception of the tension stiffening of concrete which was specified within engineering stresses. However, for the sake of simplicity, the difference between the Cauchy and the 2nd Piola-Kirchhoff stresses is neglected and the 2nd Piola-Kirchhoff stresses are directly substituted into formulae. Considering the small importance of tensile concrete strength this simplification causes only negligible inaccuracy.

The adopted formulation is suitable for structures with large deflections, large rotations but small strains. In other words it accounts for all terms of the geometric equations but the strain increments are applied suddenly. The geometric equations for the shell element have been in addition simplified by the Von Karman assumptions. For large strain analysis the Updated rate Lagrangian formulation with an appropriate material model had to be used.

Constitutive equations for both two and three dimensional analysis of reinforced concrete were considered. Smearred crack models are emphasized.

For two dimensional analysis isoparametric elements with a

variable number of nodes (four through nine) with Lagrangian approximation of geometry and displacements are used. It should be pointed out that the bilinear (i.e. four node) element formulation failed in cases when shear behavior was important (due to low shear stiffness). With the quadratic formulation no problems were experienced and therefore the eight or nine elements are highly recommended.

A new but simple material model for concrete has been developed. This is a smeared-type linear model which accounts for various failure criteria. Failure of concrete is checked by Cowan criterion (the combination of Mohr-Coulomb and Rankine Cut off criteria), steel is checked also by Rankine Cut off criterion. In the case of material crushing no material rigidity and stresses are assumed in subsequent analysis. Cracked concrete is assumed to be an orthotropic material with unaffected properties in the direction parallel to crack and small residual rigidity and stresses perpendicular to crack. Also shear stiffness is considered as a small residual value. A tension stiffening model is provided in which the descending part of stress-strain diagram is modeled by a smooth hyperbolic function. It improves significantly the convergence properties of an analysis because the usual discontinuities are removed. In the case of mixed failure mode, a crushing coefficient is used in which compressive strength is reduced. Based on the current experience with this modeling of concrete it can be said that the model is suitable for tension-tension or compression-tension stress conditions when a failure of material is caused by either shear or normal tensile stresses. For high compression regimes, i.e. with stresses about 75% of compression strength or higher, the assumption of linearity is not justified. This is the penalty for a low computational cost.

For shell analysis, the degenerated Ahmad shell element using Serendipity, Lagrange and Heterosis geometry and displacement interpolating hierarchical approach is adopted. Special attention is focused on the problem of shear locking and thus full, selective and reduced integration rules are dealt

with. Some discrepancies have been found in literature concerned with rank deficiency of the elements and thus this problems was thoroughly analyzed, accounting also for element nonlinearities. Constitutive equations are assumed which are elastic-plastic for both concrete and steel materials. Also tension stiffening and compression hardening of concrete, including descending branch of material stress-strain diagram are supported. The behavior of the element proved to be very good but the generality of formulation is paid for by a high computational time. The acceptable compromise between the element accuracy and time demands might be CBR (continuum-based resultant) shell theory advocated by ref. [59]. The use of reduced integration is not suitable for materially nonlinear problems [58].

Nonlinear solution techniques were comprehensively reviewed and consequently some of them were significantly improved. A new algorithm for the solution of nonlinear equations, which is based on Newton-Raphson, Arc-length and Line search methods has been developed. The algorithm chooses the most efficient variant of these combined solution methods and solution parameters (step length, scale factor between displacement space and loading dimension, use or not of the Line searches etc.). Its computational performance is good in spite of some problems in to handling a sudden break down of structural stiffness (e.g. local collapse) in addition to discontinuities in material model (for shell).

Analysis considering shrinkage and creep has also been solved. The Step-by-step method using the Dirichlet series approximation to the creep function was adopted. Unfortunately numerical instabilities can be a serious problem, because the adopted approximation is ill conditioned. Hence a criterion was developed, which enables a decision to be made about which mode functions are to be incorporated and which are to be neglected. The recommendations provided by Bazant [33], [38], [50] for the choice of retardation times and time integration intervals were found too cautious for the present analyses.

The practical results of the work are as follows:

The nonlinear program NONSAP (from the University of Berkeley, U.S.A.) has been significantly enhanced to include the new two dimensional constitutive model for concrete, the derived algorithm for the solution of the nonlinear equations and creep and shrinkage analysis.

For shell structures the program CONCRETE (from the University of Swansea, Wales) was used, which analyses reinforced concrete shells based on the above mentioned shell theory. The original elastic-perfectly plastic material model was improved by incorporating a hardening function (Madrid parabola with descending branch of stress-strain diagram). The nonlinear solver was also implemented in this program and, similar to the NONSAP, creep and shrinkage support have been incorporated.

Much interest has also been paid to the development of graphic support software. A library has been produced which enables simple graphics accessible from Fortran 77 on all IBM-PC compatible videos, ICL CG 6400 video, HP graphic language devices (e.g. HP 7640 plotter) and also enables cooperation with the AUTOCAD system. Using this library two additional programs were developed for graphic output with CONCRETE and NONSAP. They work interactively and support plotting of geometry and deformations of structure. Many special tasks are supported such as plotting of a couple of deformations in one Figure, zooming and boxing of a structure etc.

In addition to the above software a material data preprocessor program MATERIAL has been created which is in a very user friendly form. This program enables material constants necessary for modeling of creep and shrinkage of concrete to be generated. The material models according to ACI78, CEB78 and Bazant-Panula model I and II recommendations are supported. In order to save computer time the material preprocessor allows a study of concrete behavior, subject to any particular stress history, on a simple concrete bar. In this case the analysis is very quick and hence the best adjustments of material parameters can be made be-

fore a time consuming analysis of a practical structure is carried out. The best results were experienced using the Bazant-Panula model I [48].

Finally the used methods and capabilities of the developed software were tested for analysis of sample structures. Much information about structural behavior and the accuracy of used theoretical methods has been collected. They are summarized:

-Implementation of compression hardening and softening into the elastic-plastic constitutive equations for concrete improved both the accuracy and the numerical behavior of the model.

-The new nonlinear solution algorithm can handle complicated situations of structural behavior. If the governing equations of a structure suffer from discontinuities (e.g. due to cracking), the Line search may be of help, otherwise its use is debatable. It is, however, always useful for checking the overall convergence of the algorithm.

-Simplified methods for creep and shrinkage analysis, such as the Effective modulus method etc. do not provide the acceptable accuracy near the serviceability loading conditions. Hence "full-time" analysis must be carried out. Good results were obtained using the Step-by-step method with Dirichlet's series. The proposed algorithm, which rejects excessive modal functions from Dirichlet's series, improves numerical stability of the solution.

-The density of retardation times and intervals for time integration recommended in ref. [50] has been found too high for the present analyses.

-The Bazant-Panula model I is probably the best choice from the creep and shrinkage models implemented in the material preprocessor.

-For well reinforced and relatively thin structures, simplified short-term based analyses can be used to investigate the ultimate structural conditions.

All analyses were carried out on a standard personal computer thus meeting one of the objectives of this work. It should make them very suitable for designers to use in working practice.

Suggestion for future work:

A more sophisticated material model for concrete could be used, especially for 2D analyses. The elastic-plastic model, (used in the shell analysis) works well. However, its behavior will improve if a non-associated plastic flow and nonlinear unloading stress-strain relationships are incorporated.

The current linear creep assumptions can be enhanced to include nonlinear terms. The main problem in doing this is unavailability of some well established nonlinear creep and shrinkage models for concrete.

It would be advantageous if the user can combine 2D and shell elements in one structure. Therefore the computing facilities of CONCRETE and NONSAP should be put into one program.

The ultimate structural conditions could be better investigated if the solution of structural eigenvectors and eigenmodes is supported in the software in order to deal with bifurcation points etc. more efficiently and to identify spurious local numerical mechanisms in the structure.

REFERENCES

1. Bathe, K. J., "Finite Element Procedure in Engineering", Prentice Hall, Inc., Englewood Cliffs, New Jersey.
2. Chen, W. F., Sallee, A. F., "Constitutive Equations for Engineering Materials", Vol. 1, "Elasticity and Modelling", John Wiley & Sons, 1982.
3. Šejnoha, J., "Pružnost, pevnost, plasticita", díl I, II, Vydavatelství ČVUT, Praha 1979.
4. Buyukozturk, O., Shareef, S. S., "Constitutive Modeling of Concrete in Finite Element Analysis", Computers & Structures, Vol. 21, No.3, GB 1985.
5. Dougill, J. W., "On Stable Progressively Fracturing Solids", Zeitschrift fuer Angewandte Matematik und Physik, ZAMP, Vol.27, Fasc.4, 1976.
6. Soerensen, S. I., "Endochronic Theory in Nonlinear Finite Element Analysis of Reinforced Concrete", Report No 78-1, Institut for Statik, University of Trondheim, Norway, March 1978
7. Bažant, Z. P., Kim, S. S., "Plastic Fracturing Theory for Concrete", Journal of the Eng. Mech. Division, ASCE, Vol. 105, No. EM3, June 1979.
8. Červenka V, "Konstitutivní vztahy pro beton, ČVUT.
9. S. Balakrishan, D.W. Murray, "Prediction of Response of Concrete Beams and Panels by NLFEA", Colloquium on Computation Mechanics of Concrete Structures, IABSE Delft, Aug. 26-28 1987.
10. A.A. Al-Manaser, D.V. Phillips, "Numerical Study of Some Postcracking Materials Parameters Affecting Nonlinear Solution in RC Deep Beams", Canadian Journal of Civil Eng., 1987.
11. O. Buyukozturk, S.S. Shareef, "Constitutive Modeling of Concrete in FE Analysis", Comp. & Struct., Vol. 21, No. 3, pp. 581-610, 1985.
12. F.B. Lin, Z.P. Bažant, J.C. Chern, A.H. Marchetas, "Concrete Model with Normality and Sequential Identification", Comp. &

- Struct., Vol.26, No. 6, pp 1011-1025, 1987.
13. A. Scanlon, D.R. Green, D.V. Phillips "Skew reinforced concrete panels", J. of Struct. Engng, ASCE, Vol. 117, No. 5, pp 1477-1491, May 1991.
 14. R. Borst, P. Nauta, "Non-orthogonal Cracks in a Smeared Finite Element Model", Eng. Comput., Vol.2, March 1985.
 15. H.A. Franklin, "Nonlinear Analysis of Reinforced Concrete Frames and Panels", Report No. SESM 70-5, Dep. of Civil Engineering, University of California, Berkeley 1970.
 16. M. Cervera, E. Hinton, O. Hassan, "Nonlinear Analysis of Reinforced Concrete Plate and Shell Struct. Using 20-node Isoparametric Brick Elements", Comp.& Struct., Vol.25, No. 6, pp 845-869, 1987.
 17. R.H. Dodds, Jr., "Numerical Techniques for Plasticity Computations in FE Analysis", Comp. & Struct., Vol.26, No.5, pp 767-779, 1987.
 18. P.X. Bellini, A. Chulya, "An Improved Automatic Incremental Algorithm for Efficient Solution of Nonlinear Finite Element Equations", Comp. & Struct., Vol.26, No. 1/2, pp 99-110, 1987.
 19. R.H. MacNeal, R.L. Harder, "A Refined Four-Node Membrane Element with Rotational Degrees of Freedom", Comp. & Struct., Vol. 28, No. 1, pp 75-84,1988.
 20. I. Fried, "Orthogonal Trajectory Accession to the Nonlinear Equilibrium Curve", Comp. Method in Appl. Mech. and Eng. 47, pp. 283-297, 1984.
 21. Z.P. Bazant, F.B. Lin, "Nonlocal Yield Limit Degradation", Int. Journal for Num. Methods in Eng., Vol. 26, pp. 1805-1823, 1988.
 22. B.W.R. Forde, S.F.Stiemer, "Improved Arc Length Orthogonality Methods for Nonlinear Finite Element Analysis", Comp. & Struct., Vol. 27, No. 5, pp. 625-630, 1987.
 23. A. Eriksson, "On some Path-related Measures for Nonlinear Structural Finite Element Problems", Int. Journal for Num. Methods in Eng., Vol. 26, pp. 1791-1803, 1988.

24. M. Geradin, S. Idelhsen, M. Hogge, " Computational Strategies for the Solution of Large Nonlinear Problems via Quasi-Newton Methods", *Comp. & Struct.*, Vol. 13, pp. 73-81, 1981.
25. M.A. Crisfield, "Incremental/Iterative Procedures for Non-linear Structural Analysis", *Numerical Methods for Non-linear Problems*, Ed: Taylor, Hinton, Owen, Vol.1, Pineridge Press, Sept. 1980, pp. 261-290.
26. M.A. Crisfield, "Acceleration and Damping in the Modified Newton-Raphson Method", *Comp. & Struct.*, Vol. 18, No. 3, pp. 395-407, 1984.
27. E. Riks, "Some Computational Aspects of the Stability Analysis of Nonlinear Structures", *Comp. Methods in Applied Mechanics and Engineering* 47, pp. 219-259, 1984.
28. M.A. Crisfield, J. Wills, "Solution Strategies and Softening Materials", *Comp. Methods in Applied Mech. and Engineering* 66, pp. 267-289, 1988.
29. M.A. Crisfield, "An Arc-length Method Including Line Line Search and Acceleration", *Int. Journal for Numerical Methods in Eng.*, Vol. 19, pp. 1296-1289, 1983.
30. C. Meyer, K.J. Bathe, "Nonlinear Analysis of RC Concrete in practice", *ASCE Annual Convention and Exposition*, held at Hollywood, Fla., October 27-31, 1980.
31. Comite Euro-International du Beton : "CEB Design Manual on Structural Effects on Time Dependent behaviour of Concrete", Georgi Publishing Company Saint Saphorin, Switzerland, 1984.
32. A.M. Neville, W.H. Dilger, I.J. Brooks, "Creep of Plain and Structural Concrete", *Construction Press*, London & New York, 1983.
33. Z.P. Bazant, F.H. Wittman, "Creep and shrinkage in Concrete Structures", *John Wiley & Sons*, New York, 1982.
34. "Finite Element Analysis of Reinforced Concrete", *State of the art report*, American Society of Civil Engineers, New York, 1982.
35. W.H. Glanville, "Studies in Reinforced Concrete, III-creep or

- flow of concrete under load", Building Research Tech. Pap. No. 12, Department of Scientific and Industrial Research, London 1937.
36. C.S. Whitney, "Plain and reinforced concrete arches", Jour. of Amer. Concrete Inst., Vol. 28, pp. 479-519.
 37. Z.P. Bazant, "Prediction of concrete creep effects using age-adjusted effective modulus method", J. Am. Concrete Inst., Vol. 69, No. 4, pp 212-217, 1972.
 38. Z. Bazant, T. Spencer, "Dirichlet series creep function for aging concrete", Jour. of Eng. Mech. Div., pp. 367-387, 1973.
 39. L. Jendele, "Nelineární výpočet železobetonových konstrukcí", Research work, Prague 1989.
 40. Kupfer et al., "Behavior of concrete under biaxial stresses", ACI Journal Vol. 66, No. 8, pp 656-666, 1969.
 41. A. Y. Thannon, "Ultimate load analysis of reinforced concrete stiffened shells and folded slabs used in architectural structures", Thesis, University of Swansea, June 1988.
 42. E. Hinton, D.R.J. Owen, "Finite Element Software for Plates and Shells", Swansea, 1984.
 43. E. Hinton, D.R.J. Owen, "Finite Elements in Plasticity", Peridge Press, 1980.
 44. K. J. Bathe, Wilson, "NONSAP - Users manual", program documentation.
 45. K. J. Bathe, "NONSAP - theoretical reference guide", program documentation.
 46. A.W. Hago, "Direct design of R/C slabs", Ph.D. thesis at University of Glasgow, Glasgow 1982.
 47. E. Hinton, D.R.J. Owen, "Finite Element Programming", London, 1977.
 48. Z.P. Bazant, L. Panula, "Practical prediction of time-dependent deformations of concrete ", "Part 1: Shrinkage", Material and Structures, Vol. 11, No. 65, pp. 301-316, 1978,
"Part 2: Basic Creep", Material and Structures, Vol. 11, No. 65, pp. 317-328, 1978,

- "Part 3: Drying Creep", Material and Structures, Vol. 11, No. 66, pp. 415-423, 1978,
- "Part 4: Temperature Effect on Basic Creep", Material and Structures, Vol. 11, No. 66, pp. 424-434, 1978,
49. M.R. Hollington, "A Series of Long-term Tests to Investigate the Deflection of Representative Precast Concrete Floor Component, Technical Report TRA 442, Cement and Concrete Association, 52 Grosvenor Gardens, London SW1, SBN 721004369, CI/SfB (23)/Hf/(K4c), UDC 624.072.2.012.35: 620.172/.173, April 1970.
50. Z.P. Bazant, "Mathematical Modeling of Creep and Shrinkage of Concrete", John Wiley & Sons, New York, 1986.
51. F. Dishinger, "Untersuchungen ueber die Knicksicherheit, die elastische Vervormung und das Kriechen des Betons bei Bogenbruecken", Der Bauingenieur, Vol. 18, No 33/34, pp. 487-520, No. 35/36, pp 539-552, No. 39/40, pp. 595-621, 1937.
52. I.J. Jordan, G.L. England, M.A. Khalifa, "Creep of concrete, a consistent engineering approach", Journal os Struct. Div. ASCE, Vol 99, No. ST9, pp 131-142, 1973.
- 53 R.W.Payne at al., "GENSTAT 5 Reference Manual", Clarendon Press, Oxford, 1985.
- 54 S.Ahmad, B.M.Irons, O.C.Zienkiewicz, "Analysis of thick and thin shell structures by curved finite elements", Int. J. Numer. Methods Eng.,Vol. 2, pp. 419-451, 1970.
55. E.D.L.Pugh, E.Hinton,O.C.Zienkiewicz, "A study of quadrilateral plate bending elements with reduced integration", Int. J. Numer. Methods Eng.,Vol. 12, pp. 1059-1079, 1978.
56. H.Parisch, "A critical survey of the 9-node degenerated shell element with special emphasis on thin shell applications and reduced integration, Comp. Methods Appl. Mech. Eng., Vol. 20, pp. 323-350, 1979.
57. J.H.Wilkinson, "The Algebraic Eigenvalue Problem", Oxford University Press Inc., London, 1965.
58. L.Jendele, A.H.C. Chan, D.V. Phillips, "On the rank deficien-

- cy of 'Ahmad's degenerated shell element", to be published in Eng. Comp., 1991.
59. G.M.Stanley, K.C.Park, T.J.R.Hughes, "Continuum-based resultant shell elements", FEM for plate and shell structures edited by T.J.R. Hughes and E.Hinton, Vol.1: Element technology, Pineridge Press Int., Swansea, U. K., pp. 1-45, 1990.
 60. W.F.Chen, D.J.Han, "Plasticity for Structural Engineers", Springer Verlag New York, Berlin, London, Paris, Tokyo, Heidelberg, 1988.
 61. R.Palaniswamy, S.P.Shah, "Fracture and Stress-Strain Relationship of Concrete under Triaxial Compression", Jour. of Struct. Div., ASCE, Vol. 100, pp 901-916, 1974.
 62. P.E.Peterson, "Crack Growth and Development of Fracture Zones in Plain Concrete and Similar Materials", Report. No. TVBM-1106, Division of Building Materials, University of Lund, Lund, Sweden, 1981.
 63. B.P. Sinha, K.H.Gerstle, L.G.Tulin, "Stress-Strain Relations for Concrete Under Cyclic Loading", ACI Jour., Vol. 61, No. 2, pp 195-211, 1964.
 64. G.Wishers, "Application of Effects of Compressive Loads on Concrete", Betontech., Berlin, Nos. 2 and 3, Duesseldorf, 1978.
 65. J.G.M. van Mier, "Complete Stress-Strain Behavior and Damaging Status of Concrete under Multiaxial Conditions", RILEM-CEB-CNRS, Int. Conference on Concrete under Multiaxial Conditions, Vol.1, Presses de'Universite Paul Sabatier, Toulouse, France, pp. 75-85, 1984.
 66. E.Ramm, T.A.Kompfner, "Reinforced concrete shell analysis using an inelastic large deformation finite element formulation", prepared for publishing.
 67. A.C. van Riel, W.J.Beranek, A.C.Bouma, "Tests on shell roof models of reinforced mortar", Proceeding on 2nd Symposium on concrete shell roof construction, Oslo, 1957.
 68. B.Bresler, A.C.Scordelis, "Shear Strength of Reinforced Concrete Beams", Jour. of ACI, Proceedings Vol. 60, No. 1, Jan.

1963, pp. 51-72.

69. E.Ramm, "Strategies for tracing nonlinear response near limit points", Europe-USA Workshop, Nonlinear FE analysis in struct. mech., Bochum, Germany 1980.
70. E.Riks, "An incremental approach to the solution of snapping and buckling problems", Int. Jour. Solids Structures, Vol. 15, 1979, pp. 524-551.
71. A.B.Sabir, A.C.Lock, "The application of finite element to large deflection geometrically nonlinear behavior of cylindrical shells", Variational methods in engineering, Southampton, University Press, 7/66-7/75, 1972.

